



**Università degli studi di Roma "Tor Vergata"**

**Universidad Autónoma de Madrid**

Phd in  
**CHEMICAL SCIENCE**  
XXXIII Cycle

**Molecular Materials Based on Porphyrinoids for  
Chemical Sensing and Energy Conversion Schemes**

**Víctor Mariñas Perdigón**

Supervisors:

Prof. Sara Nardis

Prof. Roberto Paolesse

Prof. Tomás Torres

Academic Year 2020/2021

## Introducción: Subftalocianinas y corroles como materiales moleculares

Material molecular es toda aquella estructura orgánica constituida por subunidades orgánicas o metalorgánicas, pudiendo ser sintetizadas de manera individual y posteriormente combinadas entre sí. Dichos materiales presentan una serie de propiedades electrónicas, ópticas y magnéticas poco convencionales. La correlación estructural existente entre estos materiales y sus propiedades permite que éstas últimas puedan ser modificadas y perfiladas, mediante diferentes metodologías sintéticas a partir de sus subunidades iniciales, lo que los convierte en sistemas muy atractivos de cara a su aplicación en diversos ámbitos tecnológicos, que abarcan desde su incorporación en células solares como materiales sensibles hasta su uso en terapia fotodinámica para el tratamiento de diferentes patologías. De entre la multitud de materiales moleculares presentes en la actualidad, los porfirinoides se encuentran entre los sistemas macrocíclicos más estudiados gracias a sus excelentes propiedades optoelectrónicas, además de su gran versatilidad sintética.

De entre los diferentes porfirinoides, las subftalocianinas (SubPcs), análogos contraídos de las ftalocianinas (Pc), destacan por encima del resto. diferencia de la estructura plana de las Pcs, estos macrociclos aromáticos presentan una estructura cóncava formada por tres unidades diiminoisoindol alrededor de un átomo de boro central, el cual presenta una disposición tetraédrica, con su posición axial ocupada. Poseen un sistema de 14 electrones- $\pi$  que se extiende principalmente alrededor de su cavidad central, siendo uno de los pocos ejemplos conocidos de compuestos aromáticos heteroatómicos curvos.

Las SubPcs poseen un característico espectro de absorción ultravioleta-visible, con dos intensas bandas, generalmente en torno a 300 y 550 nm, denominadas banda Soret y banda Q, respectivamente. Presentan una fuerte intensidad de absorción, con valores de coeficientes de absorción en torno a  $5 \times 10^4 \text{ M}^{-1} \text{ cm}^{-1}$ . También poseen una intensa emisión, con pequeños valores de desplazamiento de Stokes (5-10 nm), y energías de excitación en torno a 2.0 eV.

Las propiedades fisico-químicas de las SubPcs las convierten en moléculas excepcionales para su incorporación en multitud de dispositivos electrónicos relacionados con la óptica no lineal, fotovoltaica, electrónica o la terapia fotodinámica. En particular, su capacidad para generar estados excitados y de separación de carga de larga duración las convierte en candidatas ideales para su uso junto a otras unidades fotoactivas, ya sea mediante uniones covalentes o electroestáticas, en sistemas enfocados hacia la conversión de energía solar.

Dentro de la familia de los porfirinoides, los corroles (Cors) presentan una serie de propiedades ideales para su combinación con SubPcs. Debido a la falta de protocolos y metodologías desarrolladas para su obtención, su disponibilidad sintética fue baja hasta principios de la década de los 2000, donde el descubrimiento de metodologías que permitían su síntesis a partir de compuestos comerciales, supuso un aumento en el número de publicaciones basadas en esta clase de macrociclos de manera exponencial. Es por ello que no se encuentran tan estudiados como las porfirinas (Pors), con las que mantienen una estrecha relación. En comparación con las Pors, los Cors presentan la misma estructura molecular salvo por un enlace directo C-C entre dos de sus unidades pirrólicas, lo que hace que posean una cavidad interna menor y una simetría reducida. Sin embargo, siguen manteniendo los 18 electrones- $\pi$  aromáticos de las Pors, lo que genera una serie de propiedades interesantes. Al igual que las

Pors, son capaces de alojar metales en su cavidad interior. Entre sus propiedades destaca la posibilidad de actuar como ligandos trianiónicos, haciendo que sean capaces de alcanzar altos estados metálicos de oxidación, los cuales serían difíciles de estabilizar empleando Pors.

Sus espectros de absorción son cualitativamente similares a los de las Pors, con una intensa banda de absorción alrededor de 400-450 nm correspondiente a la banda Soret, con valores de  $\epsilon = 1-2 \times 10^5 \text{ M}^{-1} \text{ cm}^{-1}$  y tres bandas de menor intensidad en torno a 500-600 nm correspondientes a las bandas Q, con valores de  $\epsilon = 1-2 \times 10^4 \text{ M}^{-1} \text{ cm}^{-1}$ . Las Pors han sido ampliamente empleadas como materiales moleculares en sistemas de conversión energética, como por ejemplo formando díadas con Pcs, SubPcs o ferroceno (Fc). Es por ello que el uso de Cors, los cuales presentan unas características dadoras superiores en comparación con sus análogos porfirínicos, en combinación con otras unidades aceptoras como SubPcs, puede suponer una mejora de sus propiedades fotofísicas

## **Capítulo 1. Materiales basados en subftalocianinas y corroles para su uso en sistemas de conversión energética.**

En el capítulo uno, se recogen la síntesis, la caracterización y el estudio de las propiedades de una serie de sistemas fotoactivos empleados como materiales captadores de energía lumínica basados en SubPcs y Cors.

En la primera sección del capítulo, un conjunto de SubPcs se enlazó a la posición periférica de diferentes Cors, a través de una metodología de activación axial de la SubPc y posterior reacción de sustitución axial sobre la SubPc, empleando unidades fenoxi- en las posiciones *meso*- de los Cors como nucleófilos. Las díadas **4**, **5**, **6** y **7** se obtuvieron en rendimientos razonables, teniendo en cuenta la complejidad y sensibilidad de los sistemas empleados. El estudio de sus propiedades fotofísicas y redox se llevó a cabo mediante experimentos de absorción, emisión, espectroelectroquímica y espectrometría de absorción transitoria, durante una estancia predoctoral en los laboratorios del Prof. D. M. Guldi en Erlangen, Alemania. Los resultados evidenciaron estados de separación de carga para las cuatro díadas estudiadas. A pesar de que la incorporación del cobre en las subunidades Cor se llevó a cabo con intención de estudiar un cambio en sus propiedades, se encontraron tiempos y mecanismos similares de separación de carga para las díadas **5**, **6** y **7**, obteniendo los mejores tiempos para la díada **4**, con valores máximos de 534 ps en tolueno. Adicionalmente, la díada **11** demostró ser capaz de canalizar toda la energía absorbida por la molécula hacia la subunidad SubPc, reforzando su papel como antena en sistemas de transferencia energética.

En la segunda sección, se llevó a cabo la síntesis de las díadas SubPc-Cor **14** y **15** unidas a través de la posición axial del Cor. Para ello, se empleó un Cor de fósforo sustituido en sus posiciones *meso*- por unidades aceptoras. Dado el escaso número de metodologías para la introducción de diferentes funcionalidades sobre la posición axial de los Cor de fósforo, nuestros estudios preliminares se centraron en la activación de dicha posición. Para ello, se siguió una estrategia empleando diferentes derivados de triflato, sin éxito. Finalmente, aprovechando la gran afinidad mostrada por el fósforo hacia las unidades hidroxí-, se lograron introducir dos unidades diferentes de SubPc a través de enlaces  $\mu$ -oxo. Los estudios de absorción y emisión revelaron para la díada **15** una posible transferencia de energía desde la SubPc hacia el Cor. Para

la díada **14**, sin embargo, los resultados obtenidos llevaron a proponer la formación de un exciplex.

En el tercer apartado, se llevó a cabo la unión de unidades SubPc y Fc mediante un enlace etinilo. Durante este proceso, se logró optimizar la reacción de formación de la Cl-SubPcCl<sub>6</sub> **17**, incrementando su rendimiento de obtención al 67%. La síntesis de los nuevos derivados de SubPc se llevó a cabo mediante una estrategia de sustitución axial sobre la SubPc, que consiste en el uso de AlCl<sub>3</sub> y el etinil-TMS derivado en condiciones suaves. La unión entre las correspondientes SubPc-Etinilo y Fc se realizó mediante una reacción Sonogashira de acoplamiento C-C catalizada por paladio, obteniendo las díadas **21** y **22**. Estudios preliminares fotofísicos mostraron una fuerte disminución de la intensidad de emisión de ambas díadas frente a sus correspondientes subunidades de referencia. Esto, junto con los antecedentes en la combinación de SubPcs y Fc mediante diferentes tipos de enlaces, nos llevó a sugerir la presencia de un estado de separación de carga en ambos sistemas.

En el cuarto y último apartado, se llevó a cabo la incorporación de una unidad tetraciano, con propiedades electrónicas fuertemente aceptoras, en el Cor dador **23**, a través de una de sus posiciones periféricas. Para ello, un fragmento de etinilanilina fue enlazado sobre la posición *meso*- del Cor **22** mediante una reacción de Sonogashira, permitiendo la posterior introducción de la unidad tetraciano sobre el Cor **23** mediante una reacción de cicloadición-retroelectrociclación, obteniendo el TCBD-Cor **24**. Con el fin de estudiar su comportamiento en función del pH del medio, se llevaron a cabo experimentos de absorción en diferentes fases de su equilibrio de protonación/desprotonación. Actualmente, se están llevando a cabo experimentos de emisión, espectroelectroquímica y espectrometría de absorción transitoria para determinar su uso potencial en sistemas biológicos, estudiando a fondo su comportamiento fotofísico en función del pH.

## **Capítulo 2. Subftalocianinas y naftalocianinas como materiales sensibles en sistemas de gravimetría de masas**

Gracias a sus particulares propiedades fotofísicas y electrónicas, la familia de los porfirinoides ha sido extensamente empleada como material sensible en dispositivos electrónicos. Además, la versitilidad sintética de estos macrociclos y la estrecha relación entre su estructura y sus propiedades hace que estas últimas puedan ser moduladas de manera precisa y efectiva.

En el presente capítulo, se llevaron a cabo estudios preliminares en la incorporación de SubPcs y naftalocianinas (NPcs) como materiales sensibles en dispositivos de detección de gases de amplia selectividad. El dispositivo empleado está basado en un conjunto de pequeños transductores de masa, en este caso microbalanzas de cuarzo (QMBs), cubiertos por una capa sensible que corresponde a cada uno de los compuestos empleados. La interacción del analito con la capa sensible lleva a la modificación de una o varias de sus propiedades físicas. A su vez, el transductor se encarga de transformar dichas variaciones en señales eléctricas. Este dispositivo es comúnmente conocido como “nariz electrónica”, debido a su similitud con el sistema olfativo de los mamíferos, los cuales se basan en sistemas de detección no selectivos.

El sistema de detección de gases se compone de cuatro nuevas capas sensibles (SubPcs **s1**, **s2** y **s3**; Np **s5**) así como de una serie de Cors, Pcs y Pors ampliamente estudiados. De las nuevas capas introducidas, tres de ellas presentaron perfiles de sensibilidad distintivos que, en comparación con las capas sensibles ya conocidas, mostraron un conjunto diferente de afinidades frente a los compuestos volátiles orgánicos empleados. Se logró establecer una tendencia de distinción frente a la acidez del medio para las tres SubPcs empleadas, siguiendo un patrón de afinidad en función de sus propiedades electrónicas. Estos resultados convierten a las SubPcs en perfectos candidatos para su incorporación de manera general en dispositivos sensores de selectividad cruzada.

The present work has been developed as a joint PhD at the Department of Chemical Science and Technology of University of Rome Tor Vergata, under the supervision of Prof. Sara Nardis and Prof. Roberto Paolesse, and at the Department of Organic Chemistry of the Autonoma University of Madrid, under the supervision of Prof. Tomás Torres.

*Audentis Fortuna iuvat*  
«Fortune favours the bold»  
Virgil, *Aeneid*, X, 284.

## Agradecimientos

Los agradecimientos quizás sean una de las partes más sencillas y a la vez complicadas de escribir a la hora de redactar una tesis. He tenido la suerte de conocer y vivir en dos ambientes muy diferentes, sintiéndome en ambos como en casa, haciendo que esta sea posiblemente una de las mejores etapas de mi carrera.

En primer lugar, me gustaría agradecer a mis dos directores de tesis, el **Prof. Roberto Paolesse** y el **Prof. Tomás Torres**, la oportunidad dada de desarrollar estos más de tres años de trabajo en sus respectivos grupos de investigación. Vuestra inmensurable calidad científica está al nivel de vuestra calidad como personas, dejando el listón muy alto para aquellos que están por venir. No me olvido de mi supervisora directa, la **Prof. Sara Nardis**: tu criterio, sinceridad y franqueza han sido claves en el desarrollo de esta tesis. Gracias.

A riesgo de repetirme, quiero remarcar de nuevo la gran suerte de contar con el **Prof. Tomás Torres** como uno de los directores de este trabajo. No sólo eres uno de los científicos más brillantes que he tenido la suerte de conocer, sino que me has demostrado ser una grandísima persona, con cualidades que cada vez se hacen más difíciles de encontrar.

Mis andaduras en el grupo de investigación de Nanociencia y Materiales Moleculares comenzaron en 2015, durante mi trabajo de fin de máster. Gracias a mi directora de TFM por aquel entonces, **Mariví**, que con la inestimable ayuda de **Germán** me ayudaron a sacar adelante un trabajo del cual me siento muy orgulloso. Vuestros consejos han seguido acompañándome hasta el día de hoy.

Gracias a los veteranos del grupo, **Salomé, Gema, Miguel, Max, Ismael, Andrés y Gianni**, por vuestra cercanía y simpatía sea cual sea la situación. A **Esmeralda**, que no te puedes imaginar la cara que se me quedó al verte en la vitrina después de haberme dado clase en el instituto. También a todos los que habéis sido mis compañeros de la tercera planta, **Elena, Ana Belén, Vero, Asma, Alba, Marta, Miguel Ángel y Oscar**, incluidos los chicos de IMDEA, **Luis, David, Álvaro y Nico**, con los que tan buenos ratos he pasado dentro y fuera del laboratorio. No me olvido de **Sonia**, que siempre me alegraba las mañanas cuando traía palmeritas.

Gracias a mi gente del 301. Gonzalo, mi compañero de vitrinas, con el que comentaba cualquier chorrada que me pasaba por la cabeza y tantos desayunos hemos compartido donde Pirri. Giulia, con la que no se si pasaba más tiempo hablando de química o de cocina, pero que me ha enseñado que con trabajo duro y esfuerzo uno puede sacar adelante lo que se proponga. Y Jorge, ese joven chico Pedro del Hierro que tan pronto te da una charla magistral sobre Subs como de padel, pero sobre todo me ha enseñado a interesarme verdaderamente por mi trabajo, generando en mí una motivación para leer

publicaciones e ir más allá, hasta no dejar ni un cabo suelto consiguiendo, como él dice, que madurase científicamente. Dejando a un lado las bromas, han sido muchas jornadas de entrar y salir de noche, Rusia, San Sebastián, muchas tardes de té y alguna cena de venezolano. Vosotros más que nadie sabéis los buenos y malos momentos por los que he pasado estos años. Sin vuestro apoyo y consejos esta tesis no hubiese sido posible.

E come non potrebbe essere diversamente, un paragrafo doveva essere scritto in italiano. Queste parole sono piene di sincerità, e non sono abbastanza per ringraziare tutti quelli che ho conosciuto nel gruppo del Prof. Roberto Paolesse. Dal primo momento, l'accoglienza e lo spirito di gruppo che tutti mi hanno trasmesso ha fatto sì che io mi sentissi parte della loro famiglia. **Larisa, Fede, Manu, Donato, Gabrielle, Lorena, Mounika, Beatrice, Michele, Andrea, Sara, Roberto, Fabrizio**, non ho abbastanza paragrafi per descrivere tutte le volte che ognuno di voi mi ha aiutato, sempre con un sorriso. In particolare, voglio ringraziare **Roberto** e **Sara**, per avermi guidato con sapienza in questo progetto, essendo sempre brillantissimi chimichi e persone di riferimento a cui rivolgersi. A **Gabrielle**, per essere sempre pronto ad aiutare e risolvere qualche problema, non solo accademico, dimostrando di nuovo la versatilità degli ingegneri, e anche per avermi insegnato tanto su MatLab, il mondo dei sensori e le parole romane. Grazie in particolare a **Fabrizio**, chi è stato il mio collega di laboratorio dall'inizio, che sempre mi ha aiutato in tutto, mi ha lasciato aperte le porte della sua casa e mi ha mostrato il sentimento della vera cultura romana attraverso la sua famiglia. Senza tutti voi, questa bella esperienza non sarebbe stata possibile.

Gracias a mis padres, **Lola y Emilio**, que siempre me han apoyado en todas mis decisiones, desde que en el instituto decidí que quería ser universitario. A partir de ahí, el más puro azar, o más concretamente una rápida búsqueda sobre nanotecnología en Google en el momento oportuno, hizo que de la manera más inesperada llegara hasta donde hoy me encuentro.

Gracias al resto de mis familiares, amigos, gente de Roma, que de una manera u otra habéis contribuido a que esta tesis salga adelante. Gracias también a mis abuelos, **Ana y Pedro**, y a los que ya no están, **Emilia y Tomás**, que se lo orgullosos que estarían de verme llegar hasta aquí.

Y por supuesto gracias a ti, **Alba**, la persona con la que hace más de once años decidí pasar el resto de mi vida. Tú más que nadie sabes todo el trabajo que hay detrás de esto, los días fuera de casa y las noches delante de una pantalla. Tu apoyo y ánimos en los peores momentos me dieron fuerzas para seguir adelante, sin las cuales esta tesis no existiría.

## **Predoctoral stays**

Photophysical measurements were carried out in the group of Prof. Dirk M. Guldi at the Department of Chemistry and Pharmacy of Friedrich-Alexander-Universität of Erlangen-Nürnberg, Germany, in January 2020, in close collaboration with doctoral student Benedikt Platzer.

## Abbreviations and acronyms

We have used standard Organic Chemistry abbreviations and acronyms following the recommendation of the "Guidelines for authors", *J. Org. Chem.*, which can be found in the journal webpage:

[http://pubs.acs.org/paragonplus/submission/jocea/jocea\\_authguide.pdf](http://pubs.acs.org/paragonplus/submission/jocea/jocea_authguide.pdf)

In addition, the following abbreviations have been employed during this dissertation:

A	Acceptor
BODIPY	Boron-dipyrromethene
CA-RE	Cycloaddition-retroelectrocyclization
Cor	Corrole
CSS	Charge separation state
CT	Charge transfer
CS	Charge separation
CV	Cyclic voltammetry
D	Donor
<i>o</i> -DCB	<i>o</i> -Dichlorobenzene
DCTB	Trans-2-[3-(4- <i>tert</i> -Butylphenyl)-2-methyl-2-popenylidene]malononitrile
DDQ	2,3-dichloro-5,6-dicyano-1,4-benzoquinone
DCE	Dichloroethane
DIPEA	Diisopropylethylamine
DPM	Dipyrromethane
DPV	Differential pulse voltammogram
DSSC	Dye-sensitized solar cell
EET	Electronic energy transfer
Fc	Ferrocene
HF	Hydrofluoric acid
HOMO	Highest occupied molecular orbital
HQ	Hydroquinone
ISC	Intersystem crossing
$\kappa$	Transmission coefficient
$K_{eT}$	Electron transfer rate constant
$\lambda$	Total reorganization energy
LUMO	Lowest occupied molecular orbital

$V_N$	Electronic factor in the Arrhenius expression for $K_{eT}$
MALDI	Matrix-assisted laser desorption ionization
Mes	Mesityl
OFET	Organic field-effect transistor
OLED	Organic light-emitting diode
OPD	Organic photodetector
OPV	Organic photovoltaic
PAH	Polycyclic aromatic hydrocarbons
Pc	Phthalocyanine
PCE	Power conversion efficiency
PE	Potential energy
PET	Photoinduced energy transfer
PeT	Photoinduced electron transfer
PHJ	Planar heterojunction
Por	Porphyrin
SCE	Saturated calomel electrode
SubPc	Subphthalocyanine
SubPor	Subporphyrine
SWV	Square-wave voltammetry
TAS	Transient absorption spectroscopy
TBPAF <sub>6</sub>	Tetrabutylammonium hexafluorophosphate
TCBD	Tetracyanobutadiene
TFA	Trifluoroacetic acid
$\alpha,\alpha,\alpha$ -TFT	$\alpha,\alpha,\alpha$ -Trifluorotoluene

# Index

## Introduction

Subphthalocyanines as Molecular Materials.....	3
Synthesis of Subphthalocyanines .....	4
Structural isomerism and chirality of Subphthalocyanines .....	6
Synthesis of low-symmetry Subphthalocyanines .....	7
Reactivity of Subphthalocyanines.....	8
Axial reactivity .....	9
Peripheral reactivity .....	13
Ring-expansion reactions.....	15
Other reactions of Subphthalocyanines .....	15
Properties of Subphthalocyanines.....	16
Applications of Subphthalocyanines .....	18
Corroles as Molecular Materials.....	25
Synthesis of corroles.....	26
Synthesis of $\beta$ -Substituted Corroles .....	28
Synthesis of <i>meso</i> -substituted A <sub>3</sub> -Corroles .....	31
Synthesis of <i>meso</i> -substituted A <sub>2</sub> B-Corroles .....	33
Functionalization of Corroles.....	35
Functionalization at the inner core positions.....	35
Functionalization at the periphery .....	38
Properties of corroles .....	40
Applications of Corroles .....	45

## Chapter 1 - Subphthalocyanine- and Corrole-based molecular materials for energy conversion schemes

1.1. Energy challenges in a non-so-far future.....	51
1.1.1. Marcus theory of electron transfer .....	57
1.2. Specific objectives of Chapter 1.....	61
1.3. Background .....	67

1.3.1. Corroles and Subphthalocyanines as photoactive units .....	67
1.4. Synthesis and characterization of subphthalocyanine-corrole covalent systems linked through corrole <i>meso</i> - position.....	71
1.4.1. The particular case of copper corroles: noninnocent ligands as novel acceptor units .....	71
1.4.2. Results and discussion .....	72
1.4.3. Controlling direction of EET processes: synthesis of ThioSubPc-PCor dyads .....	93
1.5. Synthesis and characterization of SubPc-Cor covalent systems linked through Corrole axial position .....	100
1.5.1. Background .....	100
1.5.2. Results and discussion .....	102
1.6. Synthesis and characterization of Subphthalo-cyanine-Ferrocene covalent systems .....	119
1.6.1. State-of-the-art in Subphthalocyanine-Ferrocene dyads .....	119
1.6.2. Results and discussion .....	120
1.7. Synthesis and characterization of Tetracyano-butadiene-Corrole covalent systems .....	127
1.7.1. Background .....	127
1.7.2. Results and discussion .....	128
1.8. Summary and conclusions .....	143
1.9. Experimental section .....	146
1.9.1. Materials and general methods.....	146
1.9.2. Synthesis of precursor phthalonitriles .....	148
1.9.3. Synthesis of precursor aldehydes .....	150
1.9.5. Synthesis of chloro-substituted subphthalocyanines .....	151
1.9.7. Synthesis of subphthalocyanine-corrole axial- dyads.....	174
1.9.8. Synthesis of subphthalocyanine-ferrocene dyads .....	176
1.9.9. Synthesis of tetracyanobutadiene-corrole .....	182

## Chapter 2 - Subphthalocyanines and Naphthalocyanines as sensing materials for mass gravimetry devices

2.1. Sensors: classification and properties.....	189
--	-----

2.1.1. Chemical sensors for the detection of gas analytes .....	194
2.1.2. Multisensory analysis based on mass transducers.....	194
2.1.3. Porphyrinoids as sensing layers in mass transducers based on QMBs. ....	197
2.2. Specific objectives of Chapter 2.....	201
2.3. Results and discussion .....	203
2.3.1. Fabrication of devices .....	203
2.3.2. Device structure and experimental procedure .....	204
2.3.3. Software, interface and data acquisition .....	205
2.3.4. Analysis of the results.....	205
2.4. Summary and conclusions .....	211
2.5. Experimental section .....	213
2.5.1. Materials and instruments .....	213
2.5.2. Gas sensor array .....	213
2.5.3. Statistical analysis.....	214

# Introduction

## Subphthalocyanines as Molecular Materials

Molecular materials refer to those systems constituted by organic or metalorganic molecular subunits that can be individually synthesized and subsequently organized *via* different approaches, presenting unusual optical, electronic or magnetic properties. Subphthalocyanines (SubPcs)<sup>1</sup> are non-planar aromatic macrocycles composed by three 1,3-diiminoisoindole units N-fused around a central boron atom (Figure 1). The particular bowl-shaped geometry of SubPcs comes mainly from the tetrahedral coordination imposed by the boron, which presents a characteristic axial position, and from the intrinsic contraction of the ligand that, in comparison with phthalocyanines (Pcs), would not be able to adopt a planar disposition. They present a 14  $\pi$ -electrons system largely around its inner cavity, being one of the few known examples of heteroatomic non-planar aromatic compounds.

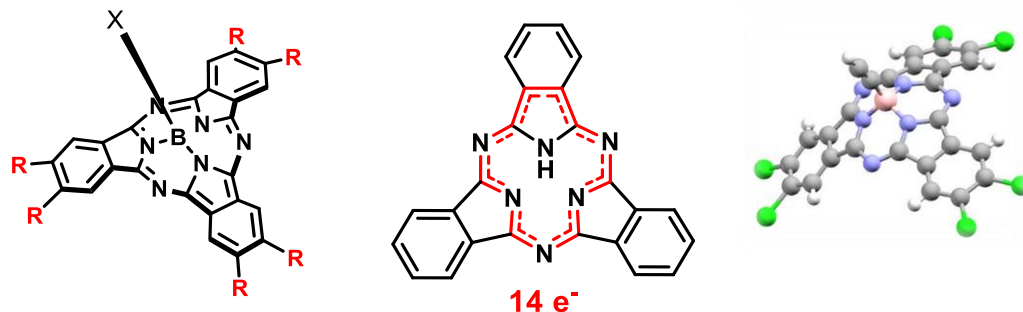
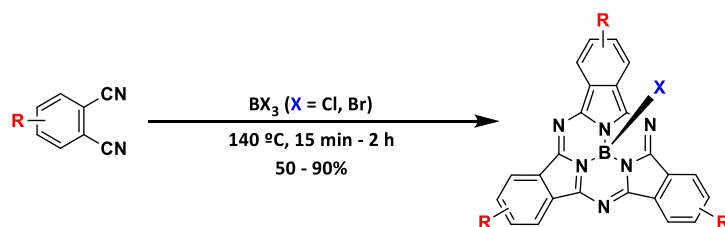


**Figure 1.** Classical representation of *meta*-substituted SubPc, the axial position being occupied by a halogen atom (left), electronic delocalization in the aromatic core (center), and ball-and-stick structure of SubPc (right).

<sup>1</sup> a) del Rey, B.; Keller, U.; Torres, T.; Rojo, G.; Agulló-López, F.; Nonell, S.; Martí, C.; Brasselet, S.; Ledoux, I.; Zyss, J. J. *Am. Chem. Soc.* **1998**, *120*, 12808. b) Claessens, C. G.; González-Rodríguez, D.; Torres, T. *Chem. Rev.* **2002**, *102*, 835. c) Torres, T. *Angew. Chem. Int. Ed.* **2006**, *45*, 2834. d) Medina, A.; Claessens, C. G. *J. Porphyrins Phthalocyanines* **2009**, *13*, 446. e) Claessens, C. G.; González-Rodríguez, D.; Rodríguez-Morgade, M. S.; Medina, A.; Torres, T. *Chem. Rev.* **2014**, *114*, 2192.

## Synthesis of Subphthalocyanines

The general methodology for the synthesis of SubPcs has been refined and optimized from the first time it was obtained in 1972 by Meller and Osko.<sup>2</sup> Attempting to synthesize a boron Pc using halo- and organoboranes as templates, they observed the formation of unexpected purple compounds, which were lastly identified as triisoidolohexaazaboraphthalenes. Currently, it implies the sequential reaction of a phthalonitrile derivative in the presence of a boron trihalide  $BX_3$  (generally  $X = Cl, Br$ ) in high boiling point aromatic solvents (such as *p*-xylene, *o*-xylene, chloronaphthalene, *o*-dichlorobenzene, or 1,2,4-trichlorobenzene) and at high temperatures (140 – 200 °C) (Scheme 1).<sup>3</sup> The presence of commercially available 1.0 M solutions of  $BCl_3$  and  $BBr_3$  in *p*-xylene, dichloromethane (DCM) and heptane allows its immediate use with a perfect control in the stoichiometry of the reaction. Additionally, other boron-based Lewis acids have been used in some situations, like  $BF_3$ ,<sup>4</sup>  $BPh_3$ ,<sup>5</sup>  $PhBF_2$ ,<sup>2</sup>  $PhBCl_2$ ,<sup>2,4</sup> or  $BuBBr_2$ ,<sup>4</sup> among others. The reactivity of the different borane derivatives with phthalonitriles follows, as observed experimentally, a tendency of  $B(Alkyl)_3 < BPh_3 < BF_3 < BCl_3 < BBr_3$ , which is in perfect agreement with their increasing Lewis Acidity.<sup>6</sup>



**Scheme 1.** General synthetic methodology for the preparation of SubPcs.

A mechanistic study of chloro-SubPc formation starting from phthalonitrile and  $BCl_3$  in aromatic solvents (*e.g.* *p*-xylene) suggests that rearrangement of the initial phthalonitrile- $BCl_3$  adduct produces (1*Z*)-3-chloro-*N*-(dichloroboryl)-1*H*-isoidol-1-imine **I**, following

<sup>2</sup> Meller, A.; Osko, A. *Monatsh. Chem.* **1972**, *103*, 150.

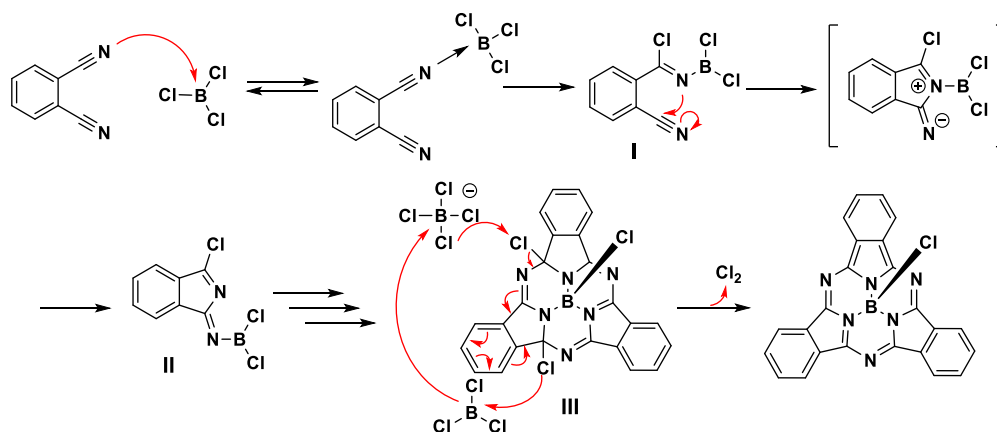
<sup>3</sup> Claessens, C. G.; González-Rodríguez, D.; del Rey, B.; Torres, T.; Mark, G.; Schuchmann, H. -P.; von Sonntag, C.; MacDonald, G.; Nohr, R. S. *Eur. J. Org. Chem.* **2003**, 2547.

<sup>4</sup> Potz, R.; Göldner, M.; Hückstädt, H.; Cornelissen, U.; Tutaß, A.; Homborg, H. *Z. Anorg. Allg. Chem.* **2000**, 626, 588.

<sup>5</sup> Geyer, M.; Plenzig, F.; Rauschnabel, J.; Hanack, M.; del Rey, B.; Sastre, A.; Torres, T. *Synthesis* **1996**, 1139.

<sup>6</sup> *Comprehensive Inorganic Chemistry*; Bailar, J. C., Emeleus, H. J., Nyholm, R., Trotman-Dickenson, A. F., Eds.; Pergamon: New York, **1973**; Vol. 1

consecutive addition of another phthalonitrile- $\text{BCl}_3$  adduct. From three molecules of **I**, the dichlorosubstituted macrocycle **III** is formed. The formation of the SubPc concludes by the elimination of chlorine, probably catalyzed by  $\text{BCl}_3$  in a concerted process (Scheme 2).<sup>7</sup> Although the presence of reactive  $\text{Cl}_2$  could lead into the formation of peripheral chlorinated sub-products, the use of an alkylaromatic solvent prevents its interaction with the macrocycle by several deactivation pathways.



**Scheme 2.** Key steps in the formation mechanism of SubPcs.

<sup>7</sup> a) Claessens, C. G.; González-Rodríguez, D.; McCallum, C. M.; Nohr, R. S.; Schuchmann, H. -P.; Torres, T. *J. Porphyrins Phthalocyanines* **2000**, 11, 18. b) Nohr, R. S.; McCallum, C. M.; Schuchmann, H. -P. *J. Porphyrins Phthalocyanines* **2010**, 14, 271.

## Structural isomerism and chirality of Subphthalocyanines

When employing low-symmetry phthalonitriles, that is, lacking of a  $C_{2v}$  point, SubPcs are obtained as a mixture of regioisomers with  $C_3$  and  $C_1$  symmetries (Figure 2). Nevertheless, due to their low aggregation tendency, they can be readily separated by HPLC<sup>8</sup> or column chromatography,<sup>9</sup> which results convenient in order to take advantage of their structural-related properties. The use of *meta*-monosubstituted phthalonitriles provides a  $C_3/C_1$  mixture following a statistical distribution ratio of 1:2, whereas the *ortho*-SubPcs are greatly influenced by electronic and steric factors, giving rise to more complex and random distributions.<sup>8b,9a,10</sup>

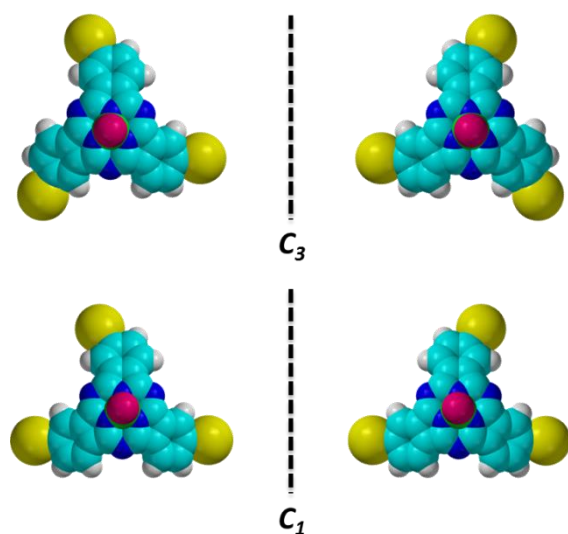


**Figure 2.** Representation of *meta*-SubPc regioisomers  $C_3/C_1$ .

The lack of inversion center of SubPcs grants them of an intrinsic chirality, properly reflected when employing unsymmetrical phthalonitriles. The racemic mixture of each of the regioisomers  $C_3/C_1$  can be separated by using an HPLC equipped with a chiral column.<sup>9b,11</sup>

<sup>8</sup> a) Hanack, M.; Geyer, M. *J. Chem. Soc., Chem. Commun.* **1994**, 2253. b) Kobayashi, N.; Nonomura, T. *Tetrahedron Lett.* **2002**, 43, 4253.

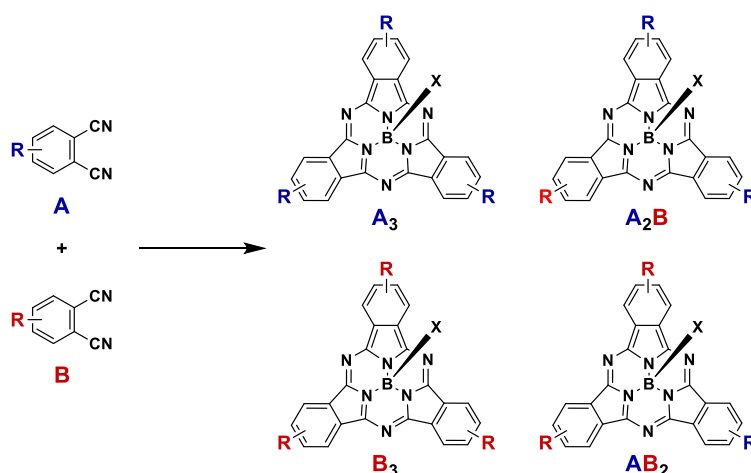
<sup>9</sup> a) Claessens, C. G.; Torres, T. *Eur. J. Org. Chem.* **2000**, 1603. b) Claessens, C. G.; Torres, T. *Tetrahedron Lett.* **2000**, 41, 6361.

<sup>10</sup> Iida, N.; Tokunaga, E.; Saito, N.; Shibata, N. *J. Fluorine Chem.* **2015**, 171, 120.

<sup>11</sup> Guilleme, J.; Mayoral, M. J.; Calbo, J.; Aragón, J.; Viruela, P. M.; Ortí, E.; Torres, T.; González-Rodríguez, D. *Angew. Chem. Int. Ed.* **2015**, 54, 2543.

## Synthesis of low-symmetry Subphthalocyanines

The synthesis of low-symmetry SubPcs is of great importance. Adding two different phthalonitriles will return a statistical distribution of  $A_3$ ,  $A_2B$ ,  $AB_2$  and  $B_3$ , that can generally be isolated by column chromatography (Scheme 3).<sup>12</sup> The mixing of isoindole units with different substitution patterns combines the physical and chemical properties of each related symmetric SubPc, obtaining a midway behaviour of those features that ultimately could lead into a fine-tuning of its electronic properties,<sup>13</sup> the establishment of additional interactions between them (e.g. push-pull systems),<sup>14</sup> or the addition of anchoring points on its periphery while preserving SubPcs electronic distribution of choice,<sup>15</sup> among others.



**Scheme 3.** Statistical distribution obtained during the synthesis of low-symmetry SubPcs.

<sup>12</sup> a) Ali, H.; Sim, S. K.; van Lier, J. E. *J. Chem. Res.* **1999**, 496. b) Stork, J. R.; Potucek, R. J.; Durfee, W. S.; Noll, B. C. *Tetrahedron Lett.* **1999**, *40*, 8055. c) Claessens, C. G.; Torres, T. *Chem. Eur. J.* **2000**, *6*, 2168. d) Zyskowski, C. D.; Kennedy, V. O. *J. Porphyrins Phthalocyanines* **2000**, *4*, 707. e) Iglesias, R. S.; Claessens, C. G.; Herranz, M. A.; Torres, T. *Org. Lett.* **2007**, *9*, 5381. f) Gonzalez-Rodríguez, D.; Claessens, C. G.; Torres, T. *J. Porphyrins Phthalocyanines* **2009**, *13*, 203.

<sup>13</sup> a) Katherine McAuliffe; Megan Kaster; Regina Szlag; Evan Trivedi. *Int. J. Mol. Sci.* **2017**, *18*, 1177. b) Zango, G.; Sakurai, T.; Urones, B.; Saeki, H.; Matsuda, W.; Martínez-Díaz, M. V.; Seki, S.; Torres, T. *Chem. Eur. J.* **2018**, *24*, 8331.

<sup>14</sup> Zango, G.; Zirzmeier, J.; Claessens, C. G.; Clark, T.; Martínez-Díaz, M. V.; Guldi, D. M.; Torres, T. *Chem. Sci.* **2015**, *6*, 5571.

<sup>15</sup> Zango, G.; Krug, M.; Krishna, S.; Mariñas, V.; Clark, T.; Martínez-Díaz, M. V.; Guldi, D. M.; Torres, T. *Chem. Sci.* **2020**, *11*, 3448.

## Reactivity of Subphthalocyanines

The reactivity of SubPcs may be classified in three main groups: (1) axial reactivity, (2) peripheral reactivity and (3) ring-expansion reactions (Figure 2). The three of them differ in the reactive center: (1) the B-X bond, (2) the functional groups located at the benzene isoindole ring and (3) the imine-type N core. Both axial and peripheral reactions produce modified SubPcs, whereas ring expansion results in the opening of the SubPc constrained ring and the incorporation of an additional isoindole unit, leading into the formation of low-symmetry  $A_3B$  Pcs.

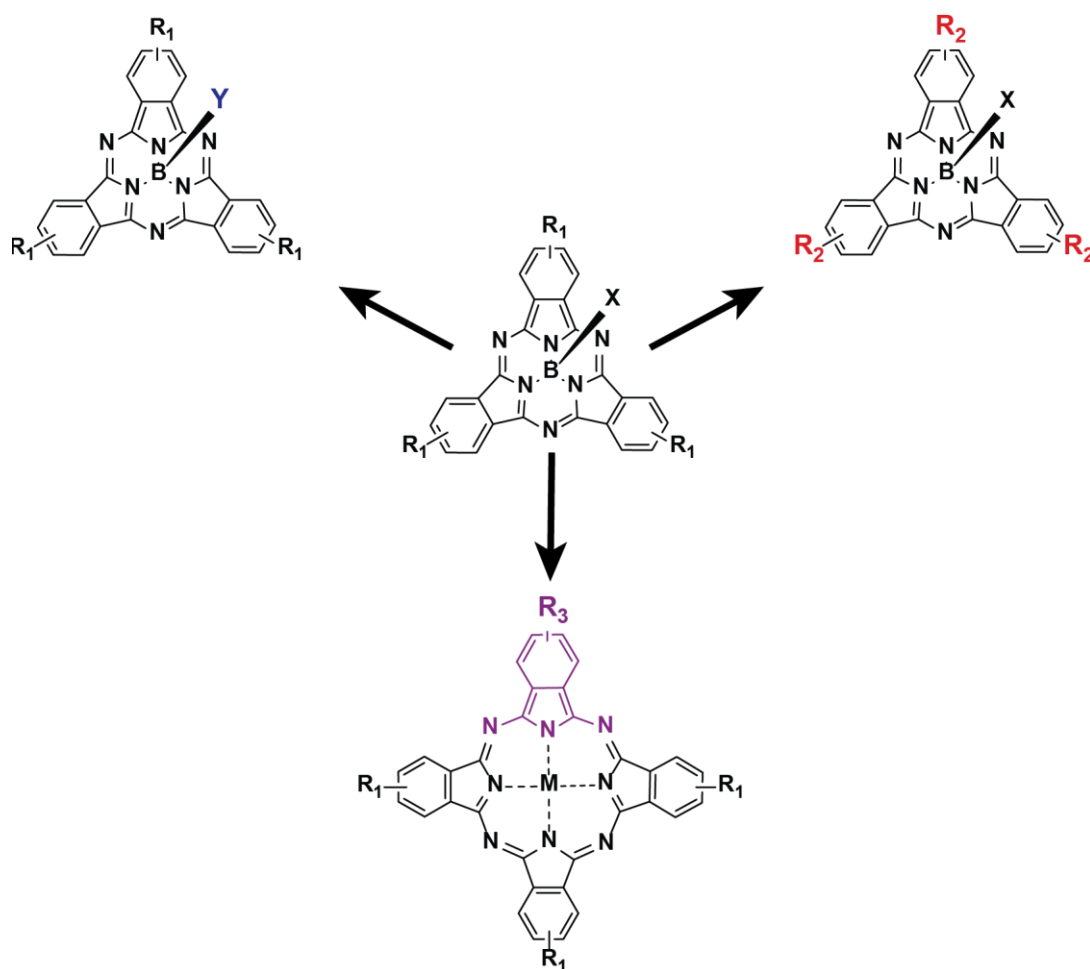


Figure 2. The three main different modes of SubPc reactivity.

Another mode of reactivity that cannot be classified within any of the groups mentioned above was reported by Rodríguez-Morgade, Torres, Sessler and co-workers.<sup>16</sup> It consists in the formation of ruthenoarene  $\pi$ -complexes of SubPcs by reaction of the aromatic rings in the macrocycle with  $[\text{Cp}^*\text{Ru}(\text{MeCN})_3]\text{PF}_6$  ( $\text{Cp}^*$  = Pentamethylcyclopenta-dienyl). The coordination of the  $\text{Cp}^*\text{Ru}$  complex with phenoxy-substituted SubPcs resulted in three different products where the metal binds either to the phenoxy ligand or the SubPc benzene isoindole ring, either from its concave or its convex side. The reaction displayed high selectivities for electron-rich aromatic rings and, to a lesser extent, for metal  $\pi$  coordination to the SubPc convex side rather than to the concave side.

### **Axial reactivity**

Substitution at the boron atom of SubPcs is a frequent methodology for its functionalization. Upon axial substitution, the electronic characteristics of the  $\pi$ -macrocycle are mostly preserved, since they are closely related only to the nature of the substituents of the benzene rings. For so, this methodology is mainly used in terms of improving its solubility or increasing the complexity of the system (*i.e.* for the developing of donor/acceptor or molecular recognition arrays).

Among the different functional groups that can be introduced into the boron, phenols have been by far the most studied and employed for several reasons: (I) commercially available reagents (II); simple and high-yielding protocols (III); enhancement of the solubility and stability of the corresponding -Cl or -Br derivatives.<sup>16</sup> The reaction is generally performed by heating a mixture of the SubPc and a high excess of the corresponding phenol in aromatic solvents (such as toluene or chlorobenzene). Sometimes, the addition of a protic base, generally a tertiary amine, is needed in order to neutralize the hydrogen halide released during the process.

A comprehensive understanding of the mechanism of the axial ligand exchange reaction between chloro-SubPcs and phenols has been provided by Guilleme *et al.*<sup>17</sup> A combination of experimental and theoretical results support an unusual bimolecular  $\sigma$ -bond metathesis mechanism in which the phenolic proton assists in weakening the boron-halogen bond concomitantly with substitution at the boron center. This mechanism would

---

<sup>16</sup> Caballero, E.; Fernández-Ariza, J.; Lynch, V. M.; Romero-Nieto, C.; Rodríguez-Morgade, M. S.; Sessler, J. L.; Guldí, D. M.; Torres, T. *Angew. Chem. Int. Ed.* **2012**, *51*, 11337.

<sup>17</sup> Guilleme, J.; Martínez-Fernández, L.; González-Rodríguez, D.; Corral, I.; Yáñez, M.; Torres, T. *J. Am. Chem. Soc.* **2014**, *136*, 14289.

also explain that (I) bromo-SubPcs react faster than chloro- and fluoro-SubPcs, since the boron-halogen bond is longer and weaker in that series; (II) SubPcs substituted with electron-donating groups at the periphery react faster as a result of the stabilization of the positive charge developed at the boron atom in the transition state; and (III) more acidic phenols accelerate the reaction, since they are able to bind more efficiently to the leaving halogen atom *via* proton coordination.

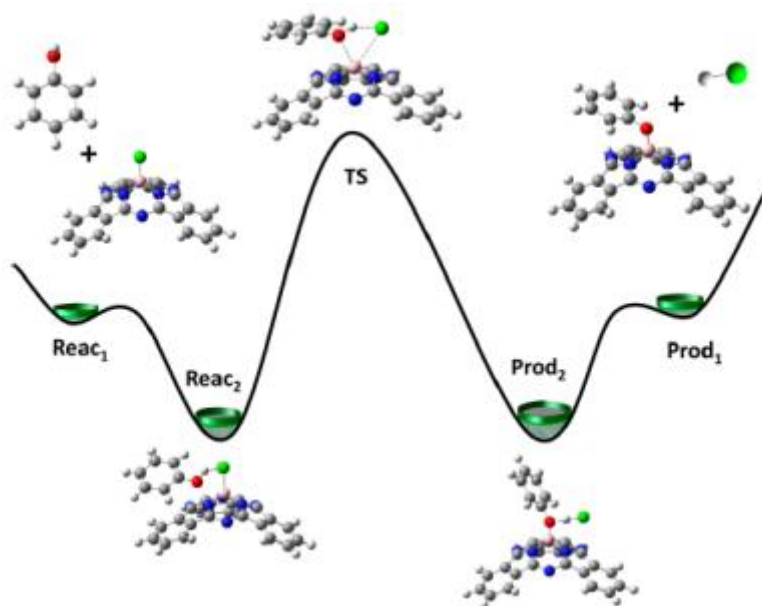


**Figure 3.** Reaction profile postulated from DFT calculations for the substitution between phenol and Cl-SubPc. Ref. 17.

Different strategies have been developed for the obtention of a variety of B-O SubPc bonds. Chloro- and bromo-SubPcs have been reported to react as well with carboxylic acids<sup>18</sup> and benzyl<sup>19</sup> or alkyl<sup>18a,20</sup> alcohols. Hydroxy-SubPcs have been obtained by refluxing

<sup>18</sup> a) Solntsev, P. V.; Spurgin, K. L.; Sabin, J. R.; Heikal, A. A.; Nemykin, V. N. *Inorg. Chem.* **2012**, *51*, 6537. b) Lessard, B. H.; Bender, T. P. *Macrom. Rapid Commun.* **2013**, *34*, 568.

<sup>19</sup> a) Romero-Nieto, C.; Medina, A.; Molina-Ontoria, A.; Claessens, C. G.; Echegoyen, L.; Martín, N.; Torres, T.; Guldi, D. M. *Chem. Commun.* **2012**, *48*, 4953. b) Ren, Y.; Hiszpanski, A. M.; Loo, Y. -L. *Chem. Mater.* **2015**, *27*, 4008. c) Konarev, D. V.; Troyanov, S. I.; Lyubovskaya, R. N. *CrystEngComm* **2015**, *17*, 3923.

<sup>20</sup> a) Xu, H.; Ng, D. K. P. *Chem. Asian J.* **2009**, *4*, 104. b) Xu, H.; Ermilov, E. A.; Röder, B.; Ng, D. K. P. *Phys. Chem. Chem. Phys.* **2010**, *12*, 7366. c) Biyiklioglu, Z.; Alp, H. *Dalton Trans.* **2016**, *45*, 3838. d) Gotfredsen, H.; Jevric, M.; Kadziola, A.; Nielsen, M. B. *Eur. J. Org. Chem.* **2016**, 17.

a suspension of the starting SubPc in water,<sup>21</sup> pyridine/water<sup>22</sup> mixtures, and acetonitrile/water<sup>23</sup> mixtures. Lastly, symmetrical<sup>24</sup> or unsymmetrical<sup>25</sup>  $\mu$ -oxo-bridged SubPc dimers have been synthesized by dehydration of hydroxyl-SubPc or by reaction of hydroxyl-SubPc with halo-SubPc, respectively.

In the last years, other general methodologies for the axial functionalization of SubPcs with different nucleophiles have appeared. For example, axial ligands can efficiently be exchanged in the presence of a Lewis acid. In 2008, Rodríguez-Morgade *et al.* reported the treatment of SubPcs bearing an axial chloride, bromide or phenoxy groups with an excess of Et<sub>2</sub>O·BF<sub>3</sub>, obtaining the corresponding fluoro-SubPcs in yields up to 80%.<sup>26</sup> Recently, the same was achieved by Yamamoto *et al.* by using AgBF<sub>4</sub>.<sup>27</sup> In the same way, chloro-SubPcs can be transformed to bromo-SubPcs by treatment with an excess of BBr<sub>3</sub>, whereas chloro- can be produced from hydroxy-, phenoxy-, or bromo-SubPcs in the presence of BCl<sub>3</sub>,<sup>28</sup> AlCl<sub>3</sub>,<sup>29</sup> or RSO<sub>2</sub>Cl.<sup>30</sup>

In the same year, the first efficient synthesis of ethynyl-boron SubPcs via replacement of the chloride ligand at the boron atom in the presence of Grignard reagents was reported by Ziesel *et al.*<sup>31</sup> A similar protocol was later employed by Yamasaki *et al.* to prepare a series of SubPcs having direct B-C bonds.<sup>32</sup> The procedure basically relied on the reaction between bromo-SubPcs and primary alkyl, secondary alkyl, or aryl Grignard reagents.

<sup>21</sup> Martínez-Díaz, M. V.; del Rey, B.; Torres, T.; Agricole, B.; Mingotaud, C.; Cuvillier, N.; Rojo, G.; Agulló-López, F. *J. Mat. Chem.* **1999**, *9*, 1521.

<sup>22</sup> Kudrevich, S. V.; Gilbert, S.; van Lier, J. E. *J. Org. Chem.* **1996**, *61*, 5706.

<sup>23</sup> del Rey, B.; Martínez-Díaz, M. V.; Barberá, J.; Torres, T. *J. Porphyrins Phthalocyanines* **2000**, *4*, 569.

<sup>24</sup> a) Kobayashi, N.; Ishizaki, T.; Ishii, K.; Konami, H. *J. Am. Chem. Soc.* **1999**, *121*, 9096. b) Yamasaki, Y.; Mori, T. *Bull. Chem. Soc. Jpn.* **2011**, *84*, 1208.

<sup>25</sup> Dang, J. D.; Fulford, M. V.; Kamino, B. A.; Paton, A. S.; Bender, T. P. *Dalton Trans.* **2015**, *44*, 4280.

<sup>26</sup> Rodríguez-Morgade, M. S.; Claessens, C. G.; Medina, A.; González-Rodríguez, D.; Gutiérrez-Puebla, E.; Monge, A.; Alkorta, I.; Elguero, J.; Torres, T. *Chem. Eur. J.* **2008**, *14*, 1342.

<sup>27</sup> Yamamoto, K.; A. Takagi, M. Hada, R. Taniwaki, T. Mizutani, Y. Kimura, Y. Takao, K. Moriwaki, F. Matsumoto, T. Ito, T. Iwai, K. Hida, T. Mizuno, T. Ohno, *Tetrahedron* **2016**, *72*, 4918.

<sup>28</sup> D. González-Rodríguez, Ph.D. Thesis, Universidad Autónoma de Madrid, Madrid, Spain, 2003.

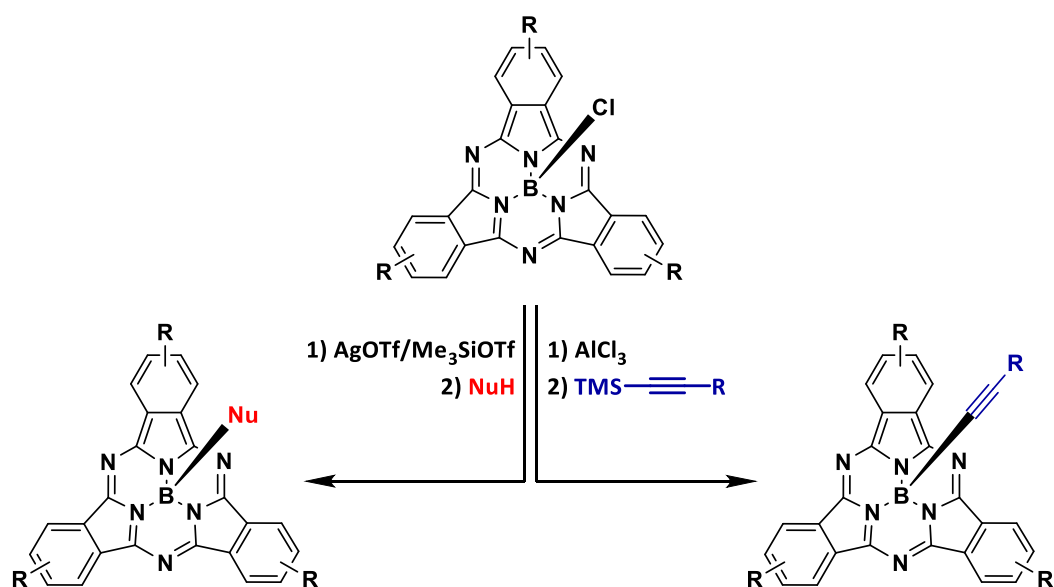
<sup>29</sup> G. E. Morse, T. P. Bender, *Inorg. Chem.* **2012**, *51*, 6460.

<sup>30</sup> Paton, A. S.; Morse, G. E.; Castelino, D.; Bender, T. P. *J. Org. Chem.* **2012**, *77*, 2531

<sup>31</sup> Camerel, F.; Ulrich, G.; Retailleau, P.; Ziesel, R. *Angew. Chem. Int. Ed.* **2008**, *47*, 8876.

<sup>32</sup> Yamasaki, Y.; Mori, T. *Chem. Lett.* **2010**, *39*, 1108.

In 2011 Guilleme *et al.* marked a watershed in the axial functionalization of SubPcs when publishing a one-pot, two-step mild synthetic methodology to efficiently exchange the chlorine atom in SubPc products by a wide range of nucleophiles (Scheme 4, left).<sup>33</sup> The first step consists in the irreversible generation of an activated triflate-SubPc intermediate by reaction with AgOTf or Me<sub>3</sub>SiOTf reagents. In the second step, the nucleophile is added and the reaction is completed within a few hours at mild temperatures. This approach not only allowed, for the first time, the incorporation of nitrogen and sulfur nucleophiles to the SubPc axial position, but also paved the way for the preparation of elaborated systems. In 2012, Bender *et al.* communicated another strategy for the activation of the axial position of SubPcs, by treatment of chloro- or bromo-SubPcs with aluminum chloride (AlCl<sub>3</sub>) prior to the addition of the nucleophile, although the scope of the reaction was limited to aromatic derivatives.<sup>29</sup>



**Scheme 4.** Mild synthetic pathways for the preparation of axially-substituted SubPcs *via* activation with ROTf (left) or AlCl<sub>3</sub> (right).

In 2016, contemporary, two different mild and versatile synthetic routes that employ TMS-protected nucleophiles as starting materials to carry out the axial ligand

<sup>33</sup> Guilleme, J.; González-Rodríguez, D.; Torres, T. *Angew. Chem. Int. Ed.* **2011**, *50*, 3506.

exchange reaction over SubPcs in one step were described.<sup>34</sup> Particularly, Nielsen *et al.* developed a methodology employing chloro-SubPcs and TMS-protected alkyne derivatives in the presence of AlCl<sub>3</sub> (Scheme 4, right).<sup>34b</sup> The direct B-C bond between the boron and the alkyne allowed for the preparation of a wide number of derivatives, even ferrocene (Fc), in mild conditions and relative high yields.

### Peripheral reactivity

Peripheral reactivity involves any reaction that produces a chemical modification of the substituents placed at the isoindole benzene rings. Functionalization of the SubPc periphery comes *via* appropriate substitution of the starting phthalonitrile or substituents transformation once the SubPc is formed. Only certain functional groups can hold SubPc cyclotrimerization conditions, so a correct synthetic route must be chosen in order to avoid undesired side reactions. Halogens, thioethers, alkyl, sulphonyl and nitro groups have proved to resist those conditions.<sup>1e</sup> On the other hand, phthalonitriles bearing amines, alkyl ethers, sulfoxides, carbonyl derivatives or unsaturated bonds, react, in several cases, with the boron halides employed during the SubPc formation, thereby restricting their use.<sup>1e</sup>

SubPcs are chemically less robust than Pcs, so special attention must be paid once a synthetic procedure is selected. As a matter of fact, SubPcs often decomposes against strong nucleophiles or protic acids, presumably *via* ring opening on their iminic positions. Pd-catalyzed cross-coupling reactions are the most extended post-functionalization strategies, being one of the main approaches for the developing of donor/acceptor systems.<sup>35</sup> Among them, iodo-substituted SubPcs have been largely used as precursors in

---

<sup>34</sup> a) Guilleme, J.; Martínez-Fernández, L.; Corral, I.; Yáñez, M.; González-Rodríguez, D.; Torres, T. *Org. Lett.* **2015**, *17*, 4722. b) Gotfredsen, H.; Jevric, M.; Broman, S. L.; Petersen, A. U.; Nielsen, M. B. *J. Org. Chem.* **2016**, *81*, 1.

<sup>35</sup> Martínez-Díaz, M.; Quintiliani, M.; Torres, T. *Synlett* **2008**, *2008*, 1.

Pd-catalyzed Sonogashira,<sup>12e,15,31,36</sup> Suzuki,<sup>37</sup> Stille<sup>37b,38</sup> and Heck<sup>39</sup> C-C bond formation reactions, as well as for Butchwald-Hatwig<sup>37b,40</sup> amination reactions, or borylation reactions.<sup>37b</sup>

Aside from metal-catalyzed cross-coupling reactions, other protocols have been successfully employed to modify SubPc peripheral positions. With the aim of increasing the water solubility of SubPcs, axial and peripheral pyridine or tertiary amine groups have been transformed into their respective quaternized salts *via* alkylation reactions.<sup>36c,39,41</sup> Dicyclohexylcarbodiimide (DCC)-mediated acylation reactions have been employed to introduce new ester functions in hydroxy-substituted SubPcs.<sup>37c,d</sup> Different deprotection conditions have also been tested for silylether groups to yield the corresponding hydroxy-substituted SubPc.<sup>37b</sup> The oxidation of sulfides to sulfoxides or sulfones employing *m*-chloroperbenzoic acid (*m*-CPBA) has been carried out.<sup>42</sup> The reduction of triple bonds attached on the SubPc core with molecular hydrogen has also been shown to proceed with moderate yields.<sup>36c</sup> Finally, the coupling of C<sub>60</sub> fullerene to SubPc-macrocycles, by the well-known cyclopropanation or Bingel reaction<sup>37d</sup> has been successfully utilized.

---

<sup>36</sup> a) del Rey, B.; Torres, T. *Tetrahedron Letters* **1997**, *38*, 5351. b) Claessens, C. G.; Torres, T. *Chem. Commun.* **2004**, *11*, 1298. c) Lapok, L.; Claessens, C. G.; Wohrle, D.; Torres, T. *Tetrahedron Lett.* **2009**, *50*, 2041. d) Sánchez-Molina, I.; Grimm, B.; Krick Calderon, R. M.; Claessens, C. G.; Guldi, D. M.; Torres, T. *J. Am. Chem. Soc.* **2013**, *135*, 10503. e) Urbani, M.; Sari, F. A.; Grätzel, M.; Nazeeruddin, M. K.; Torres, T.; Ince, M. *Chem. Asian J.* **2016**, *11*, 1223. f) Gotfredsen, H.; Holmstrøm, T.; Muñoz, A. V.; Storm, F. E.; Tortzen, C. G.; Kadziola, A.; Mikkelsen, K. V.; Hammerich, O.; Nielsen, M. B. *Org. Lett.* **2018**, *20*, 5821. g) Winterfeld, K. A.; Lavarda, G.; Guilleme, J.; Guldi, D. M.; Torres, T.; Bottari, G. *Chem. Sci.* **2019**, *10*, 10997.

<sup>37</sup> a) González-Rodríguez, D.; Carbonell, E.; Guldi, D. M.; Torres, T. *Angew. Chem. Int. Ed.* **2009**, *48*, 8032. b) Gonzalez-Rodríguez, D.; Torres, T. *Eur. J. Org. Chem.* **2009**, 1871. c) Gonzalez-Rodríguez, D.; Martínez-Díaz, M. V.; Abel, J.; Perl, A.; Huskens, J.; Echegoyen, L.; Torres, T. *Org. Lett.* **2010**, *12*, 2970. d) González-Rodríguez, D.; Carbonell, E.; de Miguel Rojas, G.; Atienza Castellanos, C.; Guldi, D. M.; Torres, T. *J. Am. Chem. Soc.* **2010**, *132*, 16488.

<sup>38</sup> Claessens, C. G.; Torres, T. *J. Am. Chem. Soc.* **2002**, *124*, 14522.

<sup>39</sup> Sánchez-Molina, I.; Soriano, A.; Claessens, C. G.; Torres, T.; Bolink, H. J. *J. Porphyrins Phthalocyanines* **2013**, *17*, 1016

<sup>40</sup> González-Rodríguez, D.; Torres, T.; Guldi, D. M.; Rivera, J.; Herranz, M. A.; Echegoyen, L. *J. Am. Chem. Soc.* **2004**, *126*, 6301.

<sup>41</sup> Spesia, M. B.; Durantini, E. N. *Dyes Pigm.* **2008**, *77*, 229.

<sup>42</sup> González-Rodríguez, D.; Torres, T. *Tetrahedron Lett.* **2009**, *50*, 860.

### Ring-expansion reactions

In 1990, nearly twenty years after their discovery, Kobayashi *et al.* renewed the interest for SubPcs by devising a method for the synthesis of unsymmetrically A<sub>3</sub>B Pcs through ring opening reaction of SubPc macrocycle (A<sub>3</sub>) in the presence of 1,3-diiminoisoindoline derivatives (B) and subsequent ring closure to a more stable Pc macrocycle.<sup>43</sup> This method was claimed to afford reasonable yields and good A<sub>3</sub>B selectivity, with a simple purification process.

After intense research by several groups it was clear that the efficiency and thus the convenience of this promising procedure depends dramatically on a number of factors, such as the nature of the peripheral substituents of the SubPc and the diiminoisoindoline precursor, the solvent, and the reaction temperature.<sup>22,24a,44</sup> During the last 20 years, further research has been devoted to the study and optimization of this procedure in diverse conditions.<sup>45</sup> Best yields obtained for the target A<sub>3</sub>B-type Pcs, in the order of 40-60%, were reported by Chauhan *et al.*<sup>45d</sup>, requiring the use of ionic solvents. Remarkably, in 2015, Jiang *et al.* obtained the first chiral A<sub>3</sub>B-type Pc by using a binaphthyl-linked phthalonitrile.<sup>46</sup>

### Other reactions of Subphthalocyanines

Recently, an addition of cyanide anions to the iminic double bonds of a SubPc, without ring opening, has been reported. The formation of these SubPc dianions comes along with an electron transfer to the solvent to produce SubPc-radical anions that ultimately result in the irreversible formation of a SubPc-dimer through their remaining carbon atom.<sup>47</sup>

<sup>43</sup> Kobayashi, N.; Kondo, R.; Nakajima, S. -I.; Osa, T. *J. Am. Chem. Soc.* **1990**, *112*, 9640.

<sup>44</sup> a) Weitemyer, A.; Kliesch, H.; Wöhrle, D. *J. Org. Chem.* **1995**, *60*, 4900. b) Sastre, A.; Torres, T.; Hanack, M. *Tetrahedron Lett.* **1995**, *36*, 8501. c) Sastre, A.; del Rey, B.; Torres, T. *J. Org. Chem.* **1996**, *61*, 8591. d) Kudrevich, S.; Brasseur, N.; La Madeleine, C.; Gilbert, S.; van Lier, J. E. *J. Med. Chem.* **1997**, *40*, 3897.

<sup>45</sup> a) Matlaba, P.; Nyokong, T. *Polyhedron* **2002**, *21*, 2463. b) Sharman, W. M.; van Lier, J. E. *J. Porphyrins Phthalocyanines* **2005**, *9*, 651. c) Padmaja, K.; Youngblood, J. W.; Wei, L.; Bocian, D. F.; Lindsey, J. S. *Inorg. Chem.* **2006**, *45*, 5479. d) Chauhan, S. M. S.; Kumari, P. *Tetrahedron* **2009**, *65*, 2518. e) Tempesti, T. C.; Álvarez, M. G.; Durantini, E. N. *Dyes Pigm.* **2011**, *91*, 6.

<sup>46</sup> Zhao, L.; Wang, K.; Shang, H.; Jiang, J. *Dyes and Pigments*, **2015**, *120*, 56.

<sup>47</sup> Konarev, D. V.; Kuzmin, A. V.; Shestakov, A. F.; Rompanen, I. A.; Lyubovskaya, R. N. *Dalton Trans.* **2020**, *49*, 16801.

## Properties of Subphthalocyanines

Like other porphyrinoids, SubPcs follow Gouterman's four orbital model,<sup>48</sup> presenting two main electronic transitions in the UV/Vis framework. At 260-370 nm, a weaker B band (namely Soret) that originates from the  $S_0 \rightarrow S_2$  transition; at 560-580 nm, a twice-intensity characteristic band (namely Q) that originates from the the  $S_0 \rightarrow S_1$  transition. Those bands appear blueshifted in comparison with Pcs, due to their smaller aromatic ring current ( $14\pi$  vs.  $18\pi$ ). Their absorption coefficients ( $\epsilon^0$ ) also decrease in both Soret and Q bands from Pcs to SubPcs, with values of  $\epsilon = 5-6 \times 10^4 \text{ M}^{-1} \text{ cm}^{-1}$  for the Q bands (vs.  $8-24 \times 10^4 \text{ M}^{-1} \text{ cm}^{-1}$  for Pcs), which may be attributed to their nonplanar structure.<sup>49</sup>

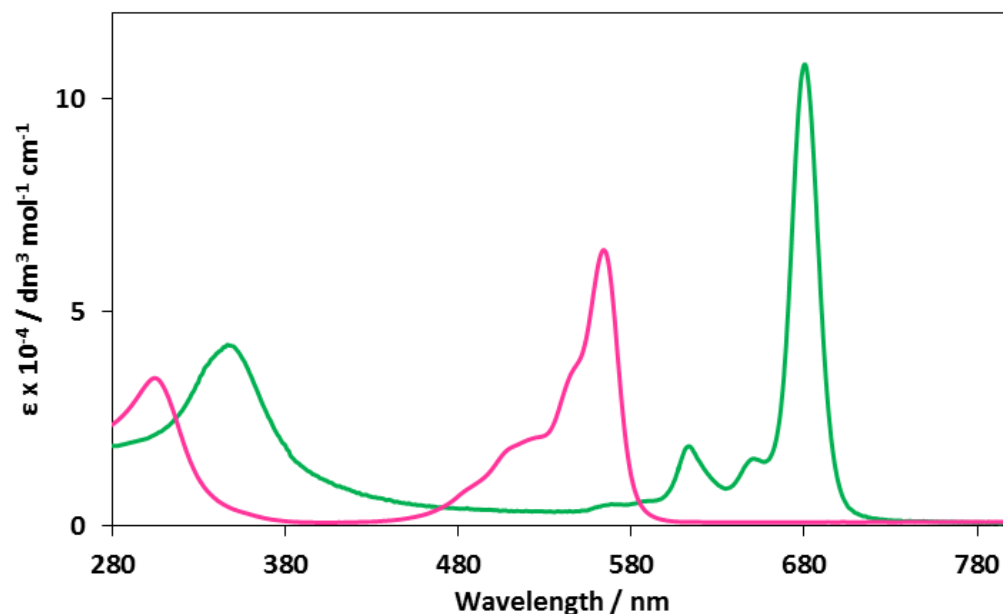


Figure 4. Comparison between typical UV-Vis profiles of SubPc (pink) and MetalloPc (green).

Whereas the electronic distribution of SubPcs remains unaffected while changing the axial substituent, the influence of the peripheral substituents becomes strongly noticeable with strong donor or acceptor moieties, the same with schemes able to expand

<sup>48</sup> a) Gouterman, M. *J. Mol. Spectrosc.* **1961**, *6*, 138. b) Spellane, P. J.; Gouterman, M.; Antipas, A.; Kim, S.; Liu, Y. C. *Inorg.Chem.* **1980**, *19*, 386.

<sup>49</sup> Kobayashi, N.; Ishizaki, T.; Ishii, K.; Konami, H. *J. Am. Chem. Soc.* **1999**, *121*, 9096.

their  $\pi$ -conjugation. In this context,  $\pi$ -donor atoms such as sulfur, nitrogen or oxygen shift the signal towards less energetic wavelengths and sometimes it goes along with a broadening of the Q band. Particularly, the presence of  $\pi$ -donor moieties such as alkoxy-, sulfonyl-, amino- or thioether groups, produces supplementary bands in the 400-500 nm region attributable to  $n \rightarrow \pi^*$  transitions due to  $\pi$ -donation from the heteroatom lone pair to the macrocycle.<sup>1e,37b,50</sup>

SubPcs are fluorescent, with their emission set at 575-670 nm, very small Stokes shifts of 10-15 nm and unusually narrow widths at half maximum of the intensity,<sup>49b</sup> due to their low geometry distortions between excited and ground states. Their emission and excitation spectra present in most cases a mirror image relationship, even though the relaxation comes from the less energetic singlet excited state. From the intersection between the two bands, singlet excited state energies of *ca.* 2.0-2.1 eV are typically derived. These values, substantially higher than those found for Pcs ( $\sim$ 1.7 eV), and similar to those for Por ( $\sim$ 2.0 eV), are consistent with the HOMO-LUMO gaps derived from cyclic voltammetry measurements.

Fluorescence quantum yields ( $\phi_F$ ) are typically around 0.2-0.5, but they can reach up to 0.95 for concrete compounds.<sup>51</sup> These yields are about the same magnitude of those of nonaggregated Pcs ( $\sim$ 0.3-0.6).<sup>52</sup> Low radiative yields (*i.e.*  $<$ 0.1) are explained in base of molecular aggregation,<sup>53</sup> fast intersystem crossing in heavy-atom substituted aromatic compounds<sup>12e</sup> or energy and charge transfer phenomena.<sup>50,54</sup> Singlet excited state lifetimes ( $\tau_s$ ) are around 2-4 ns, similar to those measured for monomeric Pcs.<sup>55</sup>

The triplet emitting transition (namely phosphorescence) is located in the NIR region at 835 nm, with triplet energies of 1.45 eV.<sup>49</sup> This provides singlet-triplet energy gaps in SubPcs of *ca.* 0.65 eV, only slightly larger than those of Pcs (0.5-0.6 eV) and Pors (0.5 eV).

---

<sup>50</sup> a) Gonzalez-Rodríguez, D.; Claessens, C. G.; Torres, T.; Liu, S. -G.; Echegoyen, L.; Vila, N.; Nonell, S. *Chem. Eur. J.* **2005**, *11*, 3881. b) Díaz, D. D.; Bolink, H. J.; Cappelli, L.; Claessens, C. G.; Coronado, E.; Torres, T. *Tetrahedron Lett.* **2007**, *48*, 4657.

<sup>51</sup> Shibata, N.; Das, B.; Tokunaga, E.; Shiro, M.; Kobayashi, N. *Chem. Eur. J.* **2010**, *16*, 7554

<sup>52</sup> a) Darwent, J. R.; Douglas, P.; Harriman, A.; Porter, G.; Richoux, M. C. *Coord. Chem. Rev.* **1982**, *44*, 83.

b) Murov, S. L.; Carmichael, I.; Hug, G. L. *Handbook of Photochemistry*; Marcel Dekker: New York, **1993**; p 1.

<sup>53</sup> Tolbin, A. Y.; Tomilova, L. G. *Mendeleev Commun.* **2008**, *18*, 286.

<sup>54</sup> a) González-Rodríguez, D.; Torres, T.; Olmstead, M. M.; Rivera, J.; Herranz, M. A.; Echegoyen, L.; Atienza Castellanos, C.; Guldí, D. M. *J. Am. Chem. Soc.* **2006**, *128*, 10680. b) Xu, H.; Jiang, X. -J.; Chan, E. Y. M.; Fong, W. -P.; Ng, D. K. P. *Org. Biomol. Chem.* **2007**, *5*, 3987.

<sup>55</sup> Darwent, J. R.; Douglas, P.; Harriman, A.; Porter, G.; Richoux, M. C. *Coord. Chem. Rev.* **1982**, *44*, 83.

Regarding their redox properties, SubPcs present the first oxidative and reductive half-wave potentials as one electron processes. The reduction is frequently reversible in the cyclic voltammetry timescale, whereas oxidation processes appear to lead into less stable charged species. Scanning at more positive or negative potentials typically reveals several redox events, which usually are electrochemically irreversible or quasi-irreversible, due to chemical modifications or to deposition of the redox species on the electrodes. The first reductive potential is generally observed between  $-1.58\text{V}^{40,56}$  and  $-0.82\text{V}^{53}$  whereas the first oxidative potential appears between  $+0.37\text{V}^{40,55}$  and  $+1.15\text{V}^{53}$  vs.  $\text{Fc}/\text{Fc}^+$  internal reference.

Absolute HOMO-LUMO energy levels have been determined *via* different techniques.<sup>57</sup> Particularly, Bender *et al.* developed a mathematical methodology for the prediction of SubPcs HOMO and LUMO energy levels, supported by semiempirical (PM3 or RM1) or DFT (B3LYP) data and experimentally corroborated.<sup>56b</sup> Those levels are not greatly affected by the nature of the axial ligand, but they are dramatically influenced by the nature of the substituents on the isoindole benzene ring. Depending on the substitution, HOMO values of SubPcs range between  $-6.8$  and  $-5.3$  eV, while LUMO values are located between  $-3.3$  and  $4.7$  eV.

## Applications of Subphthalocyanines

As a consequence of their outstanding electronic and photophysical properties, together with a rising understanding of the morphology at the nanometer-scale of the SubPc-based molecular materials, SubPcs are attracting the attention of an increasing number of chemists, physicists and materials scientists, having a deep impact in many high-technology areas, and finding applications and commercial utility as active units.

Due to their delocalized  $\pi$ -electron system, SubPcs have been widely studied in the field of nonlinear optics, focusing in the second-order effects due to their intrinsic asymmetry.<sup>58</sup> The second harmonic generation (SHG) properties of a series of peripherally

---

<sup>56</sup> González-Rodríguez, D.; Torres, T.; Herranz, M. A.; Echegoyen, L.; Carbonell, E.; Guldi, D. M. *Chem. Eur. J.* **2008**, *14*, 7670.

<sup>57</sup> a) Morse, G. E.; Helander, M. G.; Maka, J. F.; Lu, Z. -H.; Bender, T. P. *ACS Appl. Mat. Interfaces* **2010**, *2*, 1934. b) Morse, G. E.; Helander, M. G.; Stanwick, J.; Sauks, J. M.; Paton, A. S.; Lu, Z.-H.; Bender, T. P. *J. Phys. Chem. C* **2011**, *115*, 11709.

<sup>58</sup> a) de la Torre, G.; Vázquez, P.; Agulló-López, F.; Torres, T. *J. Mater. Chem.* **1998**, *8*, 1671. b) de la Torre, G.; Vázquez, P.; Agulló-López, F.; Torres, T. *Chem. Rev.* **2004**, *104*, 3723. c) Díaz-García, M. A. *J. Porphyrins Phthalocyanines* **2009**, *13*, 652.

substituted SubPcs with electron-donor and electron-acceptor groups have been extensively investigated.<sup>1a,59</sup> Third-order harmonic generation (THG) studies have also been performed on SubPcs,<sup>60</sup> reaching cubic susceptibility  $\chi^{(3)}$  values three times higher than those measured for Pcs in the same frequency range.

Organic field-effect transistors (OFETs) are the basic building blocks for many flexible integrated circuits and displays. For this purpose, OFETs consisting in vacuum sublimed SubPc films have been prepared, reaching electronic mobilities *ca.*  $10^{-5}$ - $10^{-4}$   $\text{cm}^2 \text{V}^{-1} \text{s}^{-1}$ .<sup>61</sup> Additionally, SubPcs have been employed as donor<sup>62</sup> or acceptor<sup>63</sup> materials in organic photodetectors (OPDs).

SubPcs have also shown themselves as a promising class of orange emitters with a remarkably narrow emission width and excellent electrical performance, being successfully incorporated in organic light-emitting diodes (OLEDs) by Chen *et al.*<sup>64</sup> The group of Bender has made great advances in this field observing, for the first time, orange-colored electroluminescence emission from fluorinated-SubPc-based single-layer OLEDs.<sup>65</sup> Remarkably, they synthesized a class of axially substituted phthalimido-SubPcs,<sup>64b</sup> which exhibit a high quantum yield for photoluminescence ( $\phi_F$ ), maintain a high molar extinction coefficient ( $\epsilon$ ) and have bipolar electrochemical stability, resulting in OLEDs with

---

<sup>59</sup> a) Sastre, A.; Torres, T.; Díaz-García, M. A.; Agulló-López, F.; Dhenaut, C.; Brasselet, S.; Ledoux, I.; Zyss, J. *J. Am. Chem. Soc.* **1996**, *118*, 2746. b) Torres Cebada, T.; Sastre Santos, A.; Del Rey Alvarez, B. (Universidad Autónoma de Madrid, Spain) Spain ES 2116867, 1998. c) Olbrechts, G.; Clays, K.; Wostyn, K.; Persoons, A. *Synth. Met.* **2000**, *115*, 207. d) Martín, G.; Rojo, G.; Hierro, A.; Agulló-López, F.; Ferro, V. R.; García de la Vega, J. M.; Martínez-Díaz, M. V.; Torres, T.; Ledoux, I.; Zyss, J. *J. Phys. Chem. B* **2002**, *106*, 13139. e) Claessens, C. G.; González-Rodríguez, D.; Torres, T.; Martín, G.; Agulló-López, F.; Ledoux, I.; Zyss, J.; Ferro, V. R.; García de la Vega, J. M. *J. Phys. Chem.* **2005**, *109*, 3800. f) Kim, H. M.; Cho, B. R. *J. Mater. Chem.* **2009**, *19*, 7402.

<sup>60</sup> a) Díaz-García, M. A.; Agulló-López, F.; Sastre, A.; Torres, T.; Torruellas, W. E.; Stegeman, G. I. *J. Phys. Chem.* **1995**, *99*, 14988. b) Liang, Z.; Gan, F.; Sun, Z.; Yang, X.; Ding, L.; Wang, Z. *Opt. Mater.* **2000**, *14*, 13.

<sup>61</sup> a) Yasuda, T.; Tsutsui, T. *Mol. Cryst. Liq. Cryst.* **2007**, *462*, 3. b) Castrucci, J. S.; Helander, M. G.; Morse, G. E.; Lu, Z.-H.; Yip, C. M.; Bender, T. P. *Cryst. Growth Des.* **2012**, *12*, 1095.

<sup>62</sup> a) Renshaw, C. K.; Xu, X.; Forrest, S. R. *Org. Electron.* **2010**, *11*, 175. b) Tong, X.; Forrest, S. R. *Org. Electron.* **2011**, *12*, 1822.

<sup>63</sup> Lee, K.; Lee, G. H.; Leem, D.; Lee, J.; Chung, J. W.; Bulliard, X.; Choi, H.; Park, K.; Kim, K.; Jin, Y. W.; Lee, S.; Park, S. Y. *J. Phys. Chem. C* **2014**, *118*, 13424-13431

<sup>64</sup> a) Chen, Y. -H.; Chang, J. -H.; Lee, G. -R.; Wu, I. -W.; Fang, J. -H.; Wu, C. -I.; Pi, T. -W. *Appl. Phys. Lett.* **2009**, *95*, 133302. b) Chen, Y. -H.; Chang, Y. -J.; Lee, G. -R.; Chang, J. -H.; Wu, I. -W.; Fang, J. -H.; Hsu, S. -H.; Liu, S. -W.; Wu, C. -I.; Pi, T. -W. *Org. Electron.* **2010**, *11*, 445.

<sup>65</sup> a) Helander, M. G.; Morse, G. E.; Qiu, J.; Castrucci, J. S.; Bender, T. P.; Lu, Z. -H. *ACS Appl. Mater. Interfaces* **2010**, *2*, 3147. b) Morse, G. E.; Castrucci, J. S.; Helander, M. G.; Lu, Z. -H.; Bender, T. P. *ACS Appl. Mater. Interfaces* **2011**, *3*, 3538. c) Morse, G. E.; Bender, T. P. *ACS Appl. Mater. Interfaces* **2012**, *4*, 5055.

comparable maximum efficiencies as electron transport and hole transport emitters (Figure 5).

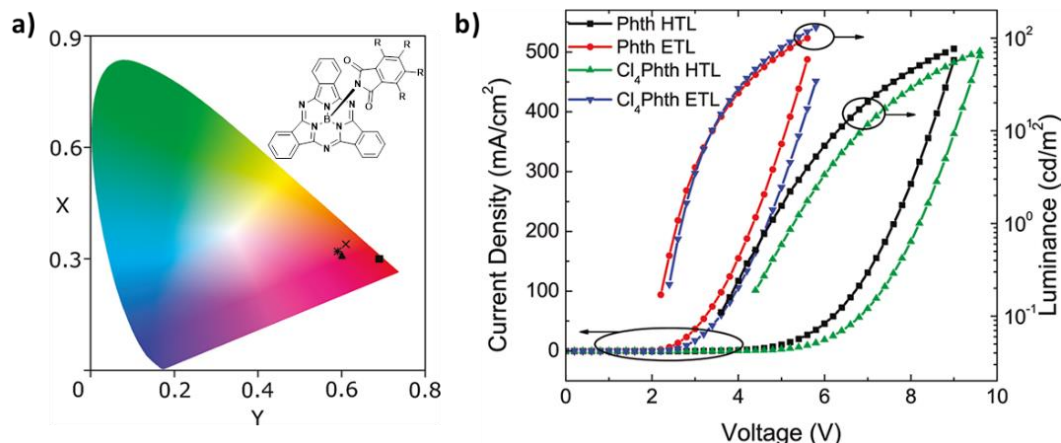


**Figure 5.** a) Structure of phthalimido-SubPcs and CIE color coordinates (symbol;  $x$ ,  $y$ ) for the light emission produced by the OLED devices; b) Luminance and current density as a function of voltage for OLED devices including SubPc as a hole transport layer (HTL) and an electron transport layer (ETL). *Ref. 64b.*

SubPcs have demonstrated to be auspicious both as electron donor and acceptor materials in organic photovoltaics (OPVs). For instance, chloro-SubPc has been extensively used as a donor material in planar heterojunction (PHJ) organic solar devices, in combination with fullerenes as the acceptor counterparts,<sup>66</sup> reaching efficiencies above 5%,<sup>66g</sup> as well as including other non-fullerene acceptors.<sup>67</sup> Importantly, Bender *et al.* demonstrated that SubPcs can not only work as donor, but also as acceptor materials, depending on the molecules they are facing.<sup>68</sup> Fullerene-free OPV based on SubPc acceptors, in combination with other kind of small molecules, have been reported. OPVs

<sup>66</sup> a) Mutolo K. L.; Mayo E. I.; Rand B. P.; Forrest S. R.; Thompson M. E. *J. Am. Chem. Soc.* **2006**, *128*, 8108; b) Gommans H.; Cheyns D.; Aernouts T.; Giroto C.; Poortmans J.; Heremans P. *Adv. Funct. Mater.* **2007**, *17*, 2653; c) Ryu I.-H.; Kim J.; Yim S.-G.; *J. Nanoelectron. Optoelectron.* **2010**, *5*, 191; d) Wang N.; Zimmerman J. D.; Tong X.; Xiao X.; Yu J.; Forrest S. R. *Appl. Phys. Lett.* **2012**, *101*, 133901; e) Kim J. Y.; Kwak J.; Noh S.; Lee C.; *J. Nanosci. Nanotechnol.* **2012**, *12*, 5724; f) Chou C.-T.; Tang W.-L.; Tai Y.; Lin C.-H.; Liu C.-H. J.; Chen L.-C.; Chen K.-H. *Thin Solid Films* **2012**, *520*, 2289. g) Lin C.-F.; Nichols V. M.; Cheng Y.-C.; Bardeen C. J.; Wei M.-K.; Liu S.-W.; Lee C.-C.; Su W.-C.; Chiu T.-L.; Han H.-C.; Chen L.-C.; Chen C.-T.; Lee J.-H. *Sol. Energy Mater. Sol. Cells* **2014**, *122*, 264.

<sup>67</sup> a) Yang, J. L.; Hatton, R. A.; Jones, T. S. *Org. Electron.* **2010**, *11*, 1399. b) Nielsen, C. B.; Voroshazi, E.; Holliday, S.; Cnops, K.; Cheyns, D.; McCulloch, I. J. *Mater. Chem. A* **2014**, *2*, 12348. c) Sullivan, P.; Collis, G. E.; Rochford, L. A.; Arantes, J. F.; Kemppinen, P. Jones, T. S.; Winzenberg, K. N. *Chem. Commun.* **2015**, *51*, 6222.

<sup>68</sup> Morse, G. E.; Gantz, J. L.; Steirer, K. X.; Armstrong, N. R.; Bender, T. P.; *ACS Appl. Mater. Interfaces* **2014**, *6*, 1515.

consisting of oligoacenes as donor materials, such as tetracene or pentacene, and Cl-SubPc and SubPcCl<sub>6</sub>-Cl as acceptor materials have been reported by Jones and Bender groups.<sup>69</sup> The incorporation of a SubPc-Cl in a PHJ OPV developed by Cnops *et al.* achieved a record with a PHJ OPV power conversion efficiency of 8.4%.<sup>70</sup> Bender *et al.* also tested the outdoor stability of SubPc-Cl as electron acceptors in PHJ devices.<sup>71</sup> Additionally, the introduction of  $\pi$ -conjugated cyano groups on the periphery of a series of SubPcs was carried out by our group, revealing charge-carrier mobility values comparable or larger than those of other known well-performing acceptor SubPcs, thus encouraging its use as n-type organic semiconductors in the fabrication of OPV devices.<sup>13</sup>

SubPcs are increasingly attracting attention in the field of optical sensors due to their remarkable photophysical properties. Initially, they have mainly been used as colorimetric and fluorescent chemodosimeters for the detection of fluoride and cyanide anions.<sup>72</sup> In this regard, Park and co-workers recently described a turn-ON water soluble SubPc-based cyanide detector.<sup>71d</sup> They have also been employed as electron mediators in electronic tongues based on phenol oxidases, with an application in the discrimination of wines.<sup>73</sup> The incorporation of SubPcs in single-walled carbon nanotubes (SWCNTs) in the electrochemical detection of Catechin in Tea extracts, or its use as an additive (*i.e.* ionophore) for ion-selective electrodes, have demonstrated a great improvement of their sensing capabilities (Figure 6).<sup>74</sup> Lately, a series of axially substituted SubPcs have demonstrated its viability as pH-fluorescence sensors in acidic media.<sup>75</sup> Interestingly, there are no precedents

---

<sup>69</sup> a) Beaumont, N.; Castrucci, J. S.; Sullivan, P.; Morse, G. E.; Paton, A. S.; Lu, Z. -H.; Bender, T. P.; Jones, T. S. *J. Phys. Chem. C* **2014**, *118*, 14813. b) Castrucci, J. S.; Josey, D. S.; Thibau, E.; Lu, Z. -H.; Bender, T. P. *J. Phys. Chem. Lett.* **2015**, *6*, 3121.

<sup>70</sup> Cnops, K.; Rand, B. P.; Cheyns, D.; Verreert, B.; Empl, M. A.; Heremans, P. *Nat Commun* **2014**, *5*, 3406.

<sup>71</sup> a) Josey, D. S.; Nyikos, S. R.; Garner, R. K.; Dovijarski, A.; Castrucci, J. S.; Wang, J. M.; Evans, G. J.; Bender, T. P. *ACS Energy Lett.* **2017**, *2*, 726. b) Josey, D. S.; Ingram, G. L.; Garner, R. K.; Wang, J. M.; Evans, G. J.; Lu, Z. -H.; Bender, T. P. *ACS Appl. Energy Mater.* **2019**, *2*, 979.

<sup>72</sup> a) Chen, K.; Tian, H.; Sheng, X. *J. Mater. Chem.* **2005**, *15*, 2676. b) Palomares, E.; Martínez-Díaz, M. V.; Torres, T.; Coronado, E. *Adv. Funct. Mater.* **2006**, *16*, 1166. c) Li, Y.; Xu, S.; Li, X.; Chen, K.; Tian, H. *Chem. Lett.* **2007**, *36*, 664. d) Arockiam, J. B.; Park, J. S. *Spectrochimica Acta Part A: Molecular and Biomolecular Spectroscopy* **2019**, *207*, 112–117.

<sup>73</sup> Gonzalez-Anton, R.; Osipova, M. M.; Garcia-Hernandez, C.; Dubinina, T. V.; Tomilova, L. G.; Garcia-Cabezon, C.; Rodriguez-Mendez, M. L. *Electrochimica Acta* **2017**, *255*, 239.

<sup>74</sup> Şenocak, A.; Basova, T.; Demirbas, E.; Durmuş, M. *Electroanalysis* **2019**, *31*, 1697.

<sup>75</sup> Skvortsov, I.A.; Zimcik, P.; Stuzhin, P. A.; Novakova, V. *Dalton Trans.* **2020**, *49*, 11090.

in gravimetry sensing SubPc-based systems. This topic will be widely discussed in *Chapter 2*.

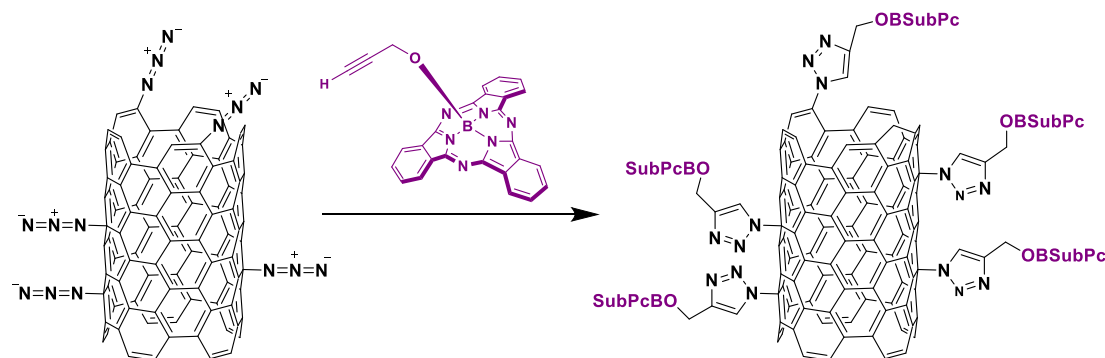


**Figure 6.** Schematic representation for the synthesis of the SWCNT-SubPc derivatives *via* Click cycloaddition reaction. *Ref 74*.

From an early stage of the SubPc chemistry, aromatic characteristics arising from the  $14\pi$ -electron conjugated system embedded in the bowl-shaped structures, such as a difference in aromaticity between the concave and convex surfaces<sup>37a,37d,16,76,77</sup> and concave-convex  $\pi$ - $\pi$  stacking interactions,<sup>11,26,76</sup> have attracted great attention due to their potential application in molecular recognition and fabrication of supramolecular architectures with fullerenes and other carbon nanostructures possessing convex  $\pi$ -conjugated surfaces. In this regard, the group of Torres achieved considerable advances reporting, for the first time, the concave-convex interaction between SubPc and  $C_{60}$  using a pocket-type SubPc dimer, which can encapsulate a  $C_{60}$  molecule in its internal cavity.<sup>36d,38,78</sup> The same group also described that even a single SubPc molecule can embrace a  $C_{60}$  (or  $C_{70}$ ) in a 2:1 stoichiometry in solution, with association constants up to  $10^5 \text{ M}^{-1}$  (Figure 7).<sup>79</sup> Nielsen and co-workers described a different design of SubPc-based fullerene receptors, featuring two SubPcs linked through a spacer that conformed a pseudo-cavity for the  $C_{60}$ .<sup>36f</sup> Very recently, the group of Torres merged those ideas in the design of a SubPc-based supramolecular EET system, obtaining formal  $\text{SubPc}^{\cdot+}\text{-C}_{60}^{\cdot-}$  charge separation states.<sup>15</sup>

<sup>76</sup> C. G. Claessens, D. González-Rodríguez, R. S. Iglesias, T. Torres, *C. R. Chim.* **2006**, *9*, 1094–1099

<sup>77</sup> Shimizu, S.; Nakano, S.; Kojima, A.; Kobayashi, N. *Angew. Chem. Int. Ed.* **2014**, *53*, 2408.

<sup>78</sup> Claessens, C. G.; Torres, T. *Chem. Commun.* **2004**, 1298.

<sup>79</sup> Sánchez-Molina, I.; Claessens, C. G.; Grimm, B.; Guldi, D. M.; Torres, T. *Chem. Sci.* **2013**, *4*, 1338.

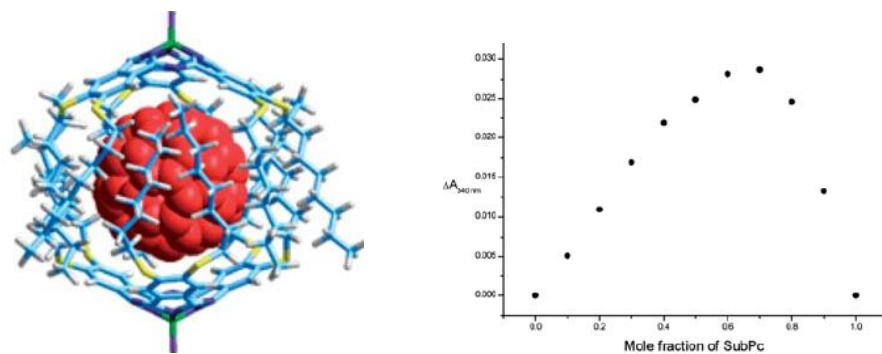


**Figure 7.** Molecular modeling of the 2:1 adduct of jellyfish-like SubPcs and C<sub>60</sub> (left). Job's Plot related to the 2:1 complex formation (right). Ref. 79.

Lastly, the singular structure of SubPcs grants them ideal attributes for their integration in artificial photosynthetic reaction centres: intense Q-bands in the solar radiation region, extinction coefficients *ca.*  $5 - 6 \times 10^4 \text{ M}^{-1}\text{cm}^{-1}$ , excitation energies of 2.0 eV, and a rigid and  $\pi$ -electronic 3D structure exhibiting intense fluorescence emission. Thus, a large number of energy/electron donor-acceptor systems mainly based on SubPcs have been prepared and studied. Most of these studies have been developed by the teams of Torres and Gludi working together.<sup>80</sup> This topic will be deeply explained in *Chapter 1*.

<sup>80</sup> Bottari, G.; de la Torre, G.; Guldi, D. M.; Torres, T. *Coordination Chemistry Reviews*, **2021**, *428*, 213605.



## Corroles as Molecular Materials

Porphyrins (Pors) are one of the most widely studied and known tetrapyrrolic macrocycles, with a constant presence in prosthetic groups of hemoproteins such as hemoglobin, myoglobin and various cytochromes. As metalloporphyrins (MPors), they have crucial roles for the correct performance of several biological systems. Reduced Pors, chlorins and bacteriochlorins, act as excellent photosensitizers, the most notable example being the magnesium-chlorin pigment present in chlorophyll. Corrins, contracted saturated Pors, are recognized as the core of vitamin B<sub>12</sub>.

Unlike Pors, chlorins and corrins, corroles (Cors) have not been found yet in nature. They present the same structure as corrins, while preserving the 18-electron  $\pi$  aromatic ring current of Pors (Figure 8). This, along with its reduced inner cavity and symmetry, results in a blooming of intriguing properties. One of the main features springing from this contraction is its ability to stabilise formally high metal oxidation states: they behave as trianionic ligands, opening the way to a series of elements at such valences hardly reachable when employing Pors.

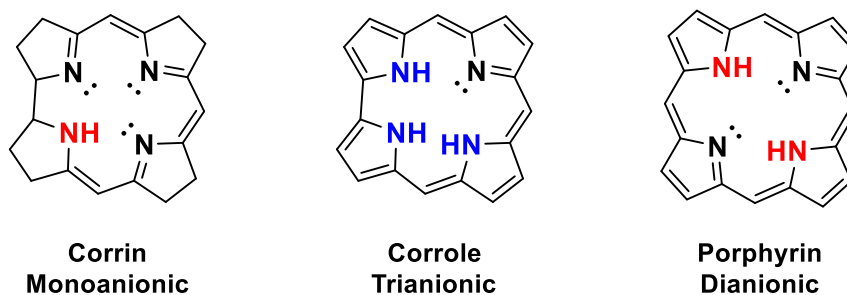


**Figure 8.** Chemical structures of free-base Corrin (left), Por (right) and Cor (center).

## Synthesis of corroles

Cors were firstly identified in 1965 by Kay and Johnson during their attempt to synthesize vitamin B<sub>12</sub>, being thought firstly as a precursor of the corrin ring.<sup>81</sup> Although results were unsuccessful, Cors were recognized as promising ligands, and a series of publications about metallo-corroles (MCors) appeared in the upcoming years after its discovery.<sup>82</sup>

Unfortunately, the tedious and difficult pyrrole chemistry needed to further explore those ligands receded them into the background until 1999 when, contemporarily, two different groups developed a one-pot synthesis from commercially available reagents.<sup>83</sup> This discovery marked a milestone in the chemistry of Cors, paving the way for a wide class of tetrapyrrolic ligands. From that moment, Cor-related publications experienced an exponential growth.

The obtention of Cors has been tackled from many different approaches.<sup>84</sup> After much effort, some of those paths have led to the development of quasi-general synthetic methodologies. Generally, the reaction relies on the formation of a linear tetrapyrrole and subsequent ring closure, obtaining the corresponding Cor. It is worth to mention that, nowadays, one of the main drawbacks for the synthesis of Cors is the competitive formation of Pors, which is generally favoured.

Structurally, the atomic positions of Cors are flagged following the assignment of Pors (Figure 9). Two different positions should be highlighted: the  $\beta$ - (2, 3, 7, 8, 12, 13, 17 and 18) and the *meso*- (5, 10 and 15). From the synthetic point of view, we can divide Cors in two main groups:  $\beta$ - and *meso*-substituted.

---

<sup>81</sup> Johnson, A. W.; Kay, I. T. *J. Chem. Soc.* **1965**, 1620.

<sup>82</sup> a) Conlon, M.; Johnson, A. W.; Overend, W. R.; Rajapaksa, D.; Elson, C. M. *J. Chem. Soc., Perkin Trans. 1*, **1973**, 2281. b) Murakami, Y.; Matsuda, Y.; Sakata, K.; Yamada, S.; Tanaka, Y.; Aoyama, Y. *Bull. Chem. Soc. Jpn.* **1981**, *54*, 163.

<sup>83</sup> a) Paolesse, R.; Mini, S.; Sagone, F.; Boschi, T.; Jaquinod, L.; Nurco, D. J.; Smith, K. M. *Chem. Commun.* **1999**, *14*, 1307. b) Gross, Z.; Galili, N.; Saltsman, I. *Angew. Chem. Int. Ed.* **1999**, *38*, 1427.

<sup>84</sup> Orłowski, R.; Gryko, D.; Gryko, D. T. *Chem. Rev.* **2017**, *4*, 3102.

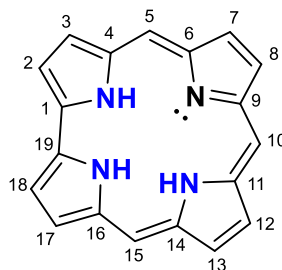


**Figure 9.** Chemical structure and numbering system of Cors.

The inner core hydrogens are not localized on three nitrogens, but rather move rapidly between them, giving rise to NH tautomers (Figure 10).<sup>85</sup> According to a detailed theoretical study by Ghosh and Jynge, it is suggested the presence of two possible tautomers, with no significant energy differences between them.<sup>86</sup> Crystal structures of free-base Cors confirm their study, since both tautomers have been experimentally observed.<sup>87</sup> Recently, it was found that individual tautomers display different fluorescence spectra.<sup>88</sup>

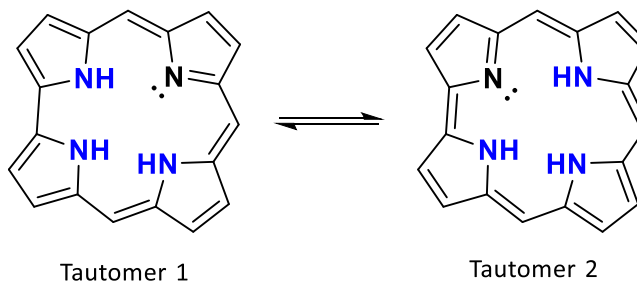


**Figure 10.** Two possible tautomers of the free-base Cors.

<sup>85</sup> Dyke, J. M.; Hush, N. S.; Williams, M. L.; Woolsey, I. S. *Mol. Phys.* **1971**, *20*, 1149–1152.

<sup>86</sup> Ghosh, A.; Jynge, K. *Chem. Eur. J.* **1997**, *3*, 823.

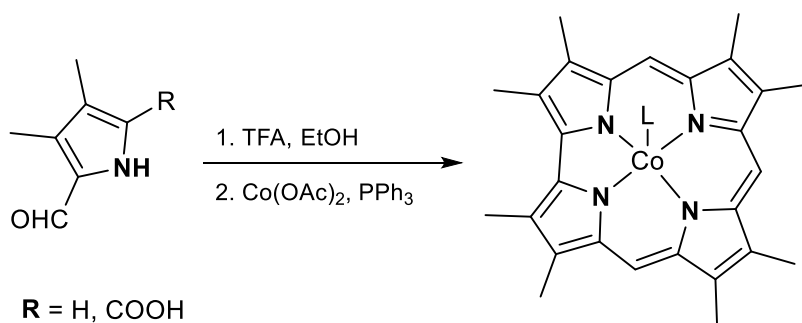
<sup>87</sup> a) Gross, Z.; Galili, N.; Simkhovich, L.; Saltsman, I.; Botoshansky, M.; Blaser, D.; Boese, R.; Goldberg, I. *Org. Lett.* **1999**, *1*, 599. b) Paolesse, R.; Marini, A.; Nardis, S.; Froiio, A.; Mandoj, F.; Nurco, D. J.; Prodi, L.; Montalti, M.; Smith, K. M. *J. Porphyrins Phthalocyanines* **2003**, *07*, 25. c) Capar, J.; Conradie, J.; Beavers, C. M.; Ghosh, A. *J. Phys. Chem. A* **2015**, *119*, 3452 d) Simkhovich, L.; Goldberg, I.; Gross, Z. *J. Inorg. Biochem.* **2000**, *80*, 235. e) Ding, T.; Harvey, J. D.; Ziegler, C. J. *J. Porphyrins Phthalocyanines* **2005**, *9*, 22.

<sup>88</sup> Kruk, M.; Ngo, T. H.; Verstappen, P.; Starukhin, A.; Hofkens, J.; Dehaen, W.; Maes, W. *J. Phys. Chem. A* **2012**, *116*, 10695.

## Synthesis of $\beta$ -Substituted Corroles

Historically,  $\beta$ -substituted Cors are referred to the first synthetic methodologies employed for the obtention of this kind of macrocycles, in which  $\beta$ -alkyl-substituted pyrroles and  $a,c$ -biladiene salts were used as starting materials. Despite intense years of research, those methodologies have prevailed as the best procedures for the obtention of symmetric and unsymmetric  $\beta$ -alkyl-substituted Cors.

The tetramerization of alkyl-pyrroles for the obtention of Cors were firstly reported by Paolesse *et al.* in 1994.<sup>89</sup> It involved the reaction of 3,4-dimethyl-pyrrole-2-carbaldehyde in presence of cobalt salts to obtain the alkyl-metallated Cor in a 10% yield (Scheme 5). Interestingly, the use of the carboxylic acid pyrrole-derivative returned the same reaction yield, probably due to a fast decarboxilation process in acidic media.



**Scheme 5.** Synthesis of Co(III)  $\beta$ -octamethyl Cor complex (L = PPh<sub>3</sub>).

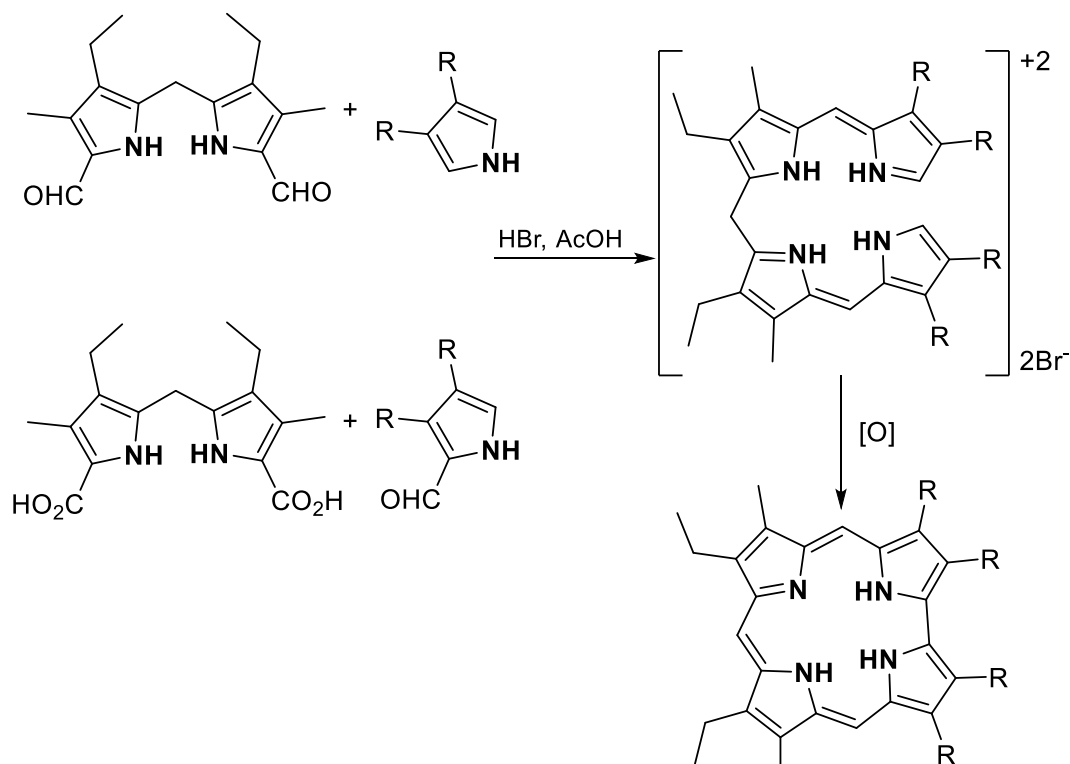
The synthesis of unsymmetrically  $\beta$ -substituted Cors *via* tetramerization was also tested.<sup>90</sup> However, the complex mixture of compounds obtained and the low global yield (*ca.* 8%) seriously limited the described methodology.

For the obtention of unsymmetrical derivatives, the use of tetrapyrrolic intermediates was required. A [2+1+1] approach involving acidic condensation in HBr of either 3,4-dialkylpyrroles with 5,5'-diformyldipyrranes or 2-formylpyrroles with dipyrroles dicarboxylic acids provided the crystalline dihydrobromide salts (Scheme 6). Subsequent photochemical oxidative cyclization in methanolic ammonia or sodium acetate solutions under light irradiation with a 200 W tungsten lamp or a medium-pressure mercury lamp led

<sup>89</sup> Paolesse, R.; Licocchia, S.; Bandoli, G.; Dolmella, A.; Boschi, T. *Inorg. Chem.* **1994**, *33*, 1171.

<sup>90</sup> Paolesse, R.; Tassoni, E.; Licocchia, S.; Paci, M.; Boschi, T. *Inorg. Chim. Acta* **1996**, *241*, 55.

into the closure of the ring with a 67% yield.<sup>79</sup> The oxidation agent could be replaced by a wide number of different oxidants, while maintaining basic conditions.<sup>91</sup> In 1994, *p*-chloranil was finally introduced as a mild oxidant by Vogel and co-workers,<sup>92</sup> significantly improving the cyclization yields. Nevertheless, preparation of the corresponding building blocks required of several tedious and highly time-consuming synthetic steps, with an overall optimized yield up to 40%.



**Scheme 6.** Synthesis of a,c-biladiene intermediates for the obtention of Cors.

<sup>91</sup> Dolphin, D.; Johnson, A. W.; Leng, J.; van den Broek, P. *J. Chem. Soc. C* **1966**, 880.

<sup>92</sup> Vogel, E.; Will, S.; Tilling, A. S.; Neumann, L.; Lex, J.; Bill, E.; Trautwein, A. X.; Wieghardt, K. *Angew. Chem., Int. Ed. Engl.* **1994**, *33*, 731.

An alternative methodology relies on the *in-situ* preparation of dibromobiladienes, starting from the corresponding dipyrroles (Figure 11).<sup>93</sup> The high reactivity of the terminal halogen atoms is the driving force of the cyclization reaction, without requirement of an oxidant agent. However, the multistep synthesis of the starting precursors limited its potential use.<sup>94</sup> Iodoarenes proved to be more reactive as compared to their bromo analogues due to the lower energy of their C-Halogen bond, yet without improving the yield.

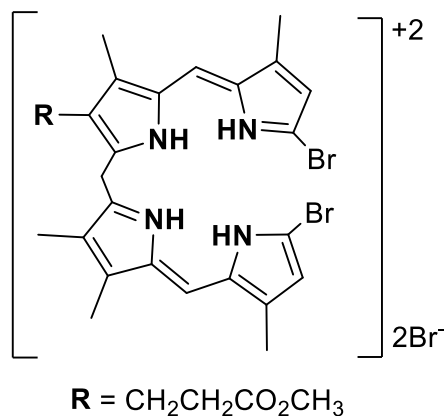


Figure 11. Structure of a,c-dibromobiladiene.

Additionally, two different approaches should be included in the synthesis of  $\beta$ -substituted Cors. Conlon *et al.* reported the reaction between a 2,2'-bipyrrrole and a dipyrrole in presence of cobalt as the templating agent, obtaining the corresponding Cor.<sup>80a,95</sup> Moreover, the ring-contraction reaction of an alkyl-thioplurin led into the formation of Cor with a stunning 60% yield.<sup>96</sup> However, the poor stability of the sulfur-based starting materials limited the interest in this methodology.

<sup>93</sup> a) Harris, R. L. N.; Johnson, A. W.; Kay, I. T. *J. Chem. Soc. C* **1966**, 22. b) Pandey, R. K.; Zhou, H.; Gerzevske, K.; Smith, K. M. *J. Chem. Soc., Chem. Commun.* **1992**, 183. c) Pandey, R. K.; Gerzevske, K. R.; Zhou, H.; Smith, K. M. *J. Chem. Soc., Perkin Trans. 1* **1994**, 971.

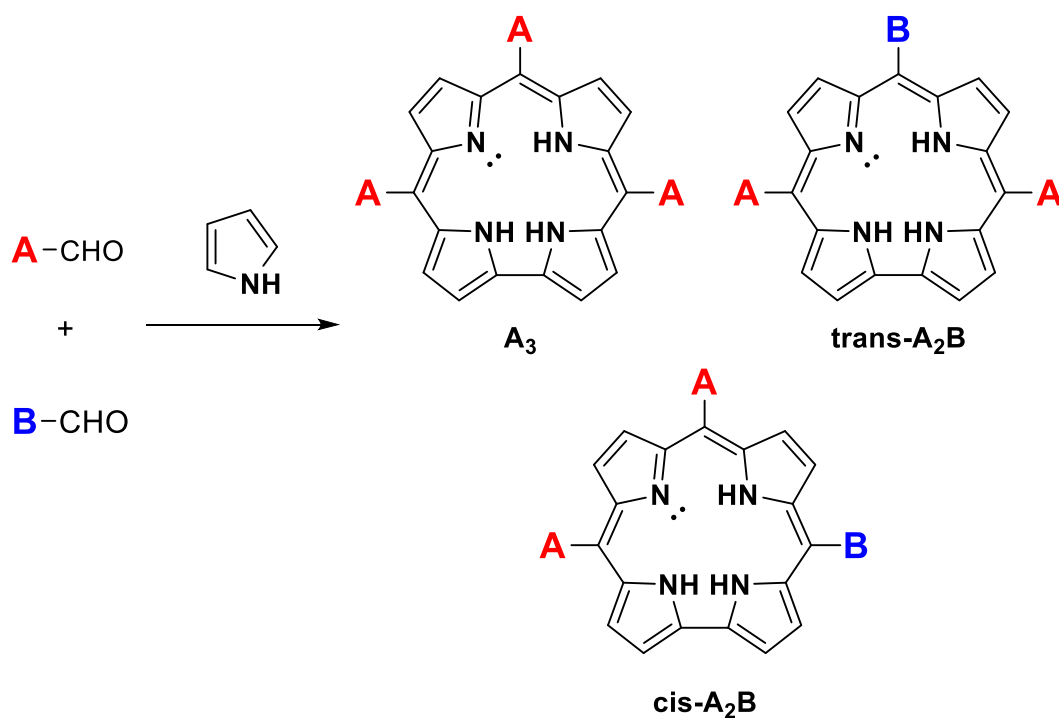
<sup>94</sup> a) Engel, J.; Gossauer, A. *J. Chem. Soc., Chem. Commun.* **1975**, 713. b) Neya, S.; Ohyama, K.; Funasaki, N. *Tetrahedron Lett.* **1997**, 38, 4113.

<sup>95</sup> Vogel, E.; Bröring, M.; Fink, J.; Rosen, D.; Schmicler, H.; Lex, J.; Chan, K. W. K.; Wu, Y.-D.; Plattner, D. A.; Nendel, M.; Houk, K. *Angew. Chem., Int. Ed. Engl.* **1995**, 34, 2511.

<sup>96</sup> a) Broadhurst, M. J.; Grigg, R.; Johnson, A. W. *J. Chem. Soc. D* **1970**, 807. b) Broadhurst, M. J.; Grigg, R.; Johnson, A. W. *J. Chem. Soc., Perkin Trans. 1* **1972**, 1124.

### Synthesis of *meso*-substituted A<sub>3</sub>-Corroles

In the last few years, the obtention of *meso*-substituted Cors, particularly by aryl fragments due to their increased stability, have become one of the preferred synthetic strategies for the preparation of new Cor derivatives. From the substitution pattern, three different types of Cors can be distinguished (Scheme 7). Cors bearing three identical substituents at their *meso* position are identified as A<sub>3</sub>-Cors, whereas those bearing two identical and one different substituent are identified as A<sub>2</sub>B-Corroles. From the adopted disposition, *trans*- and *cis*-Cors can be distinguished. *Trans*-A<sub>2</sub>B-Cors are preferred over *cis*-Cors due to their synthetic accessibility.



**Scheme 7.** Substitution patterns for the synthesis of *meso*-substituted Cors.

Despite A<sub>3</sub>-Cors can be prepared following diverse approaches, direct condensation of pyrroles and aldehydes is the simplest and main used strategy. As pointed earlier, the synthesis of Cors gets prominence when, in 1999, Paolesse<sup>83a</sup> and Gross<sup>83b</sup> described almost simultaneously a one-pot synthesis of *meso*-A<sub>3</sub>-Cors from commercially available reagents.

The methodology of Gross relied in the use of strong electro-withdrawing and highly reactive aldehydes (*i.e.* pentafluorobenzaldehyde), retrieving the best yields. Although the reaction was performed in absence of solvent, using Al<sub>2</sub>O<sub>3</sub> as a solid support and heat, those last two conditions proved to be unnecessary.<sup>87a</sup> On the other hand, the use of an organic acid such as TFA demonstrated to be crucial for an increase of the yield, acting as a catalyst in the formation of the bilane intermediate.<sup>97</sup> Gryko *et al.* refined this methodology, obtaining higher yields for the already studied Cors and smoothing the path in the obtention of new derivatives.<sup>98</sup>

Paolesse *et al.* reported a modification of the Rothmund's method<sup>99</sup> that allowed for the obtention of an extensive range of A<sub>3</sub>-Cors by adding an excess of pyrrole with respect to the aldehyde (3:1).<sup>83a,100</sup> It also follows the trend of reactivity marked by Gross, obtaining an impressive 22% yield for the 4-nitrobenzaldehyde. However, it proved to be unsuccessful for sterically hindered aldehydes such as 2,6-disubstituted derivatives.

One of the main handicaps in the synthesis of A<sub>3</sub>-Cors is the concomitant formation of the corresponding Por, reducing the yields and difficulting the purification process. To overcome this problem, Gryko and Koszarna proposed an elegant solution.<sup>101</sup> The formation of the bilane was performed in a water/methanol mixture, and catalyzed by HCl. The proportion of both solvents was optimized so that both dipyrane and tripyrane intermediates remained in solution, whereas more lipophilic tetrapyrans precipitated from the reaction mixture. Though not ideal, this methodology boosted the reaction yields, in some cases, up to a 30%. Additionally, the amount of Por obtained was minimal, greatly facilitating the purification steps.

---

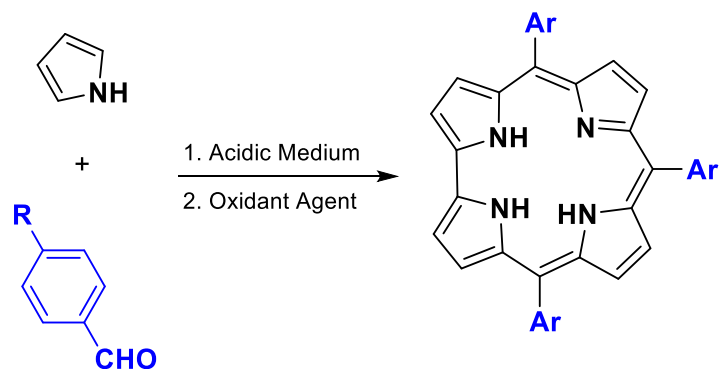
<sup>97</sup> Littler, B. J.; Miller, M. A.; Hung, C.-H.; Wagner, R. W.; O'Shea, D. F.; Boyle, P. D.; Lindsey, J. S. *J. Org. Chem.* **1999**, *64*, 1391.

<sup>98</sup> Gryko, D. T.; Koszarna, B. *Org. Biomol. Chem.* **2003**, *1*, 350.

<sup>99</sup> Lindsey, J. S. *In The Porphyrin Handbook*; Kadish, K. M.; Smith, K. M.; Guillard, R., **2000**; Vol. I.

<sup>100</sup> Paolesse, R.; Nardis, S.; Sagone, F.; Khoury, R. G. *J. Org. Chem.* **2001**, *66*, 550.

<sup>101</sup> Koszarna, B.; Gryko, D. T. *J. Org. Chem.* **2006**, *71*, 3707.

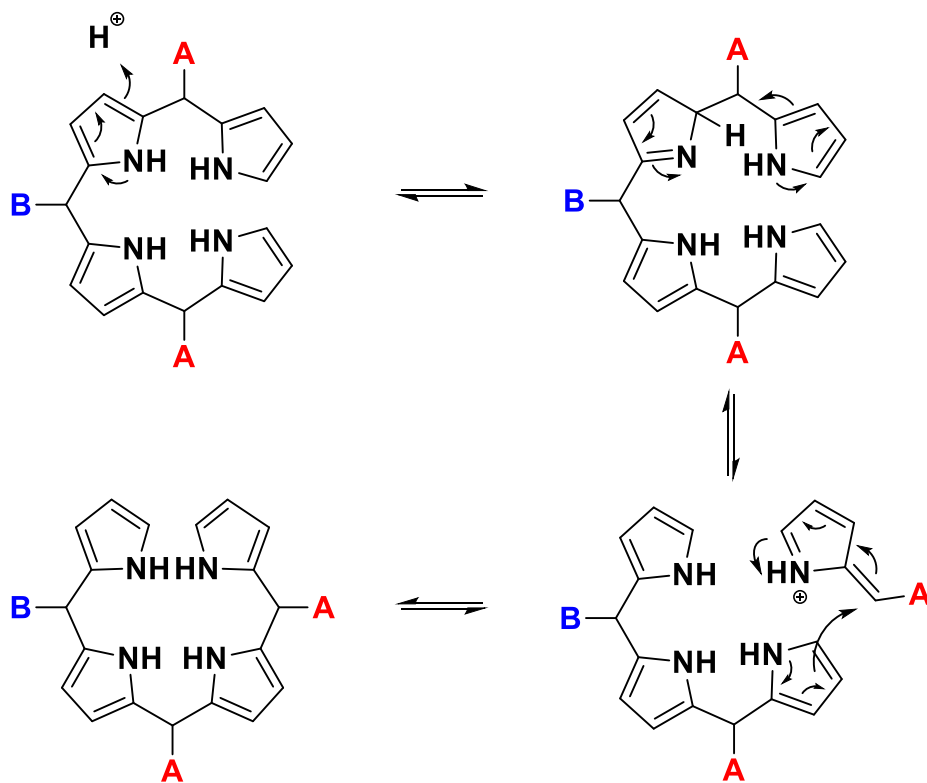


**Scheme 8.** General pathway for the obtention of A<sub>3</sub>-Cors

### **Synthesis of *meso*-substituted A<sub>2</sub>B-Corroles**

The synthesis of Cors bearing different *meso*-substituents is required in order to add functionalities and versatility to the Cor scaffold, for example, as supramolecular recognition probes or anchoring points. As mentioned above, *trans*-A<sub>2</sub>B-Cors are preferred over *cis*-A<sub>2</sub>B-Cors due to their synthetic accessibility from the corresponding dipyrromethanes (DPMs) and aldehydes.

One of the main obstacles during their preparation is the so-called *scrambling*. It consists in the rearrangement of the aldehyde subunits during dipyrroles or bilane formation, resulting in a mixture of Cors with the same molecular weight but different substitution patterns. This phenomenon is more significant if the benzylic carbon linking pyrrole units lack of steric hindrance (Scheme 9).

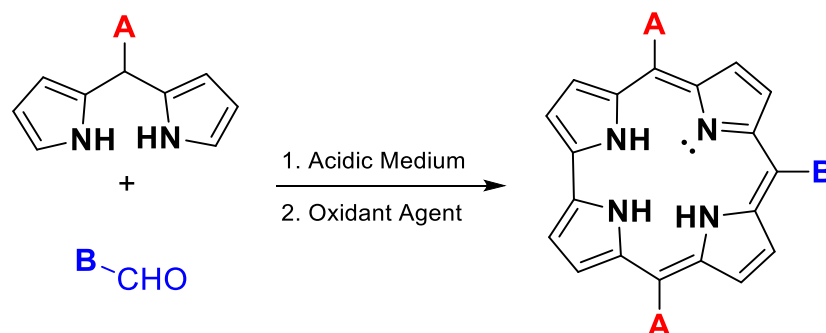


**Scheme 9.** Rearrangement process during preparation of  $A_2B$ -Cors.

Among the different pathways available for the synthesis of *trans*- $A_2B$ -Cors, the condensation of DPMs and aldehyde stands over the rest due to the synthetic availability of the starting compounds (Scheme 10). Gryko focused his studies on this topic, reporting the synthesis of the first *trans*- $A_2B$ -Cor by the non-catalyzed reaction of a DPM with an aldehyde.<sup>102</sup> However, the addition of an acid determined to be crucial: in presence of TFA, reaction times were reduced without detectable scrambling, even for unhindered DPMs.<sup>103</sup> Finally, the conditions previously developed for the obtention of  $A_3$ -Cors in MeOH/H<sub>2</sub>O were extended to the *trans*- $A_2B$ -Cors, resulting particularly effective for small and hydrophilic reactives.

<sup>102</sup> Gryko, D. T. *Chem. Commun.* **2000**, 2243.

<sup>103</sup> Gryko, D. T.; Jadach, K. *J. Org. Chem.* **2001**, *66*, 4267.



Scheme 10. General pathway for the preparation of *trans*-A<sub>2</sub>B-Cors.

## Functionalization of Corroles

The reactivity and functionalization of Cors may be classified in three main groups: (1) the inner core positions, (2) the peripheral positions and (3) the post-functionalization reactions. Due to the high number of possibilities derived from the latest, only the first two approaches will be discussed.

### Functionalization at the inner core positions

Cors give different type of reactions at its inner core, namely N-alkylation,<sup>79,104</sup> protonation, deprotonation and metal complexation. From them, protonation/deprotonation and metalation processes are the most relevant. Compared to Pors, Cors present a reduced inner cavity. A small deviation from the planarity is produced by the steric interactions and electronic repulsions between the inner protons, making them to stay slightly out of plane. Consequently, they are more acidic than Pors, being the deviated protons more accessible to nucleophiles. Correspondingly, the ability to act as trianionic ligands gets relevant in metalation processes, allowing them to coordinate high-valent metal ions. However, Cor present a non-innocent character as ligand, with ligand-to-metal charge transfer often present.

<sup>104</sup> a) Gross, Z.; Galili, N. *Angew. Chem., Int. Ed.* **1999**, *38*, 2366. b) Broadhurst, M. J.; Grigg, R.; Shelton, G.; Johnson, A. W. *J. Chem. Soc. D* **1970**, 231. c) Broadhurst, M. J.; Grigg, R.; Shelton, G.; Johnson, A. W. *J. Chem. Soc., Perkin Trans. 1* **1972**, *99*, 143. d) Rohand, T.; Dolusic, E.; Ngo, T. H.; Maes, W.; Dehaen, W. *Arkivoc* **2007**, 307. e) Naito, W.; Yasuda, N.; Morimoto, T.; Shigeta, Y.; Takaya, H.; Hisaki, I.; Maeda, H. *Org. Lett.* **2016**, *18*, 3006. f) Patra, S. K.; Sahu, K.; Patra, B.; Mondal, S.; Kar, S. *Eur. J. Org. Chem.* **2018**, 6764.

Over the course of years, Cors have accommodated a wide number of elements into its core, a number that is growing over time (Figure 12).<sup>105</sup>

1 Hydrogen <b>H</b> 1.01																	2 Helium <b>He</b> 4.00	
3 Lithium <b>Li</b> 6.94	4 Beryllium <b>Be</b> 9.01											5 Boron <b>B</b> 10.81	6 Carbon <b>C</b> 12.01	7 Nitrogen <b>N</b> 14.01	8 Oxygen <b>O</b> 16.00	9 Fluorine <b>F</b> 19.00	10 Neon <b>Ne</b> 20.18	
11 Sodium <b>Na</b> 22.99	12 Magnesium <b>Mg</b> 24.31											13 Aluminum <b>Al</b> 26.98	14 Silicon <b>Si</b> 28.09	15 Phosphorus <b>P</b> 30.97	16 Sulfur <b>S</b> 32.07	17 Chlorine <b>Cl</b> 35.45	18 Argon <b>Ar</b> 39.95	
19 Potassium <b>K</b> 39.10	20 Calcium <b>Ca</b> 40.08	21 Scandium <b>Sc</b> 44.96	22 Titanium <b>Ti</b> 47.88	23 Vanadium <b>V</b> 50.94	24 Chromium <b>Cr</b> 52.00	25 Manganese <b>Mn</b> 54.94	26 Iron <b>Fe</b> 55.85	27 Cobalt <b>Co</b> 58.93	28 Nickel <b>Ni</b> 58.69	29 Copper <b>Cu</b> 63.55	30 Zinc <b>Zn</b> 65.39	31 Gallium <b>Ga</b> 69.72	32 Germanium <b>Ge</b> 72.61	33 Arsenic <b>As</b> 74.92	34 Selenium <b>Se</b> 78.96	35 Bromine <b>Br</b> 79.90	36 Krypton <b>Kr</b> 83.80	
37 Rubidium <b>Rb</b> 85.47	38 Strontium <b>Sr</b> 87.62	39 Yttrium <b>Y</b> 88.91	40 Zirconium <b>Zr</b> 91.22	41 Niobium <b>Nb</b> 92.91	42 Molybdenum <b>Mo</b> 95.94	43 Technetium <b>Tc</b> (98)	44 Ruthenium <b>Ru</b> 101.07	45 Rhodium <b>Rh</b> 102.91	46 Palladium <b>Pd</b> 106.42	47 Silver <b>Ag</b> 107.87	48 Cadmium <b>Cd</b> 112.41	49 Indium <b>In</b> 114.82	50 Tin <b>Sn</b> 118.71	51 Antimony <b>Sb</b> 121.76	52 Tellurium <b>Te</b> 127.60	53 Iodine <b>I</b> 126.90	54 Xenon <b>Xe</b> 131.29	
55 Cesium <b>Cs</b> 132.91	56 Barium <b>Ba</b> 137.33	57-70 * Lanthanides	71 Lutetium <b>Lu</b> 174.97	72 Hafnium <b>Hf</b> 176.49	73 Tantalum <b>Ta</b> 180.95	74 Tungsten <b>W</b> 183.84	75 Rhenium <b>Re</b> 186.21	76 Osmium <b>Os</b> 190.23	77 Iridium <b>Ir</b> 192.22	78 Platinum <b>Pt</b> 195.08	79 Gold <b>Au</b> 196.97	80 Mercury <b>Hg</b> 200.59	81 Thallium <b>Tl</b> 204.38	82 Lead <b>Pb</b> 207.20	83 Bismuth <b>Bi</b> 208.98	84 Polonium <b>Po</b> (209)	85 Astatine <b>At</b> (210)	86 Radon <b>Rn</b> (222)
87 Francium <b>Fr</b> (223)	88 Radium <b>Ra</b> (226)	89-102 ** Actinides	103 Lanthanum <b>La</b> (262)	104 Rutherfordium <b>Rf</b> (267)	105 Dubnium <b>Db</b> (268)	106 Seaborgium <b>Sg</b> (271)	107 Bohrium <b>Bh</b> (272)	108 Hassium <b>Hs</b> (270)	109 Meitnerium <b>Mt</b> (276)	110 Darmstadtium <b>Ds</b> (281)	111 Roentgenium <b>Rg</b> (280)	112 Copernicium <b>Cn</b> (285)	113 Uut <b>Uut</b> (284)	114 Uuq <b>Uuq</b> (289)	115 Uup <b>Uup</b> (288)	116 Uuh <b>Uuh</b> (293)	117 Uus <b>Uus</b> (294?)	118 Uuo <b>Uuo</b> (284)
			57 Lanthanum <b>La</b> 138.91	58 Cerium <b>Ce</b> 140.12	59 Praseodymium <b>Pr</b> 140.91	60 Neodymium <b>Nd</b> 144.24	61 Promethium <b>Pm</b> (145)	62 Samarium <b>Sm</b> 150.36	63 Europium <b>Eu</b> 151.97	64 Gadolinium <b>Gd</b> 157.25	65 Terbium <b>Tb</b> 158.93	66 Dysprosium <b>Dy</b> 162.50	67 Holmium <b>Ho</b> 164.93	68 Erbium <b>Er</b> 167.26	69 Thulium <b>Tm</b> 168.93	70 Ytterbium <b>Yb</b> 173.04		
			89 Actinium <b>Ac</b> (227)	90 Thorium <b>Th</b> 232.04	91 Protactinium <b>Pa</b> 231.04	92 Uranium <b>U</b> 238.03	93 Neptunium <b>Np</b> (237)	94 Plutonium <b>Pu</b> (244)	95 Americium <b>Am</b> (243)	96 Curium <b>Cm</b> (247)	97 Berkelium <b>Bk</b> (247)	98 Californium <b>Cf</b> (251)	99 Einsteinium <b>Es</b> (252)	100 Fermium <b>Fm</b> (257)	101 Mendelevium <b>Md</b> (258)	102 Nobelium <b>No</b> (259)		

Figure 12. Periodic table highlighting the atomic elements coordinated to the inner core of Cor.

The development of metallocorrole (MCor) chemistry closely mirrors that of metalloporphyrins (MPor). Cor complexes are often prepared by combining the free-base ligand in solution or in suspension with a metal halide or acetate salt, heating or at RT. The complex is then typically isolated *via* column chromatography or precipitation.

As trianionic ligands, the most stable coordination number in MCors is the oxidation state three. According to density functional theory (DFT) calculations, gallium ion with oxidation state +3 perfectly fits the inner cavity of Cors.<sup>106</sup> For so, it is considered as a

<sup>105</sup> a) Licocchia, S.; Paolesse, R. *Metal Complexes of Corroles and Other Corrinoids*. In *Metal Complexes with Tetrapyrrole Ligands III*; Springer: Berlin, **1995**, *84*, 71. b) Buckley, H. L.; Arnold, J. *Dalton Trans.* **2015**, *44*, 30. c) Barata, J. F. B.; Neves, M. G. P. M. S.; Faustino, M. A. F.; Tomé, A. C.; Cavaleiro, *Chem. Rev.* **2017**, *117*, 3192.

<sup>106</sup> Ghosh, A.; Jynge, K. *Chem. Eur. J.* **1997**, *3*, 823.

reference for MCors, as 5,10,15,20-tetraphenylporphyrinatozinc(II) (ZnTPP) is the prototype for MPors.

Metallation of Cors is a common strategy for protecting the core against electrophilic reagents, thus conferring stability to the ligand. The introduction of concrete metal ions proved to be necessary in different selective functionalization processes, like bromination<sup>107</sup> or nitration.<sup>108</sup> Moreover, corrolate ligand supports high valence oxidation states like Fe (III) and Fe (IV), Ge (IV), Sn (IV), Cr (V), Co (IV) and Co (V), or Mn (III), among others. However, it is difficult to characterize the electronic structure of MCors due to their high electron density: the trianionic character and the high oxidation state for the metal ion facilitates the electron transfer from Cor to the metal, resulting in an oxidation state “formally” high (e.g Ni-Cor is a complex with an oxidized  $\pi$ -radical cation of Cor and Ni(II)).

The metallation/demetallation methodology is a powerful tool for the preparation of particular scaffolds requiring the use of harsh conditions that would be fatal for the free-base Cor. Despite demetallation in Pors is employed as a routinary process,<sup>109</sup> the same has resulted a challenge for Cors, where no demetallation routes were described until a few years ago. In comparison with Pors, the difficulty of demetallating Cors may be attributed to several reasons: (1) the stronger metal-nitrogen bonds due to their smaller cavity and higher ligand donor character; (2) their lower stability, leading into decomposition upon harsh reaction conditions.

In 2008, the group of Paolesse reported the first general reductive demetallation procedure, involving a mixture of  $\text{CHCl}_3$  and  $\text{H}_2\text{SO}_4$ .<sup>110</sup> The reaction proved to be effective for a series of Cu, Mn and Fe Cors, returning the corresponding free-base ligand in excellent yields. In the same year, Gosh *et al.* reported that addition of a reductant agent such as

---

<sup>107</sup> Stefanelli, M.; Naitana, M. L.; Chiarini, M.; Nardis, S.; Ricci, A.; Fronczek, F. R.; Sterzo, C. L.; Smith, K. M.; Paolesse, R.; *Eur. J. Org. Chem.* **2015**, 6811.

<sup>108</sup> a) Saltsman, I.; Mahammed, A.; Goldberg, I.; Tkachenko, E.; Botoshansky, M.; Gross, Z. *J. Am. Chem. Soc.* **2002**, *124*, 7411. b) Stefanelli, M.; Mastroianni, M.; Nardis, S.; Licoccia, S.; Fronczek, F. R.; Smith, K. M.; Zhu, W.; Ou, Z.; Kadish, K. M.; Paolesse, R. *Inorg. Chem.* **2007**, *46*, 10791. c) Mastroianni, M.; Zhu, W.; Stefanelli, M.; Nardis, S.; Fronczek, F. R.; Smith, K. M.; Ou, Z.; Kadish, K. M.; Paolesse, R. *Inorg. Chem.* **2008**, *47*, 11680. d) Stefanelli, M.; Mandoj, F.; Mastroianni, M.; Nardis, S.; Mohite, P.; Fronczek, F. R.; Smith, K. M.; Kadish, K. M.; Xiao, X.; Ou, Z.; Chen, P.; Paolesse, R. *Inorg. Chem.* **2011**, *50*, 8281.

<sup>109</sup> Fuhrhop, J. H.; Smith, K. M. In *Porphyrin and Metalloporphyrins*; Smith, K. M., Ed.; Elsevier: Amsterdam, **1975**, 757.

<sup>110</sup> Mandoj, F.; Nardis, S.; Pomarico, G.; Paolesse, R. *J. Porphyrins Phthalocyanines* **2008**, *12*, 19.

FeCl<sub>2</sub> or SnCl<sub>2</sub> resulted in an increase of the CuCors demetallation yield as well as in fewer impurities.<sup>111</sup> Subsequently, similar procedures appeared for demetallation of Cu and Mn Cors.<sup>112,113</sup> Additionally, Paolesse *et al.* reported a list of procedures for demetallation of Ag Cors.<sup>114</sup> Lastly, Grignard reagents have successfully been employed for demetallation of Sn and Ag complexes.<sup>115</sup>

### **Functionalization at the periphery**

Functionalization of Cors is performed either at the *meso*- or  $\beta$ -positions. The introduction of different chemical functionalizations can be done either from the starting pyrrole derivative, either from the already formed Cor. Generally, alkyl moieties are introduced before the formation of the macrocycle, whereas electrophilic substitutions, such as halogenation, nitration, sulfonation or acylation, are developed in the Cor structure.

Because of their reduced symmetry, peripheral functionalization reactions may result in the obtention of a large number of isomers. Consequently, several strategies should be followed in order to minimize the complexity of the mixtures, such as fine control of the relative amount of reactives, or the activation of certain positions *via* previous metallation of the ligand. However,  $\beta$ -substitution of Cors is usually highly regioselective, with pyrroles closer to the direct pyrrole-pyrrole link being more reactive.

Halogenation of the  $\beta$ -positions is particularly relevant due to the consecutive functionalization of the Cor *via* different Pd-Catalyzed cross-coupling reactions. In all cases, a halogenating agent is employed, and the substitution pattern can be slightly controlled. Regarding bromo derivatives, full bromination of free-base and metallated Cors are

---

<sup>111</sup> Capar, C.; Thomas, K. E.; Gosh, A. *J. Porphyrins Phthalocyanines* **2008**, *12*, 964.

<sup>112</sup> Ngo, T. H.; Van Rossom, W.; Dehaen, W.; Maes, W. *Org. Biomol. Chem.* **2009**, *7*, 439.

<sup>113</sup> Liu, H. Y.; Chen, L.; Yam, F.; Zhan, H. Y.; Ying, X.; Wang, X. L.; Jiang, H. F.; Chang, C. K. *Chin. Chem. Lett.* **2008**, *19*, 1000.

<sup>114</sup> Stefanelli, M.; Shen, J.; Zhu, W.; Mastroianni, M.; Mandoj, F.; Nardis, S.; Ou, Z.; Kadijah, K. M.; Fronczek, F. R.; Smith, K. M.; Paolesse, R. *Inorg. Chem.* **2009**, *48*, 6879.

<sup>115</sup> a) Sinha, W.; Kar, S. *Organometallics* **2014**, *33*, 6550. b) Patra, B.; Patra, S.K.; Mukherjee, P.; Maurya, Y.K.; Sinha, W.; Kar, S. *Eur. J. Inorg. Chem.* **2017**, 2363.

obtained employing NBS or Br<sub>2</sub> as the substitution agents.<sup>95,116</sup> Changing the solvent or the metal returns different patterns, going from mono- to hexabrominated derivatives.<sup>102,117</sup>

In the case of chloro<sup>107,118</sup> and iodo<sup>119</sup> derivatives, the methodology follows the same trend. Different proportions of halogenating agents, solvents and metal returns an apparently unsystematic pattern that can be normalized by correctly adjusting those variables. Particularly, Osuka and co-workers chlorinated the *meso*-free position of a series of electro-deficient Cors.<sup>103b-c</sup>

Formylation reactions<sup>103a,120</sup> were one of the first functionalization reactions performed over Cors. The introduction of a formyl group directly into the *meso*- or  $\beta$ -positions can be obtained by the Vilsmeier-Haack reaction over free-base and metallated Cors. The selectivity of the reaction is quite high, generally obtaining a low number of isomers.

Other functionalization methodologies include sulfonation/chlorosulfonation<sup>121</sup> carboxylation<sup>122</sup> or nitration.<sup>103a,123</sup> Once derivatized, they provide Cors of an amphiphilic character.

---

<sup>116</sup> a) Mahammed, A.; Tumanskii, B.; Gross, Z. *J. Porphyrins Phthalocyanines* **2011**, *15*, 1275. b) Wasbotten, I. H.; Wondimagegn, T.; Ghosh, A. *J. Am. Chem. Soc.* **2002**, *124*, 8104.

<sup>117</sup> a) Nardis, S.; Mandoj, F.; Paolesse, R.; Fronczek, F. R.; Smith, K. M.; Prodi, L.; Montalti, M.; Battistini, G. *Eur. J. Inorg. Chem.* **2007**, 2345. b) Du, R.-B.; Liu, C.; Shen, D.-M.; Chen, Q.-Y. *Synlett* **2009**, *16*, 2701. c) Nardis, S.; Pomarico, G.; Mandoj, F.; Fronczek, F. R.; Smith, K. M.; Paolesse, R. *J. Porphyrins Phthalocyanines* **2010**, *14*, 752.

<sup>118</sup> a) Mahammed, A.; Botoshansky, M.; Gross, Z. *Dalt. Trans.* **2012**, *41*, 10938 b) Ooi, S.; Yoneda, T.; Tanaka, T.; Osuka, *Chem. Eur. J.* **2015**, *21*, 7772. c) Ooi, S.; Tanaka, T.; Osuka, *J. Porphyrins Phthalocyanines* **2016**, *20*, 274. d) Ali, A.; Cheng, F.; Wen, W.-H.; Ying, X.; Kandhadi, J.; Wang, H.; Liu, H.-Y.; Chang, C.-K. *Chinese Chemical Letters* **2018**, *29*, 1888.

<sup>119</sup> Vestfrid, J.; Goldberg, I.; Gross, Z. *Inorg. Chem.* **2014**, *53*, 10536.

<sup>120</sup> a) Paolesse, R.; Jaquinod, L.; Senge, M. O.; Smith, K. M. *J. Org. Chem.* **1997**, *95616*, 6193. b) Paolesse, R.; Nardis, S.; Venanzi, M.; Mastroianni, M.; Russo, M.; Fronczek, F. R.; Vicente, M. G. H. *Chem. Eur. J.* **2003**, *9*, 1192. c) Vale, L. S. H. P.; Barata, J. F. B.; Santos, C. I. M.; Neves, M. G. P. M. S.; Faustino, M. A. F.; Tomé, A. C.; Silva, A. M. S.; Paz, F. A. A.; Cavaleiro, J. A. S. *J. Porphyrins Phthalocyanines* **2009**, *13*, 358.

<sup>121</sup> a) Mahammed, A.; Goldberg, I.; Gross, Z. *Org. Lett.* **2001**, *3*, 3443. b) Gross, Z.; Mahammed, A. *J. Porphyrins Phthalocyanines* **2002**, *6*, 553. c) Mahammed, A.; Gross, Z. *J. Porphyrins Phthalocyanines* **2010**, *14*, 911. d) Naitana, M. L.; Nardis, S.; Lentini, S.; Cicero, D. O.; Paolesse, R. *J. Porphyrins Phthalocyanines* **2015**, *19*, 735.

<sup>122</sup> Saltsman, I.; Goldberg, I.; Gross, Z. *Tetrahedron Lett.* **2003**, *44*, 5669.

<sup>123</sup> a) Stefanelli, M.; Mastroianni, M.; Nardis, S.; Licocchia, S.; Fronczek, F. R.; Smith, K. M.; Zhu, W.; Ou, Z.; Kadish, K. M.; Paolesse, R. *Inorg. Chem.* **2007**, *46*, 10791. b) Mastroianni, M.; Zhu, W.; Stefanelli, M.; Nardis, S.; Fronczek, F. R.; Smith, K. M.; Ou, Z.; Kadish, K. M.; Paolesse, R. *Inorg. Chem.* **2008**, *47*, 11680. c) Stefanelli, M.; Mandoj, F.;

Isocorroles are Cors in which one of the *meso*-substituted carbon atom is  $sp^3$  hybridized. Consequently, isocorrole is a non-aromatic macrocycle with dianionic character (Figure 13). A protocol for the conversion of Cors into isocorroles has been reported by Paolesse and co-workers, in which *meso*-triarylCors react with DDQ in methanol to give a mixture of two isomeric monosubstituted isocorroles.<sup>124</sup> The presence of electron-withdrawing groups difficults the reaction, and may even prevent it.

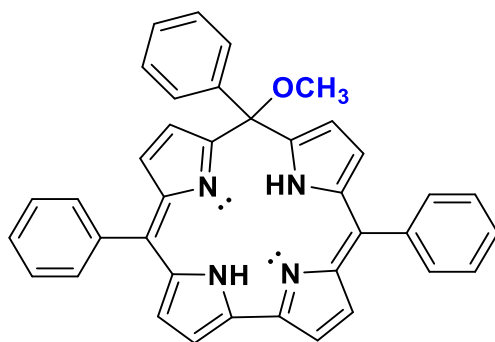


**Figure 13.** Structure of 10-methoxy-5,10,15-triphenylisocorrole.<sup>119a</sup>

The coordination behaviour of isocorroles with different metal ions has shown that the stability of the complex depends upon the coordinated metal. If a formal oxidation state higher than +2 is accessible, a metal-to-ligand charge transfer may occur, with the consequent aromatization of the isocorrole to the corresponding MCor complex. Nevertheless, Ni(II), Cu(II), Fe(III), Mn(III) and Rh(III) complexes of 10,10-dimethyl-5,15-diphenylisocorroles have been obtained, and some of their crystal structures reported.<sup>125</sup>

## Properties of corroles

The appealing properties of Cors mainly arise from the contraction of its skeleton, due to their direct pyrrole-pyrrole link. As typical tetrapyrrolic aromatic macrocycles,

---

Mastroianni, M.; Nardis, S.; Mohite, P.; Fronczek, F. R.; Smith, K. M.; Kadish, K. M.; Xiao, X.; Ou, Z.; Chen, P.; Paolesse, R. *Inorg. Chem.* **2011**, *50*, 8281. d) Stefanelli, M.; Pomarico, G.; Tortora, L.; Nardis, S.; Fronczek, F. R.; McCandless, G. T.; Smith, K. M.; Manowong, M.; Fang, Y.; Chen, P.; Kadish, K. M.; Rosa, A.; Ricciardi, G.; Paolesse, R. *Inorg. Chem.* **2012**, *51*, 6928.

<sup>124</sup> a) Nardis, S.; Pomarico, G.; Fronczek, F. R.; Vicente, M. G. H.; Paolesse, R. *Tetrahedron Lett.* **2007**, *48*, 8643.

b) Pomarico, G.; Xiao, X.; Nardis, S.; Paolesse, R.; Fronczek, F. R.; Smith, K. M.; Fang, Y.; Ou, Z.; Kadish, K. M. *Inorg. Chem.* **2010**, *49*, 5766.

<sup>125</sup> Setsune, J.; Tsukajima, A.; Okazaki, N. *J. Porphyrins Phthalocyanines* **2009**, *13*, 256.

unsubstituted free-base Cors are expected to be planar. However, several crystallographic studies have revealed important deviations from the planarity, regardless the substitution pattern (Figure 14).<sup>85b-c,91a,126</sup> A comparison between several crowded Cors and their Por analogues has been made. The crystal structures of *meso*-tris-(pentafluorophenyl)Cor ( $H_3[TPC]$ )<sup>91a</sup> and  $\beta$ -octabromo-*meso*-tris-(pentafluorophenyl)Cor ( $H_3[Br_8TPC]$ )<sup>121b,c</sup> are both distorted, being the later more deviated from the planarity. However, from the analogous Pors, *meso*-tetrakis-(pentafluorophenyl)Por ( $H_2[TPFPP]$ ) is planar, whereas  $\beta$ -octabromo-*meso*-tetrakis-(pentafluorophenyl)Por ( $H_2[Br_8TPP]$ ) is partially distorted.<sup>127</sup> On the other hand,  $\beta$ -octafluoro-*meso*-tetrakis-(pentafluorophenyl)Por ( $H_2[F_8TPP]$ ) is completely planar.<sup>128</sup> All this statements suggest that the non-planarity of the free-base Cors is mainly driven by steric interactions between the three inner protons, and slightly enhanced by the peripheral substitution pattern.

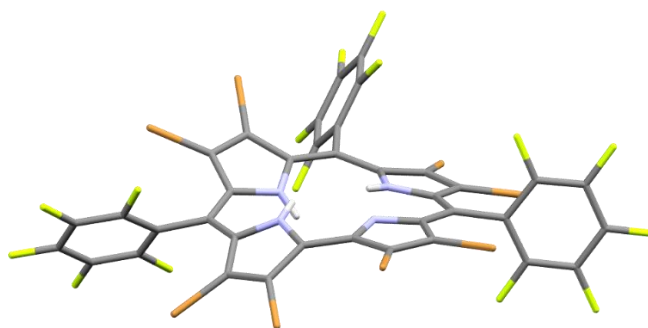


**Figure 14.** X-ray structure of  $\beta$ -octabromo-*meso*-tris(pentafluorophenyl)Cor. Ref. 121.

Metallation of Cors generally results in essentially planar macrocycles, even for peripherally crowded complexes.<sup>129</sup> This behavior supports the particular saddling of free-base Cors. However, CuCors are inherently saddled, even if they are sterically unhindered.<sup>130</sup> Its non-planarity is driven by an specific  $Cu(d_{x^2-y^2})-Cor(\pi)$  orbital interaction.

<sup>126</sup> Capar, C.; Hansen, L.-K.; Conradie, J.; Ghosh, A. *J. Porphyrins Phthalocyanines* **2010**, *14*, 509.

<sup>127</sup> Birnbaum, E. R.; Hodge, J. A.; Grinstaff, M. W.; Schaefer, W. P.; Henling, L.; Labinger, J. A.; Bercaw, J. E.; Gray, H. B. *Inorg. Chem.* **1995**, *34*, 3625.

<sup>128</sup> Leroy, J.; Bondon, A.; Toupet, L. *Acta Cryst.* **1999**, *C55*, 464.

<sup>129</sup> Thomas, K. E.; Alemayehu, A. B.; Conradie, J.; Beavers, C. M.; Ghosh, A. *Acc. Chem. Res.* **2012**, *45*, 1203.

<sup>130</sup> Alemayehu, A. B.; Gonzalez, E.; Hansen, L. K.; Ghosh, A. *Inorg. Chem.* **2009**, *48*, 7794.

Another exception comes from a family of sterically crowded silver  $\beta$ -octabromo-*meso*-tris(phenyl)Cors (Ag[Br<sub>8</sub>TPC]), which presents the same nature.<sup>131</sup> This is also an indicative of the ligand noninnocence in the Cu and Ag[Br<sub>8</sub>TPC] Cors.

As mentioned above, free-base Cors are more acidic than the corresponding porphyrins.<sup>132</sup> Different from Pors, Cors can be deprotonated in water solutions. They readily form monoanionic species in weakly basic solvents like DMF, and this behavior is enhanced when substituted by electron-withdrawing moieties. Acidic solvents are able to generate monoprotonated Cor species (Figure 15).<sup>133</sup> Both monoanionic and monocationic forms conserve its aromaticity. Particularly, the Q-bands of both species are more intense than their neutral form, and resemble those of Pors, due to the total symmetry recovery upon protonation/deprotonation.<sup>134</sup> Strongly acidic conditions, however, may disrupt the aromaticity by protonation of one of the *meso*- positions.

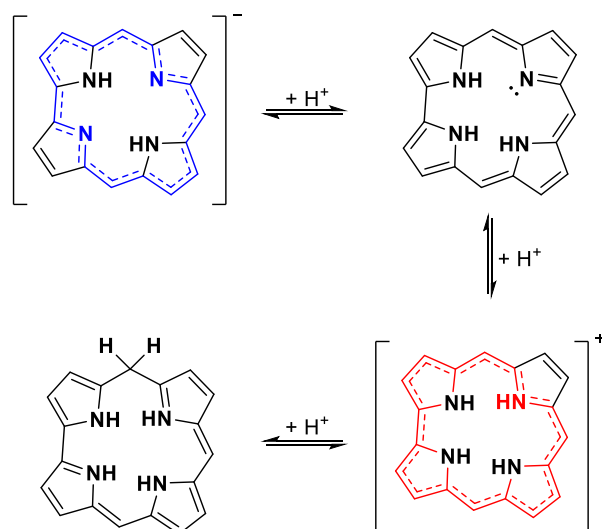


**Figure 15.** Aromatic distribution and structural changes of free-base Cors in acidic and basic media.

<sup>131</sup> a) Thomas, K. E.; Vazquez-Lima, H.; Fang, Y.; Song, Y.; Gagnon, K. J.; Beavers, C. M.; Kadish, K. M.; Ghosh, A. *Chem. Eur. J.* **2015**, *21*, 16839. b) Sarangi, R., Giles, L. J., Thomas, K. E., & Ghosh, A. *Eur. J. Inorg. Chem.* **2016**, *20*, 3225.

<sup>132</sup> Mahammed, A.; Weaver, J. J.; Gray, H. B.; Abdelas, M.; Gross, Z. *Tetrahedron Letters* **2003**, *44*, 2077.

<sup>133</sup> Paolesse, R. In *The Porphyrin Handbook*; Kadish, K. M., Smith, K. M., Guillard, R. Eds.; Academic Press: San Diego, CA, **2000**, Vol. 2, 201.

<sup>134</sup> Shen, J.; Shao, J.; Ou, Z.; E, W.; Koszarna, B.; Gryko, D. T.; Kadish, K. M. *Inorg. Chem.* **2006**, *45*, 2251.

Cors follow Gouterman's four orbital model.<sup>47</sup> Their UV/Vis spectra are qualitatively similar to those of analogous Pors presenting two main electronic transitions (Figure 16). At 400-450 nm, an intense Soret band that originates from the  $S_0 \rightarrow S_2$  transition; at 500-600 nm, three weaker Q-bands coming from the  $S_0 \rightarrow S_1$  transition. The presence of three bands instead of one may be attributed to the lack of symmetry. However, they are vibronically admitted, like Q-bands of Pors. Their absorption coefficients ( $\epsilon^\circ$ ) display values of  $\epsilon = 1-2 \times 10^5 \text{ M}^{-1} \text{ cm}^{-1}$  for the Soret band and  $1-2 \times 10^4 \text{ M}^{-1} \text{ cm}^{-1}$  for the Q-bands.

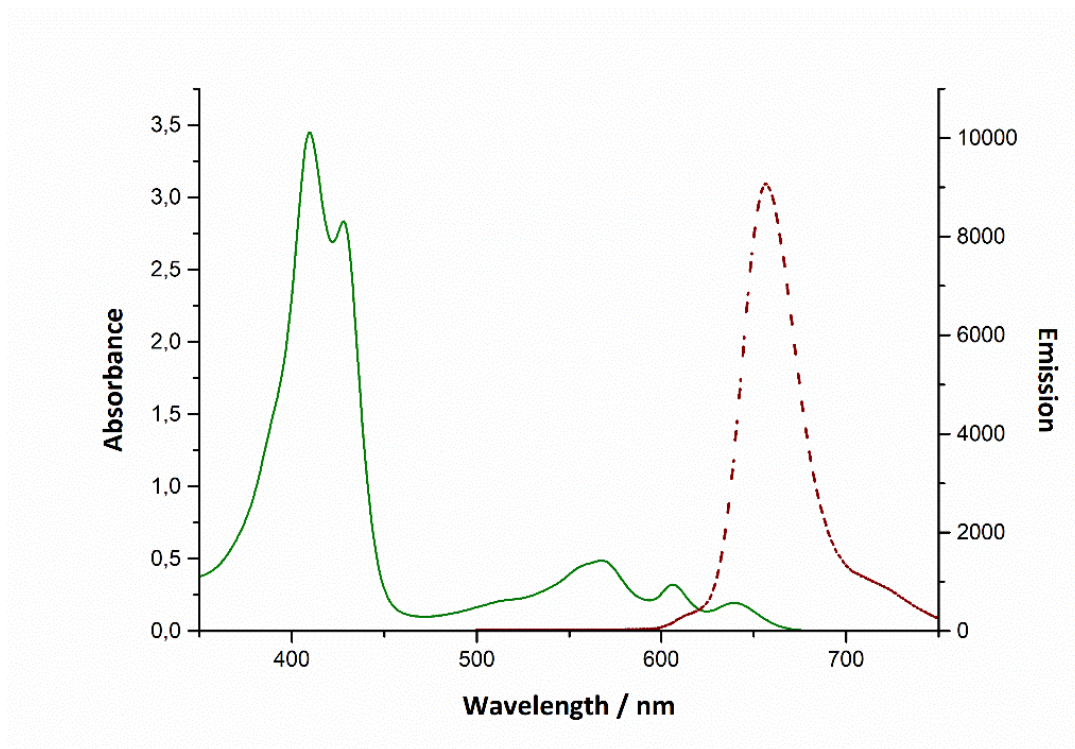


**Figure 16.** Absorption and emission spectra of 5,15-bis(Mesityl)-10-(4-Methoxyphenyl)CorroleH<sub>3</sub>.

The absorption spectra of free-base Cors are sensible to the modification of their substituents.<sup>126a</sup> Particularly, in the case of metallotriarylCors inducing a noninnocent

ligand character, such as Cu,<sup>111b</sup> FeCl,<sup>135</sup> FeNO<sup>136</sup> and MnCl,<sup>137</sup> the Soret band redshifts in response to the increasing donor character of their *meso*-aryl *para*-substituents, whereas for innocent complexes, such as Au,<sup>138</sup> CrO,<sup>139</sup> MoO or OsN<sup>140</sup> Cors, that sensitivity is not exhibited. This sensitivity is thought to arise from one or more transitions with aryl-to-Cor charge-transfer character in the Soret region, and appear only in ligands without a formal oxidation state.

Cors show an intense emission band around 600-700nm, arising from the lowest  $\pi \rightarrow \pi^*$  transition. Lifetime is at the nanosecond region, with very low Stokes shifts and fluorescence quantum yields ( $\phi_F$ ) typically around 0.10-0.20, with singlet excited states of *ca.* 1.8-2.1 eV.

Cors are easier oxidized than Pors, due to their higher electronic density. Electrochemical reduction and oxidation values highly depend on the substitution pattern, the solvent and the MCor complex.<sup>141</sup> For example, for a series of Cu complexes, first half-wave oxidation potential move from -0.11V to 0.75V vs. SCE upon increasing the electron-withdrawing substitution pattern, whereas first half-wave reduction potential goes from -1.95V to -1.03V vs. SCE.<sup>142</sup> In the case of free-base Cors, the formation of irreversible electroactive species during electrochemical studies results in a complicated redox behaviour involving multiple redox processes and multiple coupled chemical reactions from several forms of the Cor in solution (Figure 17).<sup>141</sup>

---

<sup>135</sup> a) Steene E.; Wondimagegn T.; Ghosh, A. *J. Phys. Chem. B* **2001**, *105*, 11406.; addition/correction *J. Phys. Chem. B* **2002**, *106*, 5312.; b) Roos, B. O.; Veryazov, V.; Conradie, J.; Taylor, P. R.; Ghosh, A. *J. Phys. Chem. B* **2008**, *112*, 14099.

<sup>136</sup> Vazquez-Lima, H.; Norheim, H.-K.; Einrem, R. F.; Ghosh, A. *Dalton Trans.* **2015**, *44*, 10146.

<sup>137</sup> Ghosh, A.; Steene, E.; *J. Inorg. Biochem.* **2002**, *91*, 423.

<sup>138</sup> a) A. B. Alemayehu, A. B.; Ghosh, A. *J. Porphyrins Phthalocyanines* **2011**, *15*, 106 b) Thomas, K. E.; Alemayehu, A. B.; Conradie, J. B.; Beavers, C. M.; Ghosh, A. *Inorg. Chem.* **2011**, *50*, 12844.

<sup>139</sup> Johansen, I.; Norheim, H.-K.; Larsen, S.; Alemayehu, A. B.; Conradie, J.; Ghosh, A. *J. Porphyrins Phthalocyanines* **2011**, *15*, 1335.

<sup>140</sup> Alemayehu, A.; Gagnon, K. J.; Turner, J.; Ghosh, A. *Angew. Chem. Int. Ed.* **2014**, *53*, 14411; *Angew. Chem.* **2014**, *126*, 14639.

<sup>141</sup> Fang, Y.; Ou, Z.; Kadish, K. M. *Chem. Rev.* **2017**, *117*, 3377.

<sup>142</sup> Ou, Z.; Shao, J.; Zhao, H.; Ohkubo, K.; Wasbotten, I. H.; Fukuzumi, S.; Ghosh, A.; Kadish, K. M. *J. Porphyrins Phthalocyanines* **2004**, *8*, 1236.

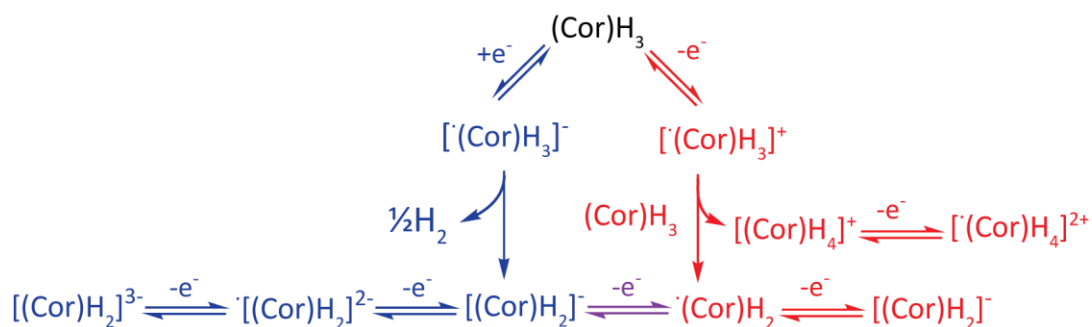


**Figure 17.** Proposed electron transfer mechanism for oxidation of  $(\text{Cor})\text{H}_3$  in PhCN. Credits: Ref. 141.

## Applications of Corroles

The growth experienced upon developing of easy an accessible synthetic methodologies have led to an exponential rise in the exploration of Cors as possible materials for diverse fields.<sup>143</sup> Thanks to its ability to stabilize high valence oxidation states, its role as catalyst has been key in oxidative, reductive and group transfer catalysis, leading into a wide number of publications.<sup>144</sup> Particularly, Cao *et al.* recently reported the improved efficiency in catalyzing the oxygen reduction reaction (ORR) by using CNT-Cobalt Cors hybrids (Figure 18).<sup>138g</sup>

<sup>143</sup> Aviv, I.; Gross, Z. *Chem. Commun.* **2007**, 20, 1987. b) Aviv-Harel, I.; Gross, Z. *Chem. Eur. J.* **2009**, 15, 8382.

<sup>144</sup> a) Gross, Z.; Golubkov, G.; Simkhovich, L. *Angew. Chem., Int. Ed.* **2000**, 39, 4045. b) Mahammed, A.; Gray, H. B.; Meier-Callahan, A. E.; Gross, Z. *J. Am. Chem. Soc.* **2003**, 125, 1162. c) Gross, Z.; Gray, H. B. *Adv. Synth. Catal.* **2004**, 364, 165. d) Dogutan, D. K.; Stoian, S. A.; McGuire, R.; Schwalbe, M.; Teets, T. S.; Nocera, D. G. *J. Am. Chem. Soc.* **2011**, 133, 131. e) Dogutan, D. K.; McGuire, R.; Nocera, D. G. *J. Am. Chem. Soc.* **2011**, 133, 9178. f) Lei, H.; Li, X.; Meng, J.; Zheng, H.; Zhang, W.; Cao, R. *ACS Catal.* **2019**, 9, 4320. g) Meng, J.; Lei, H.; Li, X.; Qi, J.; Zhang, W.; Cao, R. *ACS Catalysis* **2019**, 9, 4551.

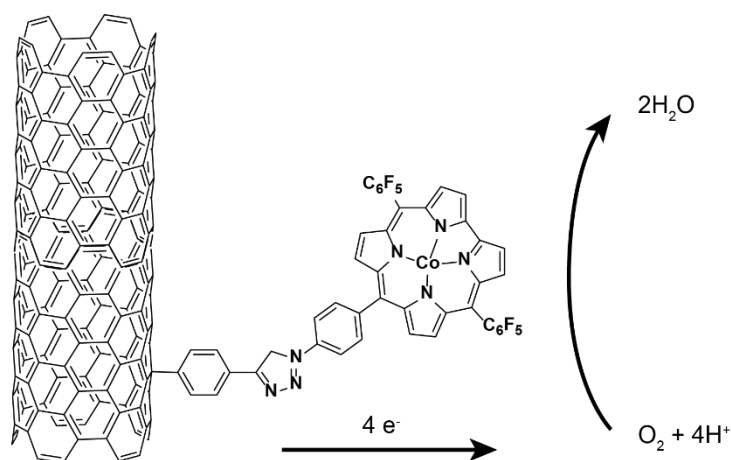


**Figure 18.** Carbon nanotubes-Cobalt Cor hybrids for the catalysis of  $O_2$  reduction reaction. *Ref. 144g.*

Due to its outstanding photophysical properties, Cors has also been tested as sensitizers in organic solar cells.<sup>145</sup> Particularly, Che *et al.* reported a solution-processed OSC based on a gold (III) Cor has been employed for the fabrication of the device, reaching power conversion efficiencies (PCE) of up to 6.0%, those values being among the best reported for both vacuum-deposited and solution-processed OSCs fabricated with metallorganic complexes.<sup>143c</sup>

Recently, an exhaustive review has been published of the use of Cors in photodynamic therapy (PDT).<sup>146</sup> In comparison with Pors, they demonstrated superior efficiency in inhibition of endothelial cell proliferation, tumor progression and metastasis.

Cors has also been extensively employed as sensing materials, with excellent results<sup>147</sup>. This topic will be deeply discussed in *Chapter 2*.

<sup>145</sup> a) Walker, D.; Chappel, S.; Mahammed, A.; Brunshwig, B. S.; Winkler, J. R.; Gray, H. B.; Zaban, A.; Gross, Z. *J. Porphyr. Phthalocyanines* **2006**, *10*, 1259. b) Lai, S.-L.; Wang, L.; Yang, C.; Chan, M.-Y.; Guan, X.; Kwok, C.-C.; Che, C.-M. *Adv. Funct. Mater.* **2014**, *24*, 4655. c) Sudhakar, K.; Giribabu, L.; Salvatori, P.; Angelis, F. D. *Phys. Status Solidi A* **2015**, *212*, 194.

<sup>146</sup> Teo, R. D.; Hwang, J. Y.; Termini, J.; Gross, Z.; Gray, H. B. *Chem. Rev.* **2017**, *117*, 2711.

<sup>147</sup> Paolesse, R.; Nardis, S.; Monti, D.; Stefanelli, M.; Di Natale, C. *Chem. Rev.* **2017**, *117*, 2517.

Its presence in energy and electron transfer arrays is constantly growing, as donor or acceptors, depending on their substitution pattern and counterparts. This will be extensively explored in *Chapter 1*.

# **Chapter 1: Subphthalocyanine- and Corrole-based molecular materials for energy conversion schemes**

## 1.1. Energy challenges in a non-so-far future

The current global economy is based on fossil fuels, in other words, fuels with an expiration date. Moreover, they are highly contaminating. Once the crude-oil and gas deposits are finished, the necessity of finding an alternative and clean primary energy source would not be an option but a requirement. For this reason, great efforts are being made in the development of technologies focused on the exploitation of alternative energy sources. Among them we can find the tidal, wind, hydroelectric, geothermic and, of course, solar energy. They all are old acquaintances, but that does not mean there is still no way for improvement.

Focusing on the solar energy, it consists in the conversion of the radiation coming from the Sun into energy, in that case electric one. It is a widely known mechanism thanks to the photosynthesis. In that process, the plants absorb the solar radiation through pigments or cytochromes, triggering a cascade of processes, culminating in the transformation of radiative into chemical energy, necessary to carry out the reduction reaction of  $\text{CO}_2$  to  $\text{O}_2$ , among other biological processes. The human being, as a dogma, has always tried to emulate nature, a master with billion years of experience upon its shoulders. With our knowledge, we try to somehow imitate and improve those energy collecting systems, generally known as antennas, due to their ability to transfer that energy from point A to point B, even when they are long separated in atomic terms. The efficiency in which they achieve this transfer, minimizing energy losses, is still far from what we are able to reach, but our investigations are in the good path. As a tool, we have designed molecular systems that pretend to emulate that cascade process.

The preparation of energy transfer arrays must be precisely designed, though only a few standards have to be taken into account in order to start developing this kind of systems. Analogously to a waterfall, energy transfer must be thermodynamically allowed. As the water in a cascade flowing in one direction, the energy in an antenna cannot go from a lower to a higher energy state, but it is transferred downwards until reaching an equilibrium state. In the antennas, those energetic states are generated from the interaction between the molecular orbitals from each of the components of our system. In molecular materials chemistry, those systems are commonly known as donor-acceptor (D-A) systems, based in this unidirectional idea. Complexity of those systems goes from a

single molecule to the junction of plenty of them, through intra- or supramolecular interactions, as in the case of cytochromes found in chloroplasts.

Within the study of those antennas, they fulfil two different processes, known as photoinduced energy transfer (PET) and photoinduced electron transfer (PeT). Understanding the mechanisms that govern those processes is crucial for adjust and modulate our synthetic systems in order to achieve the highest possible efficiency.

PET is a process in which, once the radiative energy is absorbed by one of the two elements of a D-A system, indistinctly the donor (D) or the acceptor (A), it is transferred to another one. On the other hand, in the case of the PeT process, once the radiative energy is absorbed, it is employed for the transfer of electrons between the two elements. Though similar in concept, different mechanisms are displayed for both processes.

Two different mechanisms can be found among the PET processes. Both of them are mutually exclusive, being validated depending on the distance between the donor and the acceptor, and the interactions between them. At short distances, the electron exchange energy transfer, also referred in literature as Dexter energy transfer, prevails, by the establishment of a strong orbitalic interaction. Despite being formally an energy transfer process, it arises from a simultaneous double electron transfer. Upon absorption of energy, the D fragment becomes excited, promoting an electron transfer from the lowest-occupied molecular orbital (LUMO) of D to the LUMO of A. Simultaneously, one of the electrons located at the highest-occupied molecular orbital (HOMO) of A is transferred to the hole generated at the HOMO of D. The result is an apparent energy transfer in which one excited fragment, namely exciton, returns to its ground state, with the subsequent excitation of another fragment (Figure 19, top).

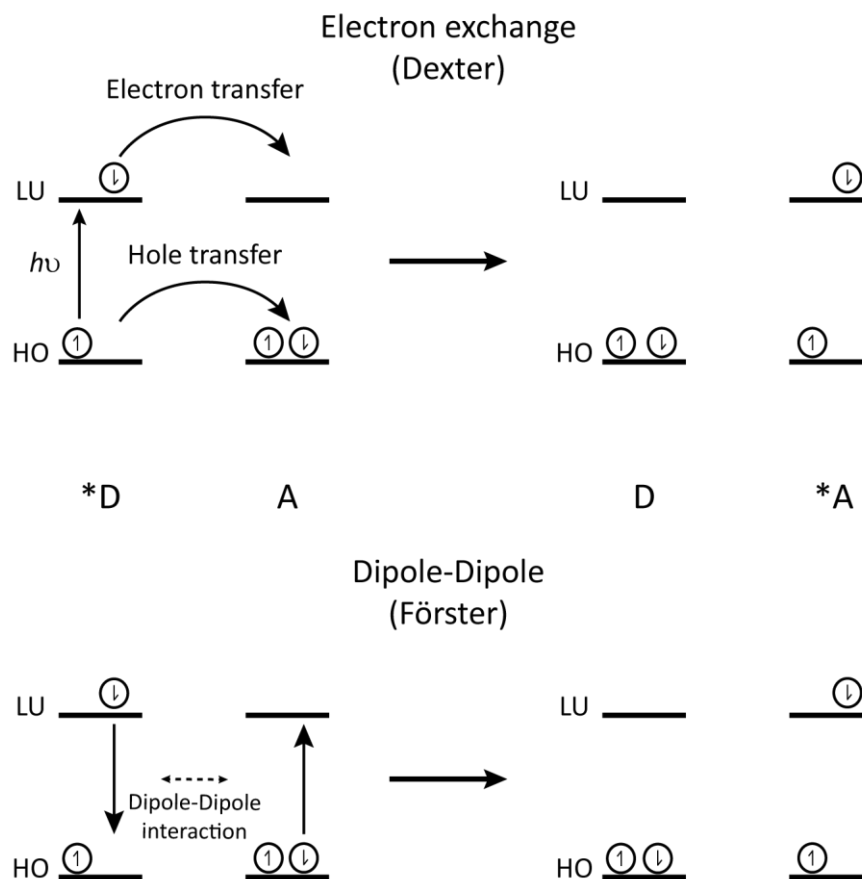


**Figure 19.** Comparison between the electron exchange and dipole-dipole of electronic energy transfer. The spin of the electrons exchanged must obey the spin conservation rules.

At longer distances, however, Dexter mechanism does not take place, since orbitalic overlapping between D and A cannot be fulfilled. This drawback makes the Dexter energy transfer constant to drop dramatically at distances generally longer than  $10 \text{ \AA}$ . Dipole-dipole energy transfer, also known as Förster energy transfer mechanism, is based on the absorption of radiative energy by an element, relaxation to its ground state and subsequent reabsorption of the irradiated energy by another element. Analogously to Dexter, the element that in first stage gets the energy absorbed and emitted is identified as D, whereas the one reabsorbing the energy is called A (Figure 19, bottom). The dipole-dipole interaction operates through an oscillating electric field produced by the excited donor (\*D), not

requiring Van der Waals contact between D and A, neither overlap of the orbitals. Since this is a mechanism based on a dipole-dipole oscillation between two elements, some conditions are required, the most important being that emission energy levels of D must overlap absorption energy levels of A. High fluorescence quantum yield values for D and high molar coefficient absorption values for A are required for the energy transfer to occur in an effective way.

As observed in Figure 20, Dexter mechanism exponentially falls upon increasing the D-A distance, whereas the Förster mechanism does in a 6-factor. Consequently, in a hypothetical exemplar, even at values of  $R_{D-A} \sim 30-40 \text{ \AA}$ , dipole-dipole energy transfer and non-radiative decay of  $^*D$  are still competitive, with no significant energy transfer coming by electron exchange. In favorable cases, the range of separation between  $^*D$  and A for energy transfer by the dipole-dipole mechanism can be much larger ( $>30 \text{ \AA}$ ) than the size of typical organic molecules ( $5-10 \text{ \AA}$ ). Therefore, Förster mechanism can be considered a more flexible process, allowing the different fragments to move in more lax separation values. Such mechanism will be always more effective if the elements involved are found in a preorganization state.

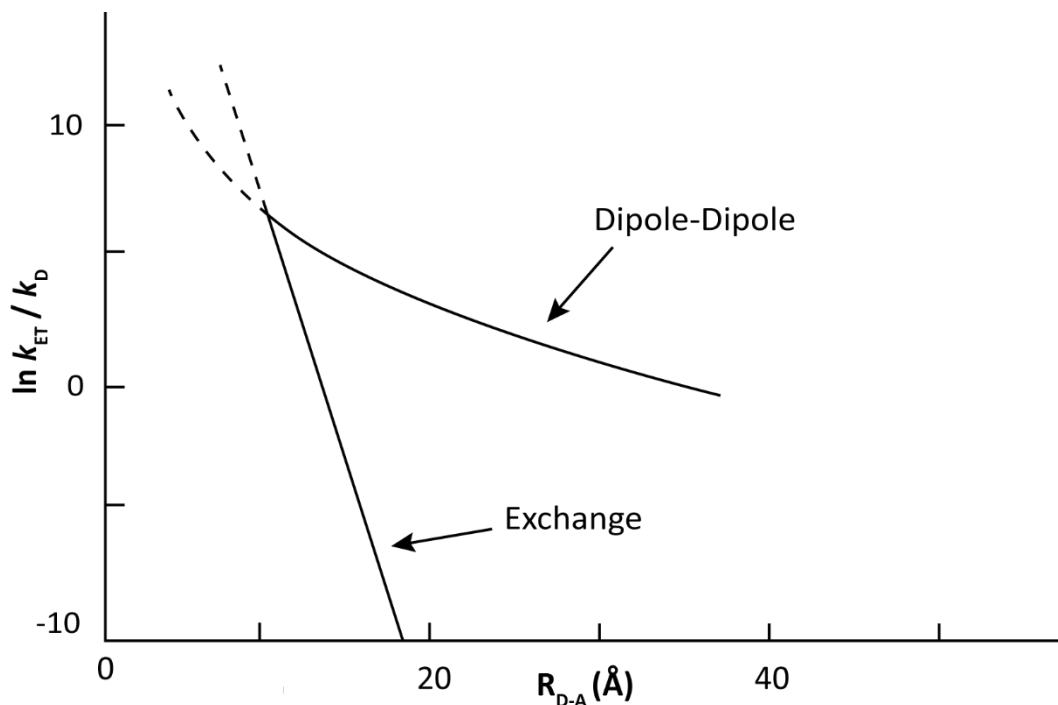


**Figure 20.** Hypothetical graphs of the rate ratio energy of energy transfer ( $k_{ET}$ ) to decay of  $^*D$  ( $k_D$ ) plotted as  $\ln k_{ET}/k_D$  vs.  $6\ln R_{DA}$  (dipole-dipole energy transfer) and vs.  $2R_{DA}/R_{DA}^0$  (exchange energy transfer).

Concerning the PeT, a simpler mechanism is *a priori* followed. However, the correct design of the involved elements required for the electron transfer to be effective can turn it into a more complicated process. During the electron transfer process, radiative energy is absorbed by D, and its electrons are excited. From the exciton, the electron located at the LUMO of  $^*D$  is transferred to the LUMO of A. A correct adjustment of the energetic levels makes none electron from the HOMO of A to be transferred back to the HOMO of D, as in the case of Dexter energy transfer. Therefore, a formal negative charge is generated upon reception of an additional electron by A, whereas a formal positive charge is generated by the hole located at the HOMO of D. This process can also happen inversely: excitation of A generates a hole into its HOMO. Next, one of the HOMO electrons of D is transferred to the HOMO of A, obtaining the same charge separated state by a different mechanism known as hole transfer. This charge transfer is the driving force of our systems, and its effectiveness at the time of conduct this transfer, our final objective.

At first glance, the electron transfer process  $D^* + A \rightarrow D^+ + A^-$  appears to be one of the simplest possible chemical reactions, since in an electron-transfer reaction no bonds appear to be formed or broken. However, this involves the creation of a pair of ions ( $D^+$  and  $A^-$ ), which will strongly interact with the solvent. Thus, the solvent may have to undergo considerable structural “reorganization” to accommodate and stabilize the new charged molecular system. Solvent reorganization and the influence of opposite charges on themselves and the solvent must be considered in the quantitative aspects of any theory of electron transfer. The change in free energy resulting from the reorganization of solvent molecules, as reactants converts into products during an electron-transfer reaction, is termed “solvent reorganization energy”.

The total reorganization energy ( $\lambda$ ) corresponds to the total internal and external reorganization energy that is required for an electron transfer to occur in an isoenergetic electron-transfer reaction. Note that  $\lambda$  is defined as an activation energy and is therefore always a positive energy value. This will be important when discussing both  $\lambda$  and the free energy change ( $\Delta G^\circ$ ) since the free energy of a reaction may be positive or negative, depending in whether the reaction is endothermic ( $\Delta G^\circ > 0$ ) or exothermic ( $\Delta G^\circ < 0$ ).

Marcus<sup>148,149</sup> proposed that the rate limiting feature of an elementary thermal electron transfer process requires only that the molecules and solvent involved in the electron transfer overcome an energy barrier at the crossing point of two potential energy (PE) surfaces.

---

<sup>148</sup> Marcus, R. A. *J. Chem. Phys.* **1956**, *24*, 966.

<sup>149</sup> Marcus, R. A. *Can. J. Chem.* **1959**, *37*, 155.

### 1.1.1. Marcus theory of electron transfer

Marcus' insight focused on an important question concerning electron transfer processes: What is the magnitude and the nature of the total reorganization energy changes required to prepare a system for electron transfer? In other words, *what is the energy required to reorganize the reactants and the solvent so that they are ready for the electron-transfer event at the crossing point along the reaction coordinate?* The energies of reactants and solvent can be conceptually divided into two types, termed *inner-* (molecular) and *outer-sphere* (supramolecular) reorganization energies. In Marcus' Theory, the term inner sphere refers to the internal molecular coordinates of the reactants and products (*i.e.* bond lengths and angles), while outer sphere refers to coordinates defining the arrangements of solvent molecules around the molecular reactants and products (supramolecular effects). Assuming that only a weak electronic interaction of the reactants (at the crossing point of two PE curves) is needed for a simple electron transfer process to occur,<sup>2</sup> the following physical model of the Arrhenius expressions was derived:

$$k_{et} = \nu_N \kappa \exp(-\Delta G^\ddagger / RT) \quad (1)$$

In equation (1), the term  $\nu_N$  is an electronic factor, effectively determining the maximum possible value for the electron transfer rate constant ( $k_{et}$ ). The transmission coefficient ( $\kappa$ ) determines the probability of the reactants that, once they reach the transition state, will successfully proceed to products. The  $\exp(-\Delta G^\ddagger/RT)$  factor represents the exponential dependence of rate on the free energy of activation as hypothesized by transition state reactivity theory.

An exemplar comparing Marcus and Libby's approaches, in which the reorganization energy was considered to occur "vertically", is depicted in Figure 21: the PE curve of the initial species (\*D-A) is represented by the parabola on the left and the energy curve of the final species (D<sup>+</sup>-A<sup>-</sup>) is represented by the parabola on the right. The x-axis represents the change in the geometry of the excited state and solvent on the way to the charge separated state. These curves are recognized as having the same form as the parabolas representing the PE as a function of separation for a harmonic oscillator. The harmonic oscillator approximation of the energy curves as parabolas allows for a powerful tool from geometry to make some remarkable predictions concerning the rate constants of

energy transfer reactions as a function of the *inner-* and *outer-*sphere reorganization energies involved in the electron transfer process.

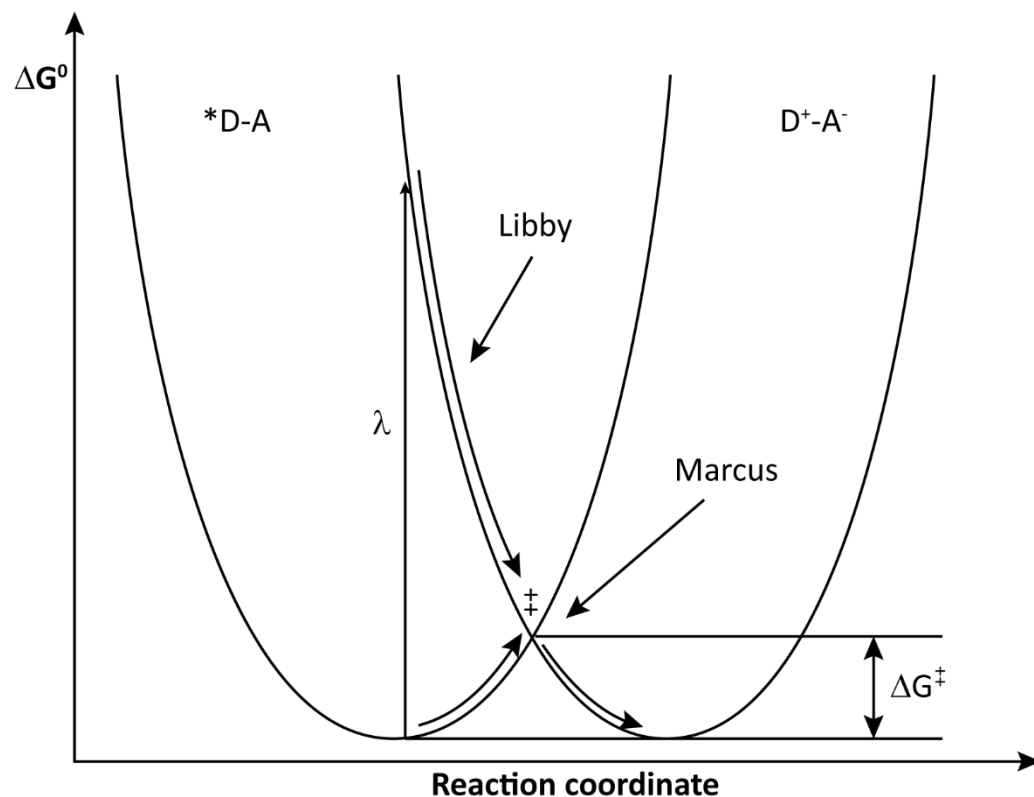


**Figure 21.** Potential energy description of an electron-transfer reaction with  $\Delta G^0 = 0$ . The point  $\ddagger$  represents the transition state. The energy  $\lambda$  is defined as the energy for the vertical jump from the ground state minimum of  $*D-A$  to the potential energy curve of  $D^+-A^-$ .

Marcus' Theory model provides a counterintuitive statement: as a reaction becomes more exothermic ( $\Delta G^0$  becomes more negative), the transition-state activation energy ( $\Delta G^\ddagger$ ) becomes smaller, until reaching a maximum electron transfer rate ( $\Delta G^\ddagger = 0$ ). However, as a reaction becomes increasingly exothermic, the values of  $\Delta G^\ddagger$  change and start increasing, reflecting a parabolic behavior. This is known as the Marcus' inverted region of electron transfer. Figure 22 shows the evolution of the PE curves as the relative *vertical* displacement of the minimum for the product curve relative to the reactant curve, leaving the reactants PE and the reaction coordinates fixed.

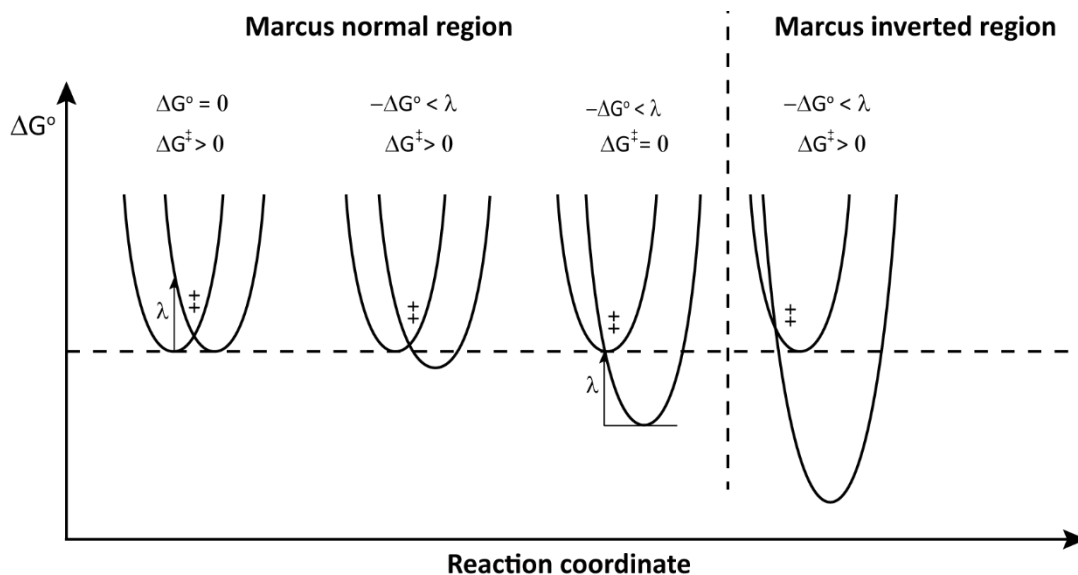


**Figure 22.** Representation of the relative vertical movement of the products curve with respect to the reactant curve. Values of  $\Delta G^\circ$  start decreasing until reaching the same value as  $\lambda$ , from which  $\Delta G^\ddagger$  equals zero.

From that behavior and equation (1), it is established the remarkable relationship between  $k_{et}$ ,  $\lambda$ ,  $\Delta G^\ddagger$ , and  $\Delta G^\circ$  given by equation (2).

$$k_{et} = \nu_N \kappa \exp(-\Delta G^\ddagger / RT) = \nu_N \kappa \exp([( -\Delta G^\circ + \lambda )^2 / 4\lambda] / RT) \quad (2)$$

This equation provides the theoretical link between the experimental rate constant ( $k_{et}$ ), the activation energy ( $\Delta G^\ddagger$ ), the reaction exothermicity ( $\Delta G^\circ$ , a negative value), and the reorganization energy ( $\lambda$ , a positive value) of an electron transfer reaction.

## 1.2. Specific objectives of Chapter 1

The main purpose of Chapter 1 is the synthesis and development of Cor- and SubPc-based D-A photoactive arrays, and their potential application as light-harvesting materials. This chapter is divided in four sections:

The first section is focused on the preparation of SubPc-Cor photoactive systems linked through one of Cor *meso*- positions, and the possibility of controlling electronic energy transfer (EET) events direction by fine-tailoring the substitution pattern (Figure 23). Although porphyrins (Pors) have been extensively employed as counterparts of Cors, the combination of SubPcs with Cors has not yet been explored. At first sight, the enhanced characteristics of the latter in comparison with Pors, such as easiness of oxidation, extended absorption range and higher extinction molar absorption coefficients, should set them as better suitable partners. In addition, the incorporation of copper corrole (CuCor) in those arrangements will be studied as an easy way to overturn the EET direction.

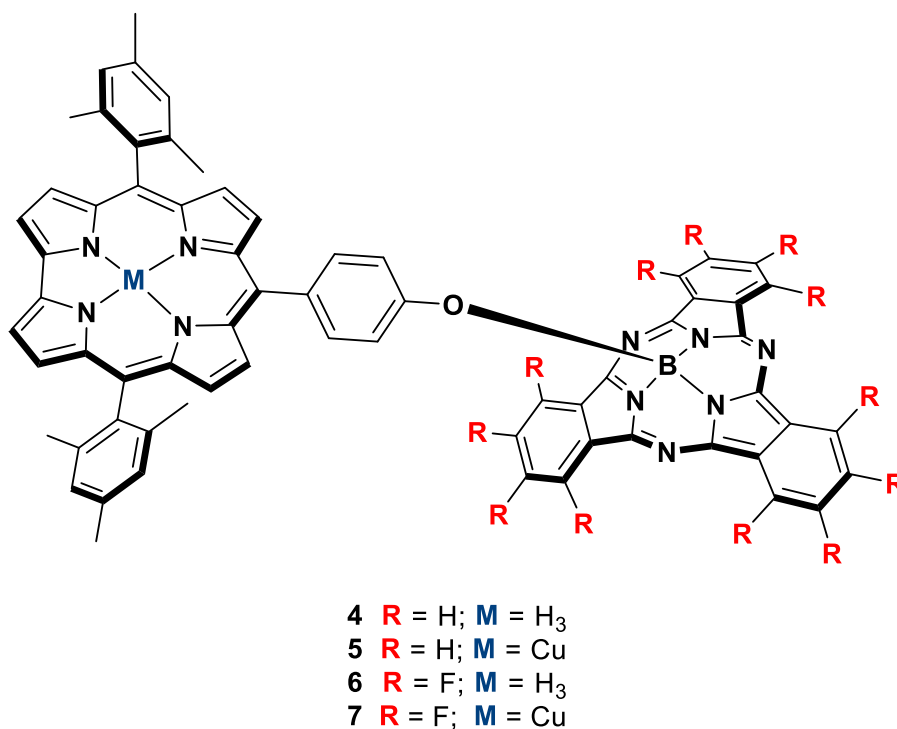


Figure 23. Schematic structure of SubPc-Cor (*meso*) dyads 4, 5, 6 and 7.

The second section is related to the preparation of SubPc-Cor photoactive systems, this time linked through Cor axial position (Figure 24). The literature lacks of examples where axial substitution of Corrs is employed. Due to its acceptor properties, P(V) complex of 5,10,15-tris(pentafluorophenyl)corrole (P-TPPCor) will be employed. Due to the reduced number of Cor inner phosphorous activation methodologies, the axial substitution reaction of these derivatives is quite unexplored. For this reason, several procedures will be tested in order to find a general substitution methodology. Finally, SubPcs will be incorporated over P-TPPCor axial position *via* a  $\mu$ -oxo bridge.

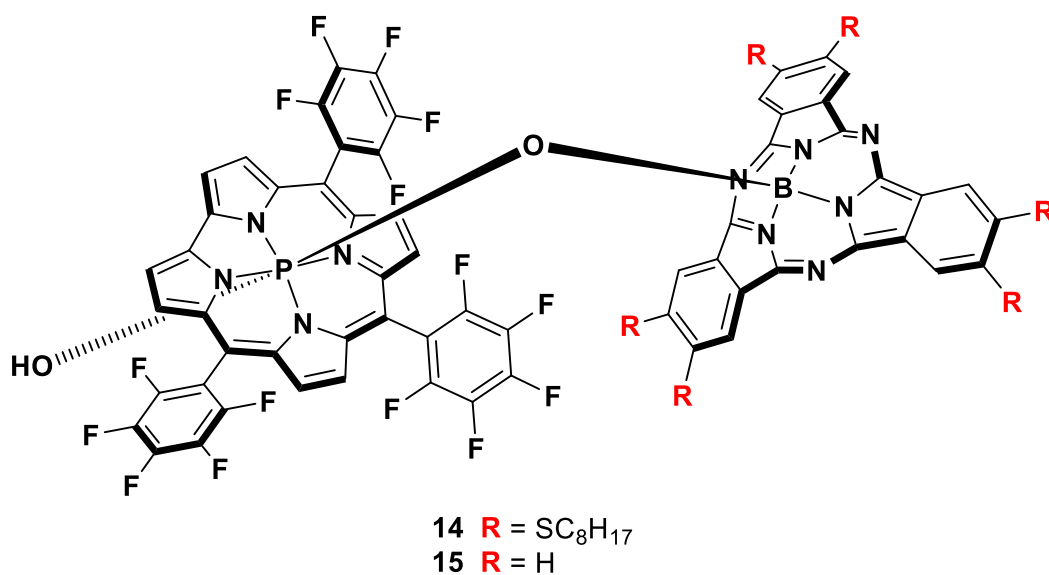


Figure 24. Schematic structure of SubPc-Cor (axial) dyads 14 and 15.

The third section comprises the synthesis of SubPc-Ferrocene (SubPc-Fc) arrays linked through an axial-ethynyl bridge (Figure 25). A methodology employing Sonogashira's palladium catalyzed cross-coupling reaction will be followed for the incorporation of new functionalization over ethynyl axially-substituted SubPcs. Additionally, the cyclotrimerization reaction of hexachloro-SubPc (SubPcCl<sub>6</sub>-Cl) will be optimized to increase the current yields.

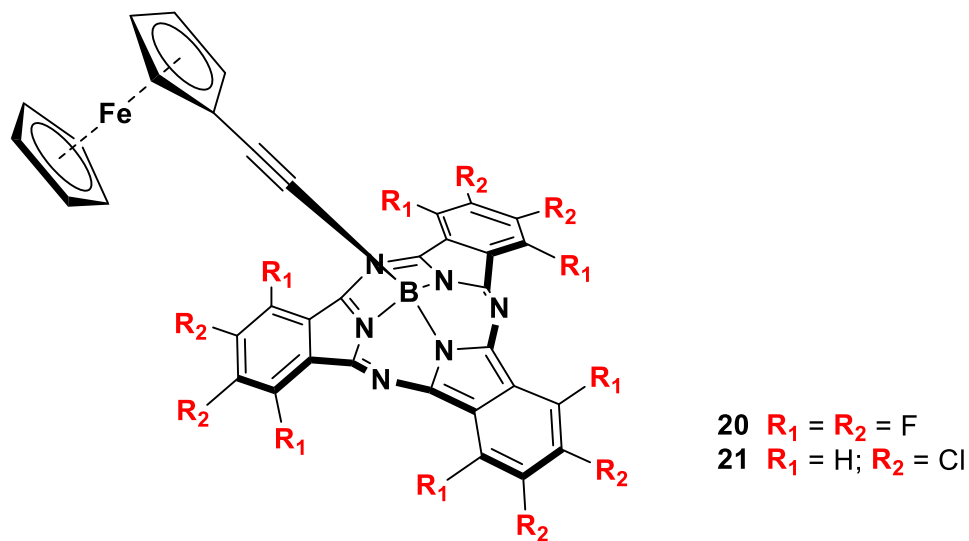


Figure 25. Schematic structure of SubPc-Fc dyads 20 and 21.

The fourth section introduces the synthesis of a tetracyanobutadiene-corrole (TCBD-Cor) photoactive array (Figure 26). Taking advantage of Cor protonation and deprotonation easiness, the photophysical properties based on its ionic state will be studied.

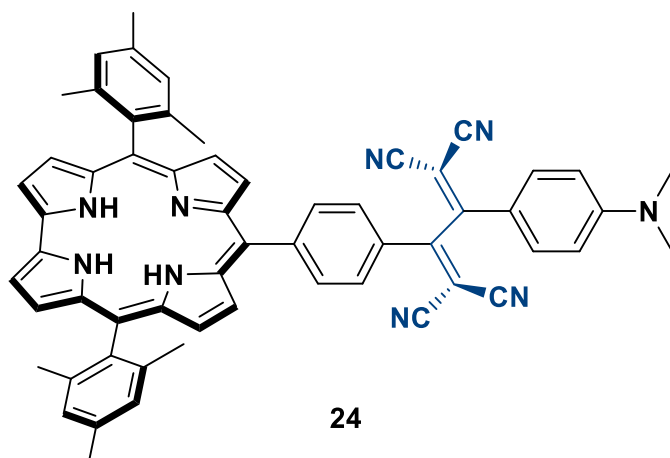


Figure 26. Schematic structure of TCBD-Cor dyad 24.

## 1.3. Background

### 1.3.1. Corroles and Subphthalocyanines as photoactive units

The particular shape and aromatic skeleton of SubPcs generates a series of optical and electronic properties that makes them suitable for their incorporation in D-A systems. In the context of solar energy conversion, their absorption in the UV-Vis frame with high excitation coefficient values confers them of high excitation energy values *ca.* 2.0 eV, which are ideal for the promotion of exergonic electron transfer processes. They are generally employed as electron acceptors, although their EET behavior can be regulated *via* fine tailoring of their substitution pattern. In this regard, our research group greatly contributed to the design of these particular systems,<sup>80</sup> and its combination with Pors,<sup>150</sup> Pcs,<sup>151</sup> Fcs<sup>152</sup> and curved carbon nanostructures,<sup>153</sup> particularly those with complementary curved surfaces *via* cooperative  $\pi$ - $\pi$  interactions,<sup>15,36a,37a,79,154</sup> have been extensively studied. In the latter, they have shown to efficiently perform EET events through intra- and supramolecular

<sup>150</sup> a) Xu, H.; Ng, D. K. P. *Inorg. Chem.* **2008**, *47*, 7921. b) El-Khouly, M. E.; Ju, D. K.; Kay, K.-Y.; D'Souza, F.; Fukuzumi, S. *Chem. Eur. J.* **2010**, *16*, 6193. c) Menting, R.; Lau, J. T. F.; Xu, H.; Ng, D. K. P.; Röder, B.; Ermilov, E. A. *Chem. Commun.* **2012**, *48*, 4597. d) Kasi Viswanath, L. C.; Shirtcliff, L. D.; Krishnan, S.; Darrell Berlin, K. *Dyes and Pigments* **2015**, *112*, 283. e) Managa, M.; Mack, J.; Gonzalez-Lucas, D.; Remiro-Buenamañana, S.; Tshangana, C.; Cammidge, A. N.; Nyokong, T. *J. Porphyrins Phthalocyanines* **2016**, *20*, 1. f) Bressan, G.; Cammidge, A. N.; Jones, G. A.; Heisler, I. A.; Gonzalez-Lucas, D.; Remiro-Buenamañana, S.; Meech, S. R. *J. Phys. Chem. A* **2019**, *123*, 5724.

<sup>151</sup> a) González-Rodríguez, D.; Claessens, C. G.; Torres, T.; Liu, S.; Echegoyen, L.; Vila, N.; Nonell, S. *Chem. Eur. J.* **2005**, *11*, 3881. b) Zhao, Z.; Cammidge, A. N.; Cook, M. J. *Chem. Commun.* **2009**, *48*, 7530. c) Fazio, E.; Winterfeld, K. A.; López-Pérez, A.; Torres, T.; Guldi, D. M.; de la Torre, G. *Nanoscale* **2018**, *10*, 22400. d) Berna, B. B.; Platzer, B.; Wolf, M.; Lavarda, G.; Nardis, S.; Galloni, P.; Torres, T.; Guldi, D. M.; Paolesse, R. *Chem. Eur. J.* **2020**, *26*, 13451.

<sup>152</sup> a) González-Rodríguez, D.; Torres, T.; Olmstead, M. M.; Rivera, J.; Herranz, M. Á.; Echegoyen, L.; Castellanos, C. A.; Guldi, D. M. *J. Am. Chem. Soc.* **2006**, *128*, 10680. b) González-Rodríguez, D.; Carbonell, E.; de Miguel Rojas, G.; Atienza Castellanos, C.; Guldi, D. M.; Torres, T. *J. Am. Chem. Soc.* **2010**, *132*, 16488. c) El-Khouly, M. E.; Kim, J.-H.; Kim, J.-H.; Kay, K.-Y.; Fukuzumi, S. *J. Phys. Chem. C* **2012**, *116*, 1970. d) Maligaspe, E.; Hauwiler, M. R.; Zatsikha, Y. V.; Hinke, J. A.; Solntsev, P. V.; Blank, D. A.; Nemykin, V. N. *Inorg. Chem.* **2014**, *53*, 9336. e) El-Khouly, M. E.; El-Kemary, M. A.; El-Refaei, A.; Kay, K.-Y.; Fukuzumi, S. *J. Porphyrins Phthalocyanines* **2016**, *20*, 1148. f) Swarts, P. J.; Conraide, J. *Inorganic Chemistry* **2020**, *59*, 7444.

<sup>153</sup> a) González-Rodríguez, D.; Torres, T.; Guldi, D. M.; Rivera, J.; Herranz, M. Á.; Echegoyen, L. *J. Am. Chem. Soc.* **2004**, *126*, 6301. b) Kc, C. B.; Lim, G. N.; D'Souza, F. *Chem. Eur. J.* **2016**, *22*, 13301.

<sup>154</sup> de la Torre, G.; Bottari, G.; Torres, T. *Advanced Energy Materials* **2017**, *7*, 1601700.

## Background

interactions. Particular examples employing boron-dipyrromethenes (BODIPYs),<sup>155</sup>  $\pi$ -extended aromatic structures<sup>156</sup> or tetracyanobutadiene (TCBD) derivatives<sup>157</sup> as their electronic counterparts have also been reported.

Over the last years, an increasing number of D-A systems involving Cors as photoactive units,<sup>158</sup> including the study of its photophysical properties,<sup>159</sup> have been described. Among them, there are several reported systems including BODIPYs,<sup>160</sup> Pors,<sup>161</sup> carbon nanostructures<sup>162</sup> and a wide number of  $\pi$ -aromatic extended organic frames and

---

<sup>155</sup> a) Ziessel, R.; Ulrich, G.; Elliott, K. J.; Harriman, A. *Chem. Eur. J.* **2009**, *15*, 4980. b) Çetindere, S.; Çoşut, B.; Yeşilot, S.; Durmuş, M.; Kılıç, A. *Dyes and Pigments* **2014**, *101*, 234.

<sup>156</sup> a) Mauldin, C. E.; Piliago, C.; Poulsen, D.; Unruh, D. A.; Woo, C.; Ma, B.; Mynar, J. L.; Fréchet, J. M. J. *ACS Appl. Mater. Interfaces* **2010**, *2*, 2833. b) Kasi Viswanath, L. C.; Shirtcliff, L. D.; Krishnan, S.; Handa, N. V.; Darrell Berlin, K. *Tetrahedron Letters* **2014**, *55*, 4199. c) El-Khouly, M. E.; El-Refaey, A.; Nam, W.; Fukuzumi, S.; Göktoğ, Ö.; Durmuş, M. *Photochem. Photobiol. Sci.* **2017**, *16*, 1512. d) Lavarda, G.; Zirzmeier, J.; Gruber, M.; Rami, P. R.; Tykewski, R. R.; Torres, T.; Guldi, D. M. *Angew. Chem. Int. Ed.* **2018**, *57*, 16291.

<sup>157</sup> a) Winterfeld, K. A.; Lavarda, G.; Guilleme, J.; Sekita, M.; Guldi, D. M.; Torres, T.; Bottari, G. *J. Am. Chem. Soc.* **2017**, *139*, 5520. b) Winterfeld, K. A.; Lavarda, G.; Guilleme, J.; Guldi, D. M.; Torres, T.; Bottari, G. *Chem. Sci.* **2019**, *10*, 10997.

<sup>158</sup> Flamigni, L.; Gryko, D. T. *Chem. Soc. Rev.* **2009**, *38*, 1635.

<sup>159</sup> Bevilacqua, A. C.; Köhler, M. H.; Piquini, P. C. *Braz J Phys* **2019**, *49*, 502.

<sup>160</sup> a) Brizet, B.; Desbois, N.; Bonnot, A.; Langlois, A.; Dubois, A.; Barbe, J.-M.; Gros, C. P.; Goze, C.; Denat, F.; Harvey, P. D. *Inorg. Chem.* **2014**, *53*, 3392. b) Chen, W.; Zhang, J.; Mack, J.; Kubheka, G.; Nyokong, T.; Shen, Z. *RSC Adv.* **2015**, *5*, 50962. c) Basumatary, B.; Raja Sekhar, A.; Ramana Reddy, R. V.; Sankar, J. *Inorg. Chem.* **2015**, *54*, 4257. d) Yan, Y.; Wu, F.; Qin, J.; Xu, H.; Shi, M.; Zhou, J.; Mack, J.; Fomo, G.; Nyokong, T.; Shen, Z. *RSC Adv.* **2016**, *6*, 72852. e) Mishra, R.; Basumatary, B.; Singhal, R.; Sharma, G. D.; Sankar, J. *ACS Appl. Mater. Interfaces* **2018**, *10*, 31462. f) Che, Y.; Yuan, X.; Cai, F.; Zhao, J.; Zhao, X.; Xu, H.; Liu, L. *Dyes and Pigments* **2019**, *171*, 107756.

<sup>161</sup> a) Hiroto, S.; Hisaki, I.; Shinokubo, H.; Osuka, A. *Angew. Chem. Int. Ed.* **2005**, *44*, 6763. b) Ngo, T. H.; Nastasi, F.; Puntoriero, F.; Campagna, S.; Dehaen, W.; Maes, W. *Eur. J. Org. Chem.* **2012**, *2012*, 5605. c) Chen, C.; Zhu, Y.-Z.; Fan, Q.-J.; Song, H.-B.; Zheng, J.-Y. *Chem. Lett.* **2013**, *42*, 936. d) Ciuciu, A. I.; Flamigni, L.; Voloshchuk, R.; Gryko, D. T. *Chem. Asian J.* **2013**, *8*, 1004. e) Murugavel, M.; Reddy, R. V. R.; Sankar, J. *RSC Adv.* **2014**, *4*, 13669. f) Murugavel, M.; Reddy, R. V. R.; Dey, D.; Sankar, J. *Chem. Eur. J.* **2015**, *21*, 14280. g) Nikolaou, V.; Karikis, K.; Farré, Y.; Charalambidis, G.; Odobel, F.; Coutsolelos, A. G. *Dalton Trans.* **2015**, *44*, 13473. h) Ngo, T. H.; Zieba, D.; Webre, W. A.; Lim, G. N.; Karr, P. A.; Kord, S.; Jin, S.; Ariga, K.; Galli, M.; Goldup, S.; Hill, J. P.; D'Souza, F. *Chem. Eur. J.* **2016**, *22*, 1301. i) Temelli, B.; Ozasik, O.; Yüksel, D. *Eur. J. Org. Chem.* **2017**, *2017*, 4905. j) Temelli, B.; Gündüz, M.; Yüksel, D. *Tetrahedron* **2018**, *74*, 4476. k) Temelli, B.; Kalkan, H. *Beilstein J. Org. Chem.* **2018**, *14*, 187.

<sup>162</sup> a) D'Souza, F.; Chitta, R.; Ohkubo, K.; Tasiar, M.; Subbaiyan, N. K.; Zandler, M. E.; Rogacki, M. K.; Gryko, D. T.; Fukuzumi, S. *J. Am. Chem. Soc.* **2008**, *130*, 14263. b) Rotas, G.; Charalambidis, G.; Glätzl, L.; Gryko, D. T.; Kahnt, A.; Coutsolelos, A. G.; Tagmatarchis, N. *Chem. Commun.* **2013**, *49*, 9128. c) Lewandowska, K.; Barszcz, B.; Wolak, J.; Graja, A.; Grzybowski, M.; Gryko, D. T. *Dyes and Pigments* **2013**, *96*, 249. d) Bursa, B.; Wróbel, D.; Lewandowska, K.; Graja, A.; Grzybowski, M.; Gryko, D. T. *Synthetic Metals* **2013**, *176*, 18. e) Li, C.; Zhang, J.; Liu, X.; Zhou, Y.; Sun, D.; Cheng, P.; Zhang, B.; Feng, Y. *RSC Adv.* **2014**, *4*, 40758. f) Wang, Y.; Wang, Z.; Guo, X.; Cui, R.; Gao, X.; Yang, S.; Chang, F.; Dong, J.; Sun, B. *J. Nanosci. Nanotech.* **2014**, *14*, 5370. g) Sudhakar, K.; Gokulnath,

polycyclic aromatic hydrocarbons (PAH).<sup>160a,161g,163</sup> Its combination with Fc<sup>163e</sup> and, very recently, with Pcs<sup>151</sup>, has also been reported. Due to their easier oxidation, in comparison with Pors, Cors generally act as the electron donor within D-A dyads. However, the application of Cors as electron acceptors has hardly been studied, primarily owing to the lack of Cor or metallo-Cor derivatives with an appropriate reduction potential.<sup>161h,164</sup> Very recently, the introduction of copper (Cu) as the metallic center have proved to be an effective strategy for engaging Cors as electron acceptors, due to the facile Cu reduction from Cu(III) to Cu(II).

Synthetic limitations avoided for many years the use of Cors as electronic counterparts, although free-base Cors show enhanced photophysical properties with respect to Pors.<sup>165</sup>

---

S.; Giribabu, L.; Lim, G. N.; Trâm, T.; D'Souza, F. *Chem. Asian J.* **2015**, *10*, 2708. h) Liu, B.; Fang, H.; Li, X.; Cai, W.; Bao, L.; Rudolf, M.; Plass, F.; Fan, L.; Lu, X.; Guldi, D. M. *Chem. Eur. J.* **2015**, *21*, 746.

<sup>163</sup> a) Tasiar, M.; Gryko, D. T.; Pielacińska, D. J.; Zaneli, A.; Flamigni, L. *Chem. Asian J.* **2010**, *5*, 130. b) Sudhakar, K.; Kanaparthi, R. K.; Kumar, C. K.; Giribabu, L. *Journal of Luminescence* **2014**, *153*, 34. c) Sudhakar, K.; Giribabu, L.; Salvatori, P.; Angelis, F. D. *Phys. Status Solidi A* **2015**, *212*, 194. d) Giribabu, L.; Sudhakar, K. *Journal of Photochemistry and Photobiology A: Chemistry* **2015**, *296*, 11. e) Kandhadi, J.; Yeduru, V.; Bangal, P. R.; Giribabu, L. *Phys. Chem. Chem. Phys.* **2015**, *17*, 26607. f) Kandhadi, J.; Cheng, F.; Wang, H.-H.; Ali, A.; Wang, L.-L.; Wang, H.; Liu, H.-Y. *Dyes and Pigments* **2017**, *143*, 368. g) Sudhakar, K.; Giribabu, L. *J Chem Sci* **2017**, *129*, 223. h) Achary, B. S.; A. R. Ramya, A. R.; Nanubolu, J. B.; Seetharaman, S.; Lim, G. N.; Jang, Y.; Francis D'Souza, F.; Giribabu, L. *New J. Chem.* **2018**, *42*, 8230. i) Cheng, F.; Wang, H.-H.; Ali, A.; Kandhadi, J.; Wang, H.; Wang, X.-L.; Liu, H.-Y. *J. Porphyrins Phthalocyanines* **2018**, *22*, 886. j) Shivaprasadachary, B.; Ramya, A. R.; Reddy, G.; Giribabu, L. *J. Porphyrins Phthalocyanines* **2020**, *24*, 693.

<sup>164</sup> Buckley, H. L.; Rubin, L. K.; Chromiński, M.; McNicholas, B. J.; Tsen, K. H. Y.; Gryko, D. T.; Arnold, J. *Inorg. Chem.* **2014**, *53*, 7941.

<sup>165</sup> a) Paolesse, R.; Sagone, F.; Macagnano, A.; Boschi, T.; Prodi, L.; Montalti, M.; Zaccheroni, N.; Bolletta, F.; Smith, K. M. *J. Porphyrins Phthalocyanines* **1999**, *7*. b) Ventura, B.; Degli Esposti, A.; Koszarna, B.; Gryko, D. T.; Flamigni, L. *New J. Chem.* **2005**, *29*, 1559. c) Ding, T.; Alemán, E. A.; Modarelli, D. A.; Ziegler, C. J. *J. Phys. Chem. A* **2005**, *109*, 7411. d) Bevilacqua, A. C.; Köhler, M. H.; Piquini, P. C. *Braz J Phys* **2019**, *49*, 502.

## 1.4. Synthesis and characterization of subphthalocyanine-corrole covalent systems linked through corrole *meso*- position

### 1.4.1. The particular case of copper corroles: noninnocent ligands as novel acceptor units

Copper corroles (CuCors) behave as noninnocent ligands: the oxidation state of the inner metal cannot be defined with a net charge, but somewhere between two integer numbers. This state emerges from a strong metal-to-ligand orbitalic interaction. Therefore, despite being Cor a trianionic ligand, the metallic complex substantially presents a Cu(II)-Corrole<sup>2-</sup> character. Previously, it was proposed that the temperature-dependent paramagnetic behavior displayed by the complex in <sup>1</sup>H-NMR and EPR spectra raised from an equilibrium between Cu(II) and Cu(III) oxidation states, with a relative small energy barrier. Ultimately, it was finally redefined as a ferromagnetic/antiferromagnetic coupling between metal and ligand unpaired electrons, presenting the same energetic barrier initially postulated (Figure 27). The great tendency for these complexes to establish this orbitalic interaction makes them even to distort the macrocycle. In the case of CuCors, the orbitalic energy levels of Cu 3d<sub>(x<sup>2</sup>-y<sup>2</sup>)</sub> and b<sub>1</sub> of Cors nearly match, favoring its interaction. Employing the same corrolate ligand with a different metal (*i.e.* Au with HOMO 5d<sub>(x<sup>2</sup>-y<sup>2</sup>)</sub>) leads to a totally planar complex, even for extremely hindered ligands, due to the mismatched nature of the Au(5d<sub>(x<sup>2</sup>-y<sup>2</sup>)</sub>)-Cor( $\pi$ ) orbital interaction. For so, most of the noninnocent Cors are found within the first-row metal transition metal complexes.

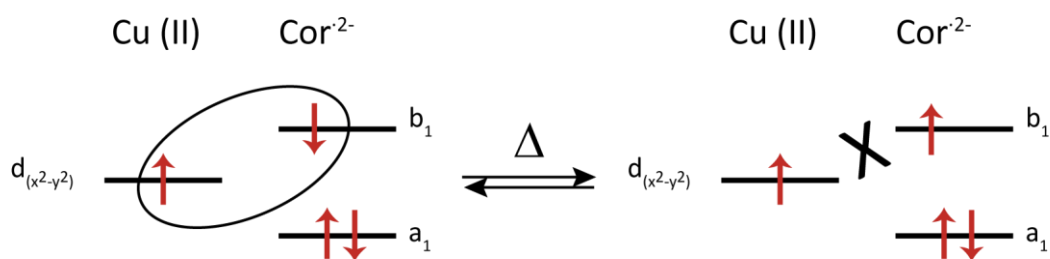


**Figure 27.** Orbitalic interaction defining the characteristic ferromagnetic/antiferromagnetic coupling of CuCor complexes between metal and ligand.

These noninnocent complexes have proven to have a great practical relevance, since they are able to act as a reservoir of electrons and holes, being able to facilitate multiple reactions, as for example in catalysis. Moreover, the possibility of introduce additional reduction potentials to photoactive systems endows versatility at these Cor complexes.

### **1.4.2. Results and discussion**

Since we are about to covalently link Cors and Subpcs, the substitution strategies and possibilities this kind of molecules can offer are introduced. In the present study, linkage from the SubPc is always directly related to its axial position. However, different substitution strategies could arise from Cors. Cor array expansion methodologies from its *meso-* position is, for several reasons, the main pathway to follow: (1) the synthetic versatility from commercially available starting materials allows for an extensive number of anchoring points; (2) its commercial and synthetic availability affords its preparation in moderate yields, either  $A_3$  or  $A_2B$ ; (3) regarding CuCors, during oxidation processes, Cor orbital from which electrons are removed (namely  $b_1$ ) have a substantial electronic density on its *meso-* positions. Therefore, the presence of the unpaired electron in that area may be assumed.<sup>166</sup> In this section, different *trans-A<sub>2</sub>B*-Cors are employed, using a phenoxy moiety as anchoring point for the formation of a B-O bond directly on the SubPc. By fine-tailoring of the substitution pattern of both Cor and SubPc, a certain control over EET processes in a series of D-A arrays composed by different elements and the study of their photophysical properties is presented.

As mentioned before, due the rich chemistry developed in the preparation of *trans-A<sub>2</sub>B*-Cors, the synthesis of Cors with specific functionalities in relatively good yields is promoted. From the SubPc point of view, one of the most recurrent axial substitution reactions at the boron atom employs phenoxy moieties. High excess of the phenoxy reagent with respect to the SubPc is required to carry out the reaction in good yields. Mechanistic studies showed that the axial substitution reaction occurred in a polar environment. Hence, the use of a polar solvent with a high boiling point should translate into an increase of the yield. Additionally, the use of a base during the axial substitution reaction with alcohols have demonstrated to help the deprotonation of the nucleophile, again increasing the yield.

---

<sup>166</sup> Wasbotten, I. H.; Wondimagegn, T.; Ghosh, A. *J. Am. Chem. Soc.* **2002**, *124*, 8104.

A study related to a deeper exploration of these statements was carried out during the Master Thesis of the candidate, obtaining enlightening results when employing  $\alpha,\alpha,\alpha$ -Trifluorotoluene ( $\alpha,\alpha,\alpha$ -TFT) and diisopropylethylamine (DIPEA) as solvent and base, respectively.<sup>167</sup> Finally, the methodology reported by Torres' research group for the activation of SubPc axial position employing triflate derivatives allowed for the preparation of SubPc-Phenoxy derivatives using a small excess of the nucleophile in mild conditions, relative smaller reaction times and higher yields. The development of this methodology paved the way for the design of complex systems in which the use of the excess required of the nucleophile, the long reaction and the tedious purification processes, made difficult their preparation.

#### 1.4.2.1. Synthesis of *meso*-phenoxy corroles **1a** and **1b**

In this context, the synthesis of a *trans*-A<sub>2</sub>B-Cor using two mesityl and one phenoxy units at their meso position allowed for the preparation of a robust molecule in moderate yields. For the synthesis of *trans*-A<sub>2</sub>B-Cor, dipyrromethanes (DPM) are generally required. Mesityl-dipyrromethane (Mes-DPM) was synthesized in high yield, following a mild methodology developed by Dolenský and co-workers.<sup>168</sup> A specific approach developed by Gryko and co-workers was used for the synthesis of *trans*-A<sub>2</sub>B-Cors.<sup>169</sup> Thus, the reaction between Mes-DPM and the corresponding aldehyde in a H<sub>2</sub>O/MeOH mixture, catalyzed by diluted HCl, with concomitant ring closure in CHCl<sub>3</sub>, employing *p*-chloranil as a mild oxidant, afforded the desired free-base Cor **1a** (Scheme 8).

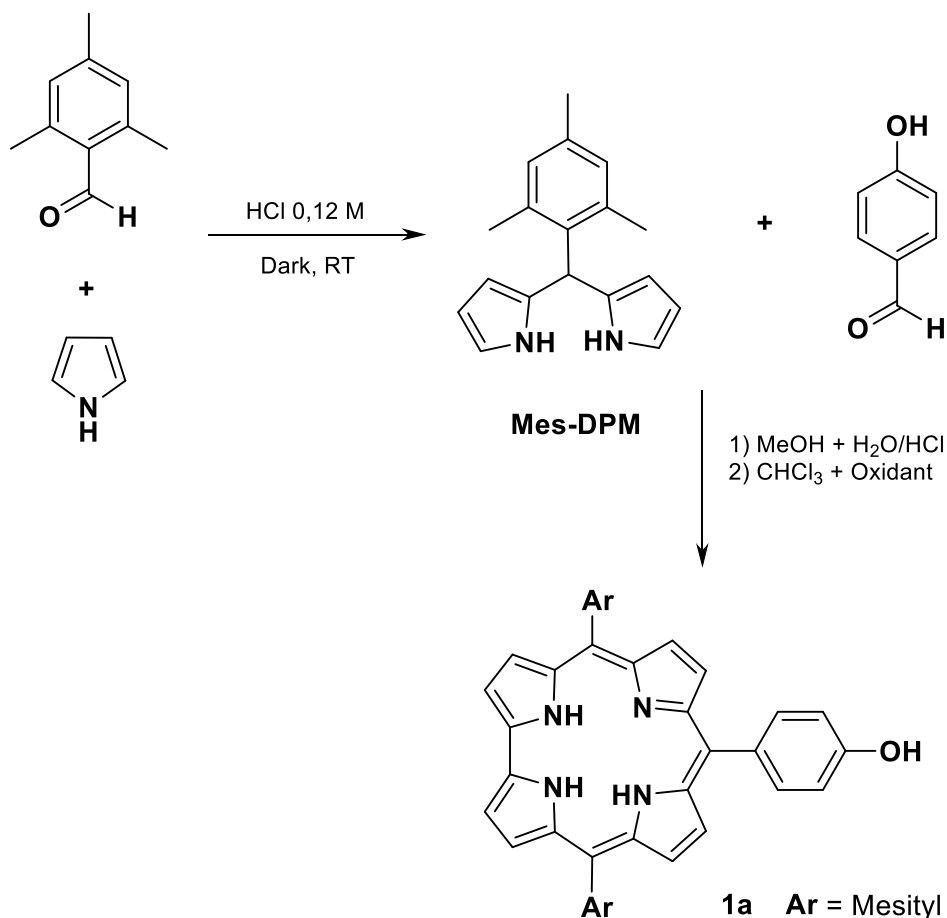
---

<sup>167</sup> Mariñas Perdígón, V., Master Thesis, Science Faculty, Autonoma University of Madrid, **2016**. Torres et al.

<sup>168</sup> Král, V.; Vašek, P.; Dolenský, B. *Collect. Czech. Chem. Commun.* **2004**, *69*, 1126.

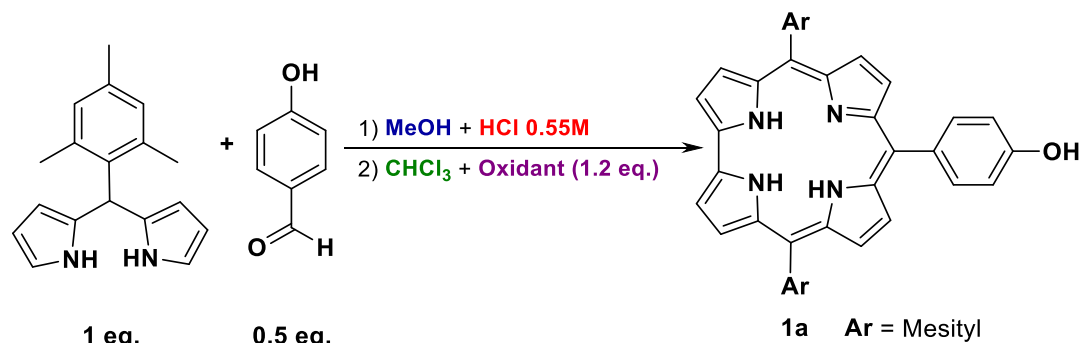
<sup>169</sup> Koszarna, B.; Gryko, D. T. *J. Org. Chem.* **2006**, *71*, 3707.

Synthesis and characterization of SubPc-Cor covalent systems linked through Cor meso- position



**Scheme 8.** Synthetic route and general conditions for the preparation of Cor **1a**.

As reflected by the author, the ratio between the different components of the reaction is imperative for the preparation of the desired Cor, requiring a surgical solubility control of our objective molecules, due to the many other consecutive condensation reactions happening concurrently. With this in mind, a statistical study was carried out in order to maximize the global reaction yield. Although the starting Mes-DPM can be directly used after filtration of the crude reaction without additional treatments, its purification *via* column chromatography proved to be crucial for the effectiveness of the next steps. A relationship between the equivalents of the starting materials, as well as the ratio of the solvents for controlling the solubility of the different reaction products, allowed for the preparation of **1a** in moderate yields (Table 1).

**Table 1.** Reaction condition's scope for the obtention of A<sub>2</sub>B-Cor **1a**.

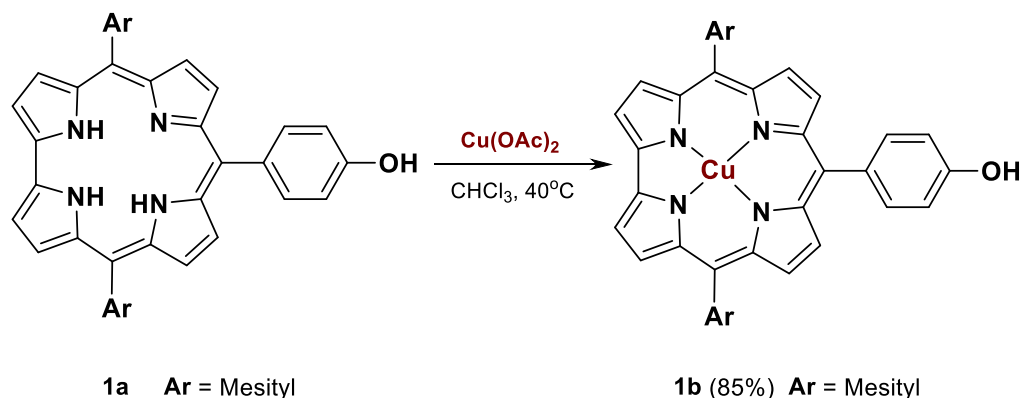
	DPM (mmol)	Aldehyde (mmol)	MeOH (mL)	HCl (mL)	CHCl <sub>3</sub> (mL)	Oxidant	Yield (%)
1	0.5	0.25	50	26.25	125	<i>p</i> -chloranil	15
2	1	0.5	100	52.5	250	<i>p</i> -chloranil	15
3	1	0.5	50	52.5	250	<i>p</i> -chloranil	37
4	1	0.5	50	52.5	250	DDQ	22
5	1	0.5	75	52.5	250	DDQ	13
6	1	0.5	100	52.5	250	DDQ	--
7	2	1	100	105	500	DDQ	13

As depicted above, the relationship between the different reagents, as well as the ratio between the HCl and CHCl<sub>3</sub>, was kept constant. Scaling the reaction did not have influence in the yield (entries 1-2). However, half-reduction of the MeOH volume dramatically increased the yield of **1a** up to 37% (entry 3). The use of a stronger oxidant such as DDQ led into cleaner reactions, obtaining less side-products, yet reducing the yield (entry 4). Increasing the ratio of MeOH reduced the amount of **1a**, or even avoided its obtention (entries 5-6). Scaling of the reaction by keeping the conditions of entry 4 also led to reduced yields (entry 7).

After the synthesis of the free-base Cor **1a**, the insertion of Cu into its core was selected for several reasons (Scheme 9): (1) Due to their higher electrodonating character and constrained core, free-base Cors are prone to deprotonation and are exposed to different decomposition pathways; (2) Cu allows for straightforward metalation and demetallation processes in almost quantitative yields, thus increasing the overall yield of

## Synthesis and characterization of SubPc-Cor covalent systems linked through Cor meso- position

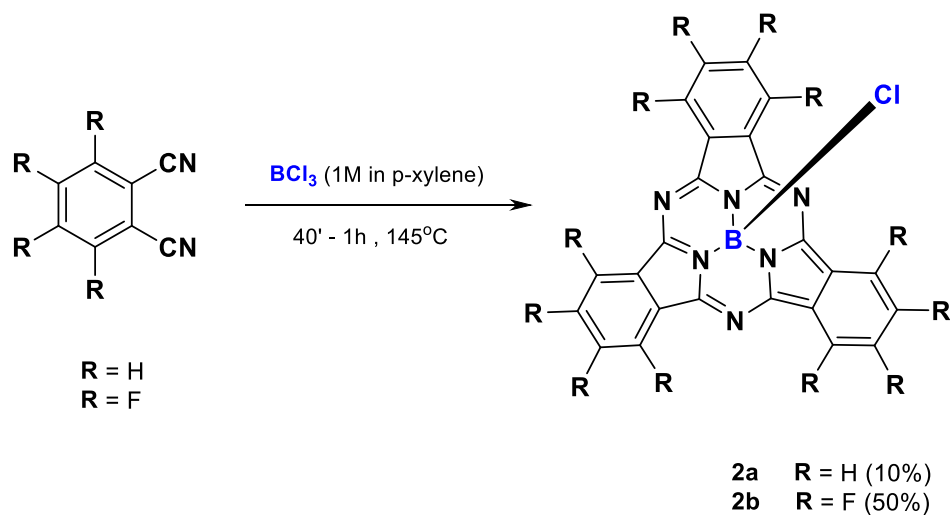
the reaction while protecting the core; (3) Its electronic structure introduces new redox potentials and characteristics, which can be useful for the field of molecular materials.



**Scheme 9.** Preparation of metalloporphyrin-complex **1b** by Cu metallation of  $\text{A}_2\text{B-Cor}$  **1a**.

### 1.4.2.2. Synthesis of SubPcs **2a** and **2b**

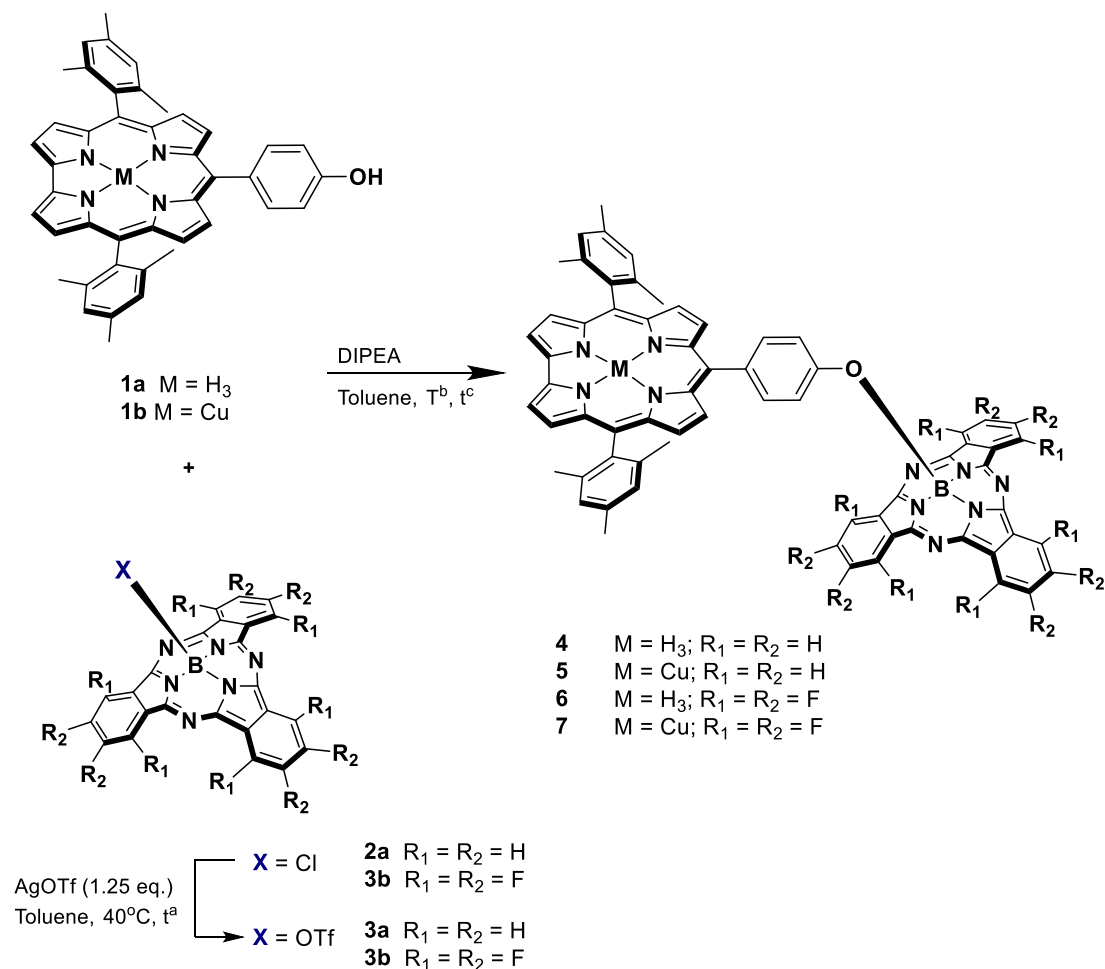
For the synthesis of SubPcs **2a** and **2b**, standard cyclotrimerization conditions were employed. 1 equiv. of phthalonitrile in the presence of  $\text{BCl}_3$  (3 equiv. in *p*-xylene) at different temperatures led to the formation of the expected chloro-SubPc products. The temperature and reaction times for each product differed upon the nature of the phthalonitrile, as could be followed by TLC (Scheme 10).



**Scheme 10.** Synthetic route for the preparation of SubPcs **2a** and **2b**.

### 1.4.2.3. Assembly of SubPc-Cor dyads **4**, **5**, **6** and **7**

SubPc-Cor assemblies were prepared by using the triflate activation methodology previously developed by our group. From a global point of view, the reaction took place milder and faster for **5** > **4** > **7** > **6**, reflecting the combination between Cors and SubPcs reactivity (Scheme 11).



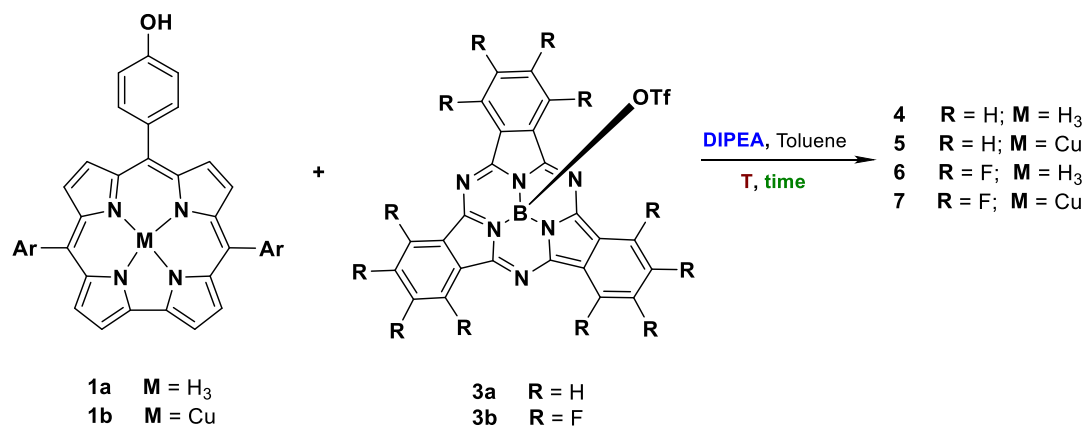
**Scheme 11.** Synthetic route for the preparation of SubPc-Cor dyads **4**, **5**, **6** and **7** via activation of SubPc axial position. a) t = 2h for **2a**; t = 6h and T = 40°C for **2b**. b) and c) different values reflected in Table 2.

For the Cu derivatives **5** and **7**, the reaction showed to be cleaner than for the free-base Cor dyads **4** and **6**, as observed by TLC, without detectable traces of radical or cationic

Synthesis and characterization of SubPc-Cor covalent systems linked through Cor meso- position

species. On the other hand, whereas in the case of the SubPcH<sub>12</sub> dyads **4** and **5** reactions were completed in a few hours at room temperature, for the case of SubPcF<sub>12</sub> dyads **6** and **7** an increase of temperature and higher reaction times were needed. In particular, in the case of dyad **6**, an additional amount of Cor and DIPEA were required in order to complete the reaction. This may be attributed to the combination of the minor reactivity presented by the SubPcF<sub>12</sub> derivative and the decreased availability of the free-base Cor, subjected to several decomposition and deactivation pathways. The difference in reactivity between all the units has a direct influence in the yield, as can be seen in Table 2.

**Table 2.** Reaction conditions for the synthesis of SubPc-Cor dyads **4**, **5**, **6** and **7**. Ar = Mesityl.



	Cor (eq.)	SubPc (eq.)	DIPEA (eq.)	T (°C)	t (hours)	Yield (%)
<b>4</b>	1	1	1.25	40	24	30
<b>5</b>	1	1	1.25	40	24	32
<b>6</b>	2	1	1.75	60	24	15
<b>7</b>	1.5	1	1.75	60	24	20

The structures of **4**, **5**, **6** and **7** were determined by <sup>1</sup>H-NMR, <sup>13</sup>C-NMR, UV-Vis and mass spectrometry (MS). In <sup>1</sup>H-NMR spectra, the free-base Cor dyads **4** and **6** exhibits a group of signals between 8.0 and 9.0 ppm, characteristic of Cor β-pyrrolic protons. The assignment is being made based on the number and integration of these signals. Besides, the doublets around 7.53 and 5.73 ppm corresponds to the phenoxy ring of the Cor. In comparison with the starting materials, the later signal appears upfield, which is a typical feature of the straight connection of phenols into SubPc boron atom, due to the presence of an anisotropic ring current. In the case of SubPcH<sub>12</sub> dyads **4** and **5**, the multiplets

appearing at 7.94 and 8.94 ppm corresponding to SubPc *outer*- and *inner*-phenyl protons, along with the shielded phenoxy ring protons, confirms the coupling (Figure 28).

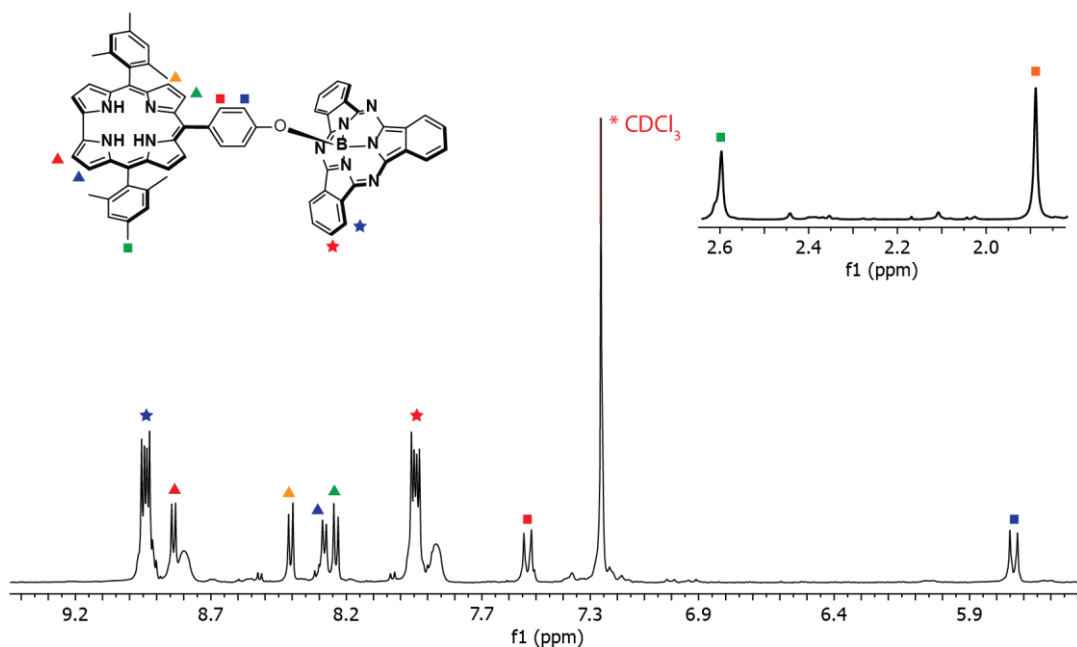


**Figure 28.**  $^1\text{H-NMR}$  (300 MHz) spectrum in  $\text{CDCl}_3$  at  $25^\circ\text{C}$  of SubPc-Cor **4**. *m*-Mesityl protons are located under  $\text{CDCl}_3$  signal (ca. 7.26 ppm).

For the CuCor dyads **5** and **7**, the antiferromagnetic coupling previously described for those noninnocent complexes leads to a paramagnetic behavior of the Cor. The spin coupling effect induced by the complex increases the relaxation times of the protons, thus not making them visible in our acquisition times. Even though its presence does not allow to record Cor  $\beta$ -pyrrolic protons, the spectrum can still be followed from the external phenoxy ring and the alkyl-mesityl protons, which are not influenced by its presence (Figure 29).

Synthesis and characterization of SubPc-Cor covalent systems linked through Cor meso- position

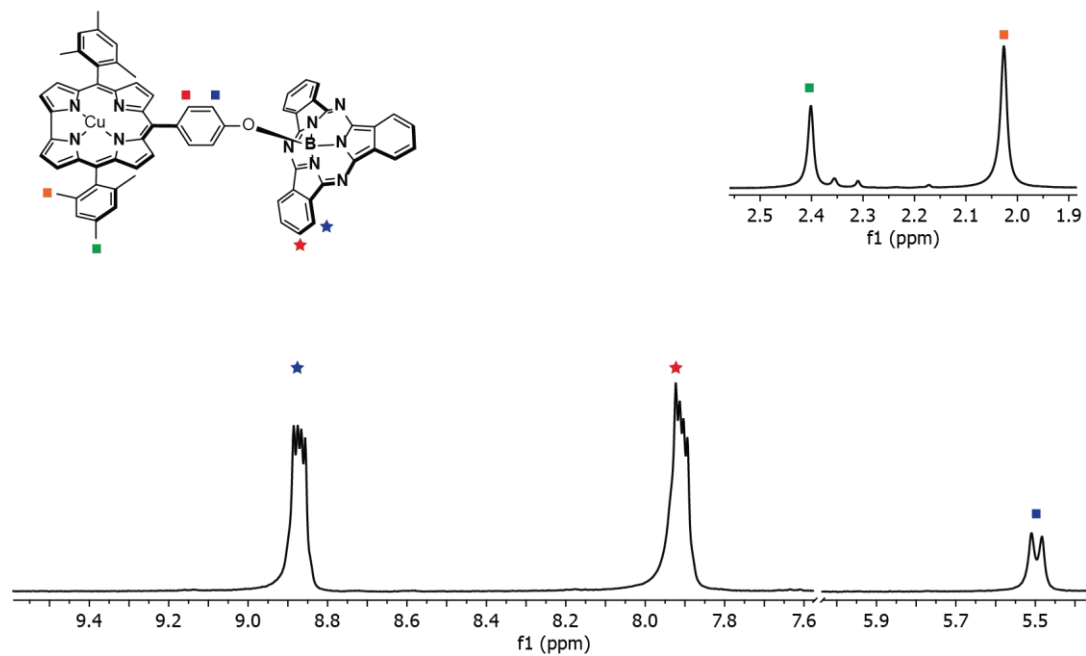
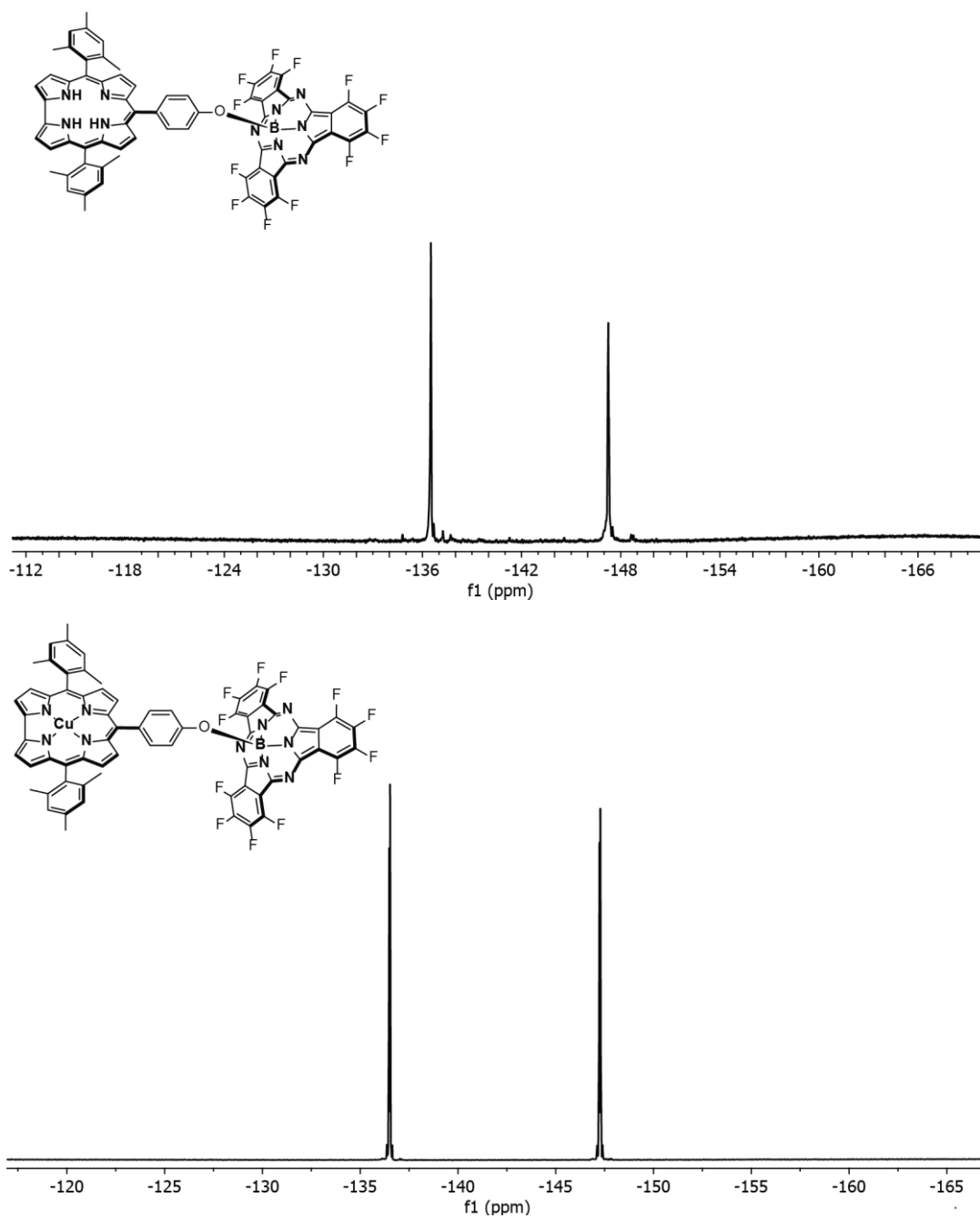


Figure 29. <sup>1</sup>H-NMR (300 MHz) spectrum in CDCl<sub>3</sub> at 25°C of SubPc-Cor 5.

In the case of SubPc-Cor dyads 6 and 7, the presence of two signals at -136.50 and -147.23 ppm in <sup>19</sup>F-NMR spectra confirmed the same conclusion (Figure 30).



**Figure 30.**  $^{19}\text{F}$ -NMR (300 MHz) spectrum in  $\text{CDCl}_3$  at  $25^\circ\text{C}$  of SubPc-Cor **6** (top) and **7** (bottom).

#### 1.4.2.4. Steady-state absorption and emission studies of SubPc-Cor dyads 4-7

Steady-state absorption spectra have been acquired in toluene (Tol) and benzonitrile (PhCN) (Figure 31, bottom). The different compounds employed as references are listed below (Figure 31, top). The reference Cor absorption generally consists of the dominant Soret band region with maxima at 403 and 431 nm for **1aR** and **1bR**, respectively, and several Q bands between 500 and 650 nm. SubPc absorption is found below *ca.* 350 nm and between 450 and 600 nm where it maximizes at a Q band at 562 and 572 nm for **2aR** and **2bR**, respectively. The dyad absorption closely fits their corresponding building blocks both in intensity and peak position with Q-bands at 563 and 573 nm for **4/5** and **6/7**, respectively. Hence, little to no ground state interaction is assumed between the moieties within the dyads.

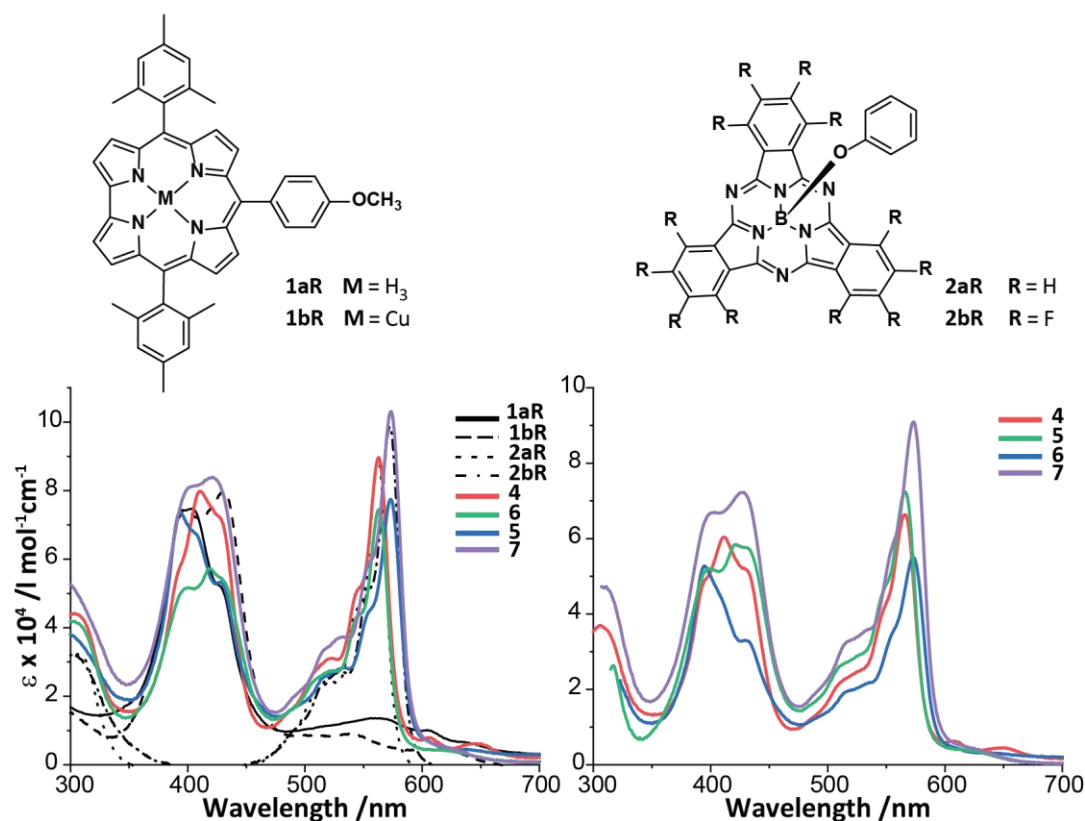


**Figure 31.** (Top) Chemical structure of SubPc and Cor references **1aR**, **1bR**, **2aR** and **2bR**, and (bottom) steady-state absorption spectra of SubPc-Cor dyads **4**, **5**, **6** and **7** in toluene (bottom, left) and PhCN (bottom, right), along with references **1aR**, **1bR**, **2aR** and **2bR** in toluene (bottom, left).

Fluorescence emission was obtained in toluene and PhCN (Figure 32). Emission maxima were found at 652 and 569/577 nm for the references Cor **1aR** and SubPcs **2aR** and **2bR**, while CuCor **1bR** showed no emission, probably arising from a heavy-atom effect. SubPc-Cor dyad **4** presents mostly Cor emission, regardless of the excitation wavelength. Still, a fraction of SubPc emission occurs upon SubPc excitation, being more pronounced in PhCN. Therefore, energy transfer towards the Cor can be assumed. Emission from SubPc-Cor dyad **6** does not fit the position of the involved moieties at 534 nm, but appears to be stronger upon excitation into the SubPc. Both Cu-dyads **5** and **7** solely show SubPc-centered emission upon excitation into the corresponding Q-bands. Fluorescence quantum yields ( $\Phi_{\text{F}}$ ) of the dyads were generally weak, with values *ca.* 0.01, contrasting the measured references at *ca.* 0.1-0.2 (Table 3).

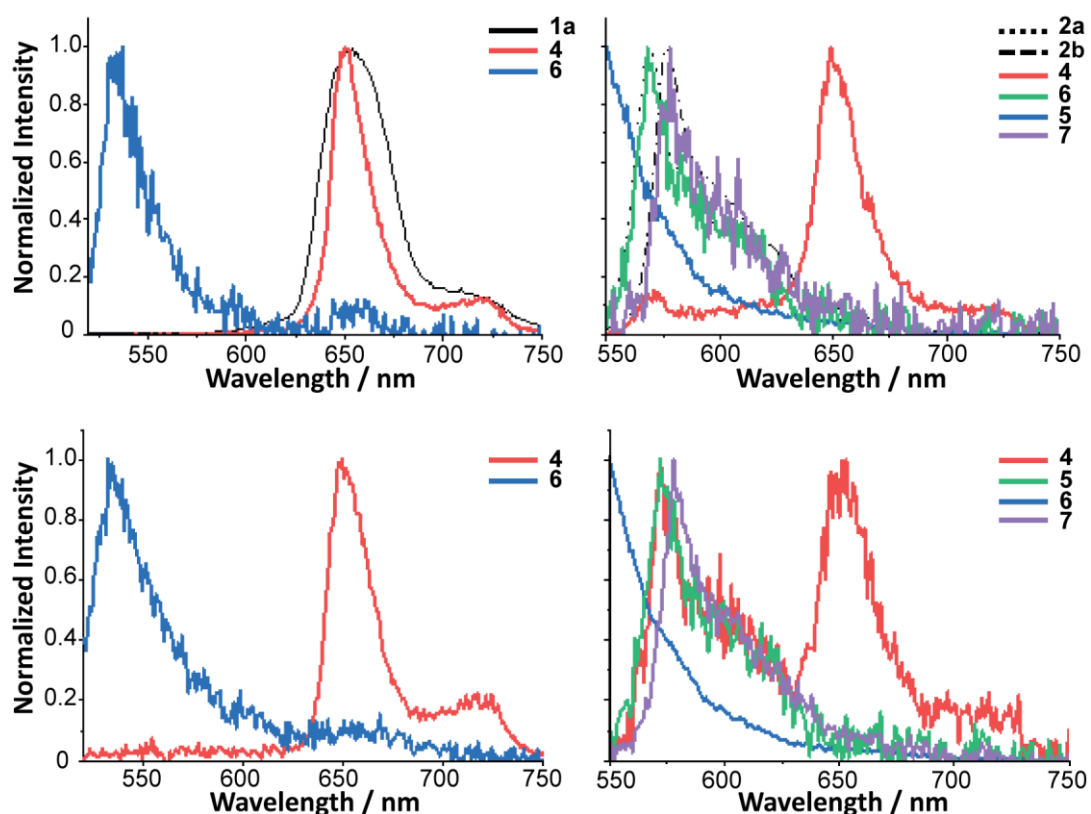


**Figure 32.** Fluorescence emission spectra of SubPc-Cor dyads **4**, **5**, **6** and **7** at 420 nm in toluene (top, left) and PhCN (bottom, left), and at 540 nm in toluene (top, right) and PhCN (bottom, right), along with references **1aR**, **2aR** and **2bR** at 420 nm (top, left) and 540 nm (top, right) in toluene.

**Table 3.** Fluorescence emission maxima and quantum yields ( $\Phi$ ) of SubPc-Cor dyads **4**, **5**, **6** and **7** in toluene and PhCN (in brackets) and references **1aR**, **1bR**, **2aR** and **2bR** at RT. H<sub>2</sub>TTP and SubPcF<sub>12</sub>-OPh were used as references for Cor- and SubPc-centered emission, respectively.<sup>170,171</sup>

	420 nm		540 nm	
	Emi <sub>max</sub> / nm	$\Phi_{Fl}$	Emi <sub>max</sub> / nm	$\Phi_{Fl}$
<b>1aR</b>	652	0.10		
<b>1bR</b>	-	-		
<b>2aR</b>			569	0.17
<b>2bR</b>			577	0.17
<b>4</b>	650	0.02 (0.01)	570/650	0.01 (<0.01)
<b>5</b>	534	<0.01 (<0.01)	<550	0.03 (<0.03)
<b>6</b>			570	<0.01 (<0.01)
<b>7</b>			578	<0.01 (<0.01)

#### 1.4.2.5. Electrochemical studies of SubPc and Cor references 1ar, 1br, 2ar and 2br

Since no apparent ground-state interaction has been detected, neither in toluene or PhCN for the SubPc-Cor dyads, only SubPc and Cor references were studied in terms of electrochemistry, in order to determine their reduction and oxidation potential values. Cyclic voltammograms (CV) and differential pulse voltammograms (DPV) of the reference Cors and SubPcs were conducted in a 0.1 M TBAPF<sub>6</sub> dichloromethane (DCM) solution, while Fc/Fc<sup>+</sup> couple acted as an internal standard (Figure 33). Free-base Cor **1aR** features three reversible reductions at -1.44/-1.17/-0.31 V vs. Ag (-1.78/-1.51/-0.65 V vs. Fc/Fc<sup>+</sup>) as well as one oxidation at +0.44 V vs. Ag (+0.10 V vs. Fc/Fc<sup>+</sup>). A set of two reductions and oxidations each is visible for CuCor **1bR** at -0.96/-0.40 V vs. Ag (-1.32/-0.76 V vs Fc/Fc<sup>+</sup>) and +0.57/+1.29 V vs. Ag (+0.21/0.93 V vs. Fc/Fc<sup>+</sup>). The SubPc **2aR** shows reversible conversions at -1.90/-1.65/-1.19 (-2.27/-2.02/-1.56 V vs. Fc/Fc<sup>+</sup>) and +0.94 V vs. Ag (+0.57 V vs. Fc/Fc<sup>+</sup>). Finally, the perfluorinated SubPc **2bR** features reductions at -1.34/-0.94/-0.65 (-1.74/-1.34/-1.05 V vs. Fc/Fc<sup>+</sup>) and an oxidation at +1.38 V vs. Ag (+0.98 V vs. Fc/Fc<sup>+</sup>) (Table 4). The corresponding Cor<sup>+</sup>-SubPc<sup>-</sup> charge-separated states (CSSs) can consequently be expected at energies of about 1.66, 1.77, 1.15 and 1.26 eV (corresponding to excitations with 984, 1078, 700 and 747 nm) for the dyads **4**, **5**, **6** and **7** in DCM, respectively.

<sup>170</sup> Seybold, P. G.; Gouterman, M. *J. Mol. Spectrosc.*, **1969**, *31*, 1-13.

<sup>171</sup> Rudolf, M.; Trukhina, O.; Perles, J.; Feng, L.; Akasaka, T.; Torres, T.; Guldi, D. M. *Chem. Sci.* **2015**, *6*, 4141.

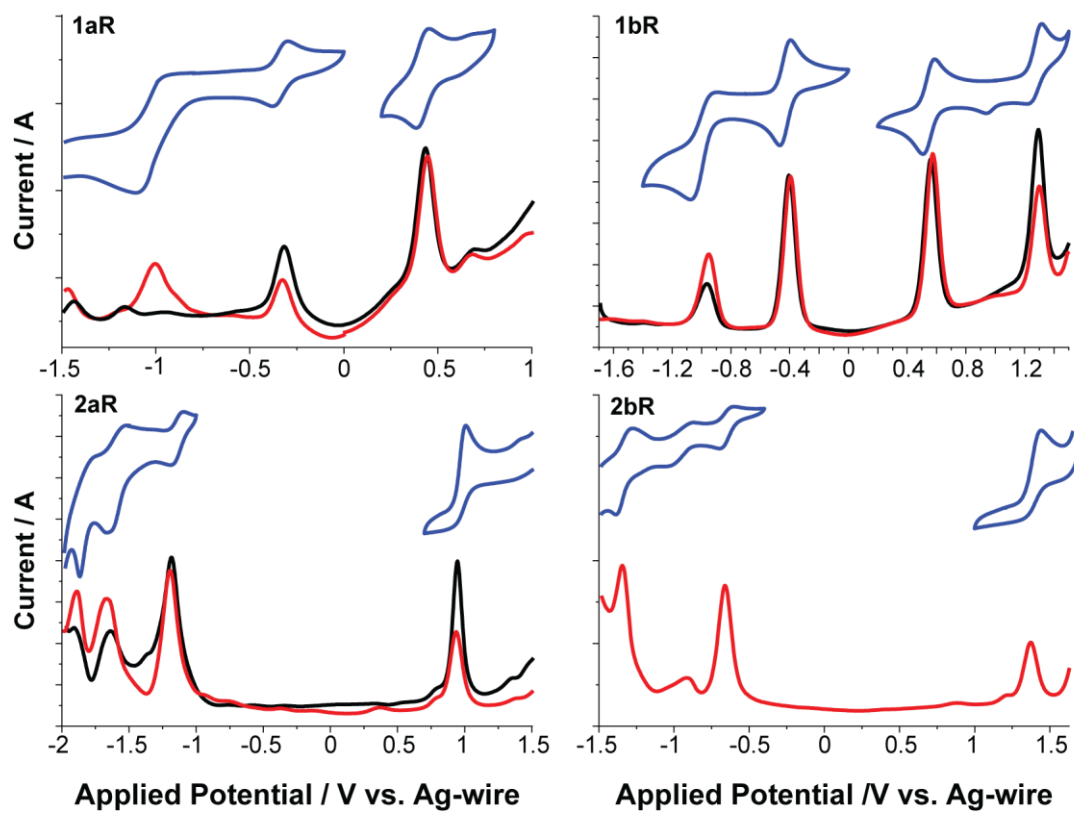


**Figure 33.** DPV (upscan: black; downscan: red) and CV (blue) of references **1aR** (top, left), **1bR** (top, right), **2aR** (bottom, left) and **2bR** (bottom, right) in purged DCM 0.1 M TBAPF<sub>6</sub> solution at RT.

*Synthesis and characterization of SubPc-Cor covalent systems linked through Cor meso- position*

**Table 4.** Reduction and oxidation potentials of references **1aR**, **1bR**, **2aR** and **2bR** vs. Ag-wire and Fc/Fc<sup>+</sup> (in brackets) in purged DCM 0.1M TBAPF<sub>6</sub> solution at RT. Working electrode: C; Counter electrode: Pt; Pseudo-reference electrode: Ag.

	E <sub>3rd Red.</sub> / V	E <sub>2nd Red.</sub> / V	E <sub>1st Red.</sub> / V	E <sub>1st Ox.</sub> / V	E <sub>2nd Ox.</sub> / V
<b>1aR</b>	-1.44	-1.17	-0.31	+0.44	
	(-1.78)	(-1.51)	(-0.65)	(+0.10)	
<b>1bR</b>		-0.96	-0.40	+0.57	+1.29
		(-1.32)	(-0.76)	(+0.21)	(+0.93)
<b>2aR</b>	-1.90	-1.65	-1.19	+0.94	
	(-2.27)	(-2.02)	(-1.56)	(+0.57)	
<b>2bR</b>	-1.34	-0.94	-0.65	+1.38	
	(-1.74)	(-1.34)	(-1.05)	(+0.98)	

#### 1.4.2.6. Spectroelectrochemistry of SubPc-Cor dyads 4-7

Differential absorption spectra of the oxidized or reduced species were obtained upon application of a bias voltage to a solution of the respective Cor or SubPc reference (Working electrode: Pt-mesh; Counter electrode: Pt-wire; Reference electrode: Ag-wire) (Figure 34). Spectra are dominated by the respective ground state bleaches around 420 and 570 nm for Cors and SubPcs, respectively. The one-electron oxidized Cor **1aR** features differential maxima at 394/454/600/634/670 and minima at 415/433/567/610 nm. Signals are found at 389/480/590/660 and 433/532 nm for the oxidized CuCor **1bR**. SubPc **2aR** features maxima and minima at 598 and 510/564 nm while the respective signals occur at 600/650 and 455/522/570 nm for the perfluorinated SubPc **2bR** upon application of a sufficient negative bias.

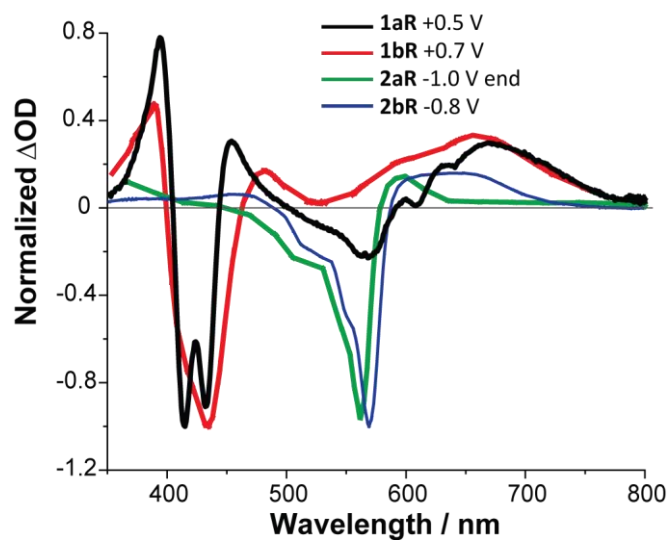


**Figure 34.** Differential absorption of one-electron oxidized reference Cors **1aR** (black) and **1bR** (red), and one electron reduced reference SubPcs **2aR** (green) and **2bR** (blue) in DCM (0.1 M TBAPF<sub>6</sub> as electrolyte) at 25°C.

#### **1.4.2.7. Transient Absorption Spectroscopy of SubPc-Cor dyads 4-7**

In order to investigate the extremely fast energy and electron-transfer processes happening in a photosynthetic system upon absorption of radiant energy, ultrafast techniques down to a femtosecond resolution must be employed. This allows for the tracking of the energy migration within the system (e.g. intersystem crossing (ISC) processes from singlet to triplet states) and for the detection of new chemical species, such as charge-separated states, in real time. This can be done by using femtosecond transient absorption spectroscopy techniques.

#### **References**

Femtosecond transient absorption of the reference Cors and SubPcs was measured in toluene upon excitation at 420 and 550 nm, respectively, to gain insight into excited state dynamics. Free-base Cor **1aR** shows internal conversion and vibrational relaxation with corresponding lifetimes of 6.1 and 74 ps (Figure S-TAS1). Ultimately the first singlet excited state undergoes ISC to populate the triplet excited state within 1.4 ns. The transient spectra are mostly defined by a strong ground state bleach around 420 nm as well as two maxima in the NIR around 1100 and 1200 nm. In CuCor **1bR**, its heavy central atom as well as open shell nature funnels a much faster singlet-to-triplet conversion (Figure S-TAS2). The second singlet excited state  $S_2$ , characterized by its distinct and broad 600 nm maximum, decays with only 1.9 ps to form the  $S_1$  which undergoes ISC with 11 ps. Finally, we propose the population of a Cu-centered species with 159 ps mostly defined by the lack of the Cor ground-state bleaching. SubPc **2aR** initially undergoes vibrational relaxation from the unrelaxed to the relaxed  $S_1$ , both characterized by a strong ground state bleach around 560 nm, a more pronounced maximum around 620 nm and shoulder at 950 and 1100 nm, with 9.1 ps followed by a decay into the triplet excited state with 1.2 ns (Figure S-TAS3). Similar dynamics occur for the perfluorinated SubPc **2bR**, with its ground state bleach around 570 nm, and lifetimes of 14 ps and 1.0 ns (Figure S-TAS4).

#### **SubPc-Cor dyads**

The four SubPc-Cor dyads were excited into the Cor Soret-band at 420 nm and the SubPc Q-bands at 550 nm both in toluene and the significantly more polar PhCN. Coexcitation of both moieties had to be considered upon 550 nm excitation for all molecules. The Cor  $S_2$  of dyad **4** is initially populated upon excitation at 420 nm in toluene

and features characteristic maxima at about 460 and 1200 nm as well as the 420 nm ground state bleaching (Figure 35). Subsequently, conversion into the unrelaxed and relaxed  $S_1$  occurs with 6.1 and 74 ps. Two states, the Cor  $T_1$  and a proposed charge transfer (CT) or charge-separated state (CSS), are formed in parallel from the  $S_1$  with 161 ps. The population of a charged species, living for 493 ps, is supported by its two ground-state bleachings around 420 and 560 nm as well as local maxima around 590 and 620 nm which fit the absorption of the Cor cation obtained via spectroelectrochemical measurements. Coexcitation of 78 % into the SubPc  $S_1$  and 22% into the unrelaxed Cor  $S_1$  (a ratio calculated from the relative extinction coefficients) was assumed at 550 nm (Figure S-TAS5). The SubPc, with its 560 nm bleaching and broad 600-630 nm maximum, decays both into the CT/CSS (43 %) and transfers energy to the unrelaxed Cor  $S_1$  (57 %) with 1.5 ps. The Cor  $S_1$  then undergoes vibrational relaxation with 74 ps and finally decays both into the CT/CSS and Cor  $T_1$  within 180 ps. The charged species lives for 534 ps in accordance with the 420 nm experiment. The best results in PhCN were obtained including a 30 % population of the CT/CSS from the unrelaxed Cor  $S_1$  as well as an 80/20-ratio for CT/CSS and Cor  $T_1$  from the relaxed Cor  $S_1$  in the previously used models for toluene (Figures S-TAS7 and S-TAS8). Lifetimes of 6.1, 5.3, 90 and 24 ps were obtained upon excitation at 420 nm for Cor  $S_2$ , unrelaxed  $S_1$ , relaxed  $S_1$  and CT/CSS, respectively. The 550 nm experiment yields respective lifetimes of 1.8, 5.3, 104 and 24 ps.

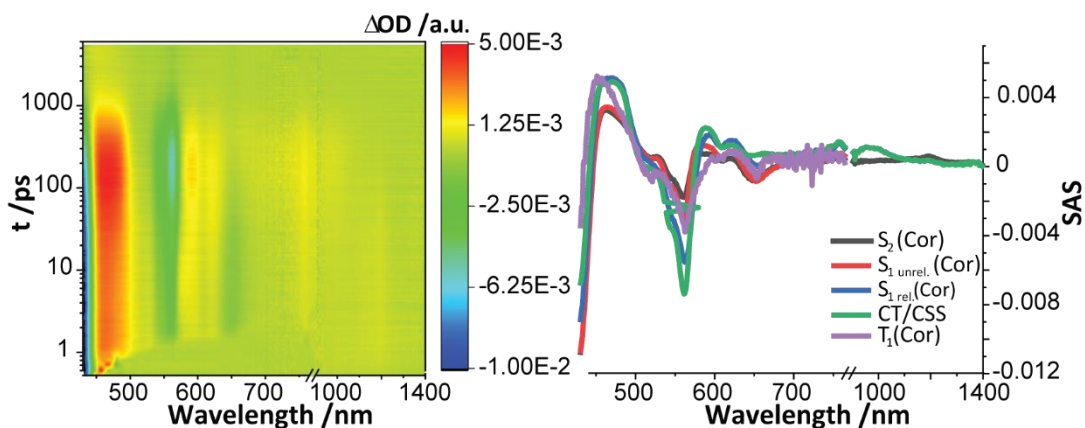


**Figure 35.** Differential absorption of SubPc-Cor **4** upon femtosecond flash photolysis with excitation at 420 nm in toluene (left) and corresponding species associated spectra of the involved transient species (right).

The perfluorinated dyad **6** shows much more rapid decays in toluene at 420 nm with a CSS living for only 22 ps after being formed directly from the Cor  $S_2$  with 3.0 ps (Figure S-

TAS10). The SubPc  $S_1$  populates the CSS with 90 % efficiency upon 550 nm excitation while transferring 10 % of its energy to the coexcited Cor  $S_1$ , which in turn decays into the CSS. Only a SubPc triplet species is ultimately obtained upon recombination. The corresponding state lifetimes are 1.3, 5.3 and 24 ps for the singlet and charged species (Figure S-TAS11). Excitation into the Cor Soret-band in PhCN yielded only three species with rather short lifetimes of 2.6, 6.4 and 21 ps (Figure 36). The second species, featuring both ground-state bleaching, succeeded the Cor  $S_2$  and was thus identified as a CSS. The final species also shows the intense SubPc bleaching but also a more pronounced 587 nm maximum. We therefore suggest another charge-separated species as the ultimate state. The occurrence of two CSS is in our view best explained by a slower adjustment of the solvent compared to toluene; the model is summarized as follows: excitation of the Cor results in the population of the  $S_2$ , which furtherly decays into the solvent-unrelaxed CSS, ultimately forming the solvent-relaxed CSS. Upon 550 nm excitation, the  $S_1$  and two CSS decay with 1.1 and 8.2/21 ps, respectively (Figure S-TAS13). Small amounts of Cor and SubPc triplet species occur upon charge-recombination and thus are populated from the relaxed CSS in parallel. In this case the coexcitation into two distinct singlet excited states could not be represented by the model due to similarity of the short lifetimes

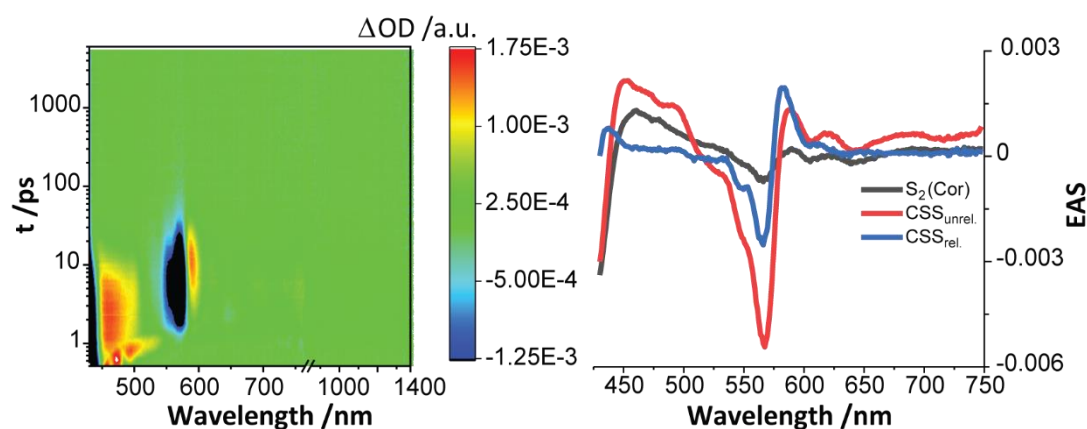


**Figure 36.** Differential absorption of SubPc-Cor **6** upon femtosecond flash photolysis with excitation at 420 nm in PhCN (left) and corresponding evolution associated spectra of the involved transient species (right).

SubPc-Cor **5** in toluene is initially excited with 420 nm into its  $S_2$  state, characterized by the ground state bleaching as well as the broad  $\sim 600$  nm maximum, followed by the CT/CSS, which in turn populates both Cor and SubPc  $T_1$  species (Figure S-TAS15). Charge-separation and recombination occur at the picosecond timescale with 1.8 and 22 ps while

the Cor  $T_1$  lives for 284 ps, coming close to the lifetime of the reference. Analysis of spectra obtained upon 550 nm excitation yields the combined Cor and SubPc  $S_1$ , CT/CSS and Cor and SubPc  $T_1$  (formed in parallel) with respective lifetimes of 2.2, 20 and 223 ps (Figure S-TAS16). Similar models were employed for measurements in PhCN; the CT/CSS was replaced by the two known solvent unrelaxed and relaxed CSS (Figures S-TAS18 & 19). Lifetimes of 1.4, 4.7, 20 and 383 ps were obtained for the Cor  $S_2$ , unrelaxed CSS, relaxed CSS and Cor  $T_1$  upon 420 nm excitation. Upon 550 nm excitation the unrelaxed CSS is formed within 3.0 and 1.0 ps from the Cor and SubPc  $S_1$ . Lifetimes of the two CSS and the Cor  $T_1$  were obtained as 7.2, 35 and 257 ps.

The transient species of SubPc-Cor **7** feature lifetimes close to the previous dyad (Figures S-TAS21). Upon excitation of the Cor in toluene, lifetimes of 1.7, 23 and 294 ps were obtained for the Cor  $S_2$ , CSS and Cor  $T_1$ , respectively. Analysis of the 550 nm excitation-data resulted in lifetimes of 0.9, 5.6, 22 and 346 ps for the Cor  $S_1$  (as combined  $S_1$  in model), SubPc  $S_1$ , CSS and Cor  $T_1$ . Initially, the  $S_1$  states could not be separated; the combined  $S_1$  thus populate the CSS (16 %) and the SubPc  $S_1$  (84 %), which in turn again forms the CSS. Measurements in PhCN once more needed the replacement of the single CSS with the two unrelaxed and relaxed CSSs. No remaining triplet signatures were visible upon 420 nm excitation where lifetimes of 0.9, 4.0 and 20 ps correspond to the Cor  $S_2$ , unrelaxed and relaxed CSS. Similar dynamics with 0.9, 4.0, 3.6 and 20 ps were obtained for Cor  $S_1$  (as combined  $S_1$  in model), SubPc  $S_1$ , unrelaxed and relaxed CSS upon 550 nm excitation. Small amounts of triplet features yielded a 332 ps lifetime for the Cor  $T_1$ .

Lifetimes corresponding to direct singlet predecessors of the CTs/CSSs and the CTs/CSSs themselves are summarized in Table 5.

**Table 5.** Excited state lifetimes of CT/CSS-predecessors and CTs/CSSs upon 420 and 550 nm (in brackets) excitation.

	Toluene (ps)		Benzonitrile (ps)	
	Singlet	CT/CSS	Singlet	CT/CSS
<b>4</b>	161	493	5.3/90	24
	(1.5/180)	(534)	(1.8/5.3/104)	(24)
<b>5</b>	3.0	22	2.6	6.4/21
	(1.3/5.3)	(24)	(1.1)	(8.3/21)
<b>6</b>	1.8	22	1.4	4.7/20
	(2.2)	(20)	(3.0/1.0)	(7.2/35)
<b>7</b>	1.7	23	0.9	4.0/20
	(0.9/5.6)	(22)	(0.9/4.0)	(3.6/20)

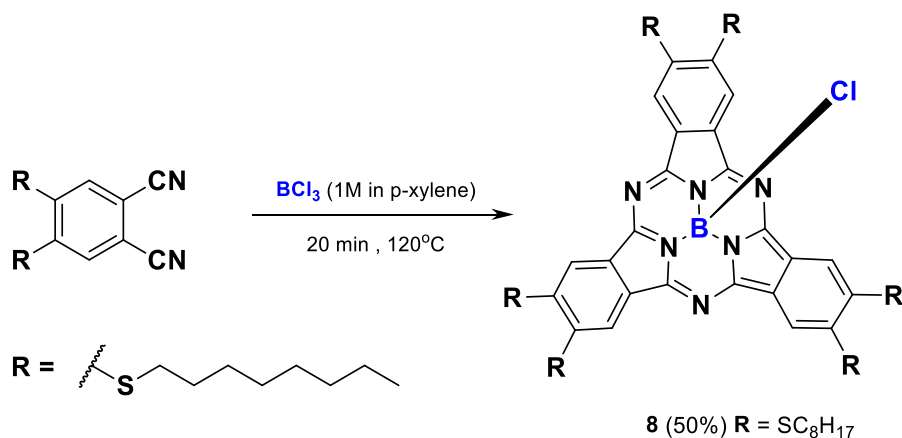
*Synthesis and characterization of SubPc-Cor covalent systems linked through Cor meso- position*

### 1.4.3. Controlling direction of EET processes: synthesis of ThioSubPc-PCor dyads

In an attempt to change the direction of the EET process of the SubPc-Cor assemblies through the *meso*-position of Cor, a qualitative approach was followed by combining the high electron deficient Phosphorus Corrole **10** with an electron rich thioether-SubPc derivative. Particularly, SubPc **8** has been chosen in order to take advantage of its already reported capability of establishing 1:1 supramolecular complex with C<sub>60</sub> and C<sub>70</sub> molecules, thanks to its jellyfish-like structure and complementary electronic features on its concave side.<sup>79</sup> They also have demonstrated to conduct efficient CT separation in combination with an electronically-suited partner.<sup>15</sup>

#### 1.4.3.1. Synthesis of SubPc **8**

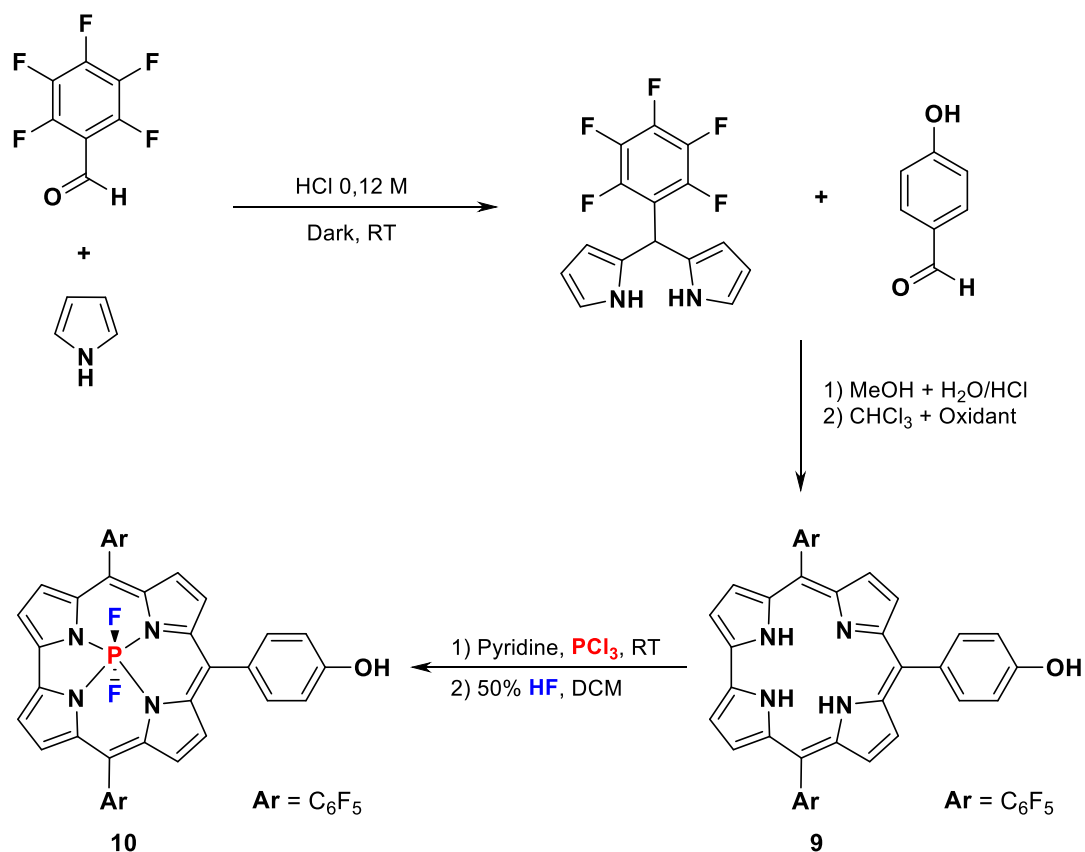
An already reported general methodology for the synthesis of thioether SubPcs was employed. Thus, starting from 4,5-dichlorophthalonitrile, the 4,5-thioether derivative was prepared. Consecutive cyclotrimerization reaction with BCl<sub>3</sub> in *p*-xylene was carried out, with the optimized conditions set for the reaction at 120°C for 20 minutes. Vacuum-evaporation of the solvent and subsequent silica-gel plug led to SubPc **8** in a 50% yield (Scheme 11). Due to the low stability of the compound, special attention should be paid in all the steps in order to minimize the formation of secondary and degradation products.



Scheme 11. Synthetic route for the preparation of SubPc **8**.

### 1.4.3.2. Synthesis of Phosphorus-Cor 10

Phosphorus Corrole (PCor) **10** was provided by Dr. Fabrizio Caroleo, from Prof. Roberto Paolesse's group. The synthesis of free-base Cor **9** was carried out employing general conditions for synthesis of electron-deficient *trans*-A<sub>2</sub>B-Cors. Subsequent metalation and axial substitution were done as previously reported by Gross *et al* (Scheme 12).<sup>172</sup>

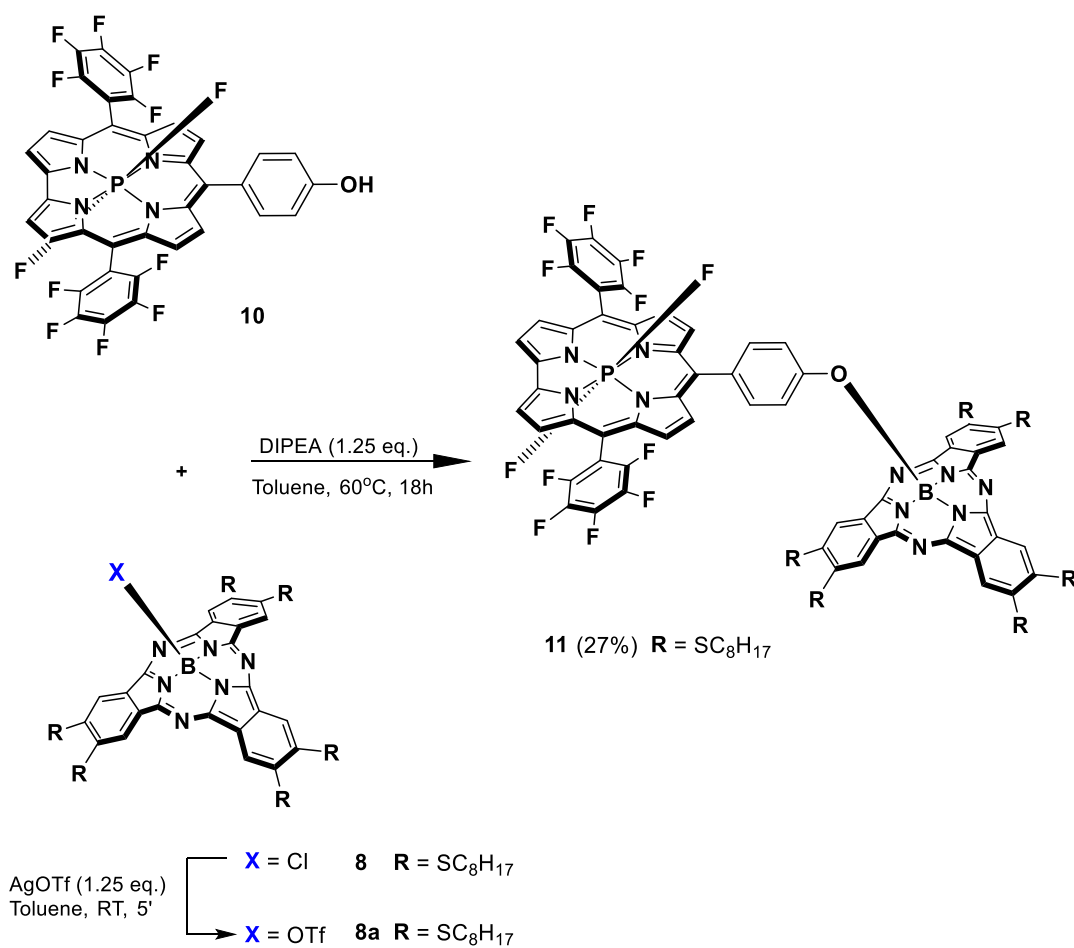


Scheme 12. Synthetic route for the preparation of Cors **9** and **10**.

<sup>172</sup> Vestfrid, J.; Kothari, R.; Kostenko, A.; Goldberg, I.; Tumanskii, B.; Gross, Z. *Inorg. Chem.* **2016**, *55*, 6061.

### 1.4.3.3. Assembling of SubPc-PCor dyad **11**

In a similar way as described in section 1.4.2.3., axial activation of SubPc **8** with AgOTf and subsequent addition of PCor **10** afforded SubPc-Cor dyad **11** in a 27% yield (Scheme 13). Although due to the high reactivity of SubPc **8** activation of its axial position may not be required, it was carried out in order to ensure the axial substitution reaction. This increased reactivity is reflected in the required activation times: whereas in the case of thioether SubPc **8** the activation reaction lasts 10 minutes at room temperature, less reactive perfluorinated SubPc **2b** requires several hours and an increase of the reaction temperature.



**Scheme 13.** Synthetic route for the preparation of SubPc-Cor dyad **11**.

SubPc-Cor dyad **11** was fully characterized by  $^1\text{H}$ -NMR,  $^{13}\text{C}$ -NMR,  $\text{B}^{11}$ -NMR,  $\text{F}^{19}$ -NMR and  $\text{P}^{31}$ -NMR, along with MS spectra. In  $^1\text{H}$ -NMR, both signals of Cor and the SubPc were observed. The 1:1 integration of the signals and the characteristic upfield shift of the phenoxy proton confirmed the formation of the dyad (Figure 37).

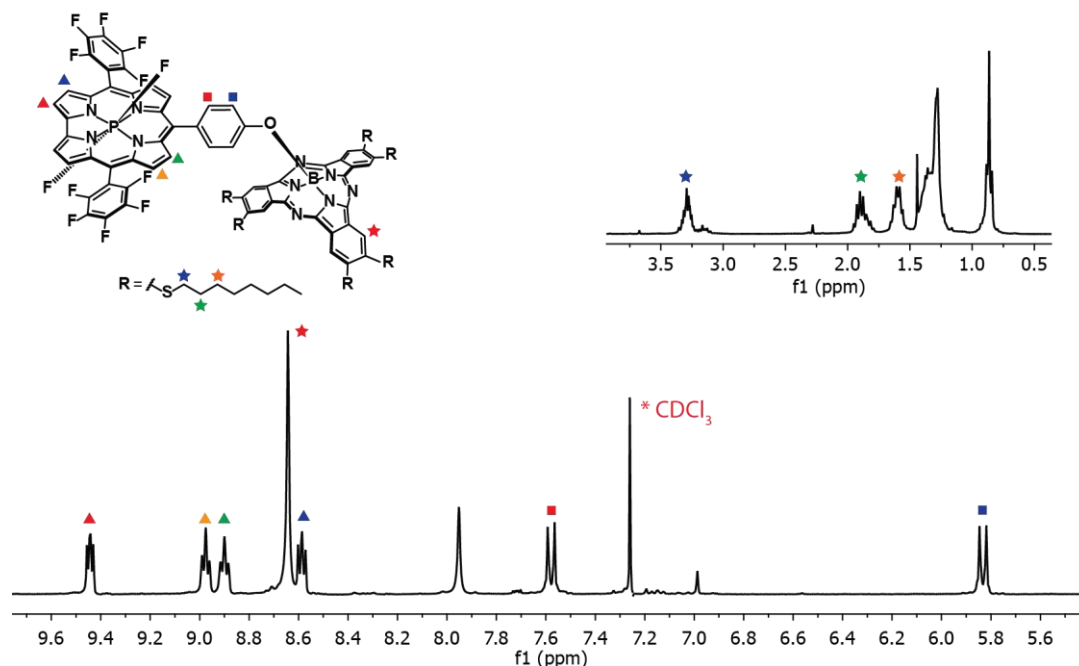
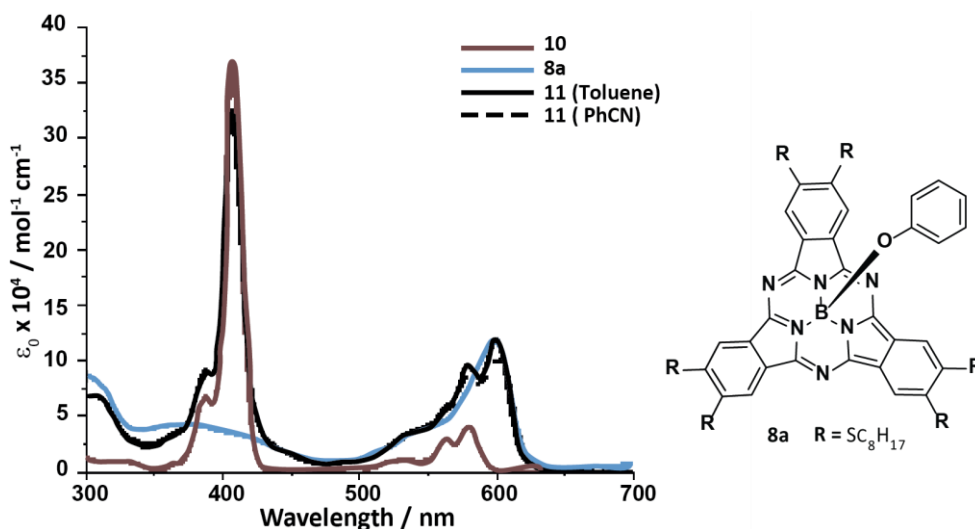


Figure 37.  $^1\text{H}$ -NMR (300 MHz) spectrum in  $\text{CDCl}_3$  at  $25^\circ\text{C}$  of SubPc-Cor dyad **11**.

#### 1.4.3.4. Optical properties of SubPc-Cor dyad **11**

The steady-state absorption spectra of SubPc-Cor dyad **11** were obtained in toluene and PhCN, and compared to its corresponding precursors (Figure 37). Dyad **11** show analogous absorption spectra as the previously observed for the SubPc-Cor dyads **4**, **5**, **6** and **7**, as a combination of both SubPc **8** and PCor **10** absorption profiles, mostly preserving their initial molar extinction coefficients. Emission spectra features different fluorescence profiles as observed for the dyads **4**, **5**, **6** and **7**. Whereas in the case of the later a strong quenching is detected, suggesting the formation of a CSS, the SubPc-Cor dyad **11** show a very intense emission from the SubPc moiety, regardless of the excitation wavelength (Figure 38). A closer look into the absorption and emission profiles of the corresponding monomers allows us to detect and overlap between Cor **10** absorption and SubPc **8**

emission. This led us to suggest an ET process from the Cor to the SubPc, probably through Förster's PET mechanism. Although these results are not in line with the previously reported in the present thesis, the linkage of two strong absorbing materials ( $\epsilon = 3.25E5$  (410 nm),  $1.17E5$  (600 nm)) funneling the energy to a concrete emission wavelength, enforces its use as an antenna. The combination of dyad **11** with  $C_{60}$  and  $C_{70}$  molecules is highly desired, due to the possibility of promote effective CSS thanks to the supramolecular interaction previously described between SubPc **8** and fullerenes.<sup>15,79</sup>



**Figure 38.** (Left) Steady-state absorption spectra of references SubPc **8R** and Cor **10** in toluene, and SubPc-Cor **11** in toluene and PhCN. (Right) Chemical structure of SubPc reference **8R**.

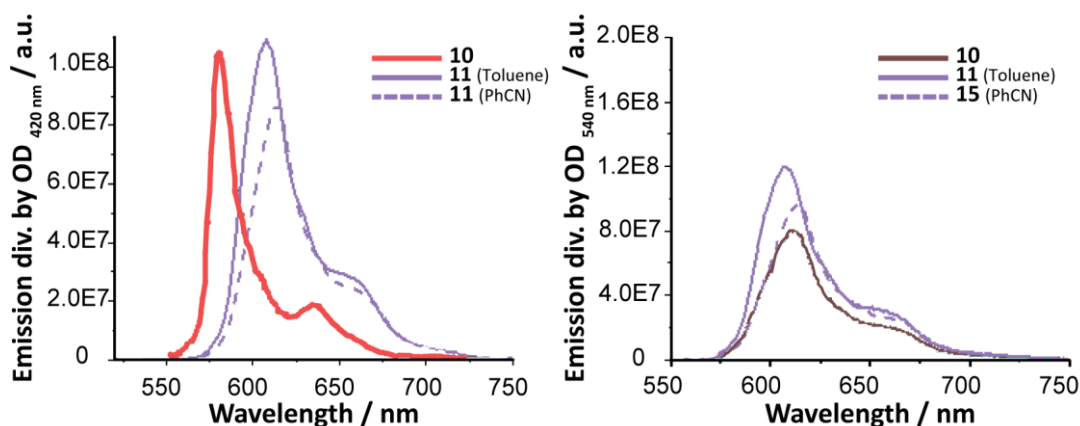


**Figure 39.** Steady-state emission spectra of references **8a** and **10** and SubPc-Cor dyad **11** (violet) at excitation wavelengths of 420 nm (left) and 540 nm (right).

*Synthesis and characterization of SubPc-Cor covalent systems linked through Cor meso- position*

## 1.5. Synthesis and characterization of SubPc-Cor covalent systems linked through Corrole axial position

### 1.5.1. Background

The coordination chemistry in the axial positions of porphyrinoids complexes has been extensively employed for the introduction of different functionalities. It allows to fine-tune the energy gaps and the photophysical properties of the complexes without modification of the macrocyclic ligand. Axial substitution chemistry in Cors, however, remains an unexplored field mainly because the weakness of the bonding of axial ligands to chelated metal ions. In general, all the compounds able to adopt a pentacoordinated structure are prone to accommodate an axial ligand.

PCors are generally obtained by refluxing the free-base ligand in presence of  $\text{POCl}_3$  or  $\text{PCl}_3$ . Except for a few specific methodologies, (*i.e.* the use of the phosphonium salt  $\text{PhPCl}_4^+$  yields the Ph- substituted phosphorus complex),<sup>173</sup> PCor is obtained as  $[\text{P}(\text{Cor})(\text{OH})]^+$ ,  $[\text{P}(\text{Cor})\text{O}]$  or  $[\text{P}(\text{Cor})(\text{OH})_2]$ . Those species are often found in equilibrium between their penta- and hexa-coordinated structures (Figure 40). This equilibrium depends on the electronic structure of the Cor, the axial ligands and the coordinating character of the solvent media.

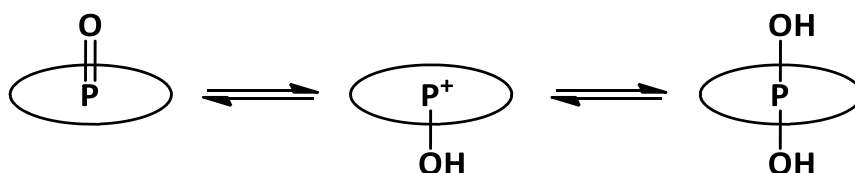


Figure 40. Equilibrium between oxo-, hydroxo- and *trans*-bishydroxo-P(V)Cors.

Hexa-coordinated complexes are more stable in coordinating solvents (*i.e.*  $\text{CH}_3\text{OH}$ ,  $\text{CH}_3\text{CN}$  or THF), whereas in non-coordinating solvents (*i.e.* Toluene,  $\text{CH}_2\text{Cl}_2$ ,  $\text{CHCl}_3$  or  $\text{C}_6\text{H}_6$ ) the hexa-coordinated P(V)Cor complexes suffer from axial ligand dissociation. For stabilizing the hexa-coordinated geometry of P(V)Cors in non-coordinating solvents, Ravikanth *et al.*

<sup>173</sup> Gilhula, J. C.; Radosevich, A. T. *Chem. Sci.* **2019**, *10*, 7177.

employed moderately bulkier, electron-donating axial silyloxy groups to restrict the axial ligand dissociation through electronic factors.<sup>174</sup>

As stated above, axial substitution is useful in order to add functionalities to the complex while leaving free Cor *meso*- and  $\beta$ - positions, where further modifications can be performed (*i.e.* addition of iodine in beta for its use in triplet-triplet annihilation systems).<sup>175</sup> Particularly for PCors, the lack of strategies developed for the introduction of different moieties once the metals are complexed is one of the main drawbacks for the exploitation of this chemistry.

Several advances have been made in order to expand its coordination chemistry. The first axial substitution reactions were reported by Kadish *et al.* employing Grignard reagents for the formation of different P-C bonds, in addition to a dihydrido substituted complex using lithium aluminum hydride (LiAlH<sub>4</sub>).<sup>176</sup> Additionally, the hydroxy ligands of an hexacoordinated P(V)Cor can be easily substituted by fluoro upon treatment with diluted HF, being later on impossible to remove.<sup>177</sup> Axial hydroxy ligands are so labile that they can be substituted by simply subjecting the P(V) complex to a column chromatography with small amounts of coordinating solvents in the mobile phase.<sup>178</sup> Reflux on alcoholic solvents after 24h gave axially solvent substituted Cors up to 30% yield. An elegant modification developed by Gross and co-workers included the addition of small amounts of TFA, obtaining almost quantitative conversions in just a few minutes at room temperature.<sup>179</sup> In the proposed mechanism, the acid catalyzes the reaction by removal of one molecule of H<sub>2</sub>O, allowing for the introduction of one solvent molecule. It should be noted that, in all the reported examples, the nucleophile is employed as the reaction solvent, although some groups reported the axial ligand substitution reaction employing almost stoichiometric

---

<sup>174</sup> Chatterjee, T.; Lee, W.-Z.; Ravikanth, M. *Dalton Trans.* **2016**, 45, 7815.

<sup>175</sup> Mahammed, A.; Chen, K.; Vestfrid, J.; Zhao, J.; Gross, Z. *Chem. Sci.* **2019**, 10, 7091.

<sup>176</sup> Kadish, K. M.; Ou, Z.; Adamian, V. A.; Guillard, R.; Gros, C. P.; Erben, C.; Will, S.; Vogel, E. *Inorg. Chem.* **2000**, 39, 5675.

<sup>177</sup> Vestfrid, J.; Kothari, R.; Kostenko, A.; Goldberg, I.; Tumanskii, B.; Gross, Z. *Inorg. Chem.* **2016**, 55, 6061.

<sup>178</sup> Gao, D.; Azarias, C.; D'Aléo, A.; Giorgi, M.; Siri, O.; Balaban, T. S.; Jacquemin, D.; Canard, G. *Eur. J. Inorg. Chem.* **2017**, 780.

<sup>179</sup> Chen, Q.; Xiao, Z.; Fite, S.; Mizrahi, A.; Fridman, N.; Zhan, X.; Keisar, O.; Cohen, Y.; Gross, Z. *Chem. Eur. J.* **2019**, 25, 11383.

amounts of nucleophile.<sup>173,180</sup> In particular, Ravikanth and co-workers activated the oxygen at the axial position by deprotonation of the hydroxy ligand for the introduction of silyloxy groups.<sup>173</sup>

It is worth pointing out that, in most of the cases, a high excess of the nucleophile with respect to the Cor is needed in order to replace the axial ligand. We cannot help but notice the resemblance with the axial substitution reaction of SubPcs, in which a high excess of nucleophile was required in order to carry out the reaction. An activation of the P(V) axial position is needed for the introduction of more complex molecules, in which and excess is not advisable.

## **1.5.2. Results and discussion**

### **1.5.2.1. Activation of axial position of PCors.**

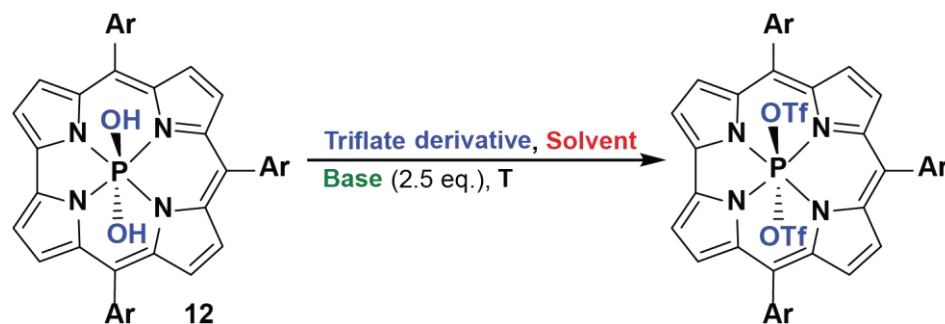
The difficulties with the introduction of new functionalities in the axial position of PCors, and our group previous experience in the activation of the boron position of SubPcs, led us to attempt developing a methodology for the activation of the phosphorus axial position.

P(V)Cors may be considered as electrophilic phosphonium cations with a square pyramidal geometry imposed by the macrocycle's binding pocket, displaying a marked sensitivity to hydroxylic and halide functionalization. Due to their high oxygen affinity, the use of triflate as counterpart anion should be favored. For that, different conditions employing triflic anhydride as triflate source have been tested (Table 7).

---

<sup>180</sup> a) Giribabu, L.; Kandhadi, J.; Kanaparthi, R. K. *J Fluoresc.* **2014**, *24*, 569. b) Achary, B.S.; Ramya, A.R; Nanubolu, J. B.; Seetharaman, S.; Lim, G. N.; Jang, Y.; D'Souza, F.; Giribabu, L. *New J. Chem.* **2018**, *42*, 8230.

**Table 7.** Reaction scope for the axial position activation of PCor **12**. a) After 24h, and excess of <sup>t</sup>Bu-PhOH was added in all cases. Ar = C<sub>6</sub>F<sub>5</sub>



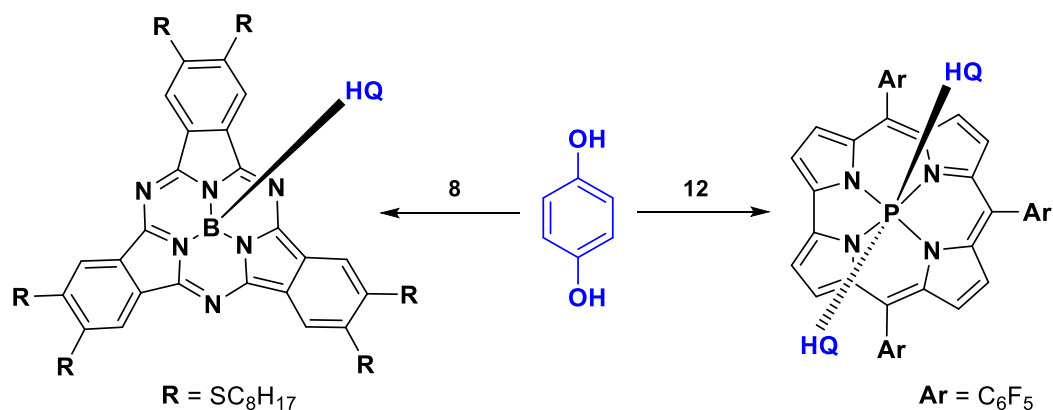
	Triflate	Solvent	Base	T (°C)
1 <sup>a</sup>	Tf <sub>2</sub> O	Toluene	DIPEA	80
2 <sup>a</sup>	Tf <sub>2</sub> O	Toluene	Pyridine	80
3 <sup>a</sup>	Tf <sub>2</sub> O	DCE	DIPEA	80
4 <sup>a</sup>	Tf <sub>2</sub> O	DCE	Pyridine	80
5 <sup>a</sup>	Sc(OTf) <sub>3</sub>	Toluene	-	80-100
6 <sup>a</sup>	Sc(OTf) <sub>3</sub>	DCE	-	80-100

In order to avoid the incorporation of the solvent into the axial position, non-coordinating solvents have been employed. Dichloroethane (DCE) has been tested instead of DCM for increasing the temperature. After 24h, no evidence of the triflate derivative formation was observed, neither by TLC or UV/Vis. In all cases, an excess of 4-*Tert*-Butylphenol (~50 eq.) was added in order to confirm a possible non-detectable axial position activation, without success.

Further reactions were attempted employing scandium triflate (Sc(OTf)<sub>3</sub>) as source, which is typically employed in organic synthesis as a robust lewis acid catalyst. Similar results were obtained, but no trace of an activated PCor could be detected (Table 7, entries 5-6).

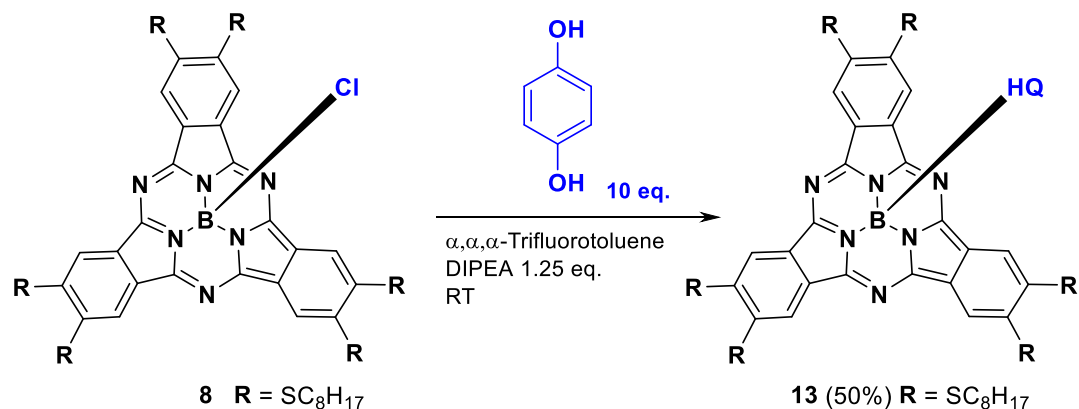
### 1.5.2.2. Alternative strategies for the axial substitution reaction in PCors

The bad results obtained in the activation of the axial position of PCors led us to test the already described strategies for the axial substitution reaction. Following the same strategy employed in the synthesis of SubPc-Cor dyads through their *meso*-position, hexasubstituted-thioether SubPc **8** has been employed for its connection with the energetically suited PCor **12**, which **10** was provided by Dr. Fabrizio Caroleo, from Prof. Roberto Paolesse's group. Hydroquinone (HQ) has been largely employed as a connector between SubPcs and different molecular units. To avoid a multisubstitution reaction between PCor and the HQ fragment, the approach was tackled from the axial substitution of the SubPc (Scheme 13).



Scheme 13. Two different axial substitution hydroquinone (HQ) routes over SubPc **8** (left) and PCor **12** (right).

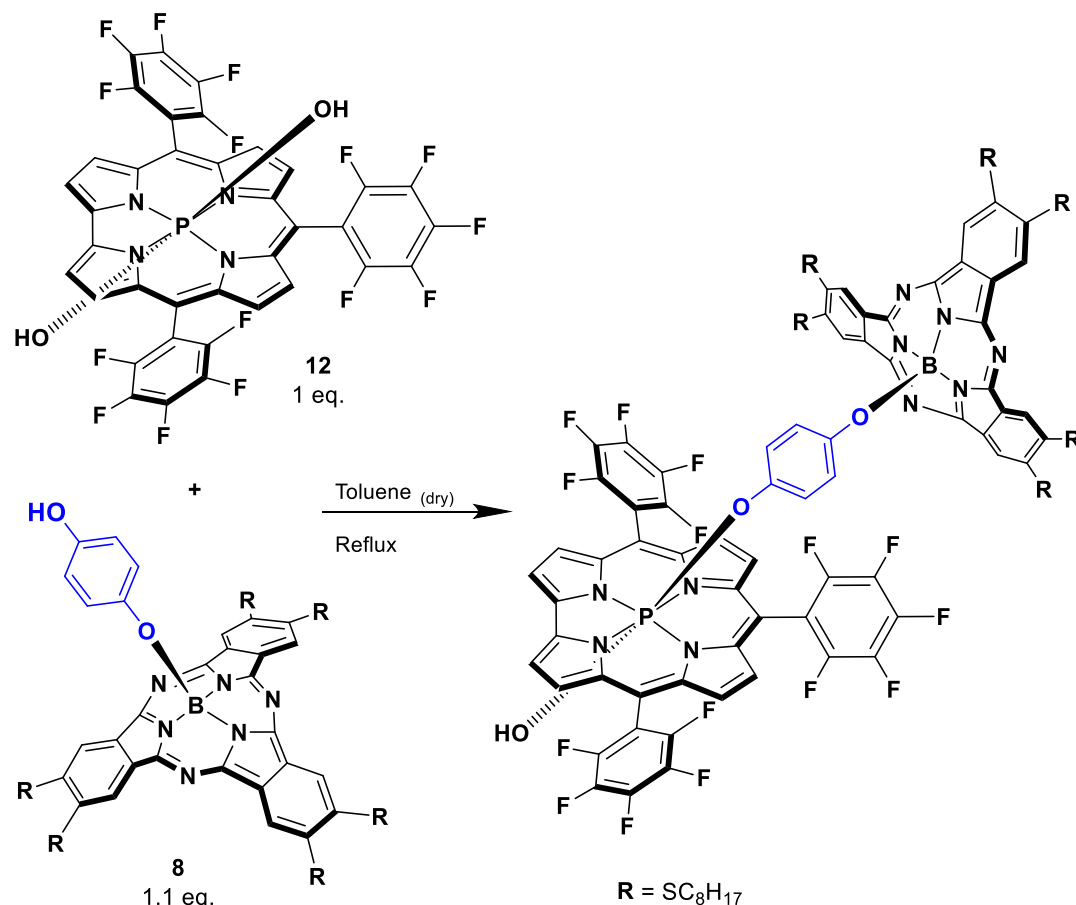
For the synthesis of SubPc **13**, the methodology previously described in section 1.4.3.1. was followed. Due to the high hydrolysis tendency for of SubPc **8**, cyclotrimerization reaction, vacuum-removal of the solvent and successive axial substitution reaction with an excess of HQ was carried out. Subsequent purification *via* silica-gel column chromatography led to SubPc **13** in an estimated 50% yield (Scheme 14).



**Scheme 14.** Synthetic route for the preparation of SubPc-HQ **13**

Subsequently, reaction conditions employing stoichiometric amounts of SubPc **13** and PCor **12** were applied, following the reaction by TLC.<sup>179</sup> However, after 6 hours, no new spots neither changes in the initial ones were observed. With respect to the recently strategy presented by Gross and co-workers,<sup>178</sup> a catalytic amount of TFA was added in order to activate the axial position of PCor (Scheme 15). However, no changes were observed, probably due to the lower number of nucleophile equivalents. An addition of 10-fold extra equivalents, followed by an increase in temperature led to decomposition of SubPc, probably due to *meso*-Nitrogen protonation and subsequent ring opening, an already known mechanism.

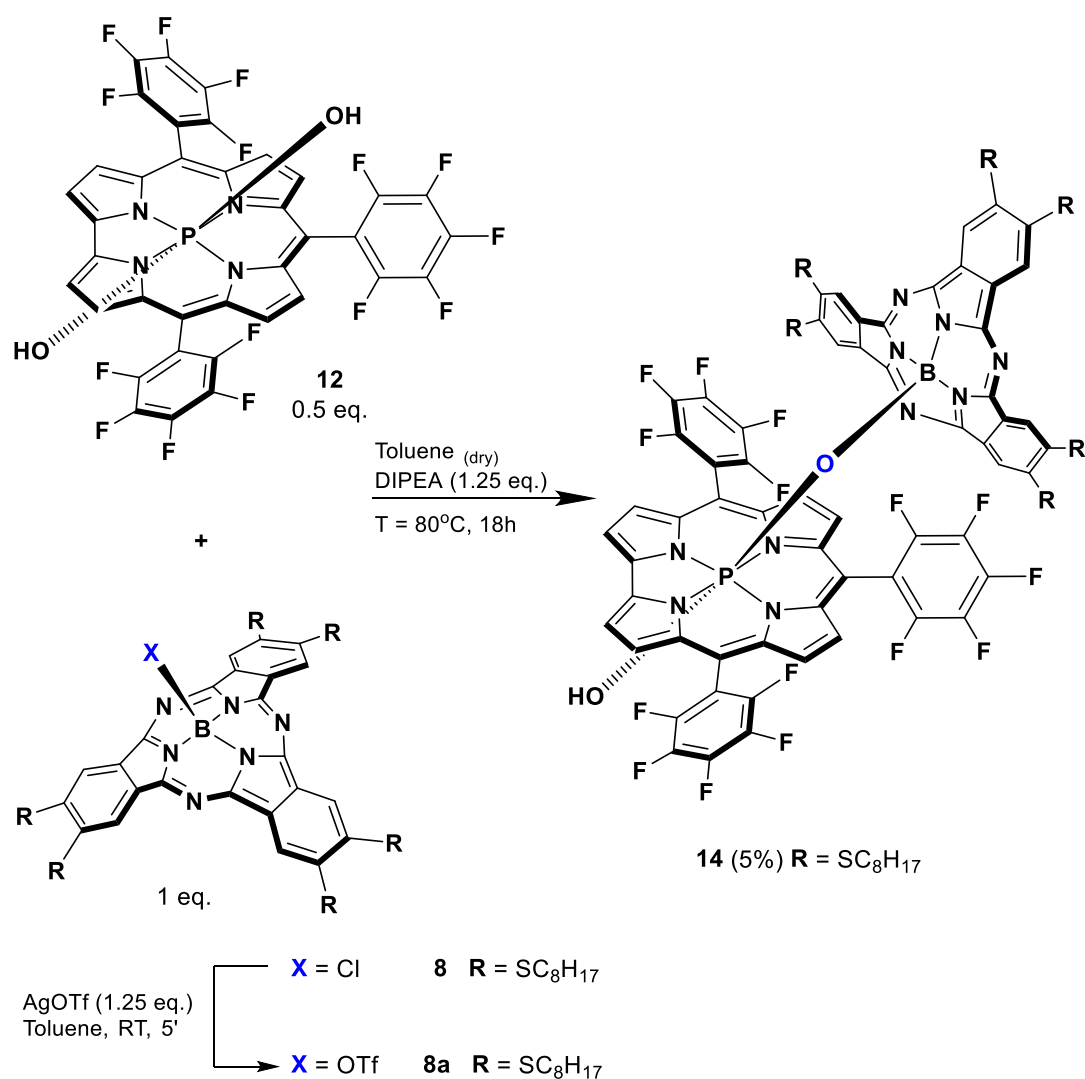
Synthesis and characterization of SubPc-Cor covalent systems linked through Cor axial position



Scheme 15. Synthetic route attempted for the preparation of SubPc-HQ-PCor dyad.

Those discouraging results led us to swap the direction of the reaction. Since in the later PCor **12** was formally acting as an electrophile and SubPc **8** as a nucleophile, we decided to try the other way around. Whereas the axial substitution reaction of PCor is in a dead end, the same for SubPcs is widely studied. At first instance, the use of a bridge was mandatory in order to avoid autoquenching of the resulting exciton in EET processes. However, the lack of results led us to discard the use of an intermediate link. The phosphorus hydroxy axial ligands may be deprotonated in a similar manner that Ravikanth's report,<sup>173</sup> in a way generally employed for SubPcs phenolic axial substitution reactions. Consequently, freshly synthesized SubPc **8** was added over a solution of PCor **12**, and the reaction was followed by TLC (Scheme 16). Although thioether SubPcs are known to be

highly reactive due to its prominent donor character, silver triflate activation methodology was employed in order to ensure the effectiveness of the reaction.



**Scheme 16.** Synthetic route for the preparation of SubPc-O-PCor dyad **14**.

Although unreacted PCor **12** was still present, a new blue spot appeared. <sup>1</sup>H-NMR spectrum in CDCl<sub>3</sub> led to signals corresponding to the thioether chains of the SubPc and the β-position of Cor. Although bad resolved, integration of the signals suggested the

Synthesis and characterization of SubPc-Cor covalent systems linked through Cor axial position

presence of the monosubstituted compound (Figure 41). Mass spectrometry confirmed the presence of dyad **14** (Figure 42).

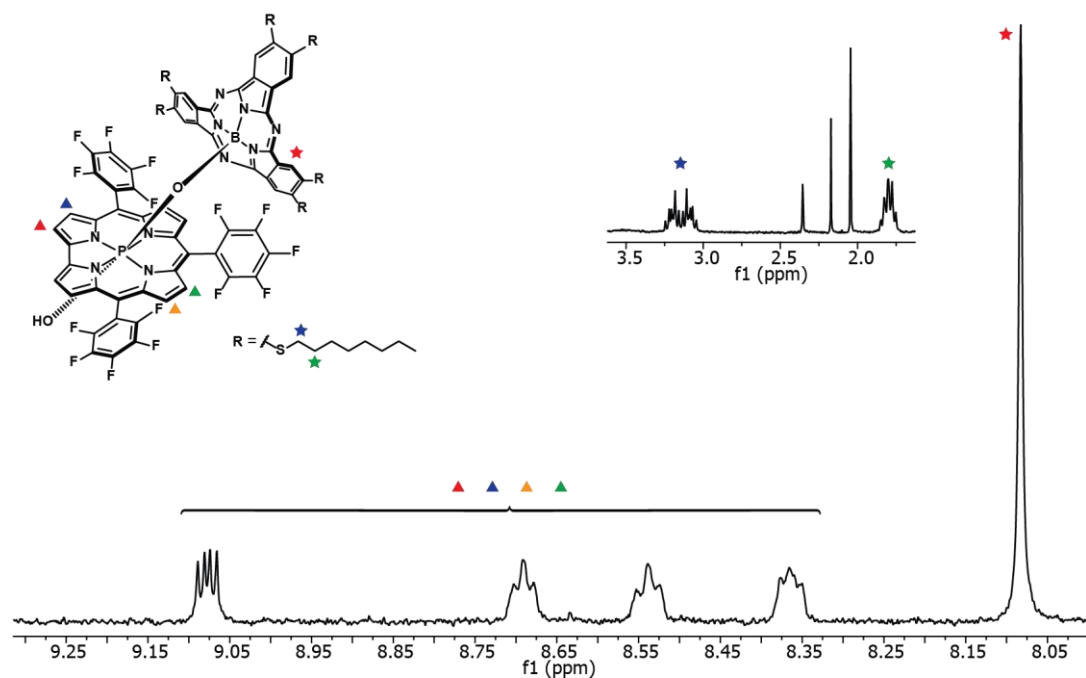
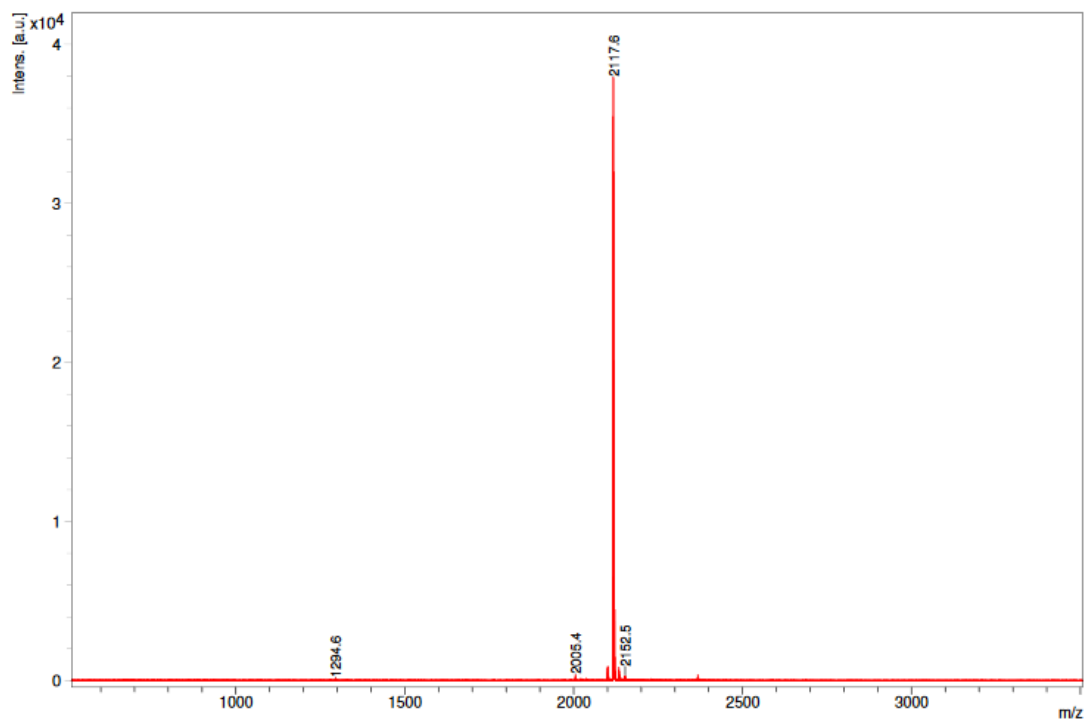


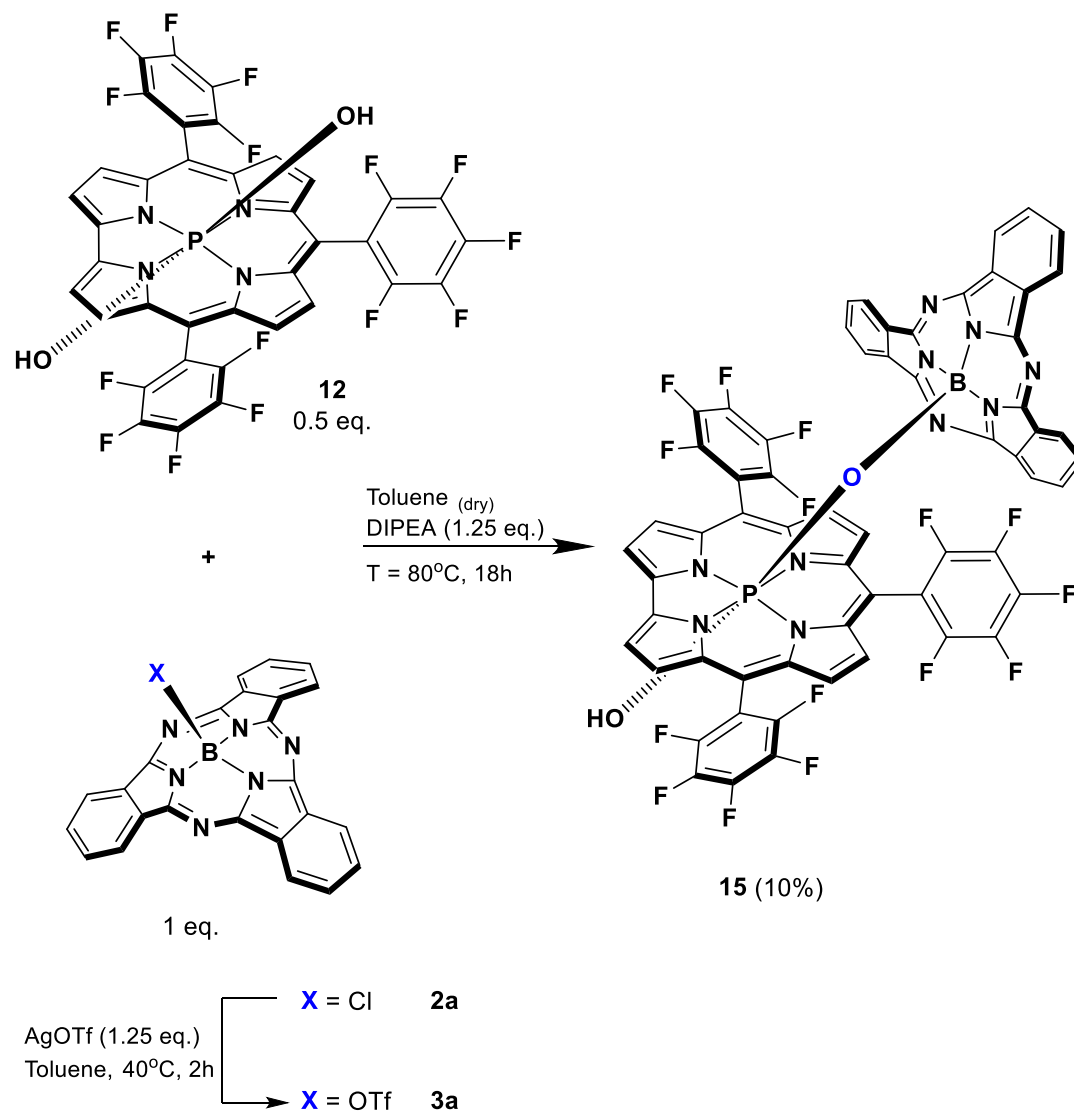
Figure 41. <sup>1</sup>H-NMR (300 MHz) spectrum in CDCl<sub>3</sub> of SubPc-Cor dyad **14** at 25°C. Ar = C<sub>6</sub>F<sub>5</sub>.



**Figure 42.** MALDI mass spectrometry assay of SubPc-Cor dyad **14**. Matrix: DCTB.

In order to confirm the effectiveness of the reaction, the same was tried employing SubPc **2a**. A new brown spot could be observed by TLC, reflecting the combination of the absorption bands of both Cor **13** and SubPc **2a** (Scheme 17).

Synthesis and characterization of SubPc-Cor covalent systems linked through Cor axial position



Scheme 17. Synthetic route for the preparation of SubPc-Cor dyad 15.

$^1\text{H-NMR}$  spectra of SubPc-Cor **15** featured signals corresponding to both SubPc **2a** and PCor **12** fragments (Figure 43). In the same way as SubPc-Cor **14**, signal integration suggested the presence of only one SubPc. Mass spectrometry confirmed the presence of SubPc-Cor dyad **15**, without any traces of the disubstituted triad (Figure 44).

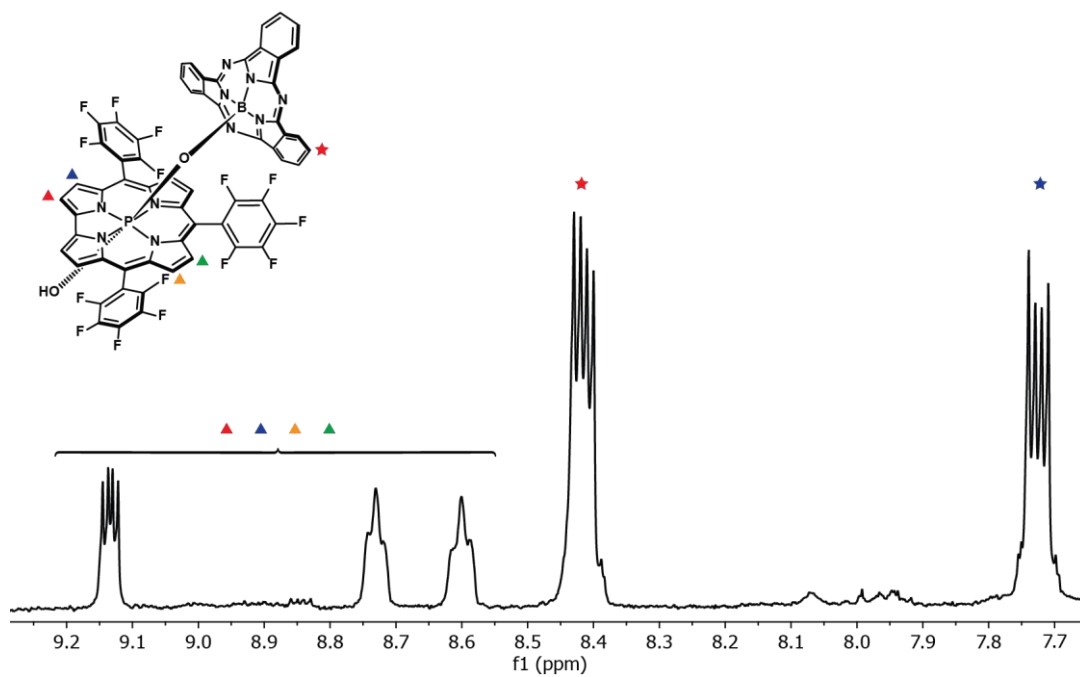


**Figure 43.** <sup>1</sup>H-NMR (300 MHz) spectrum in CDCl<sub>3</sub> of SubPc-Cor dyad **15** at 25°C. Overlap of pyrrole β- and SubPc *ortho*-protons at 8.30 ppm.

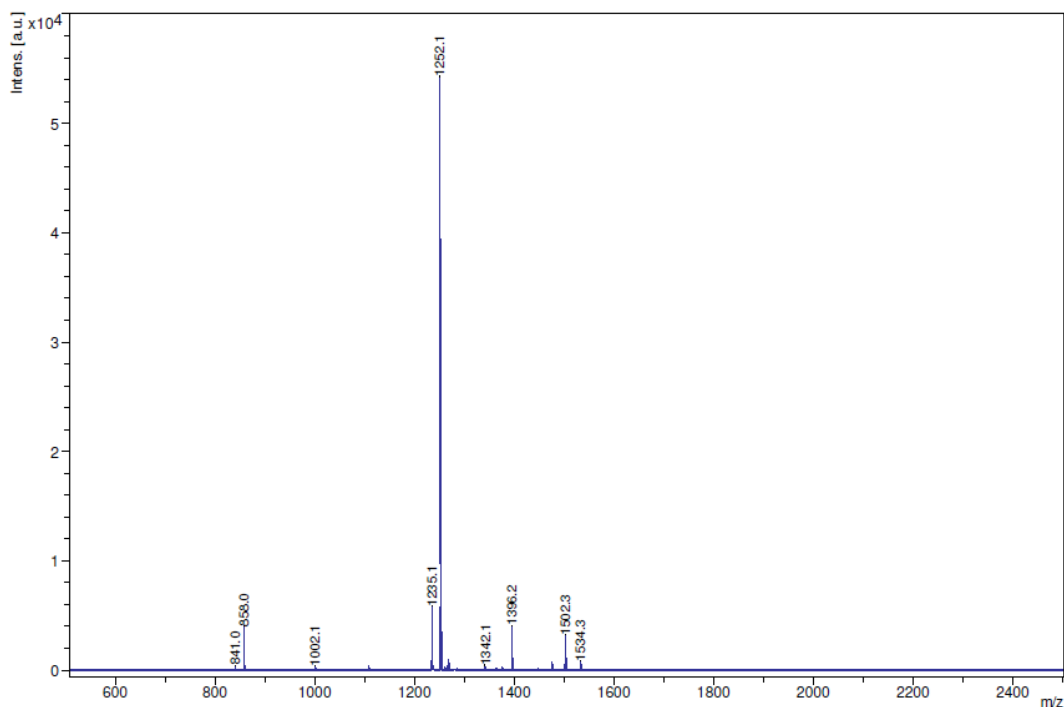
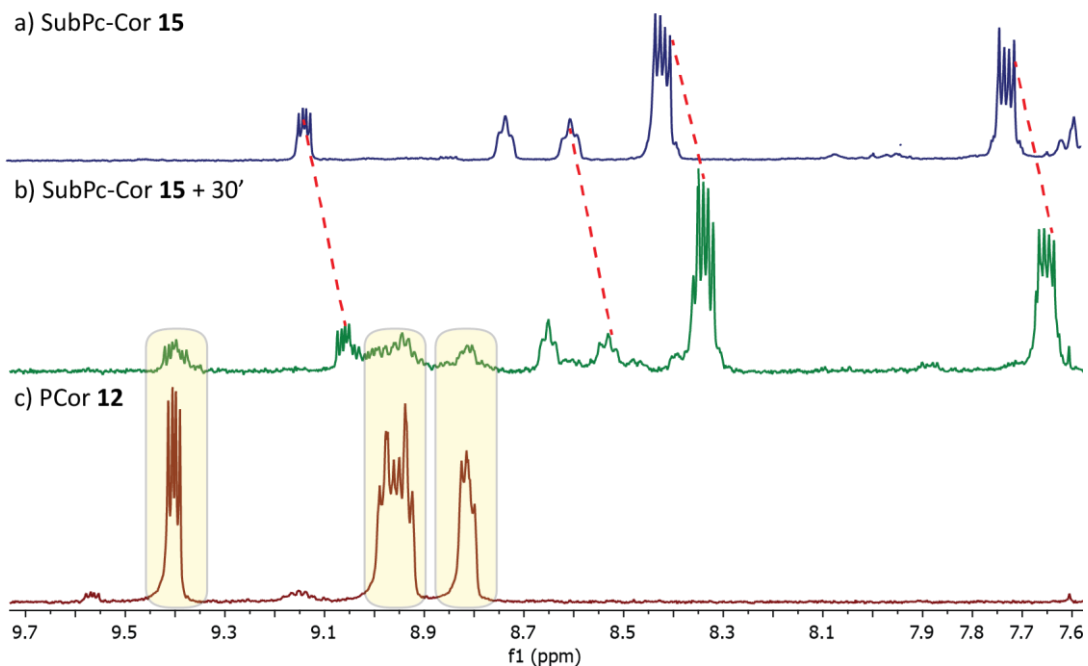


Figure 44. MALDI mass spectrometry assay of SubPc-Cor dyad **15**. Matrix: DCTB.

Regarding the possible dynamic behavior of the complexes, SubPc-Cor **14** stability was tested by performing two TLC plates in different solvents. In DCM only one blue spot could be observed, corresponding to the isolated dyad. On the other hand, in methanol, several blue spots, associated to SubPc related subproducts, and a reddish spot, appeared. The later corresponds to PCor **12**, reflecting the dynamic behaviour of these complexes in the presence of coordinating solvents.

A closer look into the  $^1\text{H-NMR}$  spectra of **14** and **15** reflects a similar trend. Focusing on the  $\beta$ -pyrrolic protons of Cor, bad resolution of their corresponding signals suggests an internal equilibrium involving different arrangements. Moreover,  $^1\text{H-NMR}$  spectrum of dyad **15** in  $\text{CDCl}_3$  was recorded thirteen minutes after the first running (Figure 45, b), showing signals of compound **15** slightly shifted to lower ppm, along with low-intensity multiplets corresponding to compound **12** (Figure 45, c), being an indication of the axial ligand dynamic equilibrium experienced by P(V)Cors, specially in non-coordinating solvents.



**Figure 45.**  $^1\text{H-NMR}$  (300 MHz) spectra in  $\text{CDCl}_3$  at  $25^\circ\text{C}$  of a) SubPc-Cor dyad **15**, b) SubPc-Cor dyad **15** after 30 minutes and c) PCor **12**.

### 1.5.2.3. Optical properties of SubPc-Cor dyads **14** and **15**

Steady-state absorption spectrum of references **2a** and **12** have been acquired in toluene. Absorption of SubPc-Cor dyad **15** in toluene featured signals closely resembling the combination of Cor **12** and SubPc **2a** absorption bands. Absorption maxima were found at 415 and 562 nm, while their intensity where in order to their corresponding building blocks (Figure 46, left).

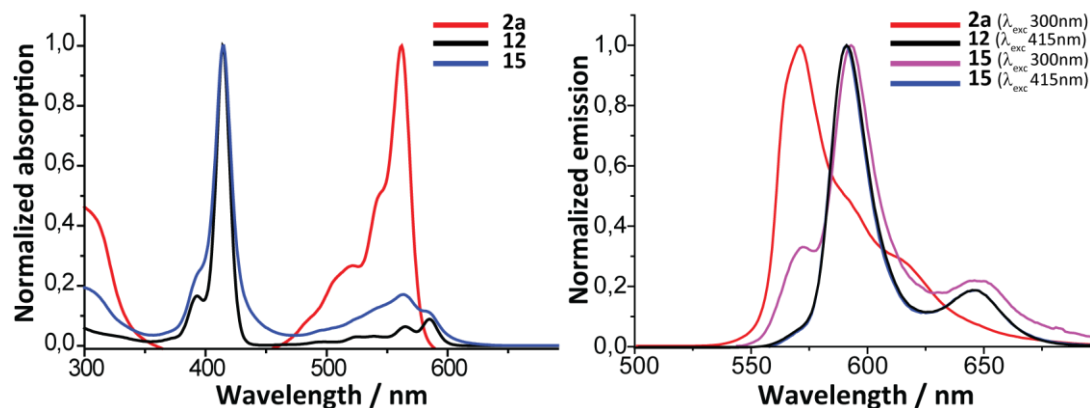


**Figure 46.** (left) Steady-state absorption spectra of SubPc **2a** (red), Cor **12** (black) and SubPc-Cor **15** (blue) in toluene, and (right) steady-state emission spectra of SubPc **2a** (red,  $\lambda_{exc} = 300\text{nm}$ ), Cor **12** (black  $\lambda_{exc} = 415\text{nm}$ ), and SubPc-Cor **15** (pink  $\lambda_{exc} = 300\text{nm}$ ; blue  $\lambda_{exc} = 415\text{nm}$ ) in toluene.

Emission of SubPc-Cor **15** was recorded in toluene. Regardless of the chosen band of excitation, the dyad shows a very intense emission arising from the PCor moiety (Figure 46, right). Therefore, a PET process can be assumed. In this case, due to the proximity of both molecules, none statement regarding the energy transfer mechanism followed can be done.

Steady-state absorption spectrum of SubPc-Cor **14** in toluene showed features resembling the combination of both monomers. However, both Soret and Q bands present broad profiles, indicating a strong electronic interaction between both independent fragments at the ground-state level (Figure 47).

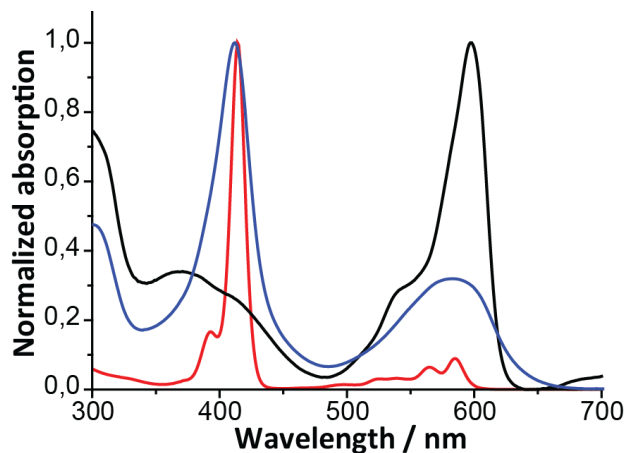


**Figure 47.** Steady-state absorption spectra of SubPc **8** (blue), Cor **12** (red) and SubPc-Cor **14** (black) in toluene.

Emission of dyad **14** in toluene showed some particular features. Excitation at 300 nm, corresponding to SubPc **8** Soret band, showed SubPc emission, whereas excitation at 411 nm, corresponding to Cor **12** Soret band, showed both Cor and SubPc emission profiles. In addition, both spectra are mostly defined by a dominant intense broad and structureless band at longer wavelengths relative to the emission of the monomers, with absorption maxima at 675 nm, that it is not characteristic of none of the individual components of the complex (Figure 48, left). It experiences a hypsochromic shift of 10 nm when increasing solvent polarity, from toluene to THF, while the signals corresponding to SubPc and Cor emission remain fixed (Figure 48, right), along with a decrease in the emission intensity. Thus, solvent dependence presented by the broad and structureless band *ca.* 675-685 nm suggests an emission arising from a polar excited state. Although a solvatochromic shift when increasing polarity is expected, the decrease in the emission intensity and the low distance between the donor and the acceptor fragments, led us to propose the formation of an excited complex, namely *exciplex*. However, the conduction of further studies (*i.e.* femtosecond transient absorption spectroscopy) must be considered in order to elucidate its nature.

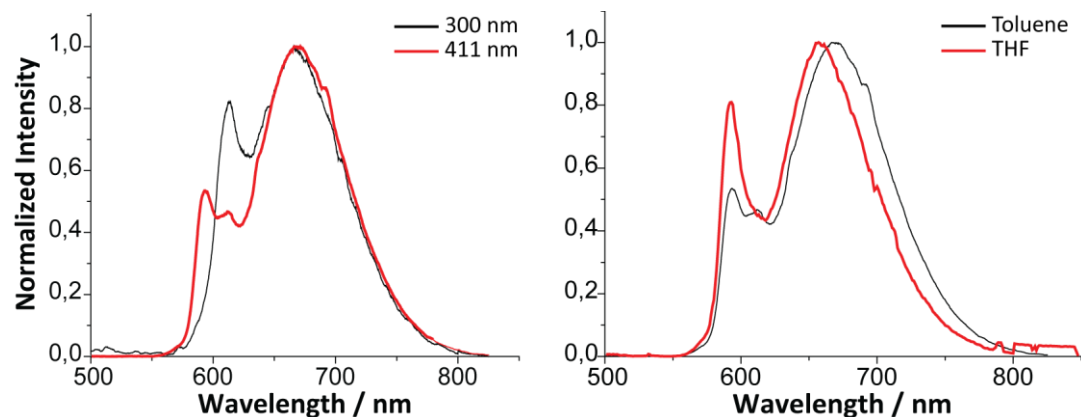


**Figure 48.** (Left) Steady-state emission spectra of SubPc-Cor **14** upon excitation at 300 nm (black) and 411 nm (red) in toluene. (Right) Steady-state emission spectra of SubPc-Cor **14** upon excitation at 411 nm in toluene (black) and THF (red).

*Exciplexes* are electronically excited complexes of definite stoichiometry. They can be better described as excited state complexes stabilized by charge transfer interactions. To form an exciplex  $(AB)^*$ , first a compound A (which can be a molecule or atom) in the ground state undergoes an excitation process such as photon absorption ( $h\nu_{exc}$ ), although other excitation mechanisms are possible. The excited compound  $A^*$  then forms an excited state complex  $(AB)^*$  with ground-state compound B. This association is driven by the existence of a local energy minimum. The excimer formation is also accompanied by a reduction of the distance between the molecules. Such a species give rise to electrostatic interactions between closely spaced electron donors and acceptors in their ground and excited states.

The stability of these complexes can be easily explained appealing to the molecular orbital's theory. If we consider an interaction between D and A, the major electronic interactions will involve their HOMO and LUMO. According to the rules of perturbation theory, the HOMO and LUMO of D will interact with the HOMO and LUMO of A to yield two new HOMOs of the ground-state exciplex. The new HOMOs and LUMOs are split in energy to the original HOMOs and LUMOs of D and A, as shown in Figure 49. In the ground-state, the four electrons that occupied the HOMOs of A and D occupy the new set of orbitals according to the Aufbau principle and fill the lowest-energy orbital. Two electrons are stabilized in the bonding orbital and two in the non-bonding orbital, cancelling each other, and being the neat energy gained for this interaction equal to zero. However, in the excited

state, since one of the partners is excited, *three* electrons are stabilized (bonding orbitals) and one is destabilized (non-bonding orbital). Thus, a net gain in energy is achieved by its interaction

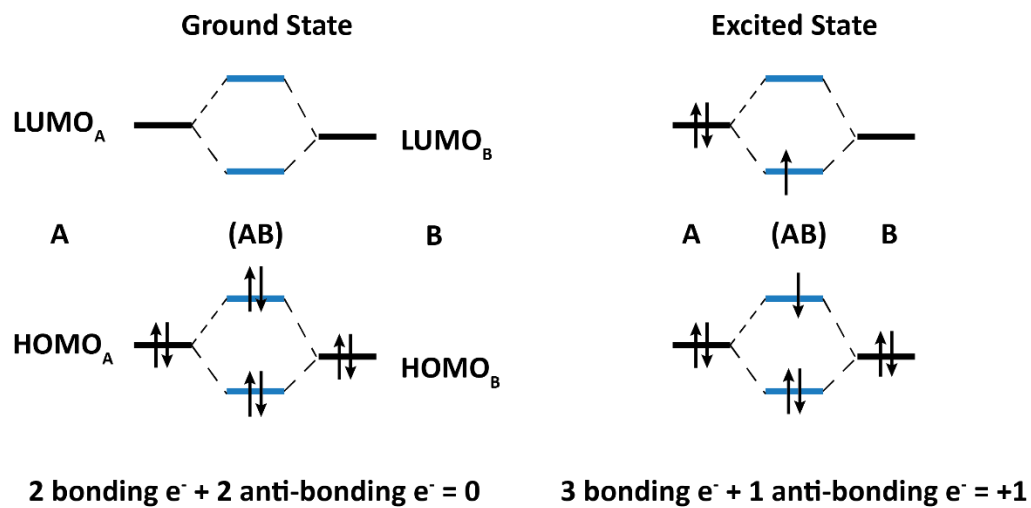


Figure 48. Orbital interactions of D-A pairs and D<sup>-\*</sup>-A exciplex.

## 1.6. Synthesis and characterization of Subphthalocyanine-Ferrocene covalent systems

### 1.6.1. State-of-the-art in Subphthalocyanine-Ferrocene dyads

From the family of metallocenes, Fc is by far the most extensively researched. Considered as the prototype of this sandwich-type organometallic compounds, it presents significant stability and a great synthetic versatility, being able to react in multiple ways such as Friedel-Crafts acylation and alkylation reactions; moreover, its cyclopentadienyl units can be sulfonated, formylated, or metallated with *n*-butyllithium, opening the way to a wide range of post-functionalization reactions. Additionally, they have proven to be greatly useful in many applications, particularly in electrochemistry as an internal reference, relying on the robust redox behavior of the Fe<sup>2+</sup>/Fe<sup>3+</sup> couple. For so, they have been largely chosen as the D moiety in a vast number of D-A systems. Particularly in the case of SubPcs, they have been incorporated into its axial position by several means, either directly attached to the boron atom,<sup>181</sup> or by using different connectors and spacers like ethyne-,<sup>35,182</sup> phenoxy-,<sup>183</sup> carboxyphenoxy-,<sup>184</sup> ether-,<sup>33</sup> carboxy-<sup>35,185,186</sup> or methylaminophenoxy-<sup>187</sup> groups. In many of these examples, PeT events occur, leading into the generation of SubPc<sup>-</sup>-Fc<sup>+</sup> CSSs.<sup>35,37,38,40</sup> They have also been successfully introduced into SubPc periphery as tri- and hexaferrocenyl-substituted SubPcs.<sup>188</sup> In that case, although its influence into SubPc conjugated system leads to broad and bathochromically shifted Q-Absorption bands with maximum at *ca.* 600-650 nm, they induce a strong perturbation of the electronic structure,

<sup>181</sup> Maligaspe, E.; Hauwiller, M. R.; Zatsikha, Y. V.; Hinke, J. A.; Solntsev, P. V.; Blank, D. A.; Nemykin, V. N. *Inorg. Chem.* **2014**, *53*, 9336.

<sup>182</sup> Gotfredsen, H.; Jevric, M.; Broman, S.L.; Petersen, A. U.; Nielsen, M.B. *J. Org. Chem.* **2016**, *81*, 1.

<sup>183</sup> a) González-Rodríguez, D.; Carbonell, E.; de Miguel Rojas, G.; Atienza Castellanos, C.; Guldi, D. M.; Torres, T. *J. Am. Chem. Soc.* **2010**, *132*, 16488. b) El-Khouly, M. E.; El-Kemary, M. A.; El-Refaei, A.; Kay, K.-Y.; Fukuzumi, S. *J. Porphyrins Phthalocyanines* **2016**, *20*, 1148.

<sup>184</sup> González-Rodríguez, D.; Torres, T.; Olmstead, M. M.; Rivera, J.; Herranz, M. A.; Echegoyen, L.; Atienza Castellanos, C.; Guldi, D. M. *J. Am. Chem. Soc.* **2006**, *128*, 10680.

<sup>185</sup> Solntsev, P. V.; Spurgin, K. L.; Sabin, J. R.; Heikal, A. A.; Nemykin, V. N. *Inorg. Chem.* **2012**, *51*, 6537.

<sup>186</sup> Swarts, P. J.; Conraide, J. *Inorganic Chemistry* **2020**, *59*, 7444.

<sup>187</sup> El-Khouly, M. E.; Kim, J.-H.; Kay, K.-Y.; Fukuzumi, S. *J. Phys. Chem. C* **2012**, *116*, 19709.

<sup>188</sup> Fernández-Ariza, J.; Calderón, R. M. K.; Perles, J.; Rodríguez-Morgade, M. S.; Guldi, D. M.; Torres, T. *Chem. Commun.* **2017**, *53*, 8525.

which results in rapid deactivation of excited states as a means to prevent energy or electron transfer.

Peripheral chlorination of SubPcs have demonstrated to induce major shifts in the HOMO/LUMO energy gaps of the SubPc and their corresponding redox potentials.<sup>189</sup> Over the last years, they have been employed as acceptor materials by means of substituting fullerenes in both planar- and bulk-heterojunction solar cells. Thus, a power conversion efficiency (PCE) up to 4.0% for SubPcCl<sub>6</sub>-Cl in BHJ solar cells was achieved by our group, which was the highest reported value for solution-processed SubPc-based solar cells.<sup>190</sup> These results led us to investigate this molecule as a counterpart vs. the simple donor Fc in D-A systems.

## 1.6.2. Results and discussion

### 1.6.2.1. Synthesis of precursor SubPcs 16 and 17

The synthesis of the different precursors, perfluorinated SubPc **16** and hexachlorosubstituted SubPc **17**, were reported long time ago. However, whereas for the synthesis of SubPc **16** the methodology is optimized, thus obtaining yields of 60% at laboratory scale starting from commercially available tetrafluorophthalonitrile, the same for SubPc **17** has not yet been optimized, giving rise to scarce yields close to 10% starting from the non-so-available 4,5-dichlorophthalonitrile (**17a**). Although commercial, the latter is generally obtained after long time-consuming synthetic steps from 4,5-dichlorophthalic acid. Bender *et al.* developed a methodology for the synthesis of **17** at gram-scale, with yields up to a 90%. However, we could not be able to reproduce them. Instead, a modified procedure for the preparation of the later was developed by us at lab-scale in which the **17** was obtained in an impressive 60% yield. Reaction conditions were optimized, observing maximum yields when a 1-to-1 reaction between 4,5-dichlorophthalonitrile and BCl<sub>3</sub> in *p*-xylene was conducted, diluting the solution in a 1:10 v/v proportion with *o*-dichlorobenzene as co-solvent (Table 8, entries 4-5). The use of a high-boiling point aromatic solvent determined to be crucial in order to increase the reflux temperature up to

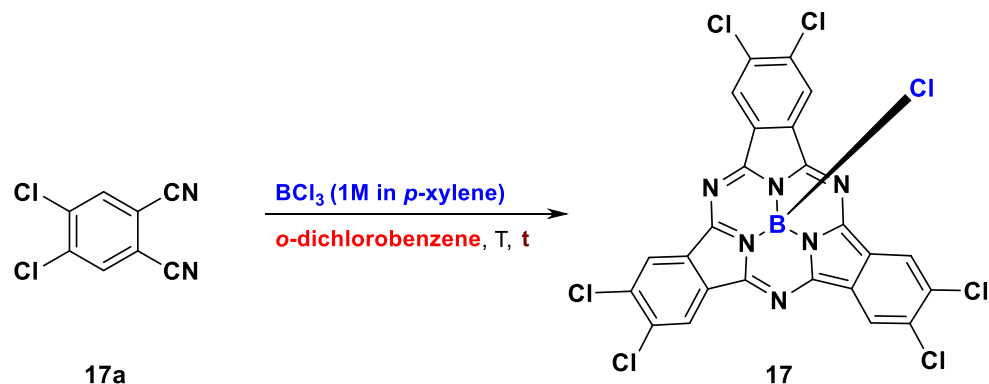
---

<sup>189</sup> a) Beaumont, N.; Castrucci, J. S.; Sullivan, P.; Morse, G. E.; Paton, A. S.; Lu, Z. H.; Bender, T. P.; Jones, T. S. *J. Phys. Chem. C* **2014**, *118*, 14813. b) Castrucci, J. S.; Josey, D. S.; Thibau, E.; Lu, Z. H.; Bender, T. P. *J. Phys. Chem. Lett.* **2015**, *6*, 3121.

<sup>190</sup> Duan, C.; Zango, G.; García Iglesias, M.; Colberts, F. J. M.; Wienk, M. M.; Martínez-Díaz, M. V.; Janssen, R. A. J.; Torres, T. *Angew. Chem., Int. Ed.* **2017**, *56*, 148.

180,5°C. Furthermore, the addition of  $\text{BCl}_3$  in *p*-xylene over the previously dissolved 4,5-dichlorophthalonitrile **17a**, and not the opposite way, determined to be critical for initiate the reaction in diluted conditions.

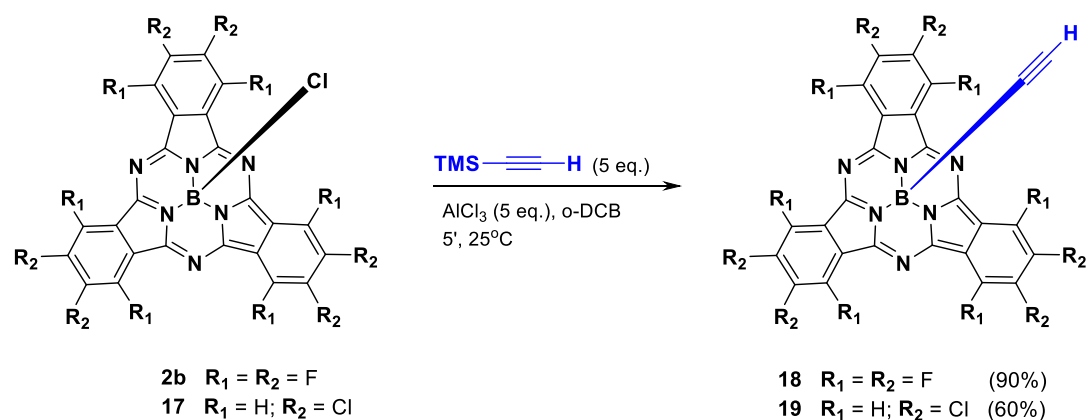
**Table 8.** Conditions scope for the optimization in the synthesis of SubPc **17**. a) In all cases, *o*-DCB is employed as a co-solvent. b) Reaction performed under microwave irradiation. c) 1-chloronaphtalene as co-solvent. d) Irradiation under 540 W.



	Phthal. (mmol)	$\text{BCl}_3$ (mL)	<i>o</i> -DCB (ml) <sup>a</sup>	T (°C)	Time	Yield (%)
<b>1</b>	3	3	-	145	40 min.	6.27
<b>2<sup>b</sup></b>	0.25	0.25	1 <sup>c</sup>	200 <sup>d</sup>	5 min.	6.12
<b>3</b>	0.25	0.6	3	180.5	20 hours	16
<b>4</b>	0.25	0.25	2	180.5	20 hours	49
<b>5</b>	1	1	8	180.5	20 hours	67

### 1.6.2.2. Synthesis of ethynyl-substituted SubPcs **18** and **19**

Employing the mild and versatile methodology developed by Nielsen *et al.* for the preparation of axially ethynyl-substituted SubPc derivatives,<sup>34b</sup> TMS-Ethynyl was used for its introduction over SubPc axial position. Addition of AlCl<sub>3</sub> over a deoxygenated solution of precursor SubPc-Cl leads into the formation of the SubPcCl[AlCl<sub>3</sub>] complex, which presents an intense blue color due to its coordination with SubPc *meso*-nitrogens. Once the color shifted, TMS-protected ethynyl fragment was added, thus obtaining SubPc **18** and **19** in a 90 and 50% yield, respectively (Scheme 17).



**Scheme 17.** Synthetic route for the preparation of SubPcs **18** and **19**.

The structure of both SubPc **18** and **19** was confirmed by H<sup>1</sup>-NMR, C<sup>13</sup>-NMR, B<sup>10</sup>-NMR, F<sup>19</sup>-NMR and mass spectrometry. In H<sup>1</sup>-NMR, a signal corresponding to the ethynyl terminal proton was assigned for each SubPc. Moreover, single crystals of the novel SubPc-Fc **19** suitable for X-ray diffraction analysis were obtained by slow diffusion of *n*-hexane into a chloroform solution of the corresponding SubPc derivative (Figure 49). They organize through π-π stacking concave-convex SubPc interactions, displaying slip-stacked columns (Figure 50, left). Each axial-ethynyl unit gives rise to up to three (B-C-CH...N) and (B-C-CH...C) interactions with an upper SubPc imino and its adjacent carbon units. Moreover, the ethynyl group interacts with two vicinal SubPcs, one through a (B-C-C...H) interaction and the other two (B-C-C...Cl) and (B-C...Cl) through the same Cl- atom.

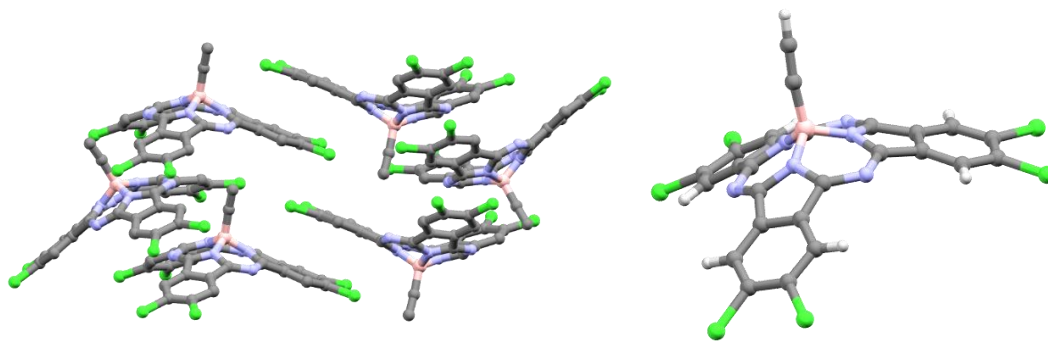
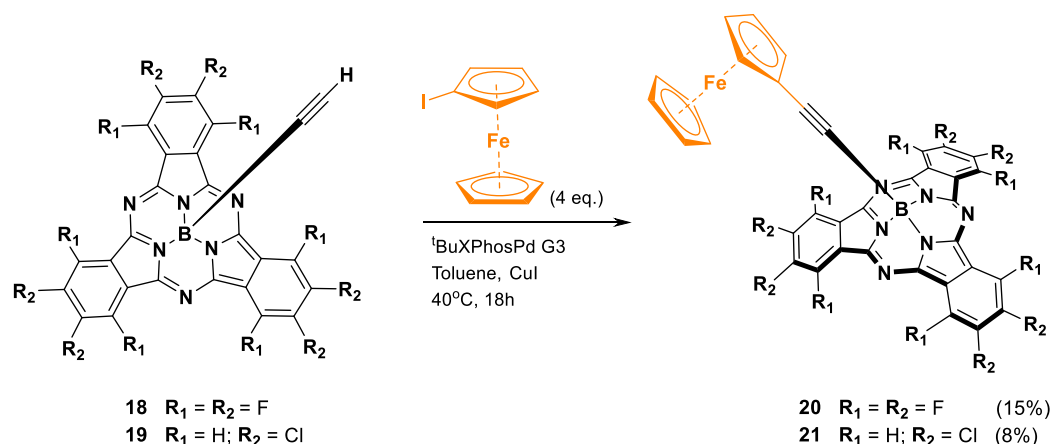


**Figure 49.** (Left) Lateral view of a portion of the X-Ray crystal structure of SubPc **19** showing the slip-stacked columnar arrangement. (Right) Lateral view of the X-Ray crystal structure of a single molecule of SubPc **19**. Chloroform molecules of crystallization have been omitted for clarity.

### 1.6.2.3. Synthesis of SubPc-Fc **20** and **21**

For the combination between axially ethynyl-substituted SubPcs **18** and **19** and Fc, a methodology was developed trusting in the widely known Palladium-catalyzed Sonogashira cross-coupling reaction. The reaction was initially carried out using Sonogashira conditions firstly employed for the coupling between Iodo-SubPcs and axially-substituted ethynyl SubPc derivatives. However, upon total consumption of the starting SubPc **18**, a unique product was detected by TLC, which was later determined as the homocoupling side product. Different catalyzers and ratios were employed in order to promote the reaction of SubPc-Fc dyad **20** as the main product. Particularly, <sup>t</sup>BuXPhos G3 has been used in combination with palladium for the catalysis of copper-free cross-coupling reactions, thus avoiding the formation of homocoupling products by Glaser reaction. The use of a preformed <sup>t</sup>BuXPhos Pd G3 along with an increase of the base amount lead into the formation of SubPc-Fc dyad **20** as the main product. Although a catalytic amount of CuI was added, no traces of homocoupling side products were detected. For the coupling between SubPc **19** and I-Fc, the same conditions used for the later were employed (Scheme 18). SubPc-Fc dyad **21** was obtained, although formation of the homocoupling product could not be avoided. The same reaction without the addition of CuI proved not to be successful. Additionally, during the purification process, both products presented similar R<sub>f</sub> values in a wide combination of mobile phases. All these drawbacks reduced the yield to a modest 8%.



**Scheme 18.** Synthetic route for the preparation of SubPc-Fc dyads **20** and **21**.

Characterization of both **20** and **21** dyads by  $^1\text{H-NMR}$  and mass spectrometry confirmed its structure. Signals for the Fc fragment can be detected around 3.80 ppm as a singlet and two triplets for the cyclopentadienyl and monosubstituted-cyclopentadienyl, respectively. Particularly for SubPc-Fc **21**, signals of SubPc  $\beta$  protons at 8.89 ppm are observed (Figure 50).

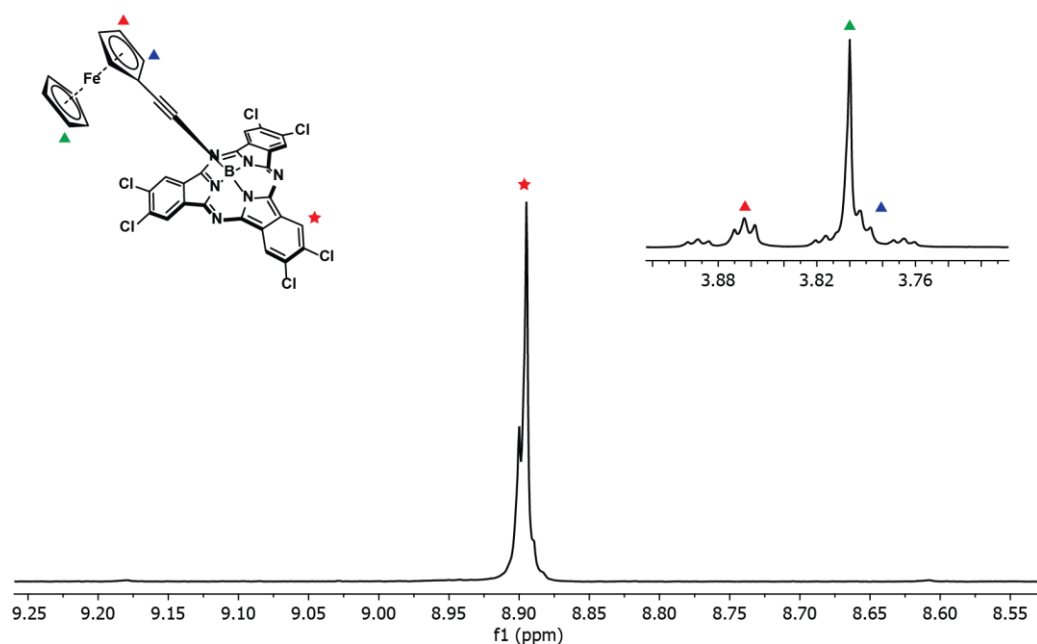


**Figure 50.**  $^1\text{H-NMR}$  (300 MHz) spectrum in  $\text{CDCl}_3$  of SubPc-Cor dyad **21** at  $25^\circ\text{C}$ .

#### 1.6.2.4. Optical properties of SubPc-Fc dyads **20** and **21**

A comparison between steady-state absorption spectra of SubPc-Fc dyads **20** and **21**, along with their respective reference SubPcs **18** and **19**, returns almost identical profiles, thus indicating negligible interactions in the ground-state between SubPc and its Fc counterpart (Figure 51). Emission spectra of both SubPc-Fc dyads, however, experiences a strong quenching with respect to the starting SubPcs. Therefore, the presence of a CSS can be assumed.

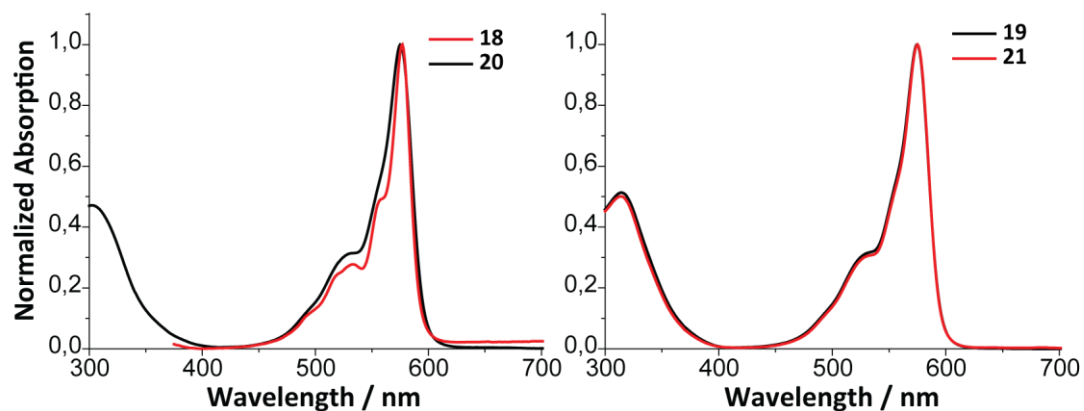


**Figure 51.** (Left) Steady-state absorption spectra of SubPc **18** (red) and SubPc-Ferrocene **20** (black). (Right) Steady-state absorption spectra of SubPc **19** (red) and SubPc-Ferrocene **21** (black).

## 1.7. Synthesis and characterization of Tetracyano-butadiene-Corrole covalent systems

### 1.7.1. Background

Tetracyanobutadiene (TCBD) is a strong electron acceptor, which its use has been increasing over the last decade due to its easiness of introduction in different molecules and arrays, by a [2+2] cycloaddition-retroelectrocyclization (CA-RE) reaction with tetracyanoethylene over activated alkynes. It has been largely employed as an electroactive counterpart in several D-A systems, where PET processes have been observed, in combination with anilines,<sup>191</sup> tetracyanoanthraquinodimethanes,<sup>192</sup> truxenes<sup>193</sup>, fullerenes<sup>194</sup> or curannulenes,<sup>195</sup> as well with Pors.<sup>196</sup> Moreover, in the family of porphyrinoids, our research group has made great efforts in the investigation of this interesting fragments by its introduction in Pc-,<sup>197</sup> SubPor-<sup>198</sup> or SubPc-based systems.<sup>199</sup> In this regard, exhaustive investigations have been made for the elucidation of the properties arising from their particular structural features, resulting from the quasi-orthogonal arrangement of its two dicyanovinyl (DCV) halves and the restricted rotation of the C-C bond

<sup>191</sup> Michinobu, T.; Boudon, C.; Gisselbrecht, J.-P.; Seiler, P.; Frank, B.; Moonen, N. N. P.; Gross, M.; Diederich, F. *Chem. - Eur. J.* **2006**, *12*, 1889.

<sup>192</sup> García, R.; Calbo, J.; Viruela, R.; Herranz, M. Á.; Orti, E.; Martín, N. *ChemPlusChem* **2018**, *83*, 300.

<sup>193</sup> Sharma, R.; Thomas, M. B.; Misra, R.; D'Souza, F. *Angew. Chem., Int. Ed.* **2019**, *58*, 4350.

<sup>194</sup> Yamada, M.; Rivera-Fuentes, P.; Schweizer, W. B.; Diederich, F. *Angew. Chem., Int. Ed.* **2010**, *49*, 3532.

<sup>195</sup> Wu, Y.-L.; Stuparu, M. C.; Boudon, C.; Gisselbrecht, J.-P.; Schweizer, W. B.; Baldrige, K. K.; Siegel, J. S.; Diederich, F. *J. Org. Chem.* **2012**, *77*, 11014.

<sup>196</sup> a) Koszelewski, D.; Nowak-Krol, A.; Gryko, D. T. *Chem. - Asian J.* **2012**, *7*, 1887. b) Tancini, F.; Monti, F.; Howes, K.; Belbakra, A.; Listorti, A.; Schweizer, W. B.; Reutenauer, P.; Alonso-Gomez, J.-L.; Chiorboli, C.; Urner, L. M.; Gisselbrecht, J.-P.; Boudon, C.; Armaroli, N.; Diederich, F. *Chem. - Eur. J.* **2014**, *20*, 202. c) Reekie, T. A.; Sekita, M.; Urner, L. M.; Bauroth, S.; Ruhlmann, L.; Gisselbrecht, J.-P.; Boudon, C.; Trapp, N.; Clark, T.; Guldi, D. M.; Diederich, F. *Chem. - Eur. J.* **2017**, *23*, 6357.

<sup>197</sup> Sekita, M.; Ballesteros, B.; Diederich, F.; Guldi, D. M.; Bottari, G.; Torres, T. *Angew. Chem., Int. Ed.* **2016**, *55*, 5560.

<sup>198</sup> Winterfeld, K. A.; Lavarda, G.; Yoshida, K.; Bayerlein, M. J.; Kise, K.; Tanaka, T.; Osuka, A.; Guldi, D. M.; Torres, T.; Bottari, G. *J. Am. Chem. Soc.* **2020**, *142*, 7920.

<sup>199</sup> a) Winterfeld, K. A.; Lavarda, G.; Guilleme, J.; Sekita, M.; Guldi, D. M.; Torres, T.; Bottari, G. *J. Am. Chem. Soc.* **2017**, *139*, 5520. b) Muñoz, A. V.; Gotfredsen, H.; Jevric, M.; Kadziola, A.; Hammerich, O.; Nielsen, M. B. *J. Org. Chem.* **2018**, *83*, 2227. c) Winterfeld, K. A.; Lavarda, G.; Guilleme, J.; Guldi, D. M.; Torres, T.; Bottari, G. *Chem. Sci.* **2019**, *10*, 10997.

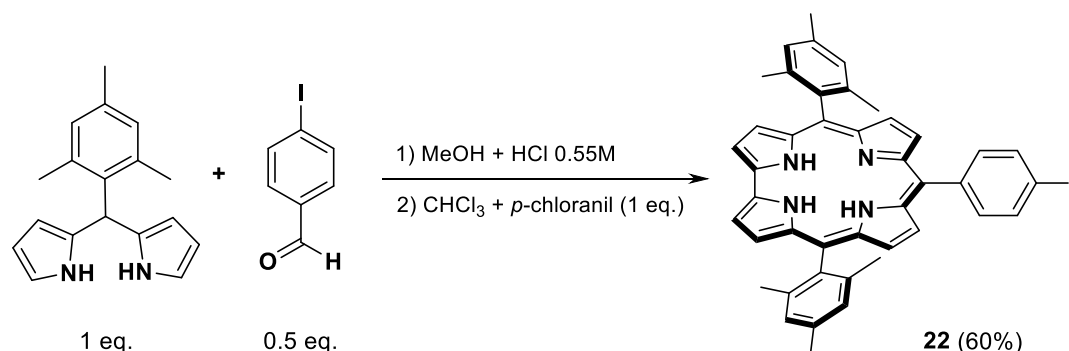
connecting them. As a consequence, atropoisomers, which are stereoisomers arising from this hindered rotation, are formed.<sup>198a</sup>

The isolation of TCBD atropoisomers is not a straightforward task, and can be only be accomplished for certain molecules in some experimental conditions, due to the configuration lability of the enantiopure species. Particularly, in the case of SubPc-TCBD reported systems, the surprising configurational stability of the enantiopure fragments allowed for a deep study and understanding of the behavior regarding this kind of systems.<sup>200</sup>

## 1.7.2. Results and discussion

### 1.7.2.1. Synthesis of Cor derivatives 22, 23 and 24

The synthesis of Cor **22** was synthesized following the same methodology employed for the preparation of *trans*-A<sub>2</sub>B-Cors, using Mes-DPM and 4-iodobenzaldehyde as starting materials, to fulfil both electronic and structural features (Scheme 18). Although commercially available, 4-iodobenzaldehyde was synthesized from the cheaper 1,4-diiodobenzene.

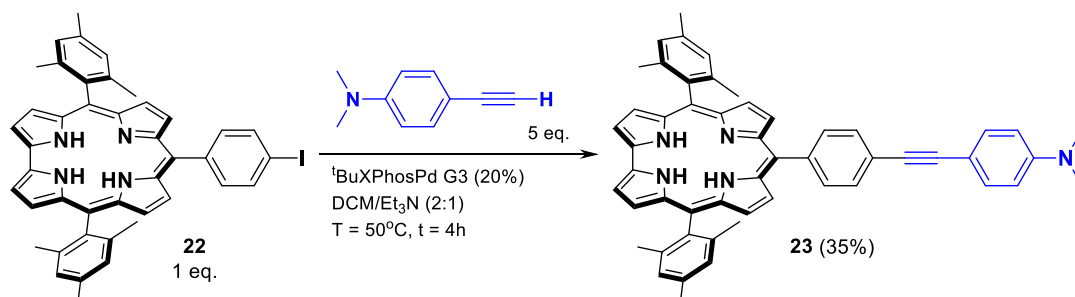


**Scheme 18.** Synthetic route for the preparation of Cor **22**.

Subsequently, Sonogashira palladium-catalyzed C-C cross-coupling reaction was performed (Scheme 19). In order to avoid the introduction of Cu into Cor inner cavity, copper-free conditions were employed, particularly using <sup>t</sup>BuXPhos G3 as our catalyst ligand. 4-Ethynyl-N,N-dimethylaniline was selected as the alkyne counterpart, in order to fulfil the CA-RE electronic requirements. Although THF has been largely employed as an

<sup>200</sup> Lavarda, G.; Bhattacharjee, N.; Brancato, G.; Torres, T.; Bottari, G. *Angew. Chem. Int. Ed.* **2020**, *59*, 21224.

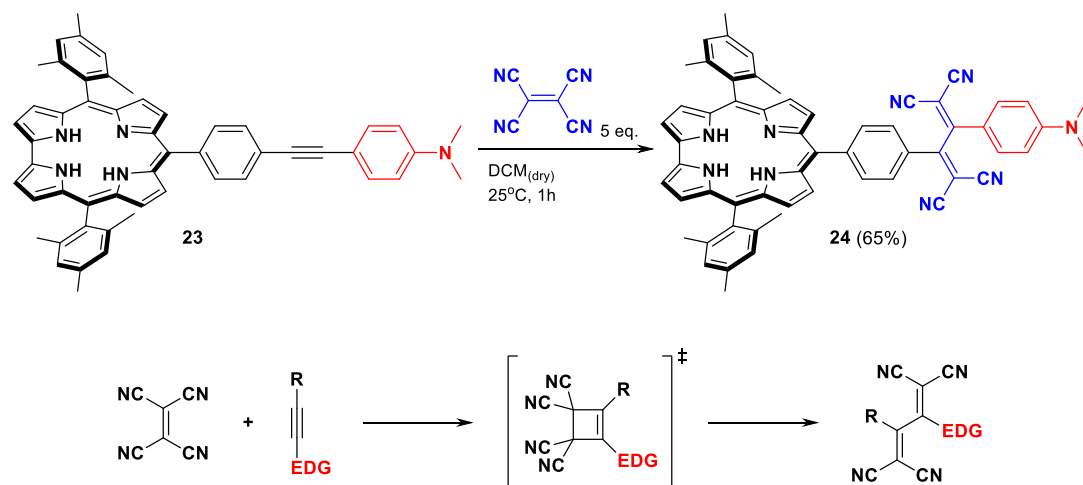
efficient solvent in Sonogashira reactions, is generally avoided in Cor chemistry due to its tendency of introduction into its *meso*-position, with consequent formation of the corresponding isoCorrole. DCM is successfully employed as the reaction solvent, leading into the formation of Cor **23** in 60% yield.



**Scheme 19.** Synthetic route for the preparation of Cor **23**.

Ultimately, CA-RE reaction between Cor **23** and tetracyanoethylene was performed, giving rise to Cor-TCBD **24** in a 65% yield (Scheme 20, top). At the end of the reaction, total consumption of the starting Cor **24** and the appearance of two new spots are observed in TLC. However, upon purification in column chromatography, only one product was recovered. This spot could be ascribed as the retro-electrocyclization intermediate (Scheme 20, bottom). Attempts for its isolation were carried out by performing all the synthetic operations in absence of light, without success.

## Synthesis and characterization of TCBD-Cor covalent systems



**Scheme 20.** (Top) Synthetic route for the obtention of TCBD-Cor **24** and (bottom) general mechanism for the CA-RE reaction. EDG: Electro-donating group.

All the reported molecules were characterized by means of NMR and mass spectrometry. Regarding the  $^1\text{H-NMR}$  spectra, signals of  $\beta$ -pyrrolic and *meso*-phenyl aromatic protons were observed around 7.00-8.00 ppm for Cor **22**, as well as mesityl aliphatic protons between 1.90-3.10 ppm (Figure 52, top). Next, the attachment of 4-Ethynyl-N,N-dimethylaniline was determined by the appearance of aniline aromatic doublets at the aromatic area as well as the aliphatic protons of the N-methyl groups at 3.04 ppm (Figure 52, bottom).

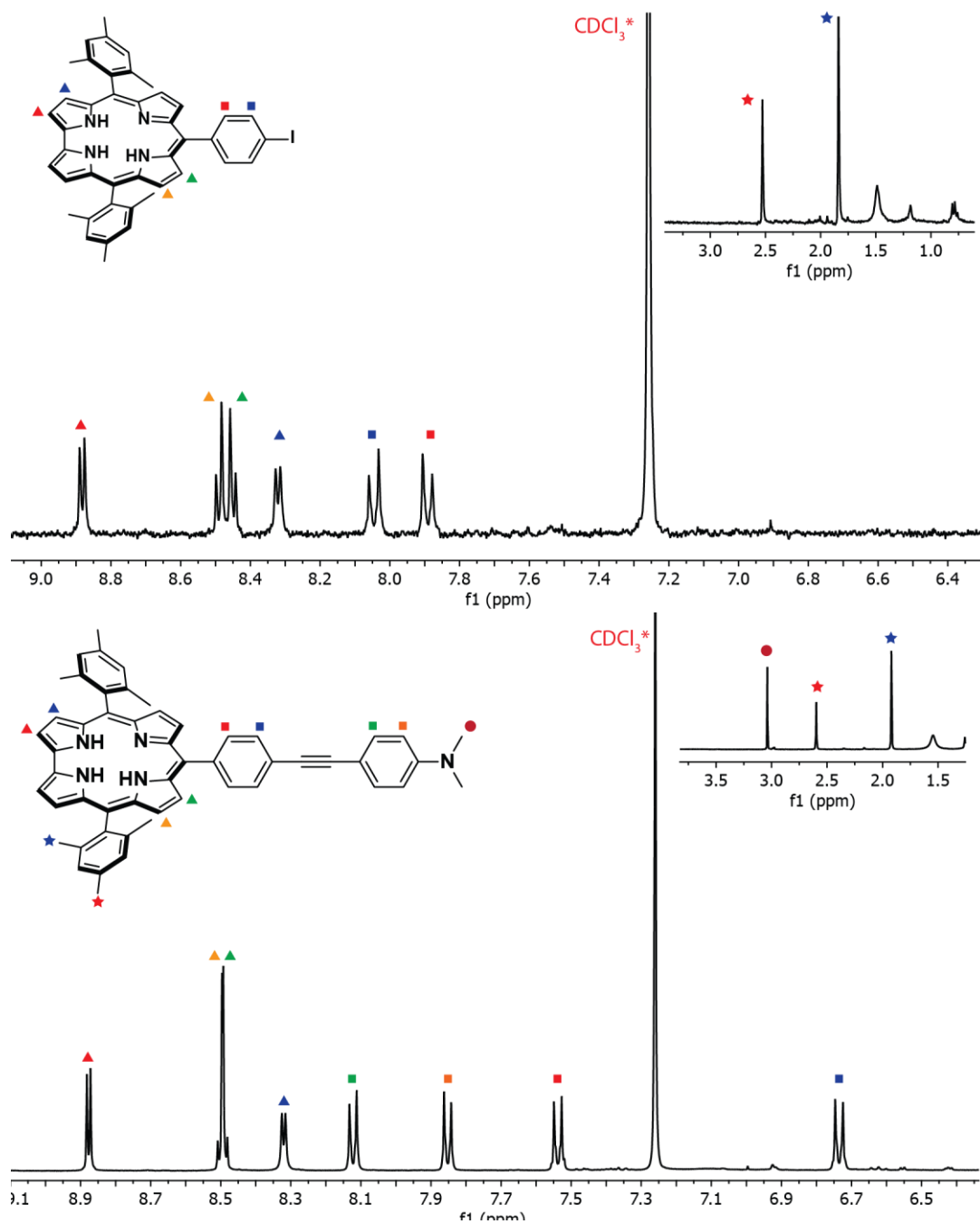


**Figure 52.** <sup>1</sup>H-NMR spectra (300 MHz) of Cor **22** (top) and Cor **23** (bottom) in CDCl<sub>3</sub> at 25°C. *m*-Mesityl protons located under CDCl<sub>3</sub> signal (*ca.* 7.26 ppm).

Finally, the introduction of the tetracyanoethylene unit, although without the appearance of any additional signal, can be detected due to structural and electronic disruptions in the molecule (Figure 53). Limiting the rotation of the molecule in one of its axes leads into a rupture in the relaxation dynamics, splitting the quasi-singlet corresponding to four  $\beta$ -pyrrole protons into two doublets. In the same way, a signal corresponding to one of the *m*-Mesityl protons, generally covered by the  $\text{CDCl}_3$  signal, is spotted at 7.25 ppm. Additionally, the signals of the aromatic protons close to the alkynyl position (from both Cor and aniline sides) undergo shielding and appear at higher ppm, mainly due to the presence of the newly introduced high electron withdrawing TCBD fragment.

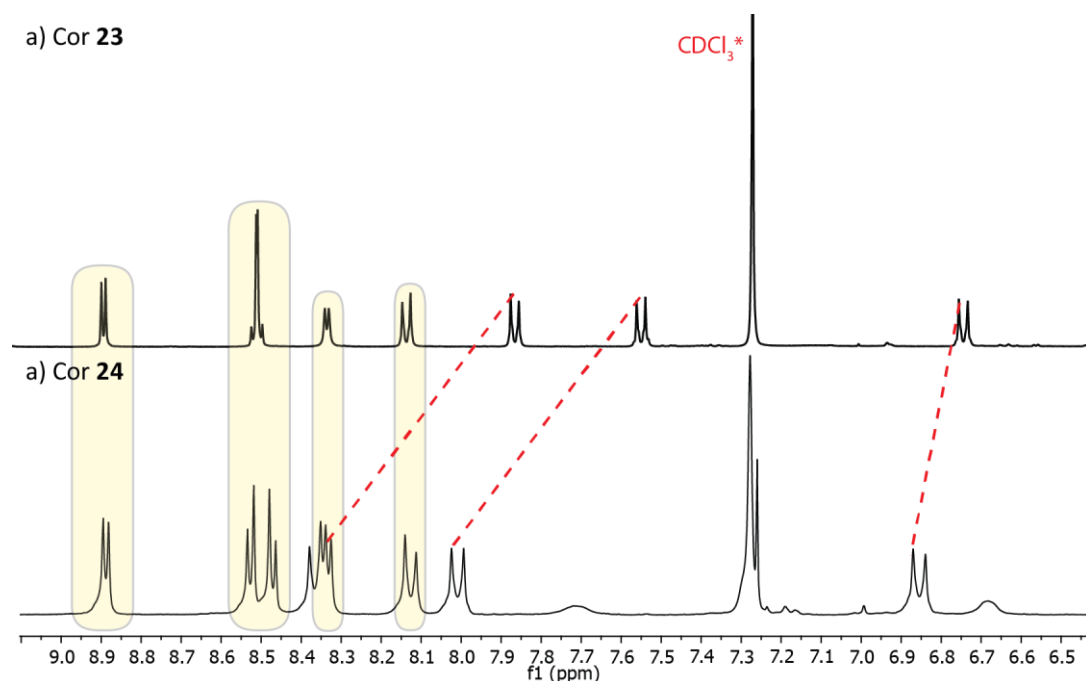


**Figure 53.**  $^1\text{H-NMR}$  spectra (300 MHz) of Cor **23** (a) and Cor **24** (b) in  $\text{CDCl}_3$  at  $25^\circ\text{C}$ , representing the chemical shifts upon introduction of the TCBD unit.

### 1.7.2.2. Electrochemistry of Cor derivatives 22, 23 and 24

As remarked in the introduction of the present thesis, electrochemistry of free-base Cors demonstrated to be particularly intricate mainly for two reasons: (1) free-base Cors possess high deprotonation constants in organic solvents, establishing an equilibrium between  $[(\text{Cor})\text{H}_3]$  and  $[(\text{Cor})\text{H}_2]^-$  species. This equilibrium is highly dependent on Cor substitution pattern and solvent, and it could be found totally displaced to the  $[(\text{Cor})\text{H}_2]^-$  form;<sup>201</sup> (2) one-electron oxidation of free-base  $[(\text{Cor})\text{H}_3]$  promotes the formation of  $[(\text{Cor})\text{H}_4]^+$ . Additionally, one-electron reduction of free-base  $[(\text{Cor})\text{H}_3]$  promotes the formation of  $[(\text{Cor})\text{H}_2]^-$ . All three forms of the metal-free Cor are electroactive, and it usually translates in complicated redox behavior involving multiple processes and multiple coupled chemical reactions from several forms of the Cor in solution. For a better understanding, the scheme depicted in the *Introduction* is recovered below (Figure 54)

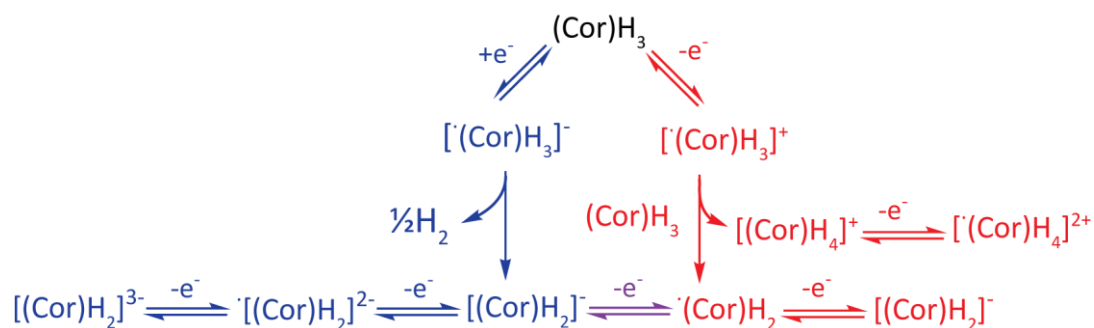


**Figure 54.** Proposed electron transfer mechanism for one-electron oxidation (red) and reduction (blue) processes of  $(\text{Cor})\text{H}_3$  in PhCN.<sup>129</sup>

Kadish and co-workers were able to identify all the species reported above by means of electrochemical and spectroelectrochemical experiments in PhCN, allowing for the easy recognition of a vast number of free-base Cor main electrochemical processes.

Electrochemical experiments, namely cyclic voltammetry, square-wave voltammetry (SWV) and differential-pulse voltammetry, were conducted in a 0.1 M TBAPF<sub>6</sub> DCM solution. Deoxygenation of the objective Cor solution was performed prior to recording of the measure. Saturated calomel electrode (SCE) and Fc couple (Fc/Fc<sup>+</sup>) were

<sup>201</sup> Kruk, M.; Ngo, T. H.; Savva, V.; Starukhin, A.; Dehaen, W.; Maes, W. *J. Phys. Chem. A* **2012**, *8*.

employed as internal reference. All the experiments were carried out at room temperature (25°C).

Electrochemical measurements of Cor **22** were conducted in order to identify the main electronic events of the molecule. Figure 55 show the voltammograms of compound **22**. Focusing on the oxidation window (Figure 55, left), several peaks are revealed as irreversible and coupled processes. Previous research work allows for its identification, since they are assigned to different electrochemically active species. Therefore, the first anodic peak potential at 0.1 V/s scan rate located at  $E_p = 0.54$  V corresponds to the oxidation of  $(\text{Cor})\text{H}_3$  into  $[(\text{Cor})\text{H}_3]^+$ , that irreversibly evolves into  $[(\text{Cor})\text{H}_2]$  and  $[(\text{Cor})\text{H}_4]^+$ . Two reversible coupled potentials are located between  $E_{pc} = 0.66$  and 0.94 V, corresponding to  $[(\text{Cor})\text{H}_2]$  and  $[(\text{Cor})\text{H}_4]^+$  oxidations, respectively. There are followed by two additional reversible and irreversible oxidations at  $E_p = 1.34$  V and  $E_p = 1.63$  V, respectively, being the later just on the edge of the solvent potential window and unable to be assigned to any process.

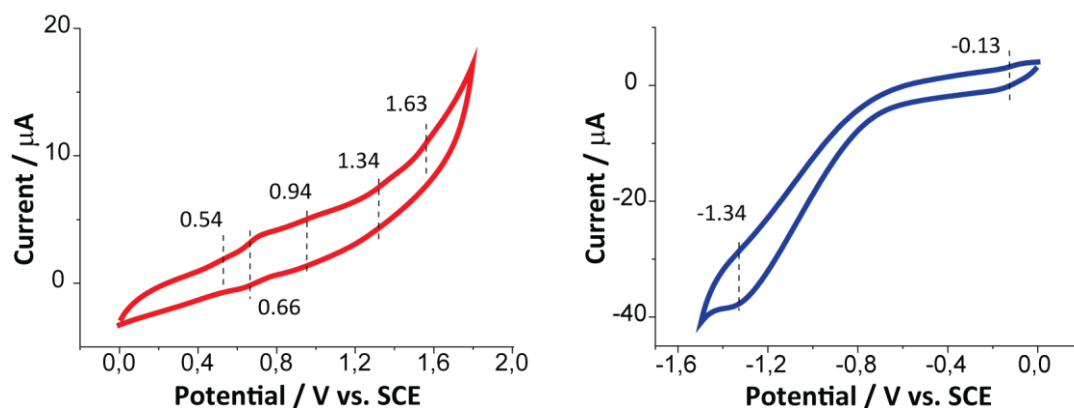


**Figure 55.** CVs representing the oxidation (left) and reduction (right) of Cor **22** in DCM, 0.1 M TBAPF<sub>6</sub> at 25°C. Scan rate: 0.1 V/s.

The reduction frame (Figure 55, right) presents an irreversible peak at  $E_p = -1.34$  V, corresponding to the transformation of  $(\text{Cor})\text{H}_3$  into  $[(\text{Cor})\text{H}_3]^-$ , that ultimately leads into the irreversible loose of molecular hydrogen and its transformation into  $[(\text{Cor})\text{H}_2]^-$ . Additionally, a reversible peak is spotted at  $E_p = -0.13$  V for the one-electron reduction of  $[(\text{Cor})\text{H}_2]$ .

Interestingly, full registration of the CV starting from negative potential values raised two unassigned pseudo-irreversible signals at  $E_p = -0.46$  and  $-1.06$  V (Figure 56). From the first oxidation and reduction potentials corresponding to  $(\text{Cor})\text{H}_3$ , a HOMO-LUMO band gap of 1.88 eV has been calculated. A scheme involving all the species and potentials is depicted in Figure 57.

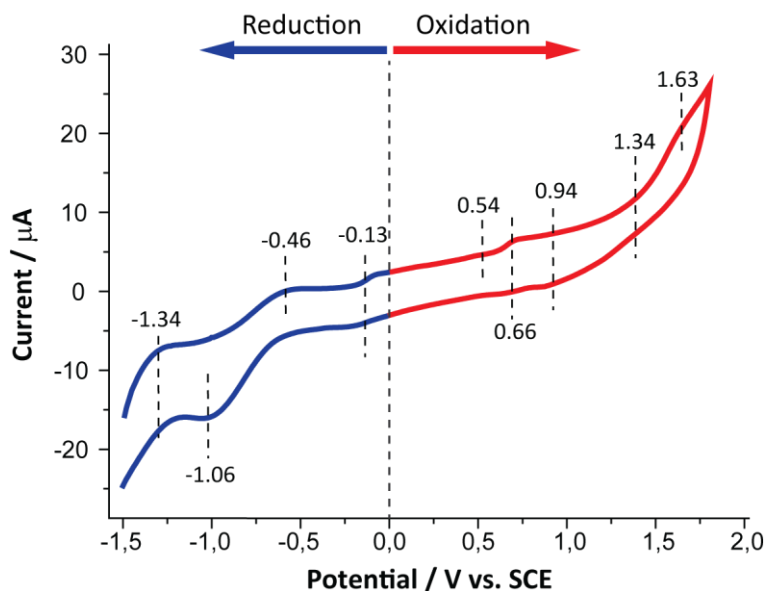


**Figure 56.** Cyclic voltammogram illustrating the full redox window of Cor **22** in DCM, 0.1 M TBAPF<sub>6</sub> at 25°C. Scan rate: 0.1 V/s.

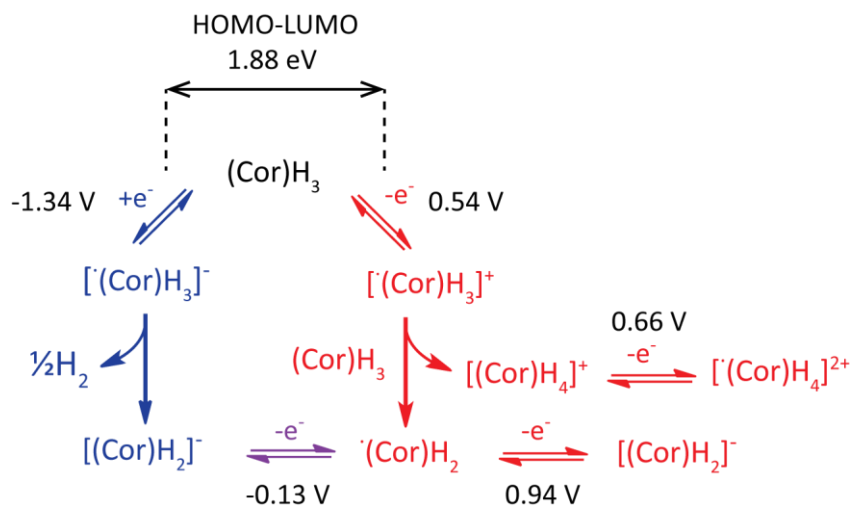


**Figure 57.** One-electron oxidation (red) and reduction (blue) processes happening during the electrochemical measurement of Cor **22** in DCM vs. SCE.

Once the main metal-free Cor potentials are resolved, the study of the precedent molecules can be resolved in an easier way. Oxidation Cor **23** showed a similar pattern than the obtained for Cor **22**. The introduction of the donor Ethynyl-aniline in *meso*- induces a shift to less potential values in the main oxidation events (Figure 58, left). Analogously, it induces a shift to high potential values in the main reduction events, introducing a new potential value of  $E_p = -0.84$  V, corresponding to the reduction of the newly introduced amine (Figure 58, right).

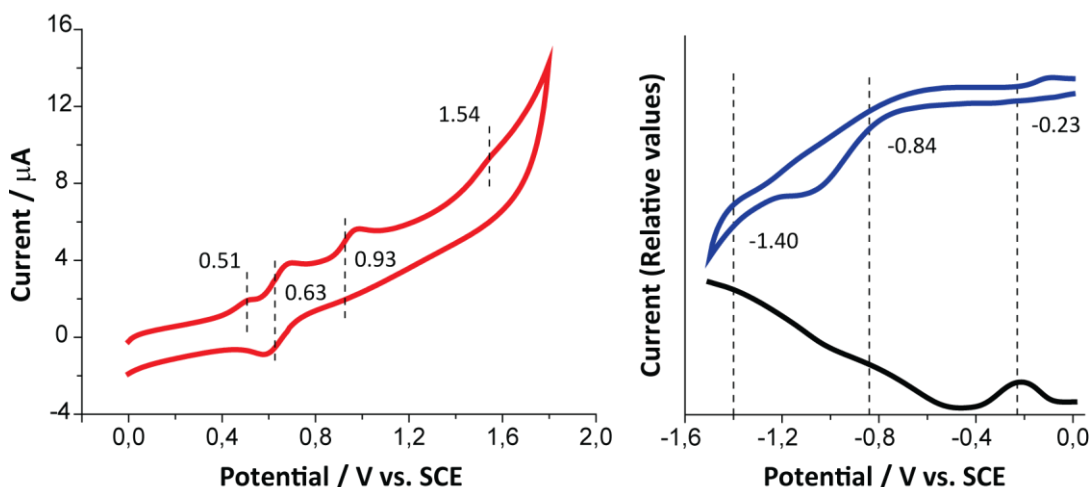


**Figure 58.** (Left) CV representing the oxidation and (right) CV (up) and DPV (down) representing the reduction of Cor **23** in DCM, 0.1 M TBAPF<sub>6</sub> at 25°C. Scan rate: 25 mV/s.

For the TCBD-Cor **24**, oxidation showed a voltammogram in which only oxidation of (Cor)H<sub>3</sub> into [(Cor)H<sub>3</sub>]<sup>+</sup> and oxidation of [(Cor)H<sub>2</sub>] into [(Cor)H<sub>2</sub>]<sup>+</sup> can be detected, along with reversible and irreversible peaks at 1.33 and 1.54 V, respectively, without detection of the corresponding oxidation of [(Cor)H<sub>4</sub>]<sup>+</sup> (Figure 59, left). The reduction of TCBD-Cor **24** introduces two new peaks at -0.58 and 1.69 V for the one-electron reductions of the TCBD unit (Figure 59, right). At -0.16 and -1.40 V, the reductions of [(Cor)H<sub>2</sub>]<sup>-</sup> and (Cor)H<sub>3</sub>, respectively. At -0.90 V, the reduction of the aniline is observed. The electrochemical data corresponding to the measured compounds can be compared in Table 8.

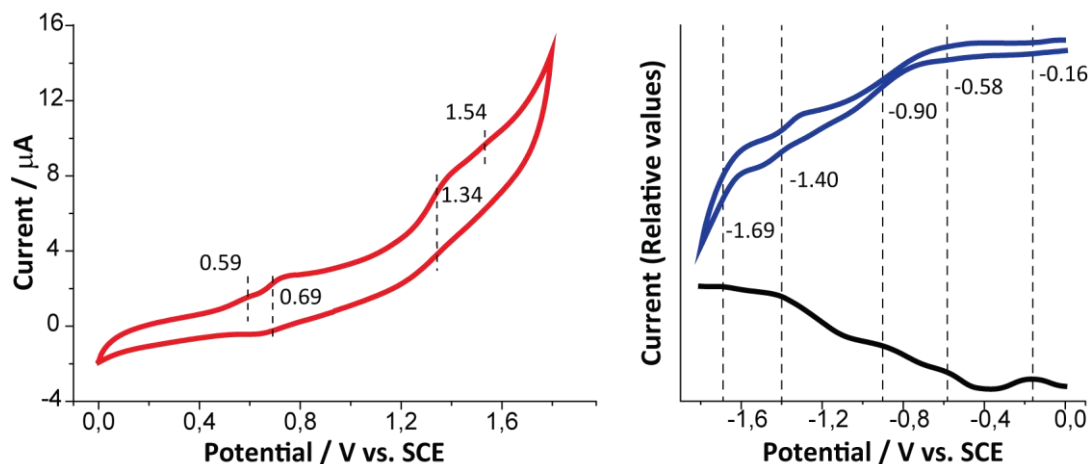


**Figure 59.** (Left) CV representing the oxidation and (right) CV (red) and SWV (black) representing the reduction of TCBD-Cor **24** in DCM, 0.1 M TBAPF<sub>6</sub> at 25°C. Scan rate: 50 mV/s.

**Table 9.** Electrochemical data (in V vs. SCE) in DCM, 0.1M TBAPF<sub>6</sub> at 25°C of Cors **22**, **23** and **24**, corresponding to: a) Cor, b) Aniline, c) TCBD.

Corrole	E <sub>red5</sub> <sup>c</sup>	E <sub>red4</sub> <sup>a</sup>	E <sub>red3</sub> <sup>b</sup>	E <sub>red2</sub> <sup>c</sup>	E <sub>red1</sub> <sup>a</sup>	E <sub>ox1</sub> <sup>a,c</sup>	E <sub>ox2</sub> <sup>a</sup>	E <sub>ox3</sub> <sup>a</sup>	E <sub>ox4</sub> <sup>a</sup>	E <sub>ox5</sub> <sup>a,c</sup>
<b>22</b>		-1.34			-0.13	0.54	0.66	0.94	1.34	1.63
<b>23</b>		-1.40 <sup>d</sup>	-0.84 <sup>d</sup>		-0.23	0.51	0.63	0.93		1.54
<b>24</b>	-1.69 <sup>e</sup>	-1.40	-0.90 <sup>e</sup>	-0.58 <sup>e</sup>	-0.16	0.59	0.69		1.34	1.54

<sup>a</sup>Since these oxidation/reduction processes are irreversible, only anodic/cationic peak potentials are reported.

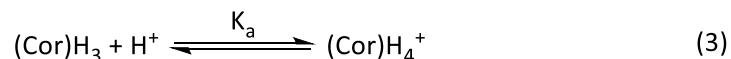
<sup>d</sup>Peak potential by DPV. <sup>e</sup>Peak potential by SWV.

### 1.7.2.3. Optical properties of Cor derivatives **22**, **23** and **24**

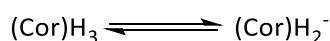
#### Determination of protonation constants of Cor derivatives **22**, **23** and **24**

The protonation and deprotonation of Cors inner core features new electronic transitions occurring at lower energies and with higher intensities than regular Cor Q-band transitions, allowing for enhanced light-harvesting properties in the red region of the spectrum. With the aim of studying the photophysical properties of TCBD-Cor **24**, a complete study was made in order to determine if the protonation or deprotonation of its inner core translates into an improvement of its ability of effectively promote charge separation (CS) and PeT processes vs. its neutral form.

Cor **24** presents two different protonation sites, that is, Cor inner core and external aniline, and the estimation of their protonation constants is needed in order to determine whether Cor is present as its mono- ( $[(\text{Cor})\text{H}_4]^+$ ) or diprotonated ( $[(\text{Cor})\text{H}_5]^{2+}$ ) form. Since all the spectroscopic data are recorded in toluene, the corresponding equilibrium constants should be considered as relative acid-dissociation constants for the reaction shown in Equation (3). It should be noted that dissociation of TFA is not taken into account and is only proportional to, but not equal to, the proton concentration in solution. The spectroscopic data were analyzed employing the methodology developed by Splan and co-workers,<sup>202</sup> which has been largely used for the determination of porphyrinoid equilibrium constants. Relative acid-dissociation constants were calculated from a plot of  $-\log[\text{TFA}]$  vs.  $\log\{[(\text{Cor})\text{H}_3]/[(\text{Cor})\text{H}_4]^+\}$ . The later was calculated from a fixed wavelengths at the Soret/Q bands of the neutral species as  $(A - A_f)/(A_o - A)$ , where  $A$  is the absorbance of the solution, and  $A_o$  and  $A_f$  are the initial and final absorbance values corresponding to the beginning and the end of the titration, respectively.



To determine the relative equilibrium constants, initial titration experiments employing increasing concentrations of TFA in toluene were performed. In order to avoid overall changes into the volume of the solution, all the samples were independently prepared, ensuring equal initial Cor concentrations in all the experiments. Prior to initiate the titration, a small amount of TFA is needed in order to neutralize the  $[(\text{Cor})\text{H}_2]^-$  present in the medium, coming from the equilibrium:



Starting with Cor **22**, it shows a well-defined isosbestic point at 470 nm. As the reaction with TFA proceeds, the Soret band redshifts and narrows from 409 to 419 nm. The 568 nm Q-band decreases, whereas the 644 nm Q-band increases (Figure 60). A linear plot of  $-\log[\text{TFA}]$  vs.  $\log\{[(\text{Cor})\text{H}_3]/[(\text{Cor})\text{H}_4]^+\}$  was obtained (Figure 60, inset). Considering

---

<sup>202</sup> Goldberg, P. K.; Pundsack, T. J.; Splan, K. E. *J. Phys. Chem. A* **2011**, *115*, 10452

different wavelengths (409, 569 and 644 nm), the zero interception with the X-Axis of the graphic returns an estimated  $pK_{a,app} = 3.7 \pm 0.1$ .

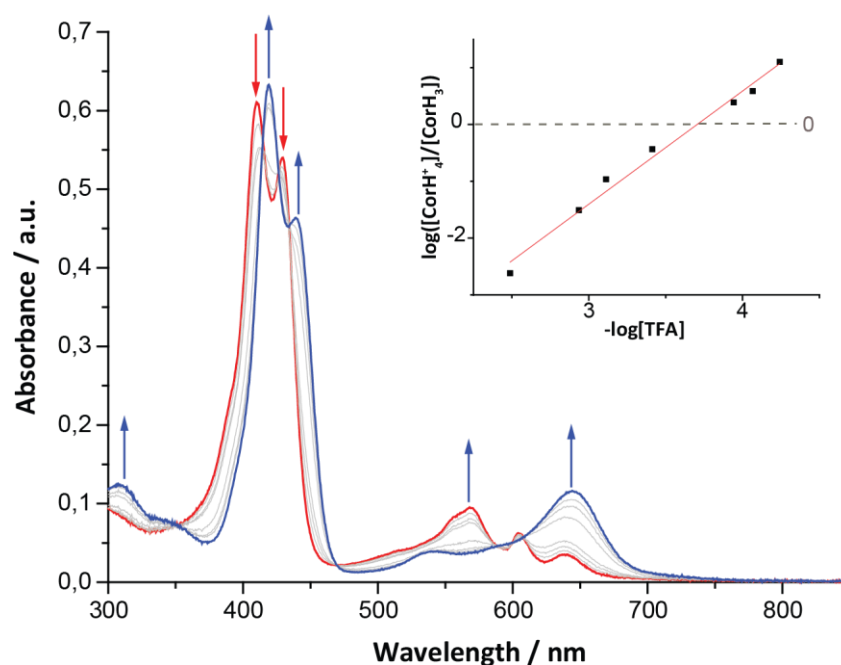


**Figure 60.** Steady-state absorption spectra of Cor **22** measured over the course of titration with TFA in Toluene (Initial stage, red. Final stage, blue). (Inset) linear plot of  $\log\left(\frac{[\text{CorH}_3]}{[\text{CorH}_4^+]}\right)$  as a function of  $-\log[\text{TFA}]$  at 569 nm.

The same methodology was employed for the rest of the molecules: Cor **23** showed two values of  $pK_{a,app} = 3.7 \pm 0.1$  and  $1.9 \pm 0.1$ , corresponding to the protonations of inner imino nitrogen and external dimethylamine, respectively (Figure 61). To confirm this assignation, the metallated Cu derivative of **23** was titrated with TFA in order to avoid protonation of Cor inner core, returning a  $pK_{a,app} = 2.3 \pm 0.1$ . Interestingly, whereas for the free base Cor **23** the protonation of the amine results in almost negligible blue shift of Soret bands in 1-2nm and an increase of the absorbance intensity for both Soret and Q bands, in the case of the CuCor derivative, the Soret band suffers a blue shift of 18 nm, remarking the Soret band sensitivity of CuCor complexes upon modification of its *meso*-aryl- substituents.

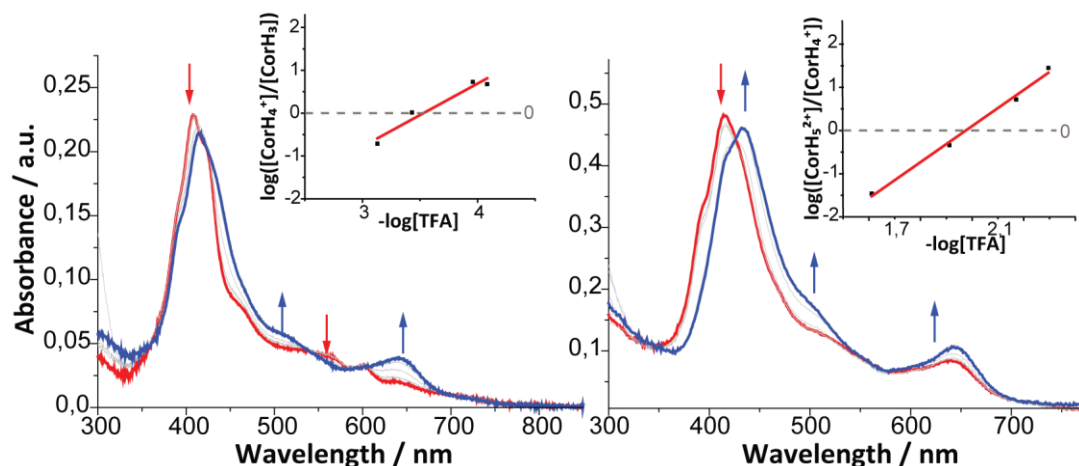


**Figure 61.** Steady-state absorption spectra of Cor **23** measured over the course of titration with TFA in Toluene (Initial stage, red. Final stage, blue). (Left) First protonation equilibrium and (right) second protonation equilibrium. (Inset) linear plot of  $\log\left(\frac{[(\text{Cor})\text{H}_{3+2n}^{+2n}]}{[(\text{Cor})\text{H}_{3+n}^{n+}]}\right)$  ( $n = 0, 1$ ) as a function of  $-\log[\text{TFA}]$  at 412 nm (left) and 445 nm (right).

Cor **24** returns again two values of  $\text{pK}_{\text{a,app}} = 3.5$  and  $2.0 \pm 0.1$ , corresponding to Cor inner core and aniline protonation, respectively (Figure 62). Interestingly, prior to addition of TFA, the UV-Vis spectrum for **24** obtained in toluene showed characteristic signals of  $[(\text{Cor})\text{H}_2]$ , with a Soret band at 417 nm an intense Q-band at 642 nm. This, along with the decreasing of inner core  $\text{pK}_{\text{a,app}}$ , are direct consequences of the presence of a high electron-withdrawing partner such as TCDB, which reduces the electronic density of the macrocycle.

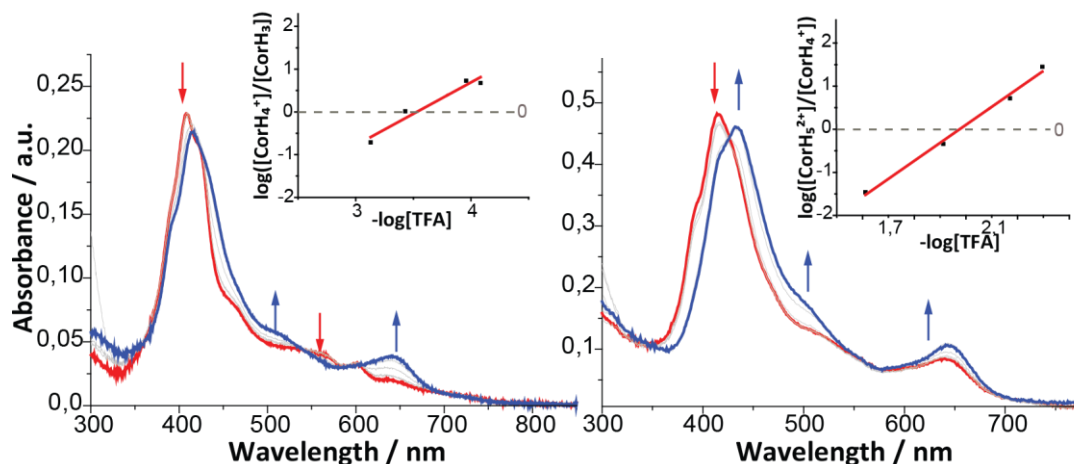


**Figure 62.** Steady-state absorption spectra of Cor **24** measured over the course of titration with TFA in Toluene (Initial stage, red. Final stage, blue). (Left) First protonation equilibrium and (right) second protonation

equilibrium. (Inset) linear plot of  $\log\left(\frac{[(\text{Cor})\text{H}_{3+2n}^{+2n}]}{[(\text{Cor})\text{H}_{3+n}^{n+}]}\right)$  ( $n = 0, 1$ ) as a function of  $-\log[\text{TFA}]$  at 412 nm (left) and 496 nm (right).

Fluorescence emission was obtained for the neutral species in toluene (Figure 63). Emission maxima were found at 659 and 650 nm for Cor **23** and Cor **24**, respectively. TCBD-Cor **24** presents a strong quenching for the Cor emission, therefore suggesting a non-radiative relaxation process upon introduction of the TCBD unit.

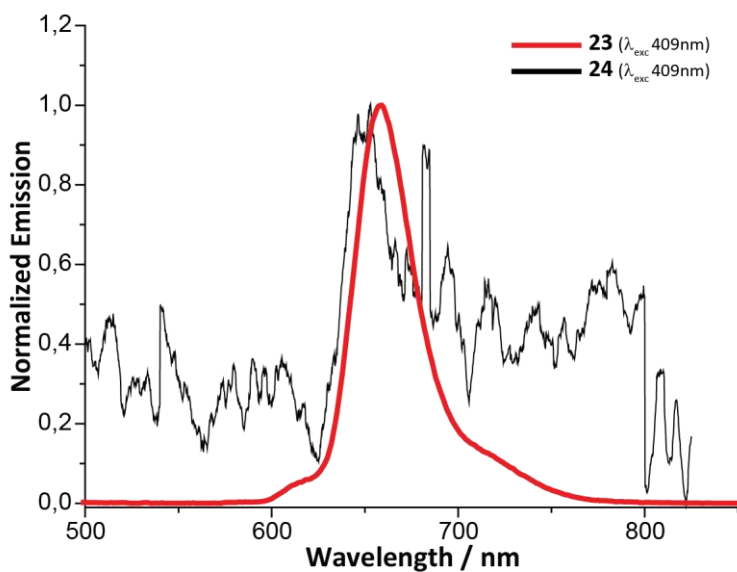


**Figure 63.** Fluorescence emission spectra of Cor **23** (red) and TCBD-Cor **24** (black) at 409 nm in toluene.

*Summay and conclusions*

## 1.8. Summary and conclusions

In this chapter, different SubPc- and Cor-based photoactive arrays as light-harvesting materials have been synthesized, characterized and their properties studied.

In the first section, a series of SubPcs have been linked at a peripheral site of Cors, by means of axial activation of the SubPc-derivative and subsequent axial substitution reaction by means of a nucleophile Cor through a *meso*-phenoxy- unit, with reasonable yields, taking into account the complexity of the systems.

The electronic, redox and photophysical properties of these systems have been studied by means of steady-state absorption and emission, spectroelectrochemistry and transient absorption experiments, conducted in the laboratories of Prof. D. M. Guldi, in part during a predoctoral stay of the candidate in Erlangen. For the series of SubPc-Cor dyads comprising donor Cors decorated with Mesityl units (**4**, **5**, **6** and **7**) a CT/CSS, to afford  $\text{Cor}^+-\text{SubPc}^-$  species, was found in all cases. Although Cu was incorporated into the dyads with the purpose of enhancing the acceptor properties of Cors, similar CT/CSS times were observed for dyads **5**, **6** and **7**. Remarkably, the best times of CSS were obtained for the SubPcH<sub>12</sub>-CorH<sub>3</sub> dyad **4**, with maximum values of 534 ps in toluene (Figure 64).

On the other hand, SubPc-PCor dyad **11** demonstrated its role as an antenna, funneling all the energy harvested by the system into the SubPc moiety. SubPc **8** was particularly designed for evaluating its ability to supramolecularly interact with fullerenes. The relatively recent publication of a CSS between SubPc **8** and C<sub>60</sub>/C<sub>70</sub> as 1:1 supramolecular complexes ( $\text{SubPc}^+-\text{C}_{60}/\text{C}_{70}^-$ ) encourages the complexation of **11** with fullerenes for the achievement of long-lived CSS.<sup>15</sup>

## Summary and conclusions

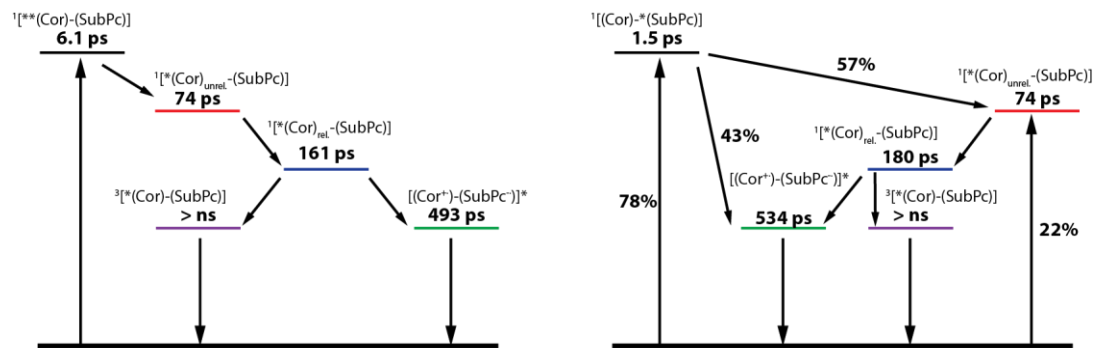


**Figure 64.** Kinetic models used for the analysis of femtosecond-resolved differential absorption of SubPc-Cor **4** upon excitation at 420 (left) and 550 nm (right) in toluene.

In the second section, the chemistry developed over PCor axial position has been studied. Although our attempts for the activation of PCor axial position were not successful, this strategy presents itself as a powerful tool in order to further functionalize these complexes, with the possibility of fine-tuning its electronic and redox properties according to the requirements of our system. We have taken advantage of the affinity of P(V) to hydroxy ligands for the introduction of two different SubPcs connected through a  $\mu$ -oxo spacer. Particularly for SubPc-Cor **14**, the formation of an exciplex has been proposed, supported by steady-state absorption and emission experiments. Although exciplexes have been for a long time considered as an undesired deactivation pathway for the obtention of CT/CSS-based systems, researchers have found an application of these phenomena in the developing white OLEDs, taking benefit of the broad and intense emission generated by those complexes.<sup>203</sup>

In the third section, two different SubPc-Fc dyads (**20** and **21**) have been synthesized. Strong emission quenching was observed for both **20** and **21**. PeT has been previously reported to occur in different SubPc-Fc arrays. Therefore, a CT/CSS can be assumed. Focusing on the SubPc-Ethynyl derivatives **18** and **19**, they are robust molecules that can be prepared in high yields and present great stability over-time. For these reasons, they are perfect candidates for its introduction as electron acceptor counter partners in more complex arrays *via* straightforward palladium-catalyzed cross-coupling or click

<sup>203</sup> a) Whei, X.; Gao, L.; Miao, Y.; Zhao, Y.; Yin, M.; Wang, H.; Xu, B. *J. Mater. Chem. C* **2020**, *8*, 2772.

b) Lee, H. L.; Jang, H. J.; Lee, J. Y. *J. Mater. Chem. C* **2020**, *8*, 10302.

reactions. Finally, the synthetic methodology for the preparation of hexachloro-SubPc **17** has been optimized, allowing for its elaboration in reasonable yields.

In the last section, push-pull TCBD-Cor dyad **24** has been prepared starting from the *meso*-iodophenyl-Cor **22**, introduction of 4-ethynylaniline *via* Sonogashira palladium-catalyzed cross-coupling reaction for obtaining **23**, and subsequent CA-RE reaction. The optical and electrochemical properties of the different Cor derivatives have been studied. With the aim of controlling its behavior according to the pH of the medium, steady-state absorption spectra have been acquired in the different stages of its protonation/deprotonation equilibria. Emission, spectroelectrochemistry and transient-absorption spectrometry experiments will be performed in order to determine their potential use as pH probes in biological systems.

## 1.9. Experimental section

In this *Experimental section*, the preparation and characterization of the compounds has been organized following the order as they appear in the text.

### 1.9.1. Materials and general methods

Chemical reagents were purchased from Aldrich Chemical Co., Alfa Aesar, Acros Organics or Fluka Chemie and were used without further purification. "Synthetic grade" solvents were used for chemical reactions and column chromatography purifications and "anhydric grade" for reactions under dry conditions. Additionally, some solvents were further dried by distillation with Na/benzophenone (THF, toluene), or with previously activated molecular sieves (3 or 4 Å), or with a solvent purifying system by Innovative Technology Inc. MD-4-PS.

**Microwave irradiation technique:** microwave reactions were carried out in a Biotage Initiator+ system. All reactions were performed in capped glass vials under argon atmosphere.

**Chromatography:** the monitoring of the reactions has been carried out by thin layer chromatography (TLC), employing aluminum sheets coated with silica gel type 60 F254 (0.2 mm thick, E. Merck). The analysis of the TLCs was carried out with an UV lamp of 254 and 365 nm. Purification and separation of the synthesized products was performed by column chromatography, using silica gel (230-400 mesh, 0.040-0.063 mm, Merck). Eluents and relative proportions of the solvents are indicated for each particular case. Size exclusion chromatography was performed using Bio-Beads S-X1 (200-400 mesh, Bio-Rad).

**Nuclear Magnetic Resonance (NMR):** monodimensional NMR spectra (<sup>1</sup>H-NMR, <sup>11</sup>B-NMR, <sup>13</sup>C-NMR, <sup>19</sup>F-NMR and <sup>31</sup>P-NMR) were recorded on a Bruker AC-300 (300 MHz) or a Bruker XRD-500 (500 MHz) instruments either in the Organic Chemistry Department or in SIdI (Servicio Interdepartamental de Investigación, Interdepartmental Investigation Service). In each case, the deuterated solvent employed is indicated between brackets. The temperature was actively controlled at 298 K unless otherwise specified. Chemical shifts ( $\delta$ ) are reported in ppm and calibrated relative to residual solvent signals using literature reference values,<sup>204</sup> and coupling constants (J) are reported in hertz (Hz). The following abbreviations are used to indicate the

---

<sup>204</sup> Fulmer, G. R.; Miller, A. J. M.; Sherden, N. H.; Gottlieb, H. E.; Nudelman, A.; Stoltz, B. M.; Bercaw, J. E.; Goldberg, K. I. *Organometallics* **2010**, *29*, 2176.

multiplicity in  $^1\text{H-NMR}$  spectra: s, singlet; d, doublet; t, triplet; q, quartet; quint, quintet; m, multiplet; bs, broad signal.

**Mass Spectrometry (MS):** mass spectra were recorded in Sidi, employing Atmospheric Pressure Chemical Ionization (APCI) or Matrix Assisted Laser Desorption/Ionization-Time of Flight (MALDI-TOF), using a MAXIS II high resolution spectrometer for APCI and a Bruker Reflex III spectrometer, with a nitrogen laser operating at 337 nm, for MALDI-TOF. The different matrixes employed are indicated for each spectrum. Mass spectrometry data are expressed in  $m/z$  units.

**Ultraviolet-visible spectroscopy (UV-Vis) and Fluorescence Spectroscopy:** spectroscopic and HPLC grade solvents were used for spectroscopic measurements. UV-Vis spectra were recorded both in the Organic Chemistry Department of UAM and the Chemical Science and Technology Department of University of Rome Tor Vergata, employing a JASCO-V660 and a Varian Cary 50 UV-Vis spectrophotometer, respectively. Fluorescence studies were carried out with a JASCO-V8600 fluorometer at the UAM.

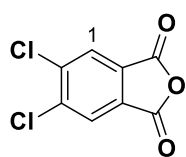
**Cyclic Voltammetry (CV) and Square Wave Voltammetry (SWV):** electrochemical measurements were performed at the Chemical Science and Technology Department of University of Rome Tor Vergata on an PalmSens potentiostat, using a standard calomel electrode (SCE) as the reference electrode, a platinum wire as the auxiliary electrode and a platinum disk (1 mm diameter) as working electrode. The measurements were carried out using anhydrous dichloromethane (DCM) solutions containing 0.1 M tetrabutylammonium hexafluorophosphate ( $\text{TBAPF}_6$ ) as supporting electrolyte, and a concentration of approximately  $10^{-3}$  M of the corresponding compound. Prior to each voltammetric measurement, the cell was degassed with  $\text{N}_{2(\text{g})}$  for 10 minutes. Ferrocene (Fc) was used as an external reference and all the potentials were given relative to the  $\text{Fc}/\text{Fc}^+$  couple. Scan rate was  $100 \text{ mV s}^{-1}$  unless otherwise specified. Compensation for internal resistance was not applied.

**X-Ray Spectroscopy:** X-Ray diffraction spectra were done in Sidi with a Bruker KAPPA APEX II CCD goniometer with kappa geometry and Mo source ( $\lambda = 0.71073 \text{ \AA}$ ). Data were collected at different temperatures, specified in each case, utilizing a system equipped with an Oxford Cryosystems dispositive. The distance between the sample and the detector is 3.5 cm. The data harvesting is done over 99% and the redundancy value is over 3. Data are corrected then with SADABS program. The intensities are calculated with SAINT program. Finally, the structures are resolved with SHELXS and refined with SHELXL.

## 1.9.2. Synthesis of precursor phthalonitriles

### 1.9.2.1 Synthesis of 4,5-dichlorophthalonitrile<sup>205</sup>

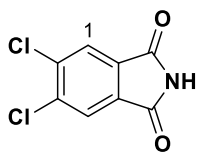
#### 4,5-Dichlorophthalic anhydride



A solution of 4,5-dichlorophthalic acid (15 g, 63.5 mmol) in acetic anhydride (25 mL) was heated to reflux while distilling the acetic acid being formed in the reaction. After 5 h the remaining acetic acid was eliminated by vacuum distillation. The solid obtained was stirred over 12 h in petroleum ether, obtaining a solid that was filtered and thoroughly washed with the same solvent (3 x 20 mL). In this way, 13.5 g (62.2 mmol) of 4,5-dichlorophthalic anhydride were obtained. Yield: 98%.

<sup>1</sup>H-NMR (300 MHz, CDCl<sub>3</sub>): δ (ppm) = 8.12 (s, 2H; H-1).

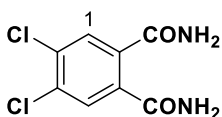
#### 4,5-Dichlorophthalimide



A mixture of 4,5-dichlorophthalic anhydride (13.5 g, 62.5 mmol) and formamide (20 mL) was heated to 200 °C for 3 h. After cooling to room temperature, the solid obtained was filtered, washed with water (1 x 20 mL) and vacuum-dried, yielding 12.4 g (57.4 mmol) of 4,5-dichlorophthalimide as a white solid. Yield: 92%.

<sup>1</sup>H-NMR (300 MHz, DMSO-*d*<sub>6</sub>): δ (ppm) = 8.10 (s, 2H; H-1).

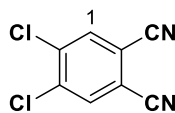
#### 4,5-Dichlorophthalamide



A suspension of 4,5-dichlorophthalimide (12.4 g, 57.7 mmol) in 33% aqueous ammonia (225 mL) was stirred for 36 h at room temperature. The white solid obtained was filtered, washed with water (3 x 15 mL) and vacuum-dried. In so doing, 11.9 g (51.1 mmol) of 4,5-dichlorophthalamide were isolated as a white solid. Yield: 89%.

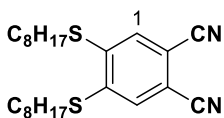
<sup>1</sup>H-NMR (300 MHz, DMSO-*d*<sub>6</sub>): δ (ppm) = 7.95 (s (broad), 2H; NH<sub>2</sub>), 7.72 (s, 2H; H-1), 7.45 (s (broad), 2H; NH<sub>2</sub>).

<sup>205</sup> Wöhrle, D.; Eskes, M.; Shigehara, K.; Yamada, A. *Synthesis* **1993**, 194.

*4,5-Dichlorophthalonitrile*

Freshly distilled thionyl chloride (42 mL) was cautiously poured over dry DMF (60 mL) at 0 °C under argon atmosphere. The mixture was vigorously stirred for 2 h at that temperature and then 4,5-dichlorophthalamide (11.9 g, 51.3 mmol) was added. After stirring for 12 h at room temperature the reaction mixture was poured onto crushed ice (100 mL), resulting in the precipitation of a slightly gray solid which was filtered and washed with water (1 x 20mL). Upon recrystallization from MeOH, 8.8 g (45 mmol) of 4,5-dichlorophthalonitrile were obtained. Yield: 88%.

$^1\text{H-NMR}$  (300 MHz,  $\text{CDCl}_3$ ):  $\delta$  (ppm) = 7.94 (s, 2H; H-1).

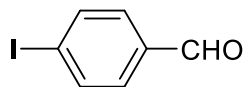
**1.9.2.2 Synthesis of 4,5-dioctylthiophthalonitrile<sup>1a</sup>**

In a 100-mL two-necked round-bottomed flask, equipped with a magnetic stirrer, rubber seal and globe, 4,5-dichlorophthalonitrile (2.4 g, 12.2 mmol), dry  $\text{K}_2\text{CO}_3$  (5.0 g, 36.2 mmol) and dry dimethylacetamide (30 mL) were placed. A stream of argon was passed through the slurry in order to remove oxygen, and then 1-octanethiol (4.6 mL, 26.8 mmol) was added. The resulting mixture was stirred at 90 °C during 8 h and poured onto 100 mL of cold water. The precipitate was filtered and collected in  $\text{CH}_2\text{Cl}_2$ . This solution was then washed with bleach (3 x 50 mL), water (3 x 50 mL) and brine solution (50 mL) and dried over  $\text{MgSO}_4$ . After filtration of the drying agent, the solvent was vacuum-evaporated and the yellow solid obtained was recrystallized from EtOH, obtaining 4.0 g (9.6 mmol) of 4,5-dioctylthiophthalonitrile as white needles. Yield: 79%.

$^1\text{H-NMR}$  (300 MHz,  $\text{CDCl}_3$ ):  $\delta$  (ppm) = 7.40 (s, 2H; H-1), 3.0 (m, 4H;  $\text{SCH}_2$ ), 1.85-1.60 (m, 4H;  $\text{SCH}_2\text{CH}_2$ ), 1.60-1.35 (m, 4H;  $\text{S}(\text{CH}_2)_2\text{CH}_2$ ), 1.35-1.15 (m, 16H;  $\text{S}(\text{CH}_2)_3(\text{CH}_2)_4$ ), 0.88 (m, 6H;  $\text{CH}_3$ ).

### 1.9.3. Synthesis of precursor aldehydes

#### Synthesis of 4-iodobenzaldehyde<sup>206</sup>



In a 100-mL two-necked round-bottomed flask, equipped with a magnetic stirrer, 1,4-diiodobenzene (2.20 g, 6.67 mmol) was dissolved in dry THF (33 mL) and cooled to -78°C. A 2.5 M solution of nBuLi in heptane (2.80 mL, 7.00 mmol) was added and the resulting mixture was stirred for 20 min. Afterwards, dry DMF (2.58 mL, 33.33 mmol) was slowly added and the solution was allowed to warm to room temperature over 2 h. The reaction was quenched by the addition of H<sub>2</sub>O (30mL), the phases were separated and the aqueous phase was extracted with Et<sub>2</sub>O (x4). The combined organic phase was washed once with H<sub>2</sub>O and brine, dried over Na<sub>2</sub>SO<sub>4</sub> and concentrated under reduced pressure. The residue was recrystallised from EtOH/H<sub>2</sub>O to afford 4-iodobenzaldehyde (0.99 g, 4.28mmol) as a white solid. Yield: 64%.

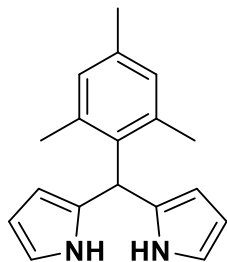
**Mp** = 77-79 °C

**<sup>1</sup>H-NMR** (400 MHz, CDCl<sub>3</sub>): δ (ppm) = 9.96 (s, 1H), 7.92 (d, J= 8.3Hz, 2H), 7.59 (d, J= 8.3Hz, 2H).

**<sup>13</sup>C-NMR** (100 MHz, CDCl<sub>3</sub>): δ (ppm) = 191.4, 138.4, 130.8, 102.8.

#### 1.9.4. Synthesis of precursor dipyrromethanes

##### Mesityl-Dipyrromethane (Mes-DPM)<sup>168</sup>

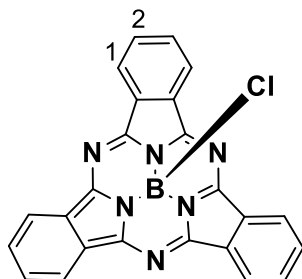


To a 2L round-bottom flask equipped with a magnetic stirrer, mesitaldehyde (1.76 mL, 12 mmol) and pyrrol (5 mL, 72 mmol) were added over a 0.12 M solution of HCl (1.2 L). The resulting mixture was stirred for 18 h under dark conditions. After filtration of the mixture, the resulting solid was subjected to column chromatography on silica gel using a mixture of DCM/heptane 5:1 as eluent. Mes-DPM was obtained as a white solid (1.19 g, 4.5 mmol). Yield: 35%.

<sup>206</sup> Kinsinger, T.; Kazmaier, U. *Org. Lett.* **2018**, *20*, 23, 7726.

### 1.9.5. Synthesis of chloro-substituted subphthalocyanines

#### Chloro-subphthalocyanato boron (III) (**2a**)<sup>3</sup>

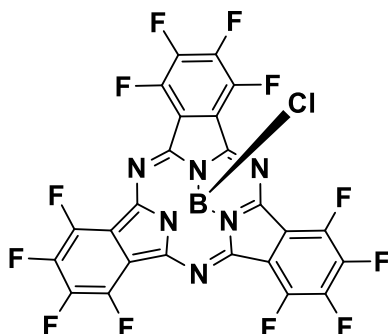


To a 25 ml round-bottom two-neck flask equipped with a reflux condenser and magnetic stirrer, a 1.0 M solution of BCl<sub>3</sub> in *p*-xylene (8 mL) was added to 3,4,5,6-tetrafluorophthalonitrile (1 g, 8 mmol) under argon atmosphere. The mixture was stirred and heated to reflux (145 °C) for 40 mins. The crude was cooled down to room temperature and flushed with argon. After evaporation of *p*-xylene under reduced pressure, the reaction flask was filled with heptane and sonicated for 30 mins. The dark solid was vacuum filtrated and washed with heptane until no color is observed, and then was further washed with methanol. The resulting solid was recovered with chloroform and dried to obtain 172 mg (0.4 mmol) of compound **2b** as a dark purple solid. Yield: 15%.

<sup>1</sup>H-NMR (300 MHz, CDCl<sub>3</sub>): δ (ppm) = 8.68 (s, 6H; H-1), 7.83 (s, 6H; H-2)

UV-vis (CHCl<sub>3</sub>): λ<sub>max</sub> (nm) (log ε (dm<sup>3</sup> mol<sup>-1</sup> cm<sup>-1</sup>)) = 565 (4.4), 529 (sh), 308 (4.1).

#### Chloro-1,2,3,4,8,9,10,11,15,16,17,18-dodecafluorosubphthalocyanato boron (III) (**2b**)<sup>3</sup>



To a 25 ml round-bottom two-neck flask equipped with a reflux condenser and magnetic stirrer, a 1.0 M solution of BCl<sub>3</sub> in *p*-xylene (5 mL) was added to 3,4,5,6-tetrafluorophthalonitrile (1 g, 5 mmol) under argon atmosphere. The mixture was stirred and heated to reflux (145 °C) for 2 hours. The crude was cooled down to room temperature and flushed with argon. After evaporation of *p*-xylene under reduced pressure, the resulting dark solid was subjected to column chromatography on silica gel using toluene/heptane 1:1

as eluent, to obtain 539 mg (0.84 mmol) of compound **2a** as a bright magenta solid. Yield: 50%.

Mp > 250 °C.

<sup>19</sup>F-NMR (470 MHz, CDCl<sub>3</sub>): δ (ppm) = -137.0 (AA'BB' system, 6F; β-SubPc), -147.7 (AA'BB' system, 6F; α-SubPc).

<sup>13</sup>C-NMR (75.5 MHz, CDCl<sub>3</sub>): δ (ppm) = 146.9, 144.8-144.1, 141.3-140.6, 115.2-114.7.

MS (MALDI-TOF, DCTB): *m/z* = 646.0 [M]<sup>+</sup>.

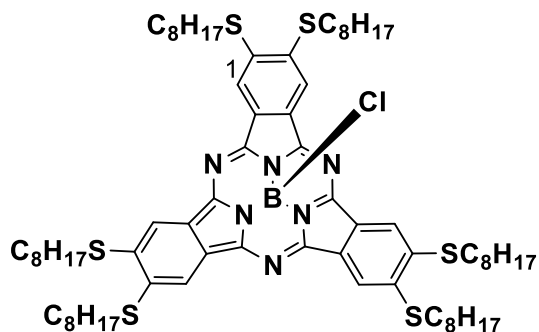
## Experimental section

**HRLSI-MS:**  $m/z$  Calcd for  $[C_{24}F_{12}N_6BCl]$ : 645.9774; Found: 645.9792.

**UV-vis** ( $CHCl_3$ ):  $\lambda_{max}$  (nm) ( $\log \epsilon$  ( $dm^3 mol^{-1} cm^{-1}$ )) = 574 (4.6), 556 (sh), 530 (sh), 311 (4.3), 277 (4.0).

**FT-IR** (KBr),  $\nu$  ( $cm^{-1}$ ): 1655, 1527, 1487, 1419, 1259, 1219, 1178, 1111, 1057, 964 (B-Cl), 883, 816, 714, 662.

### Chloro-2,3,9,10,16,17-hexa(octylthio)subphthalocyanato boron (III) (**8**)<sup>3</sup>



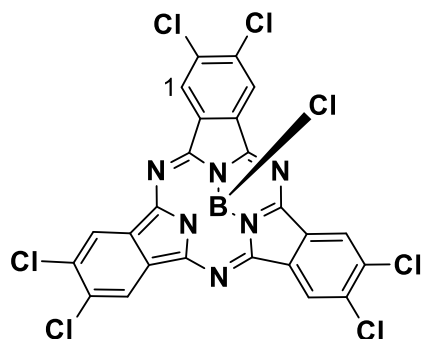
To a 25 ml round-bottom two-neck flask equipped with a reflux condenser and magnetic stirrer, a 1.0 M solution of  $BCl_3$  in *p*-xylene (2.4 mL) was added to 4,5-bis(octylthio)phthalonitrile (100 mg, 0.24 mmol) under argon atmosphere. The mixture was stirred and heated (120 °C) for 20 mins. The crude was cooled down to room temperature and flushed with argon. After evaporation of *p*-xylene under

reduced pressure, the resulting dark solid was subjected to a short column chromatography on silica gel using heptane/ethyl acetate 3:1 v/v as eluent, to obtain 63 mg (0.05 mmol) of compound **8** as a dark blue viscous solid. Yield: 60%.

**<sup>1</sup>H-NMR** (300 MHz,  $CDCl_3$ ):  $\delta$  (ppm) = 8.08 (s, 6H; H-1), 3.34-3.15 (m, 12H;  $SCH_2$ ), 1.92-1.80 (m, 12H;  $SCH_2CH_2$ ), 1.67-1.53 (m, 12H;  $S(CH_2)_2CH_2$ ), 1.44-1.22 (m, 48H;  $S(CH_2)_3(CH_2)_4$ ), 0.93-0.82 (m, 18H;  $S(CH_2)_7CH_3$ ).

**UV-vis** ( $CHCl_3$ ):  $\lambda_{max}$  (nm) ( $\log \epsilon$  ( $dm^3 mol^{-1} cm^{-1}$ )) = 603 (4.7), 555 (sh), 413 (4.1), 3.87 (4.1), 304 (4.2).

### Chloro-2,3,9,10,16,17-hexachlorosubphthalocyanato boron (III) (**17**)



To a 25 ml round-bottom two-neck flask equipped with a reflux condenser and magnetic stirrer, *o*-dichlorobenzene (8 mL) was added to 4,5-dichlorophthalonitrile (200 mg, 1 mmol) under argon atmosphere. A 1.0 M solution of  $BCl_3$  (1 mL) was added, and the mixture was stirred and heated to reflux (180.5 °C) for 20 hours. The crude was cooled down to room temperature and flushed with argon. After evaporation of solvent under reduced pressure, the resulting dark solid was subjected to column

chromatography on silica gel using toluene/heptane 1:1 v/v as eluent, to obtain 143 mg (0.23 mmol) of compound **17** as a magenta bright solid. Yield: 67%.

**Mp** > 250 °C.

**<sup>1</sup>H-NMR** (300 MHz, CDCl<sub>3</sub>): δ (ppm) = 8.93 (s, 6H; H-1).

**<sup>13</sup>C-NMR** (75.5 MHz, CDCl<sub>3</sub>): δ (ppm) = 150.5, 129.5, 123.7.

**MS** (MALDI-TOF, DCTB): *m/z* = 637.9 [M]<sup>+</sup>.

**HRLSI-MS**: *m/z* Calcd for [C<sub>24</sub>H<sub>6</sub>N<sub>6</sub>BCl<sub>7</sub>]: 633.8566; Found: 633.8532.

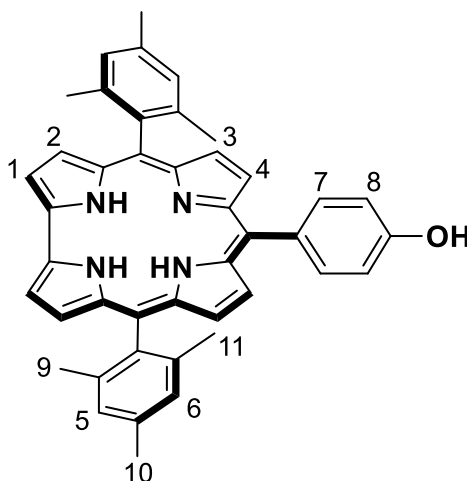
**UV-vis** (CHCl<sub>3</sub>): λ<sub>max</sub> (nm) (log ε (dm<sup>3</sup> mol<sup>-1</sup> cm<sup>-1</sup>)) = 572 (4.6), 552 (sh), 528 (4.1), 310 (4.3).

**FT-IR** (KBr), ν (cm<sup>-1</sup>): 2920, 2851, 1606, 1539, 1456, 1419, 1373, 1278, 1222, 1095 (C-Cl), 1042, 976 (B-Cl), 882, 819.

### 1.9.6. Synthesis of subphthalocyanine-corrole *meso*- dyads

#### 1.9.6.1. Synthesis of *trans*-A<sub>2</sub>B-corroles

#### **10-(4-hydroxyphenyl)-5,15-bis(2,4,6-trimethylphenyl)corrole (1a)**



To a 250 mL round-bottom flask equipped with a magnetic stirrer, 4-Hydroxybenzaldehyde (61 mg, 0.50 mmol) was added over MeOH (50 mL), and Dipyrromethane **1** (264 mg, 1.00 mmol) was added. Once upon homogenization, a HCl solution (52.5 mL, 0.55 M) was added dropwise and stirred at 25 °C for 2 hours. The mixture was extracted with CHCl<sub>3</sub> and the organic phase was washed with H<sub>2</sub>O (2x50 mL), brine (1x50 mL) and dried over Na<sub>2</sub>SO<sub>4</sub>. After filtration and solvent removal by vacuum distillation, CHCl<sub>3</sub> (250 mL) and *p*-chloranil (295 mg, 1.20 mmol) were added

and the solution stirred at 25 °C for 16 hours. Hydrazine (0.1 mL) was added and solvent was removed by vacuum distillation. The resulting solid was subjected to column chromatography on silica gel using CH<sub>2</sub>Cl<sub>2</sub> as eluent. The resulting solid was triturated with a mixture of H<sub>2</sub>O/MeOH 1:1 to afford 116 mg (0.19 mmol) of compound **1a** as a purple solid. Yield: 37%.

## Experimental section

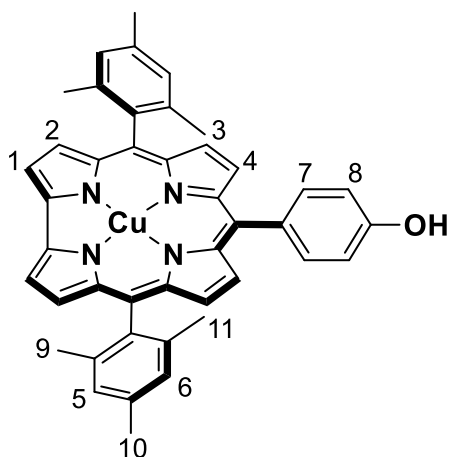
**<sup>1</sup>H-NMR** (400 MHz, CDCl<sub>3</sub>): δ (ppm) = 8.87 (d, *J* = 4.2 Hz, 2H; H-1), 8.48 (m, 4H; H-3, H-4), 8.31 (d, *J* = 4.2 Hz, 2H; H-2), 8.01 (d, *J* = 8.5 Hz, 2H; H-7), 7.18 (d, *J* = 8.5 Hz, 2H; H-8), 2.59 (s, 6H; H-10), 1.91 (s, 12H; H-9, H-11).

**MS** (MALDI-TOF, DCTB): *m/z* = 625.4 [M-H]<sup>+</sup>, 626.4 [M]<sup>+</sup>.

**<sup>13</sup>C-NMR** (126 MHz, CDCl<sub>3</sub>): δ (ppm) = 143.26, 142.70, 140.86, 140.13, 139.29, 137.72, 135.56, 133.41, 129.98, 128.30, 128.06, 126.74, 125.61, 120.63, 118.87, 115.12, 114.21, 103.75, 77.32, 77.07, 76.81, 31.91, 31.35, 30.96, 24.28, 22.72, 21.48, 21.17, 20.10, 17.76, 14.14.

**UV-Vis** (Toluene): λ<sub>max</sub> (nm) (log ε (dm<sup>3</sup> mol<sup>-1</sup> cm<sup>-1</sup>)) = 641 (3.61), 607 (3.83), 566 (4.12), 428 (4.78), 410 (4.69), 410 (4.87).

### 10-(4-hydroxyphenyl)-5,15-bis(2,4,6-trimethylphenyl)corrolato-Cu (**1b**)



To a 50 mL round-bottom flask equipped with a magnetic stirrer, Cor **1a** (43 mg, 0.069 mmol) was added over CHCl<sub>3</sub> (10 mL) and stirred at 40 °C. Cu(AcO)<sub>2</sub> (100 mg, 0.550 mmol) dissolved in hot MeOH (5 mL) was added and the solution was further stirred at 40 °C for 15 minutes. The solvent was removed by vacuum distillation and the resulting solid was subjected to a small column chromatography on silica gel using a mixture of CH<sub>2</sub>Cl<sub>2</sub>/Heptane 5:1 as eluent to obtain 40 mg (0.060 mmol) of compound **1b** as a brown solid. Yield: 85%.

**<sup>1</sup>H-NMR** (400 MHz, CDCl<sub>3</sub>): δ (ppm) = 2.59 (s, 6H; H-10), 1.91 (s, 12H; H-9, H-11).

**MS** (MALDI-TOF, DCTB): *m/z* = 686.3 [M]<sup>+</sup>.

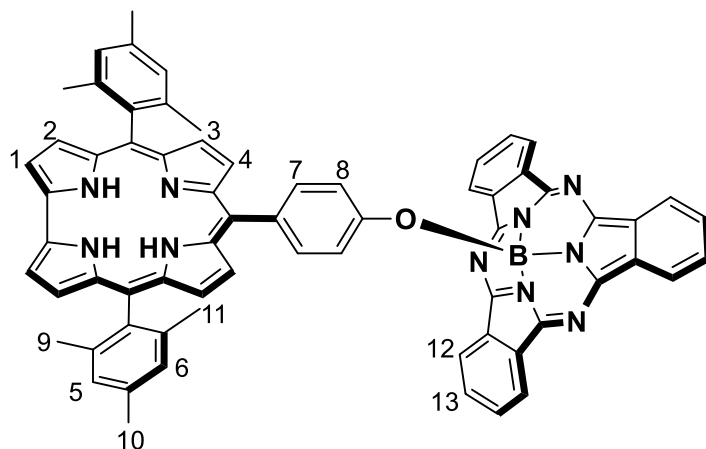
**UV-Vis** (Toluene): λ<sub>max</sub> (nm) (log ε (dm<sup>3</sup> mol<sup>-1</sup> cm<sup>-1</sup>)) = 621 (3.45), 538 (3.80), 421 (4.76), 392 (4.69).

### 1.9.6.2. Synthesis of subphthalocyanine-corrole dyads

*General procedure:*

To a 10 mL Schlenk flask equipped with a magnetic stirrer, dry toluene (3 mL) was added to a mixture of the corresponding SubPc (0.116 mmol) and AgOTf (0.144 mmol), under argon atmosphere. The mixture was stirred at 40-60 °C for 2-6 hours. The corresponding Cor (0.116 mmol) and DIPEA (0.144 mmol for SubPc-Cor dyads **4**, **5**, **7** and **11**; 0.174 mmol for SubPc-Cor dyad **6**) were then added and the suspension stirred at 40-80 °C for 24 hours (18 hours for SubPc-Cor dyad **11**). The solvent was removed by vacuum distillation and the resulting solid was subjected to column chromatography on silica gel. Each compound was further purified by size exclusion chromatography in CHCl<sub>3</sub>.

Subphthalocyanine-Corrole dyad **4**



Axial activation temperature and reaction time: 40 °C, 2h. Axial substitution temperature: 40 °C. Column chromatography on silica gel using toluene/THF 20:1 v/v as eluent. Compound **4** (50 mg, 0.04 mmol) was obtained as a dark purple solid. Yield: 30%.

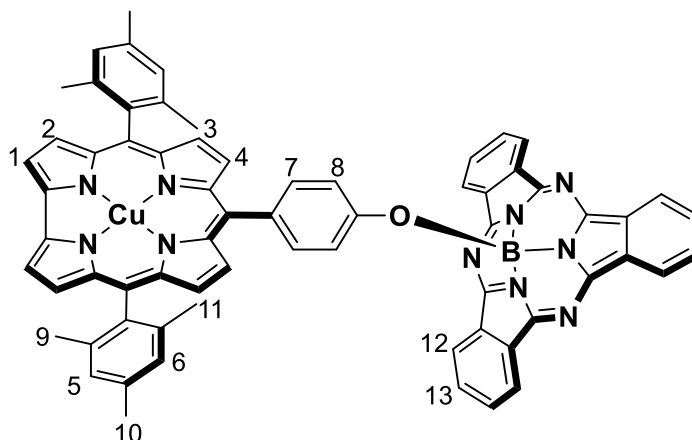
**<sup>1</sup>H-NMR** (300 MHz, CDCl<sub>3</sub>): δ (ppm) = 8.94 (dd,  $J_o = 5.9$  Hz,  $J_m = 3.1$  Hz, 6H; H-12), 8.84 (d,  $J = 4.2$  Hz, 2H; H-1), 8.39 (d,  $J = 4.7$  Hz, 2H; H-3), 8.29 (d,  $J = 4.2$  Hz, 2H; H-2), 8.22 (d,  $J = 4.7$  Hz, 2H; H-4), 7.95 (dd,  $J_o = 5.9$  Hz,  $J_m = 3.1$  Hz, 6H; H-13), 7.51 (d,  $J = 8.5$  Hz, 2H; H-7), 5.72 (d,  $J = 8.5$  Hz, 2H; H-8), 2.59 (s, 6H; H-10), 1.88 (s, 12H; H-9, H-11).

**<sup>11</sup>B-NMR** (300 MHz, CDCl<sub>3</sub>): δ (ppm) = -14.53.

**<sup>13</sup>C-NMR** (300 MHz, CDCl<sub>3</sub>): δ (ppm) = 152.20, 151.53, 139.27, 137.61, 135.72, 134.99, 134.82, 131.14, 130.99, 129.91, 129.86, 128.00, 126.33, 122.32, 122.23, 117.65, 114.98, 109.59, 33.55, 31.60, 29.70, 22.66, 21.44, 21.12, 14.12.

**MS** (APCI+):  $m/z = 1021.43$  [M]<sup>+</sup>, 627.31 [Cor+H]<sup>+</sup>.

**UV-Vis** (Toluene):  $\lambda_{\max}$  (nm) ( $\log \varepsilon$  (dm<sup>3</sup> mol<sup>-1</sup> cm<sup>-1</sup>)) = 640 (3.87), 606 (3.99), 563 (4.95), 544 (sh), 518 (4.49), 427 (4.84), 410 (4.92), 303 (4.67).

Subphthalocyanine-Corrole dyad **5**

Axial activation temperature and reaction time: 40 °C, 2h. Axial substitution temperature: 40 °C. Column chromatography on silica gel using toluene/THF 20:1 v/v as eluent. Compound **5** (40 mg, 0.037 mmol) was obtained as a dark brown solid. Yield: 32%.

**<sup>1</sup>H-NMR** (300 MHz, CDCl<sub>3</sub>): δ (ppm) = 8.87 (m, 6H; H-12), 7.90 (m, 6H; H-13), 2.40 (s, 6H; H10), 2.03 (s, 12H; H-9, H-11).

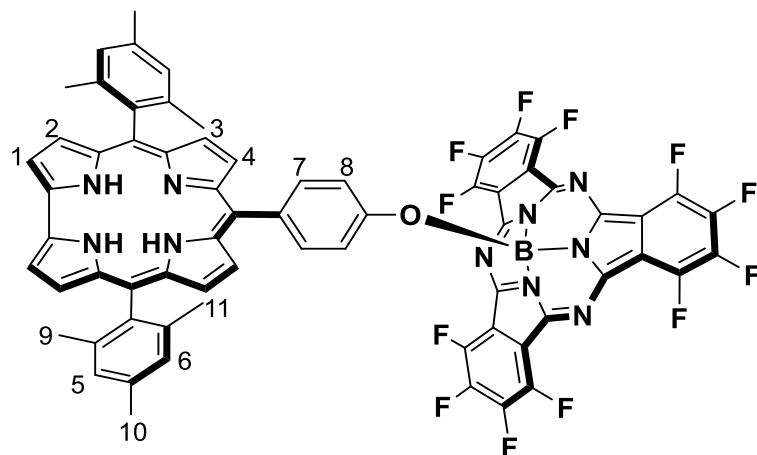
**<sup>11</sup>B-NMR** (300 MHz, CDCl<sub>3</sub>): δ (ppm) = -14.73.

**<sup>13</sup>C-NMR** (300 MHz, CDCl<sub>3</sub>): δ (ppm) = 153.37, 151.41, 137.49, 131.03, 129.90, 129.03, 128.90, 128.22, 128.09, 122.25, 120.87, 118.32, 29.70, 21.20, 19.74.

**MS** (MALDI-TOF, DCTB): *m/z* = 1080.3 [M]<sup>+</sup>.

**UV-Vis** (Toluene): λ<sub>max</sub> (nm) (log ε (dm<sup>3</sup> mol<sup>-1</sup> cm<sup>-1</sup>)) = 622 (3.52), 5.63 (4.87), 545 (4.61), 516 (4.41), 416 (4.76), 3.99 (4.71), 300 (4.64).

### Subphthalocyanine-Corrole dyad **6**



Axial activation temperature and reaction time: 60 °C, 6h. Axial substitution temperature: 80 °C. Column chromatography on silica gel using toluene/heptane 2:1 v/v as eluent. Compound **6** (22 mg, 0.018 mmol) was obtained as a dark magenta solid. Yield: 15%.

**<sup>1</sup>H-NMR** (300 MHz, CDCl<sub>3</sub>): δ (ppm) = 8.86 (d, *J* = 4.2 Hz, 2H; H-1), 8.44 (d, *J* = 4.7 Hz, 2H; H-3), 8.30 (d, *J* = 4.2 Hz, 2H; H-2), 8.21 (d, *J* = 4.7 Hz, 2H; H-4), 7.59 (d, *J* = 8.4 Hz, 2H; H-7), 5.69 (d, *J* = 8.4 Hz, 2H; H-8), 2.60 (s, 6H; H-10), 1.89 (s, 12H; H-9, H-11).

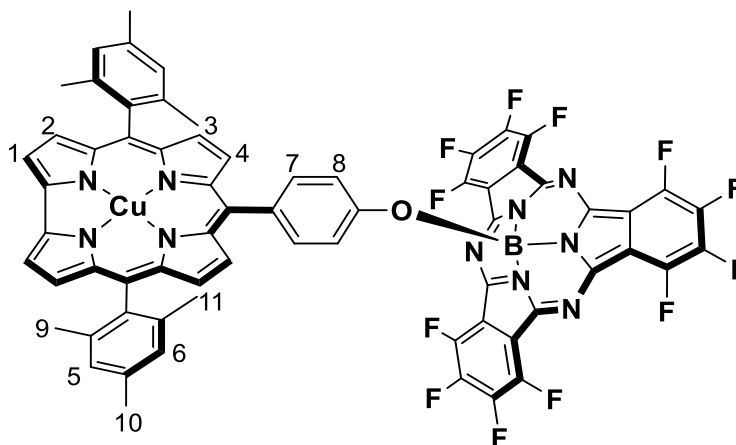
**<sup>19</sup>F-NMR** (300 MHz, CDCl<sub>3</sub>): δ (ppm) = -136.50 (AA'BB' system, 6F); -147.24 (AA'BB' system, 6F).

**<sup>11</sup>B-NMR** (300 MHz, CDCl<sub>3</sub>): δ (ppm) = -14.74.

**<sup>13</sup>C-NMR** (300 MHz, CDCl<sub>3</sub>): δ (ppm) = 148.59, 129.05, 128.24, 128.04, 125.31, 29.73, 21.48, 21.13, 1.04.

**MS** (MALDI-TOF, DCTB): *m/z* = 1235.3 [M-H]<sup>+</sup>, 1236.3 [M]<sup>+</sup>, 625.4 [Cor-H]<sup>+</sup>, 626.4 [Cor]<sup>+</sup>

**UV-Vis** (Toluene): λ<sub>max</sub> (nm) (log ε (dm<sup>3</sup> mol<sup>-1</sup> cm<sup>-1</sup>)) = 638 (3.28), 606 (3.67), 573 (4.80), 553 (sh), 528 (3.32), 428 (4.79), 408 (4.87), 394 (sh).

Subphthalocyanine-Corrole dyad **7**

Axial activation temperature and reaction time: 60 °C, 6h. Axial substitution temperature: 65 °C. Column chromatography on silica gel using toluene/heptane 2:1 v/v as eluent. Compound **7** (30 mg, 0.023 mmol) was obtained as a dark magenta solid. Yield: 20%.

**<sup>1</sup>H-NMR** (300 MHz, CDCl<sub>3</sub>): δ (ppm) = 5.48 (d, *J* = 8.2 Hz, 2H; H-8), 2.60 (s, 6H; H-10), 1.89 (s, 12H; H-9, H-11).

**<sup>19</sup>F-NMR** (300 MHz, CDCl<sub>3</sub>): δ (ppm) = -136.51 (AA'BB' system, 6F), -147.31 (AA'BB' system, 6F).

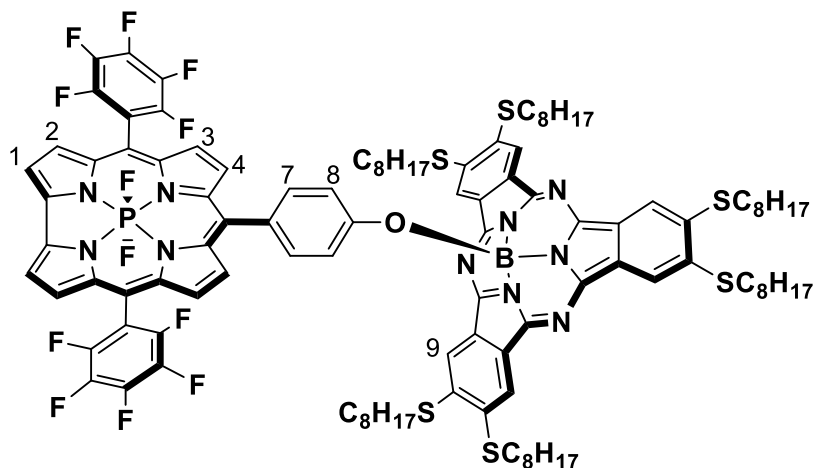
**<sup>11</sup>B-NMR** (300 MHz, CDCl<sub>3</sub>): δ (ppm) = -15.02.

**<sup>13</sup>C-NMR** (300 MHz, CDCl<sub>3</sub>): δ (ppm) = 151.80, 148.73, 148.48, 144.64, 144.50, 144.19, 141.12, 140.93, 140.71, 137.60, 130.96, 129.02, 128.73, 128.14, 121.06, 117.98, 114.98, 114.86, 29.70, 22.69, 21.20, 19.73, 14.10.

**MS** (APCI+): *m/z* = 1297.22 [M-H]<sup>+</sup>, 687.22 [Cor]<sup>+</sup>.

**UV-Vis** (Toluene): λ<sub>max</sub> (nm) (log ε (dm<sup>3</sup> mol<sup>-1</sup> cm<sup>-1</sup>)) = 619 (3.67), 573 (5.03), 554 (sh), 530 (4.58), 514 (sh), 417 (4.98), 399 (4.91).

Subphthalocyanine-Corrole dyad **11**



Axial activation temperature and reaction time: RT, 10 min. Axial substitution temperature: 60 °C. Column chromatography on silica gel using toluene/heptane 2:1 v/v as eluent. Compound **11** (64.13 mg, 0.03 mmol) was obtained as a dark purple solid. Yield: 27%.

<sup>1</sup>H-NMR (300 MHz, CDCl<sub>3</sub>): δ (ppm) = 9.44 (br t, *J* = 4.5, 3.2 Hz, 2H; β-pyrr), 8.98 (t, *J* = 4.5 Hz, 2H; β-pyrr), 8.90 (t, *J* = 4.7 Hz, 2H; β-pyrr), 8.64 (s, 6H; H-9), 8.59 (br t, 2H; β-pyrr), 7.58 (d, *J* = 8.4 Hz, 2H; H-7), 5.83 (d, *J* = 8.4 Hz, 2H; H-8), 3.28 (m, 8H; SCH<sub>2</sub>), 1.89 (m, 8H; SCH<sub>2</sub>CH<sub>2</sub>), 1.61 (m, 8H; S(CH<sub>2</sub>)<sub>2</sub>CH<sub>2</sub>), 1.35 (m, 32H; S(CH<sub>2</sub>)<sub>3</sub>(CH<sub>2</sub>)<sub>4</sub>), 0.85 (m, 12H; S(CH<sub>2</sub>)<sub>7</sub>CH<sub>3</sub>).

<sup>19</sup>F-NMR (300 MHz, CDCl<sub>3</sub>): δ (ppm) = -36.32 (1F, P-F), -39.20 (1F, P-F), -136.40 (AA'BB'C system, 4F, Ar-F), -152.00 (AA'BB'C system, 2F, Ar-F), -161.26 (AA'BB'C system, 4F, Ar-F).

<sup>11</sup>B-NMR (300 MHz, CDCl<sub>3</sub>): δ (ppm) = -14.34.

<sup>13</sup>C-NMR (300 MHz, CDCl<sub>3</sub>): δ (ppm) = 150.68, 140.72, 134.46, 128.52, 119.66, 118.25, 99.9, 33.74, 31.86, 31.82, 29.73, 29.24, 29.18, 29.16, 28.49, 22.68, 22.65, 14.07.

<sup>31</sup>P-NMR (300 MHz, CDCl<sub>3</sub>): δ (ppm) = 182.20.

MS (MALDI): *m/z* = 2047.5 [M]<sup>+</sup>, 1276.6 [SubPc-Cl].

### 1.9.6.3 Transient absorption spectroscopy

#### 1.9.6.3.1 Reference corroles and subphthalocyanines

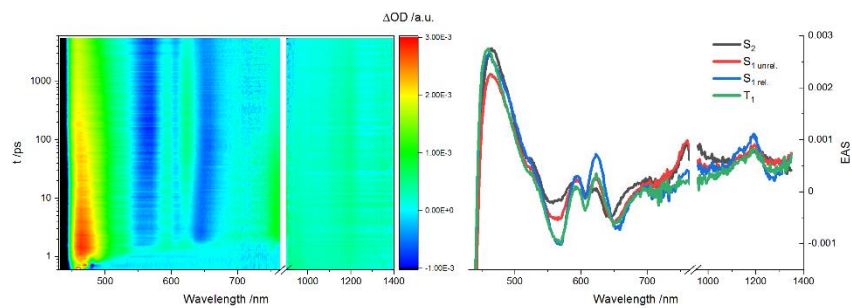


**Figure S-TAS1.** (left) Differential absorption of Ref. Cor **1aR** upon femtosecond flash photolysis with excitation at 420 nm in toluene and (right) corresponding evolution associated spectra of the involved transient species.

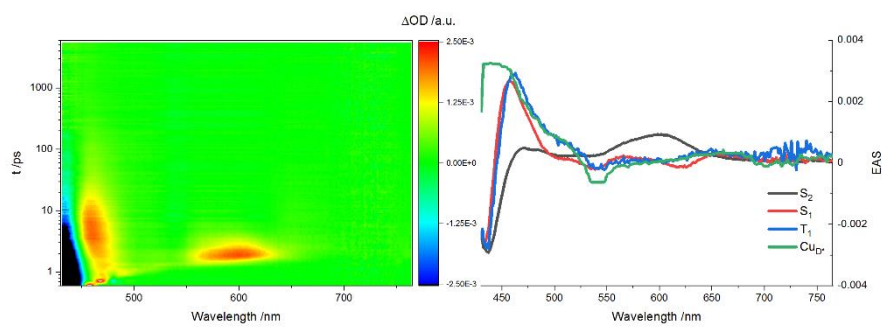


**Figure S-TAS2.** (left) Differential absorption of Ref. Cor **1bR** upon femtosecond flash photolysis with excitation at 420 nm in toluene and (right) corresponding evolution associated spectra of the involved transient species.

## Experimental section

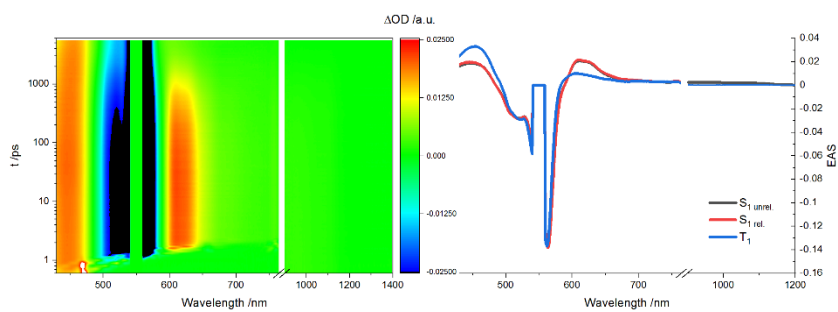


**Figure S-TAS3.** (left) Differential absorption of Ref. SubPc **2aR** upon femtosecond flash photolysis with excitation at 550 nm in toluene and (right) corresponding evolution associated spectra of the involved transient species.

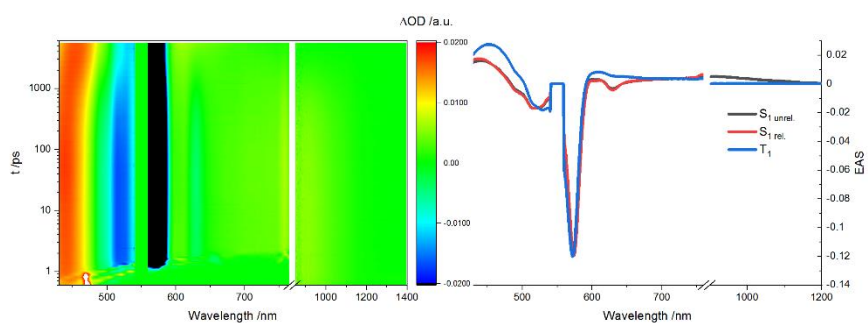


**Figure S-TAS4.** (left) Differential absorption of Ref. SubPc **2bR** upon femtosecond flash photolysis with excitation at 550 nm in toluene and (right) corresponding evolution associated spectra of the involved transient species.

## 1.8.4.3.2. Subphthalocyanine-corrrole covalent dyads

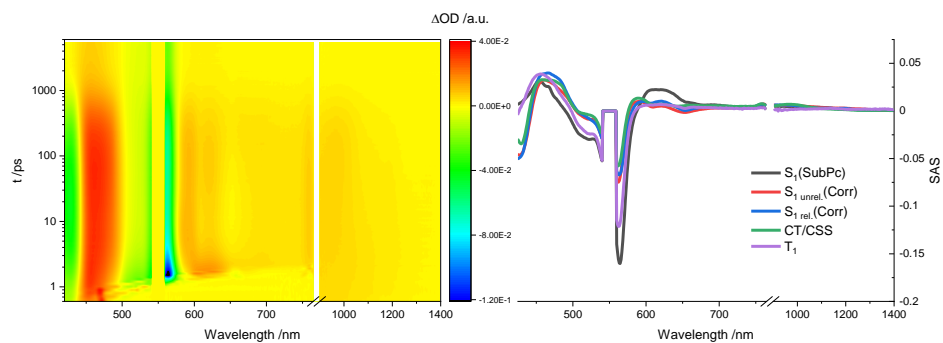


**Figure S-TAS5.** (left) Differential absorption of dyad **4** upon femtosecond flash photolysis with excitation at 550 nm in toluene and (right) corresponding species associated spectra of the involved transient species.

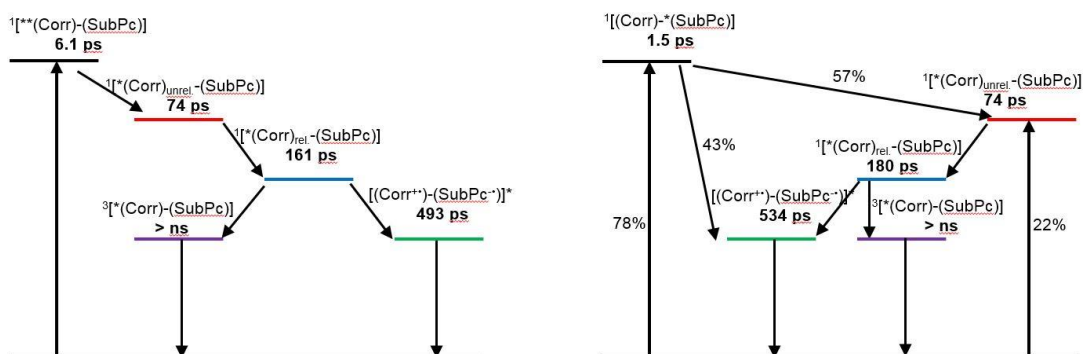


**Figure S-TAS6.** Kinetic models used for the analysis of femtosecond-resolved differential absorption of dyad **4** upon excitation at 420 (left) and 550 nm (right) in toluene.

## Experimental section

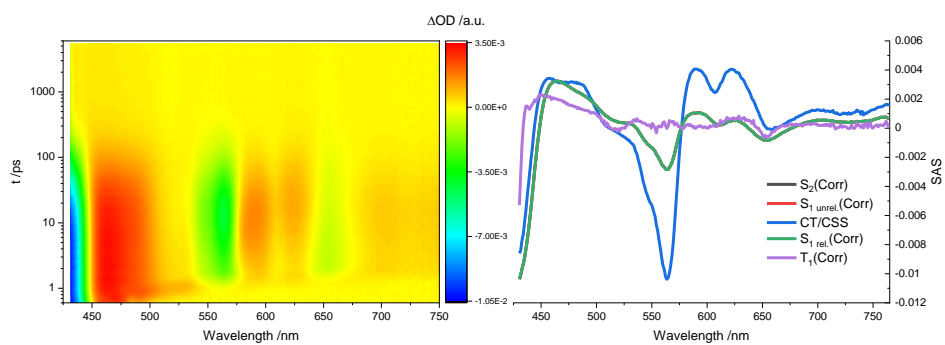


**Figure S-TAS7.** (left) Differential absorption of dyad **4** upon femtosecond flash photolysis with excitation at 420 nm in benzonitrile and (right) corresponding species associated spectra of the involved transient species.

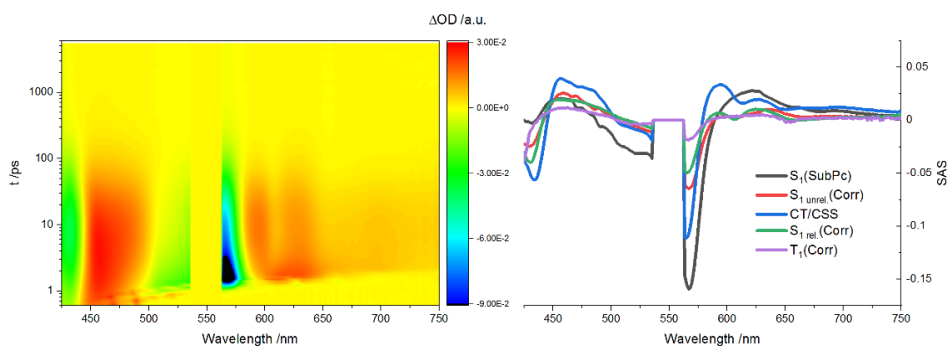


**Figure S-TAS8.** (left) Differential absorption of dyad **4** upon femtosecond flash photolysis with excitation at 550 nm in benzonitrile and (right) corresponding species associated spectra of the involved transient species.

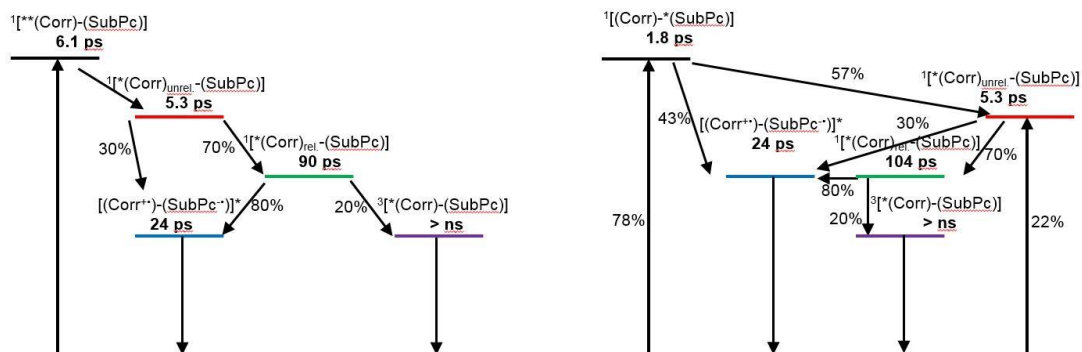


**Figure S-TAS9.** Kinetic models used for the analysis of femtosecond-resolved differential absorption of dyad **4** upon excitation at 420 (left) and 550 nm (right) in benzonitrile.

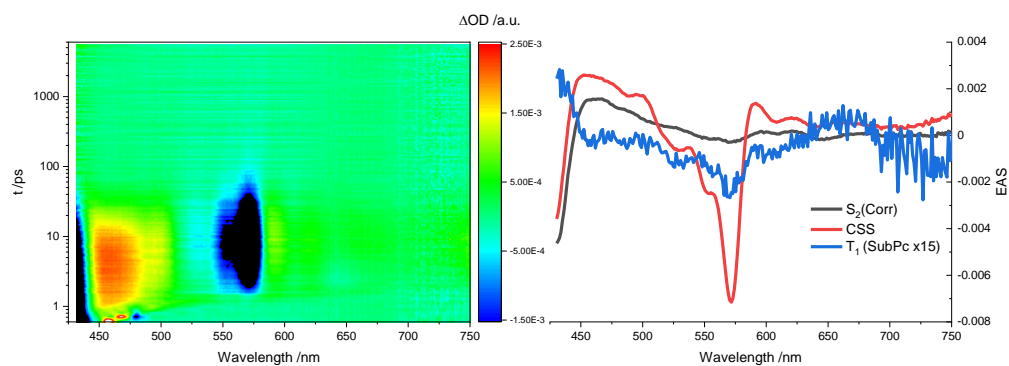


**Figure S-TAS10.** (left) Differential absorption of dyad **6** upon femtosecond flash photolysis with excitation at 420 nm in toluene and (right) corresponding evolution associated spectra of the involved transient species.

## Experimental section

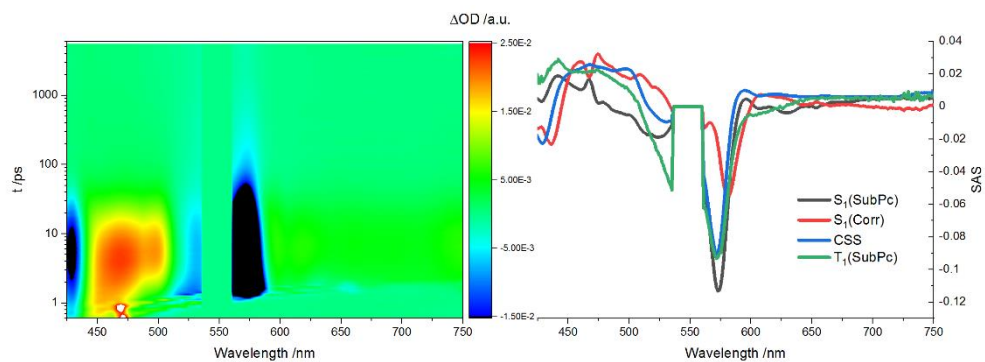


**Figure S-TAS11.** (left) Differential absorption of dyad **6** upon femtosecond flash photolysis with excitation at 550 nm in toluene and (right) corresponding species associated spectra of the involved transient species.

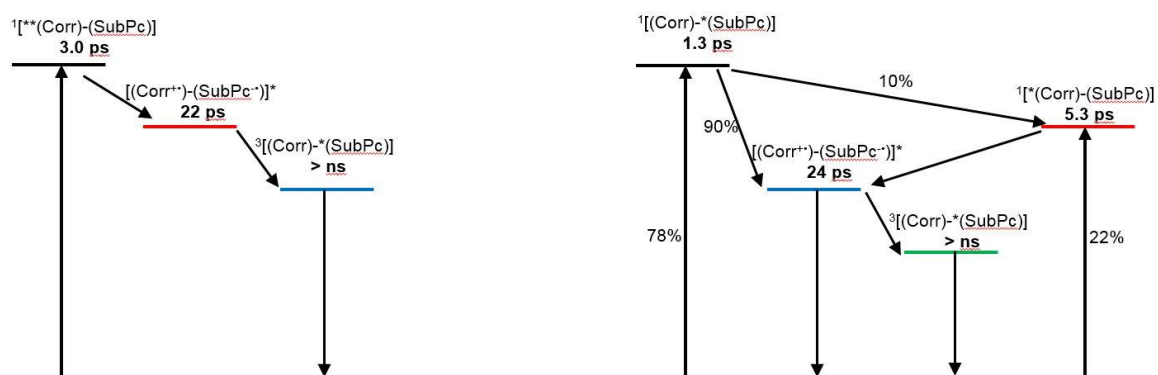


**Figure S-TAS12.** Kinetic models used for the analysis of femtosecond-resolved differential absorption of dyad **6** upon excitation at 420 (left) and 550 nm (right) in toluene.

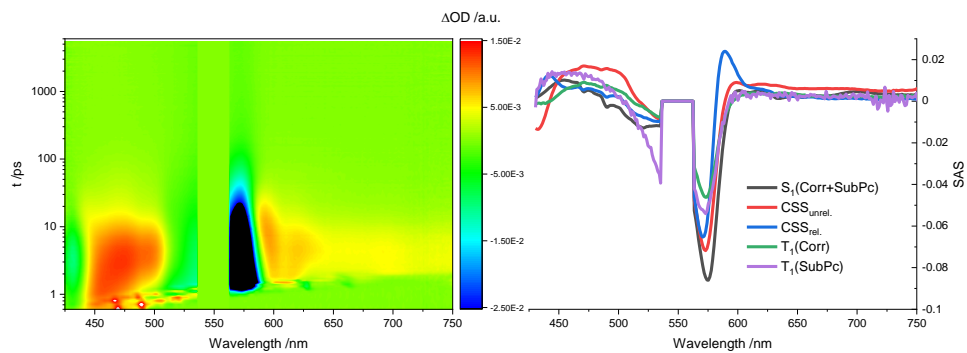


**Figure S-TAS13.** (left) Differential absorption of dyad **6** upon femtosecond flash photolysis with excitation at 550 nm in benzonitrile and (right) corresponding species associated spectra of the involved transient species.

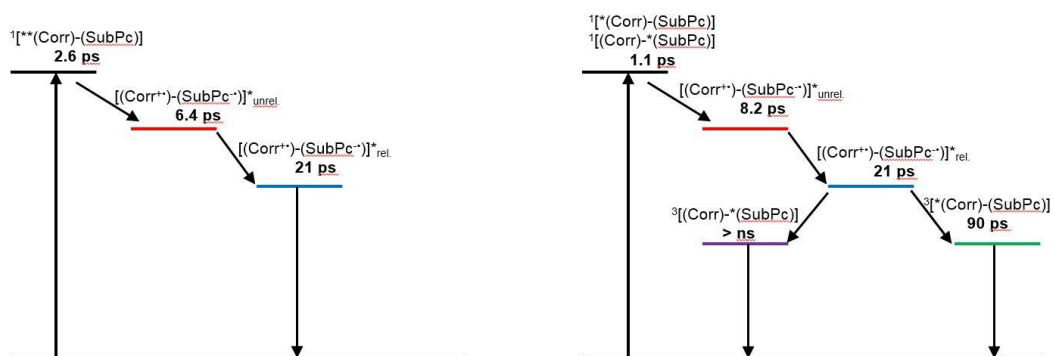


**Figure S-TAS14.** Kinetic models used for the analysis of femtosecond-resolved differential absorption of dyad **6** upon excitation at 420 (left) and 550 nm (right) in benzonitrile.

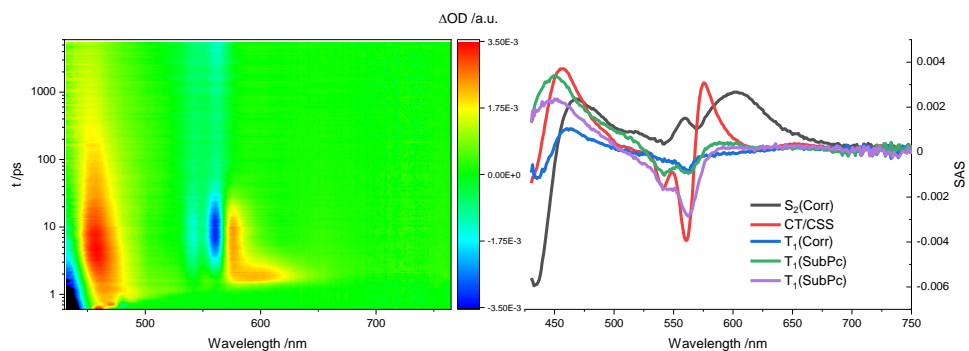


**Figure S-TAS15.** (left) Differential absorption of dyad **5** upon femtosecond flash photolysis with excitation at 420 nm in toluene and (right) corresponding species associated spectra of the involved transient species.

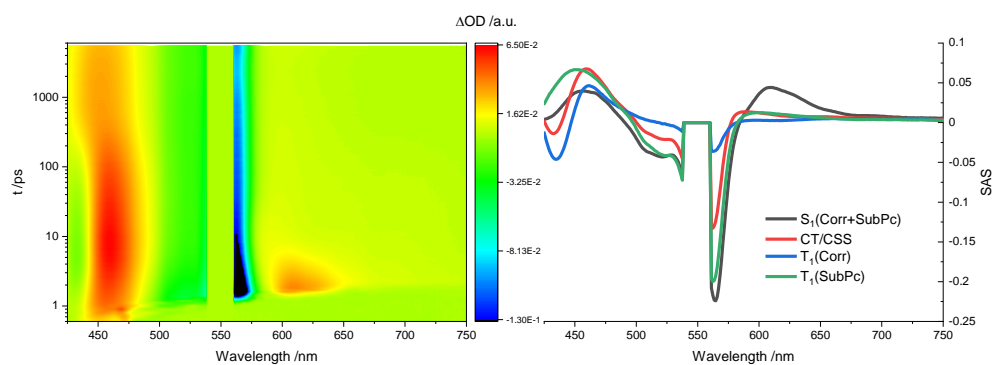


**Figure S-TAS16.** (left) Differential absorption of dyad **5** upon femtosecond flash photolysis with excitation at 550 nm in toluene and (right) corresponding species associated spectra of the involved transient species.

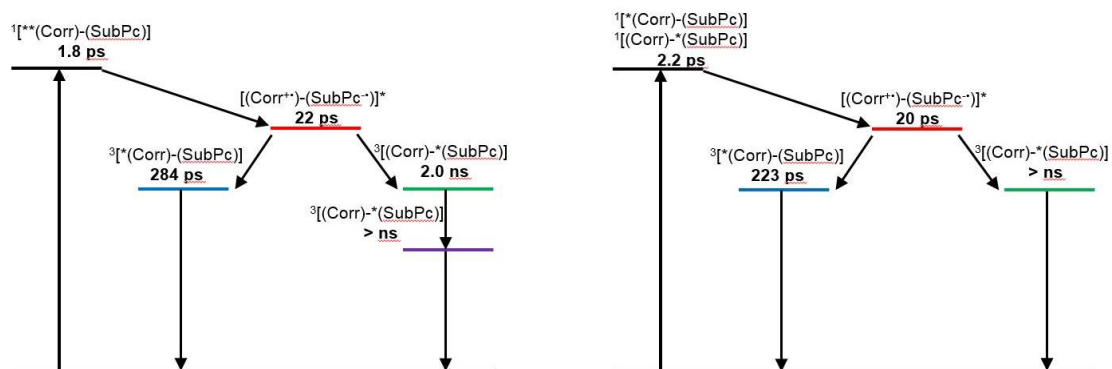


**Figure S-TAS17.** Kinetic models used for the analysis of femtosecond-resolved differential absorption of dyad 5 upon excitation at 420 (left) and 550 nm (right) in toluene.

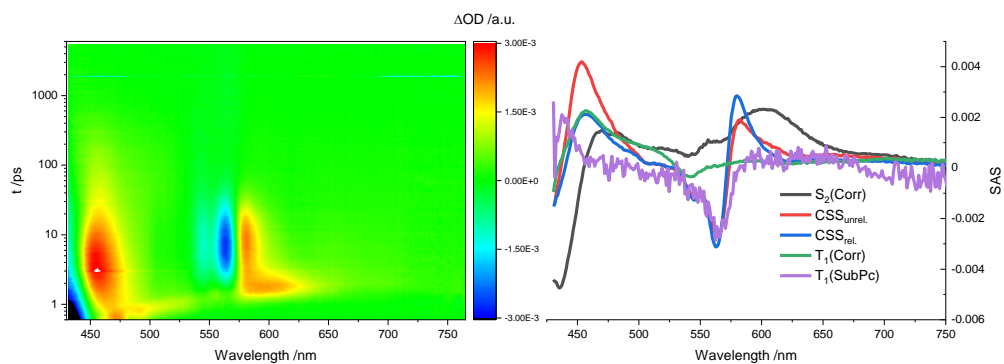


**Figure S-TAS18.** (left) Differential absorption of dyad 5 upon femtosecond flash photolysis with excitation at 420 nm in benzonitrile and (right) corresponding species associated spectra of the involved transient species.

## Experimental section

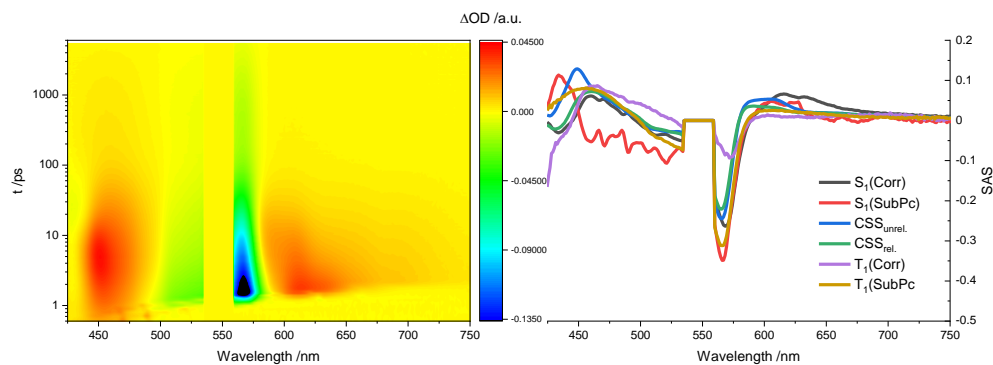


**Figure S-TAS19.** (left) Differential absorption of dyad **5** upon femtosecond flash photolysis with excitation at 550 nm in benzonitrile and (right) corresponding species associated spectra of the involved transient species.

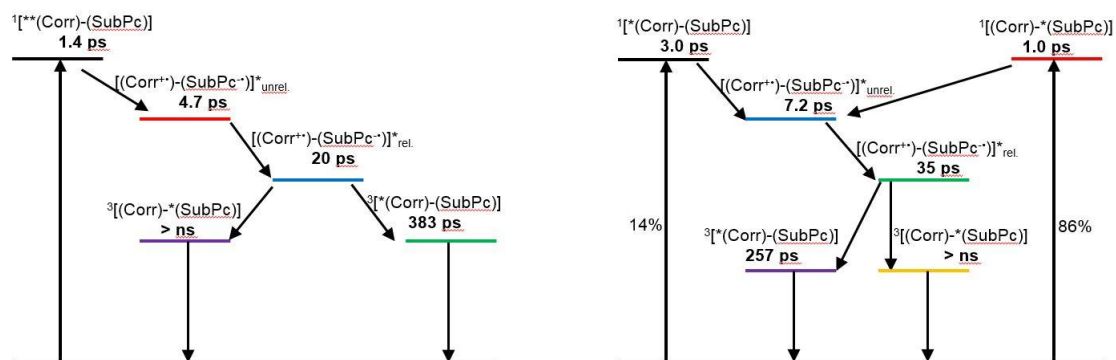


**Figure S-TAS20.** Kinetic models used for the analysis of femtosecond-resolved differential absorption of dyad **5** upon excitation at 420 (left) and 550 nm (right) in benzonitrile.

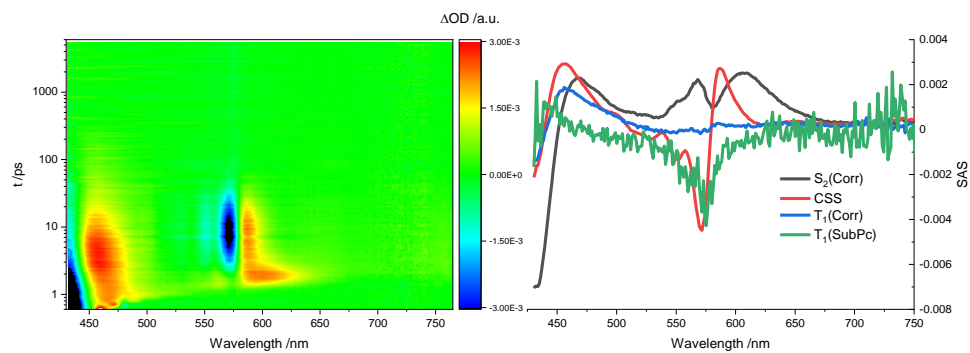


**Figure S-TAS21.** (left) Differential absorption of dyad **7** upon femtosecond flash photolysis with excitation at 420 nm in toluene and (right) corresponding species associated spectra of the involved transient species.

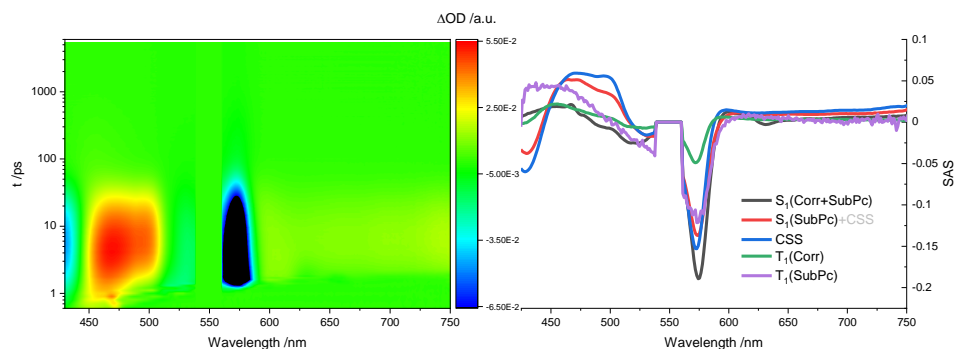


**Figure S-TAS22.** (left) Differential absorption of dyad **7** upon femtosecond flash photolysis with excitation at 550 nm in toluene and (right) corresponding species associated spectra of the involved transient species.

## Experimental section

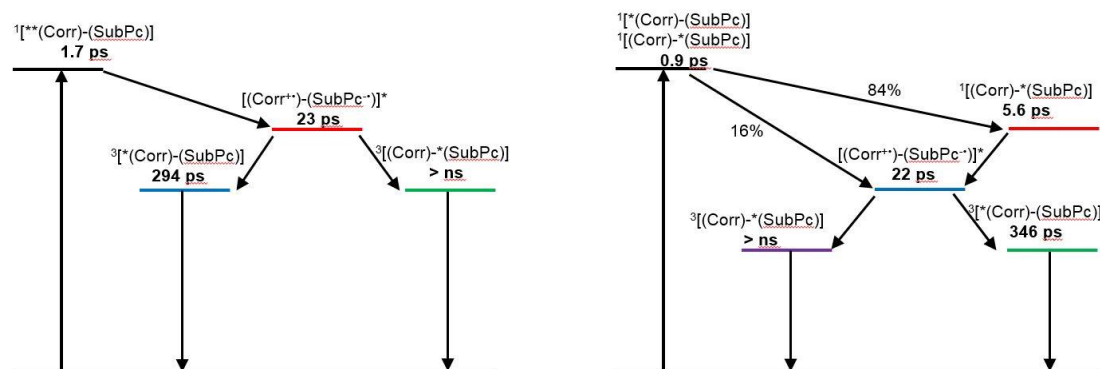


**Figure S-TAS23.** Kinetic models used for the analysis of femtosecond-resolved differential absorption of dyad **7** upon excitation at 420 (left) and 550 nm (right) in toluene.

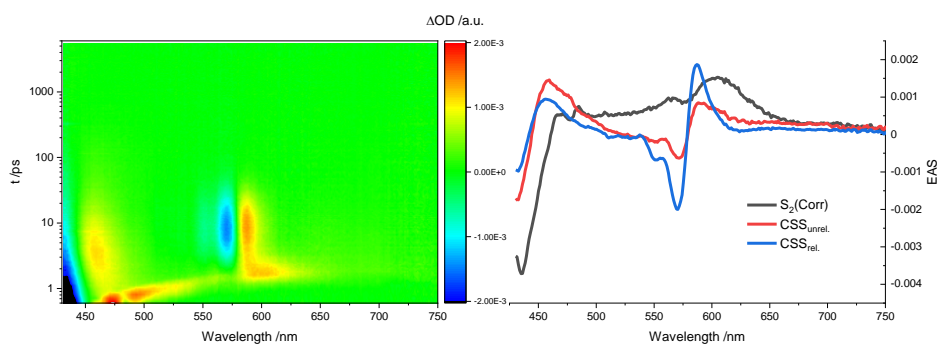


**Figure S-TAS24.** (left) Differential absorption of dyad **7** upon femtosecond flash photolysis with excitation at 420 nm in benzonitrile and (right) corresponding evolution associated spectra of the involved transient species.

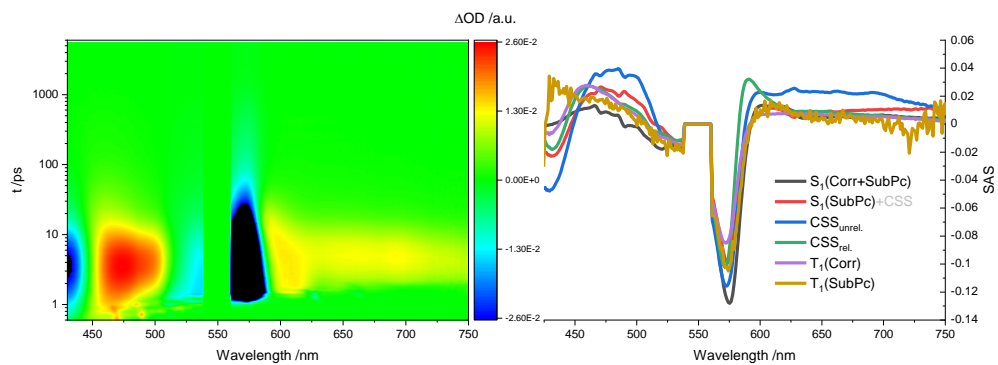


**Figure S-TAS25.** (left) Differential absorption of dyad **7** upon femtosecond flash photolysis with excitation at 550 nm in benzonitrile and (right) corresponding species associated spectra of the involved transient species.

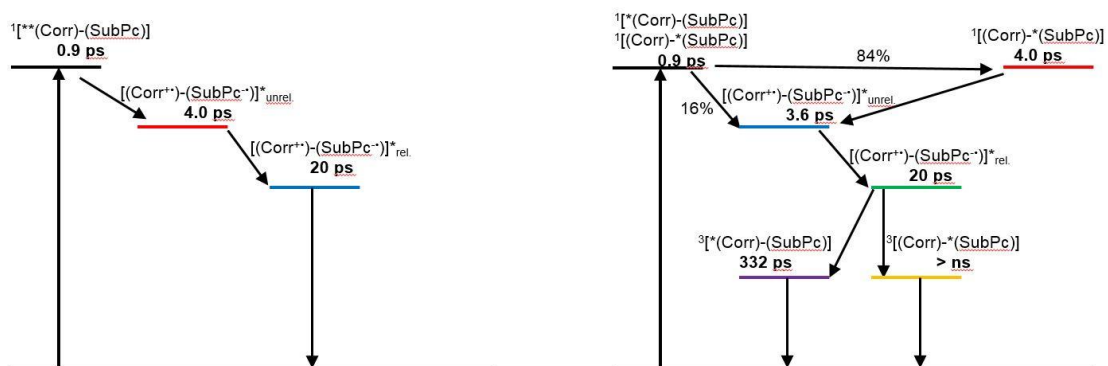
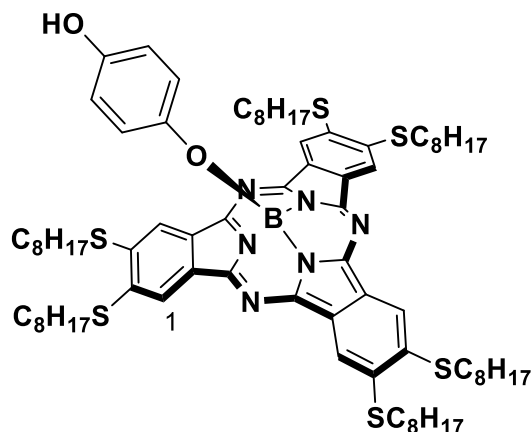


**Figure S-TAS23.** Kinetic models used for the analysis of femtosecond-resolved differential absorption of dyad **7** upon excitation at 420 (left) and 550 nm (right) in benzonitrile.

## 1.9.7. Synthesis of subphthalocyanine-corrole axial- dyads

### 1.9.7.1. Synthesis of subphthalocyanines

#### Hydroquinone-Subphthalocyanine (**13**)



To a 10 mL Schlenk flask equipped with a magnetic stirrer, dry  $\alpha,\alpha,\alpha$ -trifluorotoluene (2.5 mL) was added to a mixture of the corresponding SubPc **8** (61.20 mg, 0.047 mmol) and hydroquinone (52.00 mg, 0.472 mmol) under argon atmosphere. DIPEA (8  $\mu$ L) was added, and the mixture was stirred at room temperature for 2 hours. The solvent was removed by vacuum distillation and the resulting solid was subjected to column chromatography on silica gel using a

mixture of AcOEt/Heptane 1:15 as eluent. Compound **13** was obtained as dark blue solid (32.30 mg, 0.023 mmol). Yield: 50%.

**$^1\text{H-NMR}$**  (300 MHz,  $\text{CDCl}_3$ ):  $\delta$  (ppm) = 8.08 (s, 6H; H-1), 6.30 (d,  $J$  = 8.8 Hz, 2H; Ar-H), 5.32 (d,  $J_o$  = 8.8 Hz, 2H; Ar-H), 3.30-3.20 (m, 12H;  $\text{SCH}_2$ ), 1.90-1.80 (m, 12H;  $\text{SCH}_2\text{CH}_2$ ), 1.36-1.25 (m, 48H;  $\text{S}(\text{CH}_2)_3(\text{CH}_2)_4$ ), 0.89-0.86 (m, 18H;  $\text{S}(\text{CH}_2)_7\text{CH}_3$ ).

**$^{13}\text{C-NMR}$**  (500 MHz,  $\text{CDCl}_3$ ):  $\delta$  (ppm) = 151.18, 150.86, 146.08, 140.79, 128.83, 128.19, 119.71, 119.49, 115.68, 33.69, 33.14, 31.95, 29.34, 29.31, 29.23, 29.11, 28.55, 28.41, 22.80, 14.24.

**$^{11}\text{B-NMR}$**  (300 MHz,  $\text{CDCl}_3$ ):  $\delta$  (ppm) = 14.73

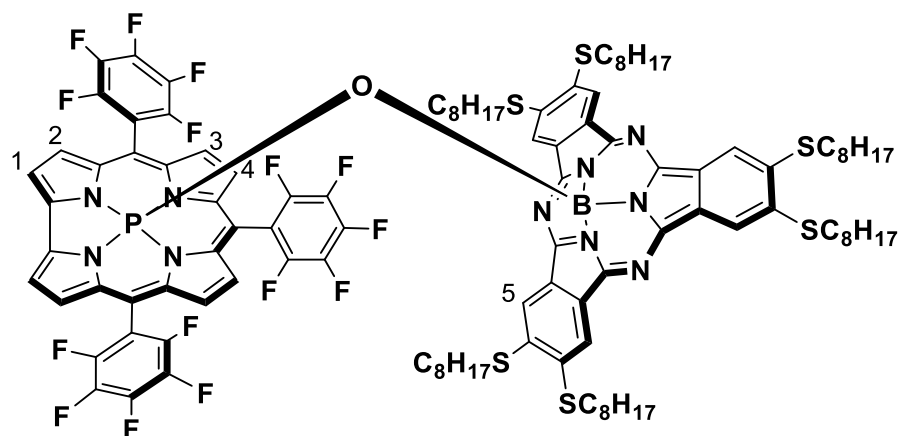
### 1.9.7.2. Synthesis of subphthalocyanine-corrole dyads

#### General procedure:

To a 10 mL Schlenk flask equipped with a magnetic stirrer, dry toluene (1 mL) was added to a mixture of the corresponding SubPc (0.030 mmol) and AgOTf (0.037 mmol), under argon atmosphere. The mixture was stirred and heated (10 mins at RT for SubPc **8**; 2 hours at 40  $^\circ\text{C}$  for SubPc **2a**). Cor **12** (0.015 mmol) and DIPEA (0.037 mmol) were added and the

suspension was stirred at 80 °C for 18 hours. The solvent was removed by vacuum distillation and the resulting solid was subjected to column chromatography on silica gel. Each compound was further purified by size exclusion chromatography in  $\text{CHCl}_3$ .

#### Subphthalocyanine-Corrole dyad (**14**)



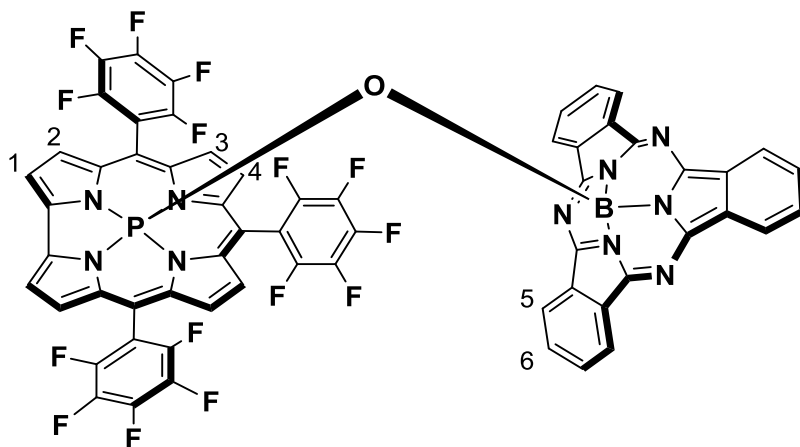
Column chromatography on silica gel using heptane/ethyl acetate 4:1 as eluent. Compound **14** (3 mg, 0.002 mmol) was obtained as a purple solid. Yield: 5%.

$^1\text{H-NMR}$  (300 MHz,  $\text{CDCl}_3$ ):  $\delta$  (ppm) = 9.08 (br dd, 2H;  $\beta$ -pyrr), 8.69 (br t, 2H;  $\beta$ -pyrr), 8.54 (br t, 2H;  $\beta$ -pyrr), 8.37 (br t, 2H;  $\beta$ -pyrr), 8.08 (s, 6H; H-5), 3.15 (m, 12H;  $\text{SCH}_2$ ), 1.80 (m, 12H;  $\text{SCH}_2\text{CH}_2$ ), 1.28 (m, 48H;  $\text{S}(\text{CH}_2)_3(\text{CH}_2)_4$ ), 0.88 (m, 18H;  $\text{S}(\text{CH}_2)_7\text{CH}_3$ ).

**MS** (MALDI-TOF, DCTB):  $m/z$  = 2117.6 [ $\text{M}$ ] $^+$

**UV-Vis** (Toluene):  $\lambda_{\text{max}}$  (nm) = 584, 563, 540 (sh), 522 (sh), 495 (sh), 415.

#### Subphthalocyanine-Corrole dyad **15**



Column chromatography on silica gel using toluene/THF 20:1 as eluent. Compound **15** (4 mg, 0.003 mmol) was obtained as a dark magenta solid. Yield: 10%.

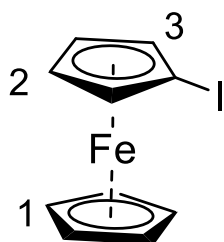
<sup>1</sup>H-NMR (300 MHz, CDCl<sub>3</sub>): δ (ppm) = 9.03 (br dd, 2H; β-pyrr), 8.62 (br t, 2H; β-pyrr), 8.49 (br t, 2H; β-pyrr), 8.31 (dd,  $J_o = 5.9$  Hz,  $J_m = 3.0$  Hz, 6H; H-5), 8.30 (br t, 2H; β-pyrr), 7.62 (dd,  $J_o = 5.9$  Hz,  $J_m = 3.0$  Hz, 6H; H-6).

MS (MALDI-TOF, DCTB):  $m/z = 1252.1$  [M]<sup>+</sup>

UV-Vis (Toluene):  $\lambda_{max}$  (nm) = 583 (br), 412 (br).

### 1.9.8. Synthesis of subphthalocyanine-ferrocene dyads

#### 1.9.8.1. Synthesis of iodo-ferrocene



To a 100 ml round-bottom three-neck flask equipped with a magnetic stirrer, dry THF (15 mL) was added over ferrocene (10.75 mmol) under argon atmosphere, and the solution was cooled to 0 °C. A 1.7 M solution of <sup>t</sup>BuLi in heptane (7 ml) was added dropwise. Dry heptane (15 mL) was added, and the temperature was reduced to -78 °C. Iodine (10.75 mmol) and dry THF (10 mL) were added, and the reaction was left to reach RT for 2 hours. The reaction was

washed with a saturated solution of NaHSO<sub>3</sub> (2x40 mL) and water (40 mL). The organic phase solvent was removed by vacuum distillation, and the resulting solid was subjected to a column chromatography on silica gel using heptane as eluent, obtaining starting ferrocene and iodo-ferrocene as an inseparable mixture.

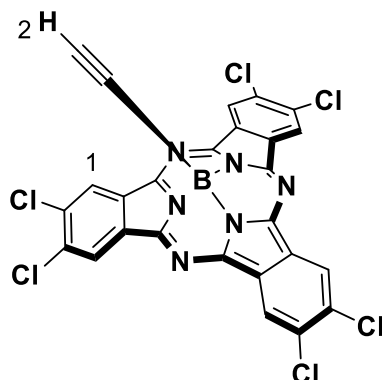


## Experimental section

**<sup>19</sup>F-NMR** (300 MHz, CDCl<sub>3</sub>):  $\delta$  (ppm) = -137.06 (AA'BB' system, 6F), -147.71 (AA'BB' system, 6F).

**UV-Vis** (CHCl<sub>3</sub>):  $\lambda_{\max}$  (nm) (log  $\epsilon$  (dm<sup>3</sup> mol<sup>-1</sup> cm<sup>-1</sup>)) = 574 (5.0), 556 (sh), 532 (4.6), 494 (sh), 308 (4.4).

### Ethynyl-2,3,9,10,16,17-hexachlorosubphthalocyanato boron (III) (**19**)



Compound **19** (151 mg, 0.24 mmol) was obtained as a dark magenta solid. Yield: 60%.

**<sup>1</sup>H-NMR** (300 MHz, CDCl<sub>3</sub>):  $\delta$  (ppm) = 8.91 (s, 6H; H-1), 1.07 (s, 1H; H-2)

**<sup>11</sup>B-NMR** (300 MHz, CDCl<sub>3</sub>):  $\delta$  (ppm) = -21.42

**<sup>13</sup>C-NMR** (300 MHz, CDCl<sub>3</sub>):  $\delta$  (ppm) = 149.40, 134.98, 129.59, 123.78

**MS** (MALDI-TOF, DCTB):  $m/z$  = 626.0 [M]<sup>+</sup>

**UV-Vis** (Toluene):  $\lambda_{\max}$  (nm) = 576, 528 (sh), 314.

**XRD**: Single crystals suitable for X-Ray diffraction analysis were obtained by vapor diffusion of hexane into a chloroform solution. Crystallographic data is summarized in the following table.

<b>Chemical formula</b>	C <sub>26.25</sub> H <sub>7.25</sub> BCl <sub>6.75</sub> N <sub>6</sub>
<b>Formula weight</b>	656.73 g/mol
<b>Temperature</b>	200(2) K
<b>Wavelength</b>	0.71073 Å
<b>Crystal size</b>	0.043 x 0.123 x 0.153 mm
<b>Crystal habit</b>	dark purple prismatic

<b>Crystal system</b>	triclinic	
<b>Space group</b>	P -1	
<b>Unit cell dimensions</b>	$a = 7.6760(7) \text{ \AA}$	$\alpha = 68.304(4)^\circ$
	$b = 25.601(2) \text{ \AA}$	$\beta = 85.593(5)^\circ$
	$c = 28.535(3) \text{ \AA}$	$\gamma = 84.612(5)^\circ$
<b>Volume</b>	$5181.9(9) \text{ \AA}^3$	
<b>Z</b>	8	
<b>Density (calculated)</b>	$1.684 \text{ g/cm}^3$	
<b>Absorption coefficient</b>	$0.773 \text{ mm}^{-1}$	
<b>F(000)</b>	2612	

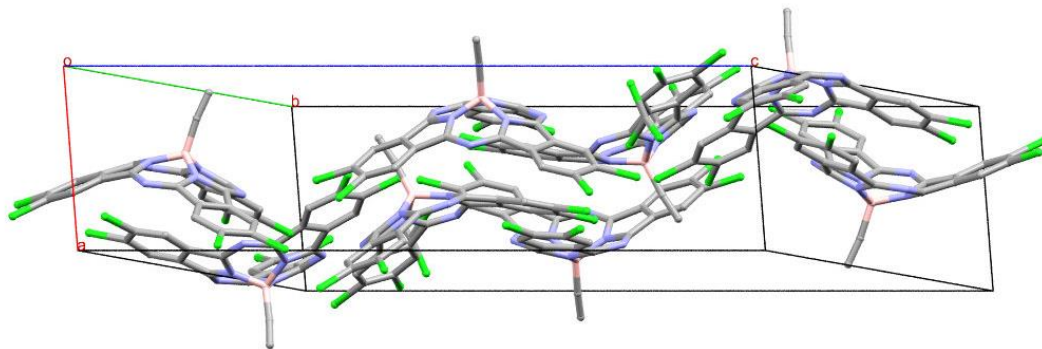


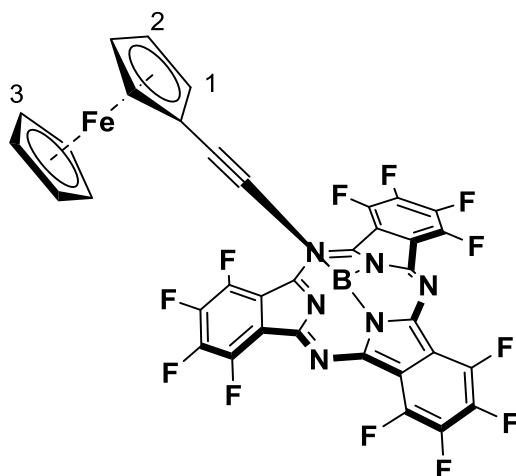
**Figure S-24.** Crystalline structure and packing of SubPc 19. Hydrogen atoms have been omitted for clarity.

### 1.9.8.3. Synthesis of subphthalocyanine-ferrocene dyads

#### General procedure

To a 10 mL Schlenk flask equipped with a magnetic stirrer, dry toluene (2 mL) and dry triethylamine (1 mL) were deoxygenated via three Freeze-Pump-Thaw cycles and added to a mixture of the corresponding SubPc (0.158 mmol), Iodo-ferrocene (0.158 mmol), <sup>t</sup>BuXPhosPd G3 (0.008 mmol) and CuI (0.008 mmol) under argon atmosphere, and the solution was stirred at 60 °C for 16 hours. The reaction slurry was dissolved in CH<sub>2</sub>Cl<sub>2</sub> and passed through a short silica plug. The solvent was removed by vacuum distillation and the resulting solid was subjected to column chromatography on silica gel using a mixture of toluene/Heptane 1:1 v/v as eluent. The desired compound was further purified by size exclusion chromatography in CHCl<sub>3</sub>.

#### Subphthalocyanine-Ferrocene **20**

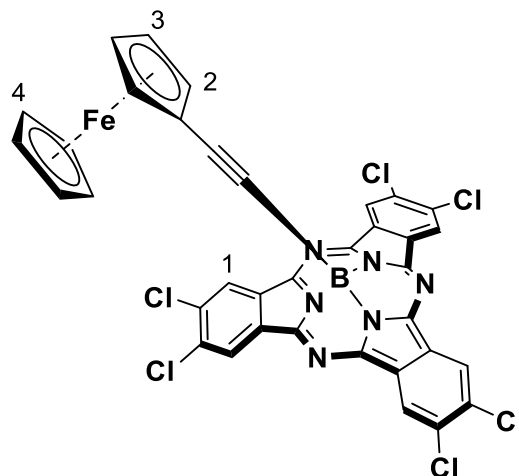


Compound **20** (20 mg, 0.024 mmol) was obtained as a dark pink solid. Yield: 15%.

<sup>1</sup>H-NMR (300 MHz, CDCl<sub>3</sub>): δ (ppm) = 3.89 (t, 2H; H-2), 3.81 (s, 5H; H-3), 3.79 (t, 2H; H-1).

MS (MALDI-TOF, DCTB): *m/z* = 820.1 [M]<sup>+</sup>

UV-Vis (CHCl<sub>3</sub>): λ<sub>max</sub> (nm) (log ε (dm<sup>3</sup> mol<sup>-1</sup> cm<sup>-1</sup>)) = 574 (5.1), 5 (sh), 303.

Subphthalocyanine-Ferrocene **21**

Compound **21** (10 mg, 0.013 mmol) was obtained as a dark pink solid. Yield: 8%.

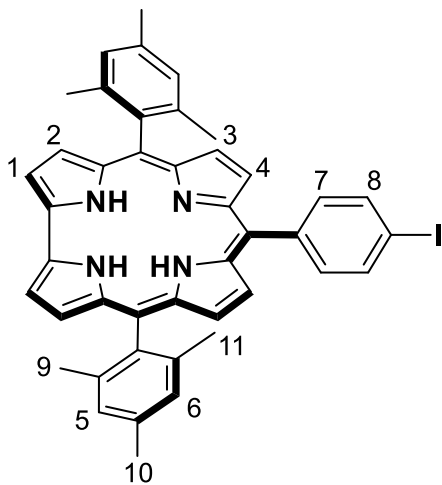
**<sup>1</sup>H-NMR** (300 MHz, CDCl<sub>3</sub>):  $\delta$  (ppm) = 8.89 (s, 6H; H-1), 3.86 (t, 2H; H-3), 3.80 (s, 5H; H-4), 3.79 (t, 2H; H-2)

**MS** (MALDI-TOF, DCTB):  $m/z$  = 810.0 [M]<sup>+</sup>

**UV-Vis** (Toluene):  $\lambda_{\text{max}}$  (nm) = 574, 527 (sh), 315.

### 1.9.9. Synthesis of tetracyanobutadiene-corrole

#### 10-(4-iodophenyl)-5,15-bis(2,4,6-trimethylphenyl)corrole (**22**)



To a 250 mL round-bottom flask equipped with a magnetic stirrer, methanol (50 mL) was added to a mixture of 4-iodobenzaldehyde (0.50 mmol) and Mes-DPM (1.00 mmol). Upon homogenization, a 0.55 M HCl solution (52.5 mL) was added dropwise and stirred at 25 °C for 2 hours. The mixture was extracted with CHCl<sub>3</sub> and the organic phase was washed with H<sub>2</sub>O (2x50 mL), brine (1x50 mL) and dried over Na<sub>2</sub>SO<sub>4</sub>. After filtration and solvent removal by vacuum distillation, CHCl<sub>3</sub> (250 mL) and *p*-chloranil (1.00 mmol) were added and the solution stirred at 25 °C for 16 hours. Hydrazine (0.1

mL) was added and solvent was removed by vacuum distillation. The resulting solid was subjected to column chromatography on silica gel using DCM/heptane 5:1 v/v as eluent. The resulting solid was triturated with a mixture of H<sub>2</sub>O/MeOH 1:1 to obtain 442 mg (0.6 mmol) of compound **22** as a purple solid. Yield: 60%.

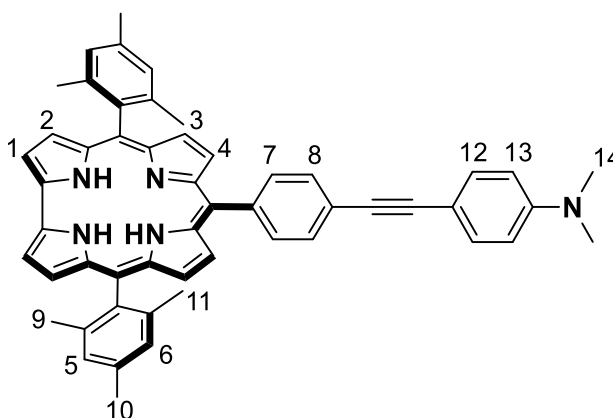
<sup>1</sup>H-NMR (400 MHz, CDCl<sub>3</sub>): δ (ppm) = 8.88 (d, *J* = 4.1 Hz, 2H; H-1), 8.47 (m, 4H; H-3, H-4), 8.32 (d, *J* = 4.1 Hz, 2H; H-2), 8.05 (d, *J* = 8.3 Hz, 2H; H-8), 7.89 (d, *J* = 8.3 Hz, 2H; H-7), 2.60 (s, 6H; H-10), 1.91 (s, 12H; H-9, H-11).

<sup>13</sup>C-NMR (500 MHz, CDCl<sub>3</sub>): δ (ppm) = 152.54, 152.50, 151.22, 147.98, 141.04, 137.59, 136.65, 136.26, 134.24, 131.56, 127.69, 127.00, 125.89, 121.91, 117.77, 112.15, 95.16, 94.36, 32.09, 29.86, 29.52, 22.85, 14.27, 1.18

MS (MALDI-TOF, DCTB): *m/z* = 736.3 [M]<sup>+</sup>

UV-Vis (Toluene): λ<sub>max</sub> (nm) (log ε (dm<sup>3</sup> mol<sup>-1</sup> cm<sup>-1</sup>)) = 409 (4.95), 429 (4.90), 565 (4.16), 604 (4.00), 637 (3.72).

**10-(4-[N,N-dimethyl-4-anilinethynyl]phenyl)-5,15-bis(2,4,6-trimethylphenyl)corrole (23)**



To a 25 mL Schlenk flask equipped with a magnetic stirrer, dry DCM (4 mL) and dry triethylamine (2 mL) were deoxygenated via three Freeze-Pump-Thaw cycles and added to a mixture of the Cor **22** (0.128 mmol), N,N-dimethyl(4-ethynyl)aniline (0.680 mmol) and <sup>t</sup>BuXPhosPd G3 (0.028 mmol) under argon atmosphere, and the solution was stirred at 50 °C for 4 hours. The reaction slurry was passed through a short silica plug. The solvent was removed by vacuum distillation and the resulting solid was subjected to column chromatography on silica gel using a mixture of DCM/Heptane 1:1 v/v as eluent to obtain 37 mg (0.05 mmol) of compound **23** as a dark green solid. Yield: 35%.

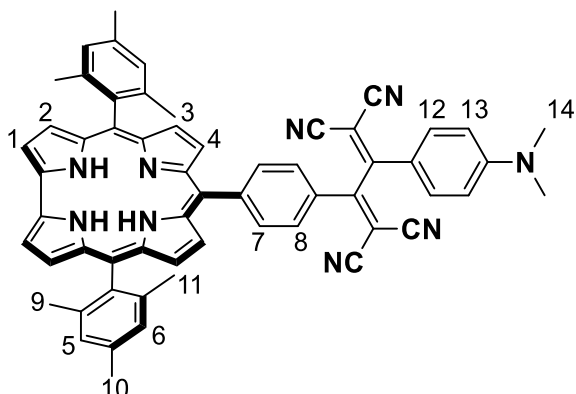
**<sup>1</sup>H-NMR** (400 MHz, CDCl<sub>3</sub>): δ (ppm) = 8.88 (d, *J* = 4.1 Hz, 2H; H-1), 8.49 (m, 4H; H-3, H-4), 8.32 (d, *J* = 4.1 Hz, 2H; H-2), 8.12 (d, *J* = 8.1 Hz, 2H; H-8), 7.85 (d, *J* = 8.1 Hz, 2H; H-7), 7.54 (d, *J* = 8.8 Hz, 2H; Ar-Aniline), 6.74 (d, *J* = 8.8 Hz, 2H; Ar-Aniline), 3.04 (s, 6H; H-14), 2.60 (s, 6H; H-10), 1.92 (s, 12H; H-9, H-11).

**<sup>13</sup>C-NMR** (300 MHz, CDCl<sub>3</sub>): δ (ppm) = 150.31, 139.49, 134.82, 133.70, 132.97, 130.38, 127.78, 125.85, 123.36, 120.34, 119.47, 111.98, 111.77, 110.59, 53.57, 40.30, 40.18, 29.85.

**MS** (MALDI-TOF, DCTB): *m/z* = 813.3 [M]<sup>+</sup>, 670.3 [M-EthynylAniline]<sup>+</sup>

**UV-Vis** (Toluene): λ<sub>max</sub> (nm) (log ε (dm<sup>3</sup> mol<sup>-1</sup> cm<sup>-1</sup>)) = 640 (3.66), 605 (3.88), 570 (4.07), 515 (sh), 432 (4.87), 412 (4.89).

**Tetracyanobutadiene-Corrole 24**



To a 25 mL Schlenk flask equipped with a magnetic stirrer, dry DCM (3 mL) was added to a mixture of the Cor **23** (0.034 mmol) and tetracyanobutadiene (0.051 mmol) under argon atmosphere, and the solution was stirred at RT for 1 hour. The solvent was removed by vacuum distillation and the resulting solid was subjected to column chromatography on silica gel using DCM as eluent to obtain 20 mg (0.02 mmol) of compound **24** as a dark green solid. Yield: 65%.

**<sup>1</sup>H-NMR** (400 MHz, CDCl<sub>3</sub>):  $\delta$  (ppm) = 8.89 (d,  $J$  = 3.9 Hz, 2H; H-1), 8.52 (d,  $J$  = 4.6 Hz, 2H; H-(3-4)) 8.47 (d,  $J$  = 4.6 Hz, 2H; H-(3-4)), 8.36 (d,  $J$  = 8.1 Hz, 2H; H-7), 8.33 (d,  $J$  = 3.8 Hz, 2H; H-2), 8.12 (d,  $J$  = 8.1 Hz, 2H; H-8), 8.00 (d,  $J$  = 8.9 Hz, 2H; Ar-Aniline), 6.85 (d,  $J$  = 8.9 Hz, 2H; Ar-Aniline), 3.24 (s, 6H; H-14), 2.61 (s, 6H; H-10), 1.92 (s, 12H; H-9, H-11).

**MS** (MALDI-TOF, DCTB):  $m/z$  = 881.4 [M]<sup>+</sup>

**UV-Vis** (Toluene):  $\lambda_{\max}$  (nm) (log  $\epsilon$  (dm<sup>3</sup> mol<sup>-1</sup> cm<sup>-1</sup>)) = 637 (sh), 600 (4.04), 567 (sh), 529 (sh), 465 (sh), 424 (sh), 409 (4.89), 390 (sh).

# Chapter 2: Subphthalocyanines and Naphthalocyanines as sensing materials for mass gravimetry devices

## 2.1. Sensors: classification and properties

The concept of chemical sensing is directly related to the identification of compounds in a complex environment or background. On this basis, gas chromatography (GC), liquid chromatography (LC) or mass spectrometry (MS) may be considered as perfect exemplars. However, for the use of those techniques, expensive equipment, highly qualified technicians and large work facilities are generally required. A valid alternative to these analytical techniques consists in the employment of chemical sensors. According to the IUPAC definition, a chemical sensor is a device that transforms chemical information, ranging from the concentration of a specific sample component to overall composition analysis, into an analytically useful signal.<sup>208</sup> On the other hand, the Cambridge institution defines chemical sensors as miniaturized devices that can deliver real-time and online information on the presence of specific compounds or ions in complex samples.<sup>209</sup> The design of low-dimension devices able to transform a wide number of chemical interactions into useful information is for so highly desirable. Sensor devices are made up by two main components: a sensing material (or receptor), whose interaction with the analyte leads to changing one or more of its physical properties, and a transducer, which transforms sensing layer variations into an electric signal.

Focusing on chemical sensors, the sensing procedure can be described as follows: the interaction with the analyte changes one or more physical properties of sensing layer (*e.g.*, temperature,  $\Delta T$ ; mass,  $\Delta m$ ; conductivity,  $\Delta \sigma$ ; work function,  $\Delta \phi$ ; refractive index,  $\Delta n$ ; permittivity,  $\Delta \epsilon$ ). The transducer is an electrical device that converts the variation of the different physical properties into electrical parameters (*e.g.*, capacitance,  $\Delta C$ ; inductance,  $\Delta L$ ; or resistance,  $\Delta R$ ). The circuit in which the sensor is connected finally gives rise to the sensing signal, in base of changes in current,  $\Delta i$ , voltage,  $\Delta V$ , or frequency,  $\Delta f$  (Figure 65).

---

<sup>208</sup> Hulanicki, A.; Glab, S.; Ingman, F. *Pure Appl. Chem.* **1991**, *63*, 1247.

<sup>209</sup> Cammann, G. G.; Guilbault, E. A.; Hal, H.; Kellner, R.; Wolfbeis, O. S. *The Cambridge Definition of Chemical Sensors, Cambridge Workshop on Chemical Sensors and Biosensors*; Cambridge University Press: New York, 1996.

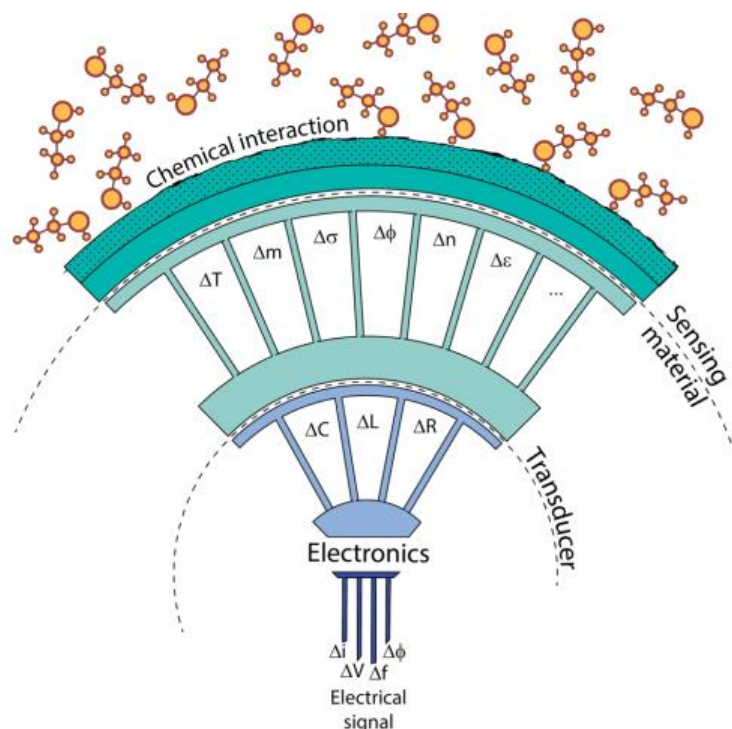


**Figure 65.** Logical structure of a chemical sensor. Upon chemical interaction between the analyte and the sensing material, variations of its physical properties occur (e.g., temperature,  $\Delta T$ ; mass,  $\Delta m$ ; conductivity,  $\Delta \sigma$ ; work function,  $\Delta \phi$ ; refractive index,  $\Delta n$ ; permittivity,  $\Delta \epsilon$ ). The transducer converts the physical variations into electrical parameters (e.g., capacitance,  $\Delta C$ ; inductance,  $\Delta L$ ; resistance,  $\Delta R$ ), that are read by the circuit in terms of electrical variations. Credits: Ref. 210.

As observed in Figure 65, the interaction of the analyte with the sensor device directly depends upon the sensing material. In this regard, macrocyclic derivatives such as porphyrinoids represent a versatile scaffold for their incorporation as sensing materials. As chromophores with an extended  $\pi$ -aromatic system, they present interesting properties that can be useful upon interaction with the different analytes. Moreover, due to a strict structure-property relationship, their synthetic flexibility allows for a fine-tune of the characteristic properties that define the different sensing layers, thus expanding the possibility of sensor's design. These features have been the basis for the development of a

large number of porphyrinoid-based sensor devices for the detection of analytes in both gaseous and liquid media (Figure 66).<sup>210</sup>

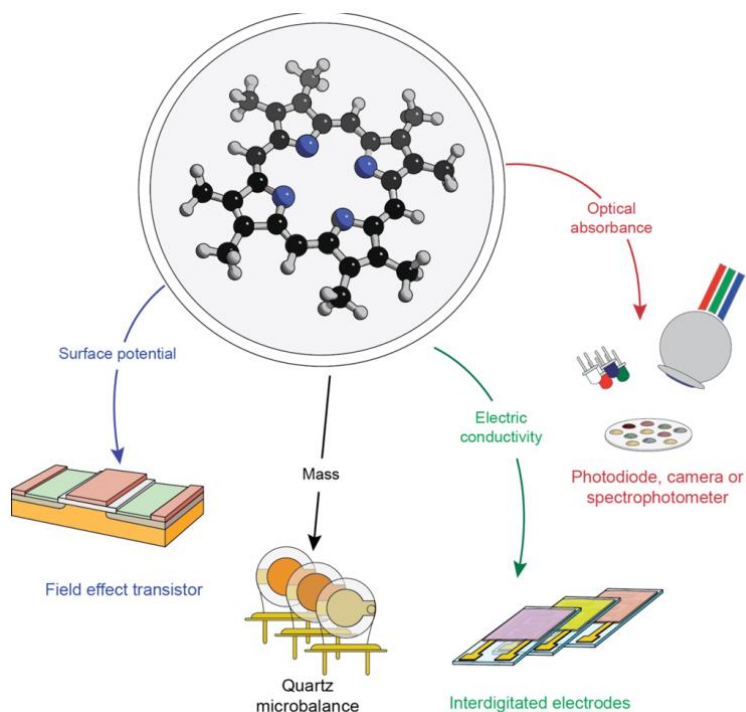


**Figure 66.** Examples of porphyrin-based chemical sensors. Credits: Ref. 210.

Sensors are defined by a series of quantitative parameters that determine the reliability of the data obtained by the device. Usually, sensor characteristics are derived by the sensor response curve that reports the variation of sensor output over the variation of target analyte concentration. Among the several definitions, we prefer to define sensitivity as the variation of the response signal with respect to the variation of the analyte concentration around a wanted concentration, corresponding to the derivative of the response curve. In other words, the slope of characteristic curve at a concentration is the

<sup>210</sup> Paolesse, R.; Nardis, S.; Monti, D.; Stefanelli, M.; Di Natale, C. *Chem. Rev.* **2017**, *117*, 2517.

sensitivity of the sensor at that concentration. In case of linear region, the sensitivity is constant. Otherwise, it must be expressed as a function of the concentration.

Resolution corresponds to the smallest variation of the analyte concentration that can be measured by the sensor around a working point. Limit of Detection (L.O.D.) is the resolution in zero, and so the minimum variation of input that provides an output signal statistically different from the noise. This feature is driven by measurement errors and is ultimately limited by the electronic noise unavoidably embedded in the sensor signal. Resolution of the sensor depends also on the electronic instrument that is applied to measure the sensor signal, being possible to obtain different resolutions for the same sensor device. Usually, it is defined as the  $3 \cdot \text{NOISE}_{\text{rms}} / \text{Sensitivity}$ , where  $\text{NOISE}_{\text{rms}}$  is the root mean square value of noise. Please note that as long as sensitivity depends on the concentration, also does resolution.

Reproducibility is the ability to produce the same response when identical chemical stimuli are applied under same conditions and directions, determining the robustness of the device. Additionally, reversibility is the ability of a sensor to return to its initial position (baseline value or zero) after the removal of the stimulus. In chemical sensors this property is correlated with the strength of interactions occurring between the analyte and the receptors. In case of strong interaction, the binding is not reversible, being the case, for example, of disposable sensors.

Although all important, the most crucial property of sensors is selectivity. Specificity is the capacity of a sensor to only respond to one chemical stimulus. This is typical, for example, of recognition mechanisms of biological systems (*e.g.* antigens-antibodies binding). Selectivity is defined as the capability of the sensor to respond mainly to one kind of analytes. In this case, the response to other analytes is not zero, but much lower than the response towards the target analyte. It is particularly important for the recognition of target compounds in complex mixtures or in presence of interferents. Generally, specificity or high selectivity occurs from a strong interaction (or multiple weak interactions) between the receptor and the analyte. Therefore, this kind of sensor are usually not reversible (this is the reason why most of biosensors are disposable systems).

From a traditional approach, higher selectivity is generally associated to best performance sensors: the interaction with motifs that could be recurrent in different

molecules, even in complex mixtures, is always desired. However, in the case of porphyrinoids, this task resulted difficult to fulfil, and the number of highly selective porphyrinoid sensors remains limited.<sup>211</sup> From the traditional point of view, low selective sensors give rise to ambiguous signals, and can only be trusted when subjected to already known samples.

In an effort to imitate nature, selectivity was found to be “*weak*” in one of receptors of the major living being’s sensing system, that is, mammals’ olfactory system. One of the main components of this system consists of the main olfactory epithelium in the nasal cavity where transduction of volatile odour occurs, and the main olfactory bulb and its connection with other parts of the brain.<sup>212</sup> The chemical olfactory neurons originate from the olfactory receptors that are transmembrane proteins endowed with specific sites where the volatile compounds interact. In the olfactory system, the combination of responses coming from low-selective receptor arrays generates a pattern that is later interpreted by the brain: each receptor is sensitive to many molecules, and each molecule is sensitive to many receptors.

The approach of biological system to odour recognition was utilized as source of inspiration for the development of sensor arrays, giving an intelligent use to those individual low-selective sensors through their combination. Instead of being selective to one concrete molecule or fragment (*e.g.* aminoacids), each individual sensors compromising the system present a certain affinity to one or more general characteristic, like polarity, H-bonding or aromaticity, so that synergies can be created among them. In this regard, the synthetic versatility of porphyrinoids provides a clear advantage, allowing the way which this system complements itself to be precisely controlled. Additionally, it is worth to note that, in case of odour recognition, selective sensors have a series of disadvantages. First, in order to fully characterize a complex mixture, a selective sensor is needed for each of the single

---

<sup>211</sup> a) Cho, Y.; Lee, S. S.; Jung, J. H. *Analyst* **2010**, *135*, 1551. b) Jaworska, E.; Naitana, M. L.; Stelmach, E.; Pomarico, G.; Wojciechowski, M.; Bulska, E.; Maksymiuk, K.; Paolesse, R.; Michalska, A. *Anal. Chem.* **2017**, *89*, 7107. c) Jaworska, E.; Pomarico, G.; Berna, B.; Maksymiuk, K.; Paolesse, R.; Michalska, A. *Sensors and Actuators B: Chemical* **2018**, *277*, 306. d) Jaworska, E.; Caroleo, F.; Natale, C. D.; Maksymiuk, K.; Paolesse, R.; Michalska, A. *J. Porphyrins Phthalocyanines* **2020**, *24*, 929.

<sup>212</sup> Ennis, M.; Puche, A. C.; Holy, T.; Shipley, M. T. Chapter 27 - The Olfactory System. In *The Rat Nervous System (Fourth Edition)*; Paxinos, G., Ed.; Academic Press: San Diego, **2015**, 761.

compounds comprising the odours (*i.e.* coffee aroma is composed by hundreds of volatiles compounds). Besides the fabrication effort of a so made array, the exact composition of odour must be *a priori* known to make the selective sensor array. Finally, so made array is not able to detect any unknown compounds, being its employment limited only to that specific task.

### **2.1.1. Chemical sensors for the detection of gas analytes**

Chemical sensor devices are mainly composed by a receptor and a transducer, as previously illustrated in Figure 1. Among all the different transducers, mass sensors allow for the detection of all the interactions undergoing between receptors and analyte. This situation perfectly suits the rich portfolio of chemical interaction mechanisms typical of porphyrinoid-based systems. Furthermore, mass transduction does not require any particular film properties such as conductivity.

### **2.1.2. Multisensory analysis based on mass transducers**

Mass transducers are able to detect the variation of mass due to the adsorption of molecules over the sensing layer. This detection mechanism is sensitive only to the molecular weight of analyte. Therefore, it can be considered a non-selective transducer since any interactions onto the sensing layer, even the weak and ubiquitous Van-der-Waals, are detected. As a consequence, their use in broad-selective sensing arrays is preferred. The most widely utilized mass transducers are the Quartz Crystal Microbalances, which consist in a slab of quartz embedded into two electrodes (generally made of gold) that oscillate thanks to piezoelectric property of quartz.

Piezoelectricity is the electric charge that is accumulated in certain solid materials, such as crystals or specific ceramics, in response to a mechanical stress and *vice versa*. Quartz is a piezoelectric material that can be made to oscillate at a defined frequency by applying an appropriate voltage driven signal, usually contacting metal electrodes into an oscillating electronic circuit. They are endowed with enough resolution (lower than 1 ng) to detect small mass variations, and the surface presented by this kind of sensors can be properly coated by the sensitive material by means of different deposition techniques.

QMBs are composed by thin quartz plates cut along a particular crystalline direction that confers the device the thickness shear resonance mode (AT cut, Figure 67). The

resonant frequency depends on the thickness of the quartz plate, according to the relationship  $f_0 = v_s/2h_q$ , where  $v_s$  is the quartz sound velocity (3750 m/s for quartz) and  $h_q$  is the thickness of the quartz. Sauerbrey demonstrated that, in a low perturbation regime, the frequency of a QMB depends on the mass deposited over the surface according to Equation (4).<sup>213</sup>

$$\Delta f = \frac{2f_0^2}{A\sqrt{\mu_q\rho_q}} \Delta m \quad (4)$$

where  $f_0$  is the fundamental resonance frequency of the quartz,  $A$  is the active area,  $\mu_q$  is the quartz shear module, and  $\rho_q$  is the quartz density. The Sauerbrey equation is strictly valid for rigid coatings that do not store elastic energy. We have recently confirmed the validity of Sauerbrey equation in case of porphyrin coating by a simple optical method.<sup>214</sup>

Quartz crystals are generally connected to oscillator circuits, so the change of frequency upon adsorption of mass on the quartz surface can be measured, resulting in a shift on the frequency of the oscillator. The theoretical (and optically validated) sensitivity of a QMB utilized is 7.20 Hz/ng.

---

<sup>213</sup> Sauerbrey, G. *Eur. Phys. J. A* **1959**, *155*, 206.

<sup>214</sup> Magna, G.; Belugina, R.; Mandoj, F.; Catini, A.; Legin, A. V.; Paolesse, R.; Di Natale, C. *Sensors and Actuators B: Chemical* **2020**, *320*, 128373.

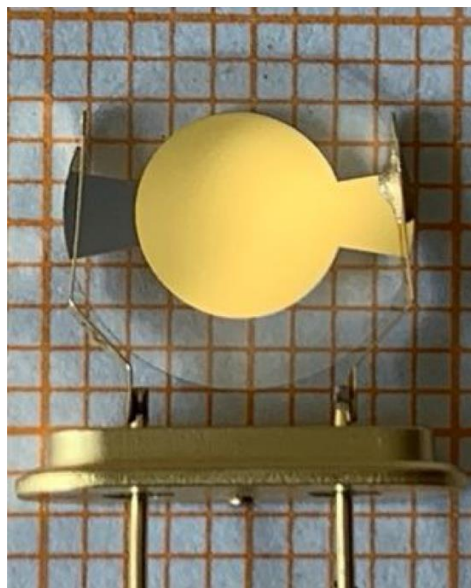


**Figure 67.** Typical QMB sensor used for chemical sensors and biosensors applications. QMBs are composed by a central quartz disc corresponding to the active surface area, held by a gold electrode pad. Credits: *Ref 214*.

The latest version of the QMB-based chemical multisensor, namely electronic nose, developed by the Paolesse and Di Natale group, is presented (Figure 68). An array of 12 QMBs coated with different porphyrin and corrole metallocomplexes is set up inside a Teflon cell. Once sealed, the volatile sample can be provided either by a mass flow controller system or by the internal microfluid system (composed by a micropump and electro-valves). The changes of frequency upon adsorption of the volatile compound over the different QMBs are transferred and recorded to a PC via USB through the interface electronic board. Time signals are elaborated in MatLab® environment to extract features, which are descriptors used to summarize the information stored into the time-signals recorded. The pattern of responses considering the features extracted by the whole array constitutes a fingerprint of the analyte that is unique for each volatile compound. Different multivariate data analysis techniques (Principal component analysis, PCA; Multiple linear regression, MLR; Partial least square regression, PLSR; Principal component regression, PCR) or chemometric techniques are employed for the extraction of the information and the analysis of the characteristics provided by every different sensor comprising the array. In this regard, the sensor array must be cross selective, that is, the differences between the individual sensors should be maximum in order to achieve distinctive profiles for each

independent molecule. Essentially, the patterns of responses of each sensor to the different VOCs should be low correlated.

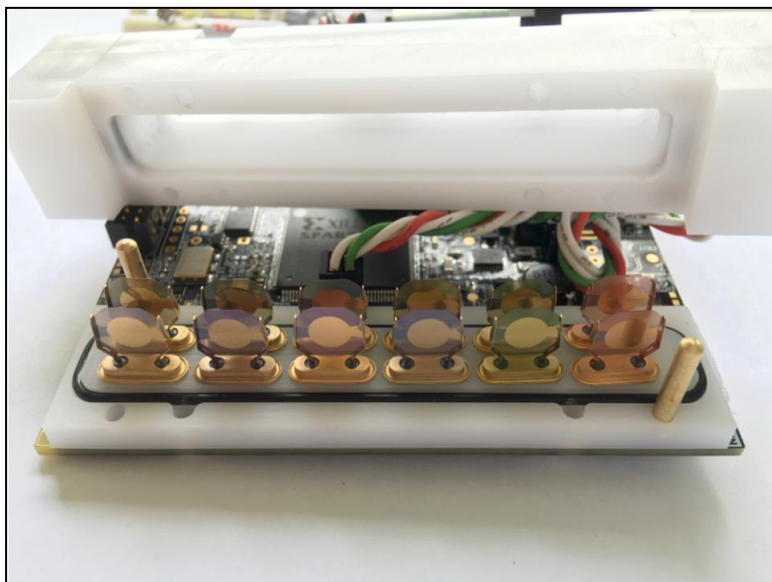


**Figure 68.** Array of 12 QMBs coated with different metal complexes of porphyrins and corroles. In the background, the interface electronic board. On top, the Teflon cell covering the QMB's array during the measure. Credits: University of Rome Tor Vergata.

### 2.1.3. Porphyrinoids as sensing layers in mass transducers based on QMBs.

As previously referred in the later section, porphyrinoids represent a versatile scaffold for its use as sensing layers, not only because their particular electronic and photophysical properties, but also for the possibility of being fine-tuned *via* a wide range of synthetic methodologies.

Porphyrins were firstly introduced as QMB-sensing layers by the group of Paolesse and Di Natale in the later nineties, in which a series of metalloporphyrin-coated QMBs were investigated for the determination of food freshness, presenting cross-selective profiles towards alcohols and amines.<sup>215</sup> Those encouraging results paved the way for the

---

<sup>215</sup> Brunink, J. A. J.; Di Natale, C.; Bungaro, F.; Davide, F. A. M.; D'Amico, A.; Paolesse, R.; Boschi, T.; Faccio, M.; Ferri, G. *Analytica Chimica Acta* **1996**, *325*, 53.

introduction of porphyrinoids as sensing materials in the development of new QMB-based sensing arrays.<sup>216</sup> A watershed was marked when their applications focused on the identification of different diseases by detection of disease-related volatile organic compounds (VOCs). Smartly, a relationship between porphyrins and cancer-related VOCs was established. Oxidative stress, one of the main pathways for the generation of those VOCs, arises from an increased activity of the cytochrome P450 enzyme, whose prosthetic group is an iron porphyrin. With the idea that the prosthetic group employed to produce the VOCs may be eventually able to detect them, an array of non-selective QMBs was designed for the detection of lung cancer.<sup>217</sup> In the light of those results, the number of publications related to the measure of human breath for the study of lung cancer started to grow exponentially,<sup>218</sup> extending the methodology for the identification of different disease-related VOCs.<sup>219</sup>

Besides the molecular structure, sensing properties are also influenced by the tridimensional arrangement of the different porphyrinoids onto the surface. Multiple examples have been reported using, for instance, porphyrins with microporous organic

---

<sup>216</sup> Di Natale, C.; Martinelli, E.; Magna, G.; Mandoj, F.; Monti, D.; Nardis, S.; Stefanelli, M.; Paolesse, R. *J. Porphyrins Phthalocyanines* **2017**, *21*, 769.

<sup>217</sup> Di Natale, C.; Macagnano, A.; Martinelli, E.; Paolesse, R.; D'Arcangelo, G.; Roscioni, C.; Finazzi-Agrò, A.; D'Amico, A. *Biosensors and Bioelectronics* **2003**, *18*, 1209.

<sup>218</sup> Capuano, R.; Santonico, M.; Pennazza, G.; Ghezzi, S.; Martinelli, E.; Roscioni, C.; Lucantoni, G.; Galluccio, G.; Paolesse, R.; Di Natale, C.; D'Amico, A. *Scientific Reports* **2015**, *5*, 16491. b) Gasparri, R.; Santonico, M.; Valentini, C.; Sedda, G.; Borri, A.; Petrella, F.; Maisonneuve, P.; Pennazza, G.; D'Amico, A.; Natale, C. D.; Paolesse, R.; Spaggiari, L. *J. Breath Res.* **2016**, *10*, 016007.

<sup>219</sup> a) D'Amico, A.; Di Natale, C.; Paolesse, R.; Macagnano, A.; Martinelli, E.; Pennazza, G.; Santonico, M.; Bernabei, M.; Roscioni, C.; Galluccio, G.; Bono, R.; Agrò, E. F.; Rullo, S. *Sensors and Actuators B: Chemical* **2008**, *130*, 458. b) Di Natale, C.; Paolesse, R.; Martinelli, E.; Capuano, R. *Analytica Chimica Acta* **2014**, *824*, 1. c) Capuano, R.; Domakoski, A. C.; Grasso, F.; Picci, L.; Catini, A.; Paolesse, R.; Sirugo, G.; Martinelli, E.; Ponzi, M.; Di Natale, C. *Sensors and Actuators B: Chemical* **2017**, *245*, 341. d) Zetola, N. M.; Modongo, C.; Matsiri, O.; Tamuhla, T.; Mbongwe, B.; Matlhagela, K.; Sepako, E.; Catini, A.; Sirugo, G.; Martinelli, E.; Paolesse, R.; Di Natale, C. *Journal of Infection* **2017**, *74*, 367. e) Capuano, R.; Spitalieri, P.; Talarico, R. V.; Catini, A.; Domakoski, A. C.; Martinelli, E.; Scioli, M. G.; Orlandi, A.; Cicconi, R.; Paolesse, R.; Novelli, G.; Di Natale, C.; Sangiuolo, F. *Sci Rep* **2018**, *8*, 11056. d) Capuano, R.; Khomenko, I.; Grasso, F.; Messina, V.; Olivieri, A.; Cappellin, L.; Paolesse, R.; Catini, A.; Ponzi, M.; Biasioli, F.; Di Natale, C. *Sci Rep* **2019**, *9*, 12360.

networks<sup>220</sup> or groups of uniform materials based on organic salts (GUMBO).<sup>221</sup> Particularly, to take advantage of this additional feature, ZnO nanoparticles (NPs) coated with porphyrins were employed as the sensing layer, observing an enhancing of the sensitivity and selectivity vs. a single porphyrin, thus adding a new degree of freedom for sensor arrays design.<sup>222</sup>

Very recently, the mass sensitivity of QMBs based on Sauerbrey equation was experimentally validated taking advantage of the outstanding absorption properties of porphyrins, even when the coating of the surface is unevenly distributed.

The exploitation of the different binding behaviors of porphyrinoids as sensing layers have prompted their simultaneous use in cross sensitive sensor arrays. The combination of corroles and porphyrins have been recently investigated by measuring an array of functionalized QMBs with model VOCs.<sup>223</sup> The results obtained evidenced a great influence in the macrocycle structure, showing higher sensitivities for the corrole in comparison with the corresponding porphyrins, paving the way for the combination of several porphyrinoids that can positively cooperate to enhance the performance of sensor arrays.

---

<sup>220</sup> Park, J. H.; Ko, J. H.; Hong, S.; Shin, Y. J.; Park, N.; Kang, S.; Lee, S. M.; Kim, H. J.; Son, S. U. *Chem. Mater.* **2015**, *27*, 5845.

<sup>221</sup> Regmi, B. P.; Galpothdeniya, W. I. S.; Siraj, N.; Webb, M. H.; Speller, N. C.; Warner, I. M. *Sensors and Actuators B: Chemical* **2015**, *209*, 172.

<sup>222</sup> Magna, G.; Dinc Zor, S.; Catini, A.; Capuano, R.; Basoli, F.; Martinelli, E.; Paolesse, R.; Di Natale, C. *Sensors and Actuators B: Chemical* **2017**, *251*, 524.

<sup>223</sup> Capuano, R.; Pomarico, G.; Paolesse, R.; Di Natale, C. *Sensors* **2015**, *15*, 8121.

## 2.2. Specific objectives of Chapter 2

The main purpose of Chapter 2 is devoted to the exploration and study of Subphthalocyanines (SubPcs) and Naphthalocyanines (NPc) as sensing materials in QMBs for its introduction in cross-selective arrays. To the best of our knowledge, the use of SubPcs as the sensing layer in QMBs or gas-detection devices is unprecedented. On the other hand, although no QMB-based NPc sensor devices have been reported, they have already been incorporated into organic thin-film transistor (OTFT) sensors for gas detection purposes, demonstrating an improved chemical vapor sensitivity and selectivity relative to vacuum-deposited Phthalocyanine (Pc) OTFTs.<sup>224</sup> Additionally, NPcs have been employed in liquid electrochemical sensing devices, presenting, along with Phthalocyanines (Pcs) and Porphyrins (Pors), a high degree of cross-selectivity towards antioxidant compounds.<sup>225</sup>

In this chapter, the preparation of three new SubPc-QMB (SubPcF<sub>12</sub>-Cl **s1**, SubPcH<sub>12</sub>-Cl **s2** and SubPcCl<sub>6</sub>-Cl **s3**) and one NPc-QMB (TTNPcNi **s4**) and its incorporation into cross-selective gas arrays, along with a series of already-known porphyrinoids, has been studied.

---

<sup>224</sup> Royer, J. E.; Zhang, C.; Kummel, A. C.; Trogler, W. C. *Langmuir* **2012**, *28*, 6192.

<sup>225</sup> Casilli, S.; De Luca, M.; Apetrei, C.; Parra, V.; Arrieta, Á. A.; Valli, L.; Jiang, J.; Rodríguez-Méndez, M. L.; De Saja, J. A. *Applied Surface Science* **2005**, *246*, 304.

## 2.3. Results and discussion

### 2.3.1. Fabrication of devices

Quartz microbalances (QMBs) with a fundamental frequency of 20 MHz were employed as mass transducers, being the gold electrode of the QMB the sensitive area of the device. As sensing compounds, a series of seven different porphyrinoids have been selected (Figure 69). For coating the sensitive surface area, different deposition techniques may be employed, namely spray coating, spin coating and drop casting. In order to maintain a standard, the mass deposited on each sensor corresponded to a frequency shift of approximately 30 kHz, equally distributed between the two electrodes.

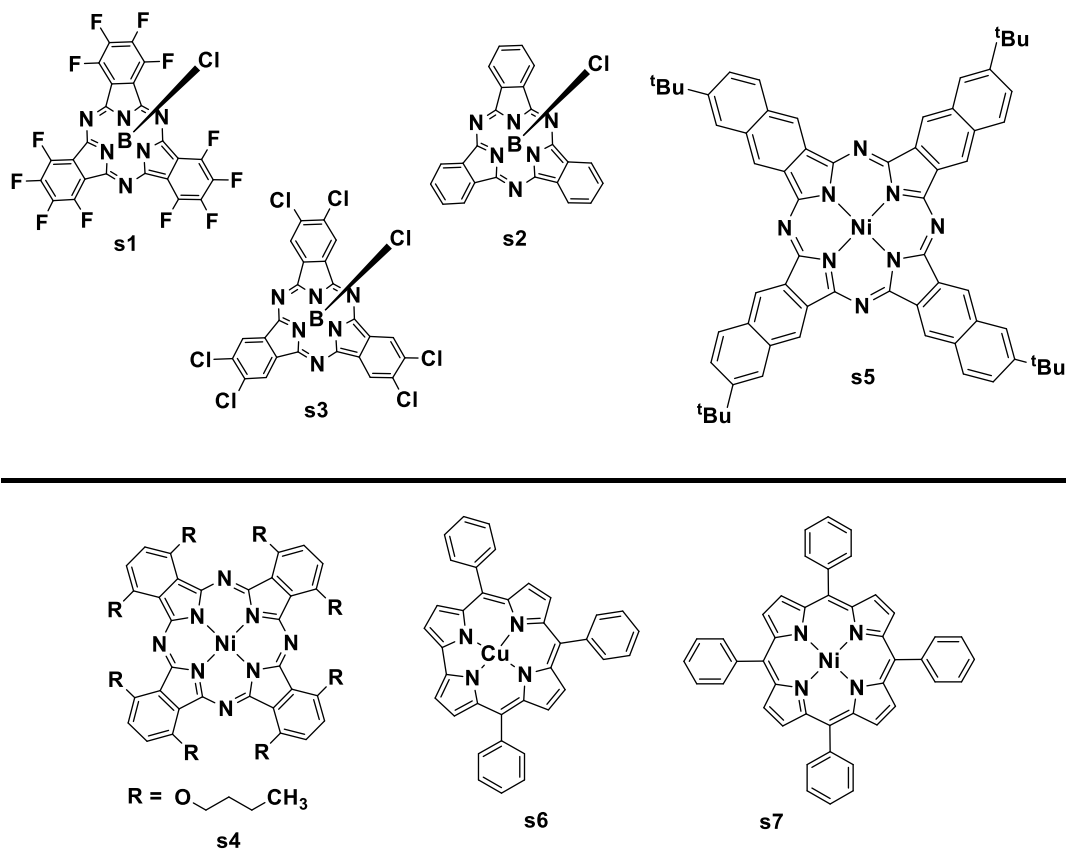


**Figure 69.** Chemical structure of the novel (top) and already studied (bottom) porphyrinoids in QMBs cross-selective arrays.

Drop casting deposition technique consists on the placement of one drop of the dissolved sensing material onto QMB's sensitive area (namely the electrodes). It is a straightforward technique with low sensing material and low time consumption. However, there is no fine control in the amount of sensitive material deposited, corresponding to a concrete shift of frequency. Additionally, upon evaporation of the casted solvent, the low homogeneity of the deposited layer promotes the generation of clusters that could disrupt the measure.

Spin coating follows the same principle that the drop casting technique. To improve the evenness of the sensing layer, QMBs are subjected to a high-revolution spin during the solvent drop, avoiding the formation of clusters and favouring the homogeneity of the layer. However, it presents the requirement of specialized equipment.

Spray coating stands as the best technique for the deposition of the organic sensing layer. Vaporization of the solved compound over the gold electrode allows for a fine-control of the mass deposited with a high grade of homogeneity. However, compound and time-consumption requirements grow exponentially in comparison with the drop casting and spin coating techniques. Additionally, it presents the requirement of spray-deposition equipment.

Spray coating was selected as the deposition technique for the QMBs described in this chapter. Nevertheless, in order to establish a direct comparison between the different deposition techniques, three different QMBs of the model NiTTPorf **s7** were introduced into the cross-selective array, in which the three different deposition approaches were independently employed for each QMB.

### **2.3.2. Device structure and experimental procedure**

The device was set up in accordance with the disposition described in Figure 4. Of the twelve available electronic oscillator circuit docks, nine were occupied by the already coated QMBs. The electronic parts of the device were in-house developed, allowing for the control of the measurement setup. On the other hand, a mass flow controller system was employed for providing carrier gas constant flow and the different dilution of saturated vapours of the volatile organic compounds (VOCs) into the measurement chamber. Saturated vapor pressures were obtained by liquid sample by a bubbler where a nitrogen flow helps the evaporation. The saturated vapor was further diluted with a carrier of gas N<sub>2</sub> at different dilution percentages by using mass-flow controllers to provide the desired sample concentration, always maintaining a total flux of 200 sccm.

Once the measurement chamber is closed, the flux circuit is directly connected to one of the chamber's sides, with an exit canal on the opposite side to facilitate the inner pressure to be kept constant.

As gas samples, probe VOCs were employed. In order to obtain a wider spectrum of responses towards chemical functionalities, different probe VOCs were selected, presenting polar (methanol (MeOH), ethanol (EtOH)), non-polar (hexane), aromatic (toluene), basic (triethylamine (TEA)), acid (acetic acid (AcOH)), or particular interactions (water, formaldehyde). Measurements of each VOC were randomly performed at four different concentrations, in frames of five minutes, with N<sub>2</sub> cleaning times of fifteen minutes between each measure. Each concentration was measured four times, with a total of sixteen measures for each VOC. In order to avoid false or corrupted results, N<sub>2</sub> was flushed through the system one hour prior and after each VOC data recording. In order to ensure the stability and robustness of the QMBs' sensing layers, control experiments were performed in between the different VOC measurements so exactly results as the initial measures were recorded.

### **2.3.3. Software, interface and data acquisition**

Acquisition of data is carried out from a MatLab® interface previously programmed by our group. The interface was specifically designed to control the electronic nose device employed for the measure procedure. Moreover, the frequency changes of all the different QMBs comprising the array can be checked in real time during the measure, allowing to control the correct performance of the device.

### **2.3.4. Analysis of the results**

All the recorded data was analyzed by means of MatLab® software. Gas responses were measured as the frequency change for each QMB upon adsorption of the different VOCs. A characteristic frequency variance profile is observed in Figure 79, presenting a good recovery of the baseline. The sensor response is calculated as the frequency change measured right before and after the addition of the volatile compound.

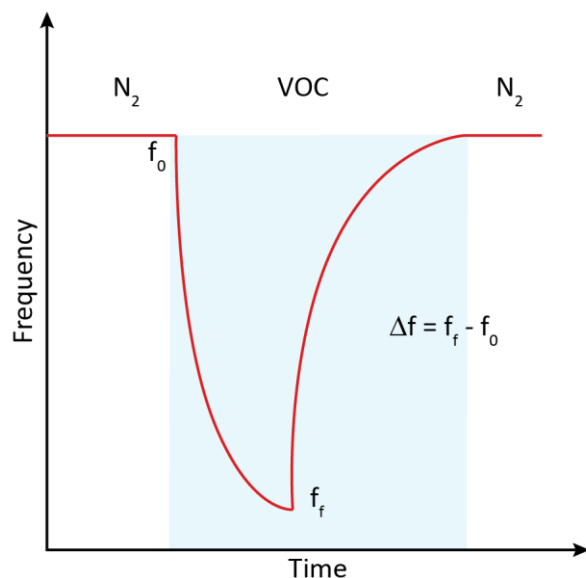


**Figure 70.** Evolution of the frequency change of a coated QMB layer exposed to % of saturated pressure of VOC. Sensor response calculated as the difference between the final and initial frequency measured upon addition and removal of the volatile compound.

It is important to take into account that, since each volatile compound is characterized by its own saturation pressure, the concentration of each compound in gas phase is different. For so, concentration values are reported in terms of parts-per-million (ppm) values, so a good relationship can be established between the different responses.

The sensitivity of the sensors of the nine compounds is calculated as the derivative of the sensor response with respect to the concentration (Figure 71). In order to do that, a linear fitting equation is considered to model the relationship between sensor responses and VOC concentrations. As a result of having linear fitting models, sensitivities result to be constant in the range considered. All the corresponding QMBs presented higher sensitivity values when exposed to formalin, with respect to the other VOCs. Sensitivities are here reported in logarithmic scale since the range of concentrations is different due to the different saturated vapor pressures of samples. Furthermore, logarithmic conversion places sensitivity measurements in a linear scale, which is more convenient for statistical analysis.

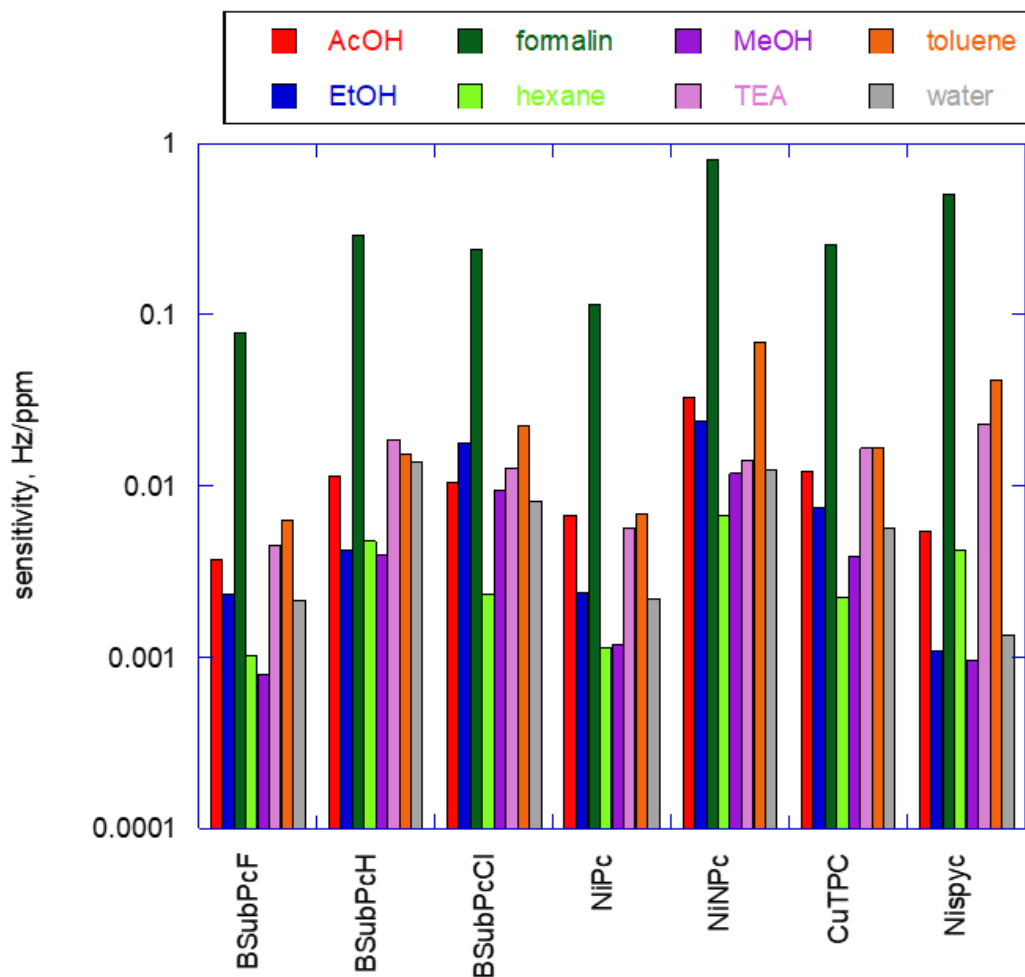


**Figure 71.** Sensitivity profiles (y-axis, Hz/ppm) of the different sensors comprising the array (x-axis) for each VOC.

At first glance, sensitivity profiles returned by SubPcF<sub>12</sub>-Cl **s1** and NiPc **s4** present a high similarity between them. Although structurally and electronically different, they are expected to perform equivalently in QMBs arrays.

A higher affinity towards EtOH than MeOH is reported by all sensors, although for SubPcH<sub>12</sub>-Cl **s2** and NiTPPorf **s7** is more difficult to discriminate between both alcohols. In six of the eight VOCs studied, NiNpc **s5** stands as the most sensitive sensor, showing lower

values for TEA. The highest sensitivity towards water is presented by SubPcH<sub>12</sub>-Cl **s2**, though the same by NiNPc **s5** is remarkable.

Returning to the different coating techniques that were employed for the deposition of NiTTPorf, comparison between the reliable spray-coated QMB and the spin-coated and drop-casted sensors reflected erratic responses, especially for the later, with disrupted frequency profiles. This result led us to discard the two later two QMBs, including in the study only results coming from the spray-coated NiTTPorf **s7**.

In order to investigate their collective behaviour, Principal Components Analysis (PCA) was performed on data considering the responses of 7 sensors to vapours of 8 different VOCs at 4 different concentrations (for each concentration, 4 repetitions were considered). For the scope, sensor responses were arranged in a matrix, being PCA calculated on the non-scaled matrix. As expected, the first Principal Component (PC1) bears the information about concentration, which is also distributed on the other components (Figure 72). PC1 contribution can be excluded order to emphasize the clustering of data. A nice distribution of the information about the compounds in PC2-PC3 is observed (Figure 73). If we consider the four quadrants of PC2-PC3 projection plane, gathering the different compounds by electron-donors (I; water, TEA), alcohols (II; EtOH, MeOH), aromatics (III; toluene) and hydrocarbons (IV; hexane). Responses close to the origin, as in the case of formalin and AcOH, are related to a low-sensitivity response from the array towards them.

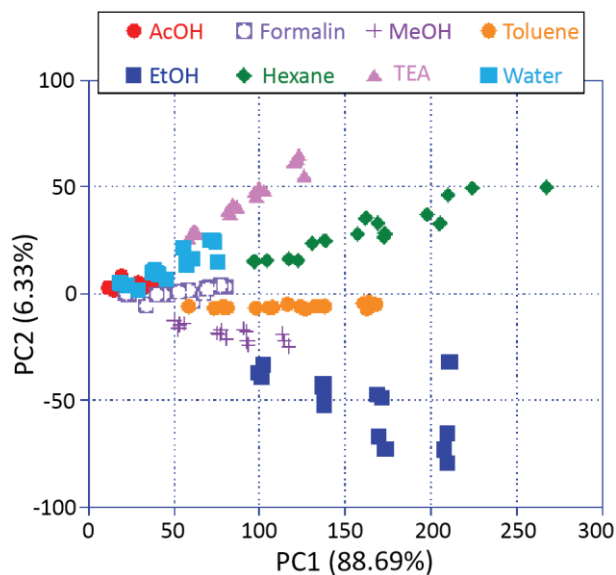


**Figure 72.** Bi-plot of the first two principal components of the analysis performed over the matrix data. A strong correlation between the first PC is observed, corresponding to the measured concentrations of VOCs.

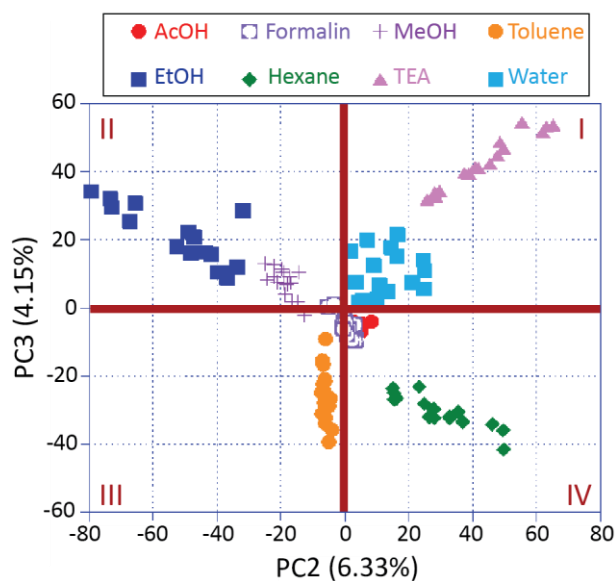


**Figure 73.** Bi-plot of the second and third principal components of the analysis performed over the matrix data. Correlation between the different points is assigned to the main supramolecular interactions established between the sensing layers and the VOCs.

By looking at bi-plot it is possible to investigate the contributions of sensors to the distribution of samples into the projection plane. In particular, PC1-PC2 plane seems to separate sensors into 3 main groups: **s7**, (**s1**, **s2**, **s4**, **s6**), and (**s3**, **s5**) (Figure 74, left). Second order differences are highlighted by PC2-PC3 plots where the different contribution of **s3** and **s5** sensors emerges in the discrimination of alcohols from aromatics (Figure 73, right). As expected, the crucial role of the  $\pi$ -extended structure of NPc **s5** is determined by its positive interaction with aromatic compounds. In addition, a relationship can be established between the electron-accepting properties of the different SubPcs (in crescent order: SubPcH<sub>12</sub>-Cl (**s2**) < SubPcCl<sub>6</sub>-Cl (**s3**) < SubPcF<sub>12</sub>-Cl (**s1**)) and the acid and basic characteristics of the VOCs (Figure 74, right). Consequently, for the most electro-deficient SubPc **s1**, an affinity towards acid compounds (AcOH) is observed. In the same way, for the less electro-deficient SubPc **s3**, interaction towards less acidic compounds such as alcohols is preferred. Finally, for the higher electron-rich SubPc **s2**, the affinity is turned towards more basic compounds, such as TEA.

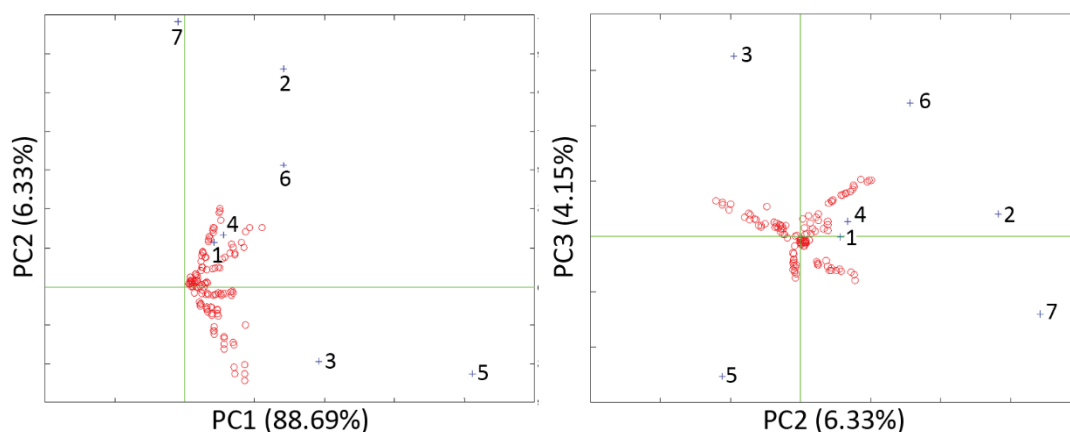


**Figure 74.** Bi-plots of the PC1-PC2 (left) and PC2-PC3 (right) highlighting the major contribution of each of the corresponding sensors to the array.

## 2.4. Summary and conclusions

Preliminary studies have been performed in the use of SubPcs and NPs as sensing materials for gas-detection devices. From the four newly introduced compounds, three of them (**s2**, **s3** and **s5**) presented distinctive sensitive profiles that, in comparison with the model QMBs employed, displayed a prominent affinity to certain interactions. A discrimination trend for the three different SubPcs (**s1**, **s2** and **s3**) was followed, being able to distinguish between acidic/basic VOCs based on its electronic density, paving the way for the fine-tune of its sensing properties *via* easy and straightforward synthetic methodologies, making them ideal candidates for its inclusion in cross-selective sensing arrays.

These results encourage us to further investigate its detection capabilities, expanding the investigation to different sensing devices and tested against real complex samples.

## 2.5. Experimental section

### 2.5.1. Materials and instruments

Organic chromophores employed as sensitive materials for the coating of QMBs were obtained as listed: SubPcF<sub>12</sub>-Cl (**s1**), SubPcH<sub>12</sub>-Cl (**s2**) and SubPcCl<sub>6</sub>-Cl (**s3**) were synthesized as previously described in Chapter 1. Nickel(II)-2,11,20,29-tetra-*tert*-butyl-2,3-naphthalocyanine (**s4**) Nickel(II)-1,4,8,11,15,18,22,25-octabutoxyphthalocyanine (**s5**) were purchased from Sigma-Aldrich. Copper(II)-5,10,15-triphenylcorrole (**s6**) and Nickel(II)-5,10,15,20-tetraphenylporphyrin (**s7**) were obtained from the “Dipartimento di Scienze e Tecnologie Chimiche” of the University of Rome Tor Vergata. Organic solvents employed as volatile organic compound, namely acetic acid, ethanol, hexane, formalin, methanol, toluene and triethylamine were purchased from Sigma-Aldrich. Acetic acid was diluted with water up to a 20% v/v. Freshly distilled water was obtained from the “Dipartimento di Scienze e Tecnologie Chimiche” of the University of Rome Tor Vergata. Additional solvents were purchased from Sigma-Aldrich and were used without further purification. Nitrogen gas (N<sub>2</sub>) was directly used from its corresponding compressed gas cylinder.

### 2.5.2. Gas sensor array

The sensor array was an ensemble of nine quartz microbalance (QMB) mass transducers. In these sensors, a slight mass change ( $\Delta m$ ) on the quartz surface results in frequency changes ( $\Delta f$ ) of the electrical output signal of an oscillator circuit at which each sensor is connected. The quantities  $\Delta m$  and  $\Delta f$  are linearly proportional in the low-perturbation regime. QMB had a fundamental frequency of 20 MHz, corresponding to a mass resolution of the order of a few nanograms. Solid films of sensitive organic chromophores were coated by drop coating, spin coating and spray coating techniques onto QMB mass transducers. Thin films of the sensing materials were deposited on both sides of

quartz disks, from  $10^{-3}$  M solutions in  $\text{CH}_2\text{Cl}_2$ . Deposition of the sensitive layer was controlled, resulting in a total frequency shift of approximately 30 KHz.

The sensor system used was the last version of a series of instruments being designed since 1996 at the University of Rome Tor Vergata. It may accommodate up to twelve QMBs in a measurement cell of approximately  $8 \text{ cm}^3$  volume. The gas sensors are completed by temperature and relative humidity sensors. Each QMB is connected to an oscillator circuit, the frequencies of the oscillator's outputs are measured taking advantage of a temperature compensated reference quartz, allowing for a frequency resolution of 0.1 Hz. Electronics are implemented in a FPGA. Gaseous samples delivery is controlled by a miniature diaphragm pump (0-200 sccm). The instrument is connected and powered via a single USB connection. Functions and the data acquisition are controlled with a in-house software running in MatLab®.

The baseline of sensor signals was measured in a constant flow of  $\text{N}_2$  gas. Saturated VOC samples were obtained by flushing  $\text{N}_2$  gas through the organic solvent compound. Concentrations of the measured VOCs were calculated by mixing VOC and  $\text{N}_2$  gas streams at different proportions, maintaining a constant total flow of 200 sccm. Concentrations ranged from 16 to 2 sccm.

### **2.5.3. Statistical analysis**

Principal Component Analysis (PCA) were used for exploration and classification purposes. All data analysis was performed in MatLab®.

# **Resumen y conclusiones**

## Introducción: Subftalocianinas y corroles como materiales moleculares

Material molecular es toda aquella estructura orgánica constituida por subunidades orgánicas o metalorgánicas, pudiendo ser sintetizadas de manera individual y posteriormente combinadas entre sí. Dichos materiales presentan una serie de propiedades electrónicas, ópticas y magnéticas poco convencionales. La correlación estructural existente entre estos materiales y sus propiedades permite que éstas últimas puedan ser modificadas y perfiladas, mediante diferentes metodologías sintéticas a partir de sus subunidades iniciales, lo que los convierte en sistemas muy atractivos de cara a su aplicación en diversos ámbitos tecnológicos, que abarcan desde su incorporación en células solares como materiales sensibles hasta su uso en terapia fotodinámica para el tratamiento de diferentes patologías. De entre la multitud de materiales moleculares presentes en la actualidad, los porfirinoides se encuentran entre los sistemas macrocíclicos más estudiados gracias a sus excelentes propiedades optoelectrónicas, además de su gran versatilidad sintética.

De entre los diferentes porfirinoides, las subftalocianinas (SubPcs), análogos contraídos de las ftalocianinas (Pc), destacan por encima del resto. diferencia de la estructura plana de las Pcs, estos macrociclos aromáticos presentan una estructura cóncava formada por tres unidades diiminoisindol alrededor de un átomo de boro central, el cual presenta una disposición tetraédrica, con su posición axial ocupada. Poseen un sistema de 14 electrones- $\pi$  que se extiende principalmente alrededor de su cavidad central, siendo uno de los pocos ejemplos conocidos de compuestos aromáticos heteroatómicos curvos.

Las SubPcs poseen un característico espectro de absorción ultravioleta-visible, con dos intensas bandas, generalmente en torno a 300 y 550 nm, denominadas banda Soret y banda Q, respectivamente. Presentan una fuerte intensidad de absorción, con valores de coeficientes de absorción en torno a  $5 \times 10^4 \text{ M}^{-1} \text{ cm}^{-1}$ . También poseen una intensa emisión, con pequeños valores de desplazamiento de Stokes (5-10 nm), y energías de excitación en torno a 2.0 eV.

Las propiedades fisico-químicas de las SubPcs las convierten en moléculas excepcionales para su incorporación en multitud de dispositivos electrónicos relacionados con la óptica no lineal, fotovoltaica, electrónica o la terapia fotodinámica. En particular, su capacidad para generar estados excitados y de separación de carga de larga duración las convierte en candidatas ideales para su uso junto a otras unidades fotoactivas, ya sea

mediante uniones covalentes o electroestáticas, en sistemas enfocados hacia la conversión de energía solar.

Dentro de la familia de los porfirinoides, los corroles (Cors) presentan una serie de propiedades ideales para su combinación con SubPcs. Debido a la falta de protocolos y metodologías desarrolladas para su obtención, su disponibilidad sintética fue baja hasta principios de la década de los 2000, donde el descubrimiento de metodologías que permitían su síntesis a partir de compuestos comerciales, supuso un aumento en el número de publicaciones basadas en esta clase de macrociclos de manera exponencial. Es por ello que no se encuentran tan estudiados como las porfirinas (Pors), con las que mantienen una estrecha relación. En comparación con las Pors, los Cors presentan la misma estructura molecular salvo por un enlace directo C-C entre dos de sus unidades pirrónicas, lo que hace que posean una cavidad interna menor y una simetría reducida. Sin embargo, siguen manteniendo los 18 electrones- $\pi$  aromáticos de las Pors, lo que genera una serie de propiedades interesantes. Al igual que las Pors, son capaces de alojar metales en su cavidad interior. Entre sus propiedades destaca la posibilidad de actuar como ligandos trianiónicos, haciendo que sean capaces de alcanzar altos estados metálicos de oxidación, los cuales serían difíciles de estabilizar empleando Pors.

Sus espectros de absorción son cualitativamente similares a los de las Pors, con una intensa banda de absorción alrededor de 400-450 nm correspondiente a la banda Soret, con valores de  $\epsilon = 1-2 \times 10^5 \text{ M}^{-1} \text{ cm}^{-1}$  y tres bandas de menor intensidad en torno a 500-600 nm correspondientes a las bandas Q, con valores de  $\epsilon = 1-2 \times 10^4 \text{ M}^{-1} \text{ cm}^{-1}$ . Las Pors han sido ampliamente empleadas como materiales moleculares en sistemas de conversión energética, como por ejemplo formando diadas con Pcs, SubPcs o ferroceno (Fc). Es por ello que el uso de Cors, los cuales presentan unas características dadoras superiores en comparación con sus análogos porfirínicos, en combinación con otras unidades aceptoras como SubPcs, puede suponer una mejora de sus propiedades fotofísicas

## **Capítulo 1. Materiales basados en subftalocianinas y corroles para su uso en sistemas de conversión energética.**

En el capítulo uno, se recogen la síntesis, la caracterización y el estudio de las propiedades de una serie de sistemas fotoactivos empleados como materiales captadores de energía lumínica basados en SubPcs y Cors.

En la primera sección del capítulo, un conjunto de SubPcs se enlazó a la posición periférica de diferentes Cors, a través de una metodología de activación axial de la SubPc y posterior reacción de sustitución axial sobre la SubPc, empleando unidades fenoxi- en las posiciones *meso*- de los Cors como nucleófilos. Las díadas **4**, **5**, **6** y **7** se obtuvieron en rendimientos razonables, teniendo en cuenta la complejidad y sensibilidad de los sistemas empleados. El estudio de sus propiedades fotofísicas y redox se llevó a cabo mediante experimentos de absorción, emisión, espectroelectroquímica y espectrometría de absorción transitoria, durante una estancia predoctoral en los laboratorios del Prof. D. M. Guldi en Erlangen, Alemania. Los resultados evidenciaron estados de separación de carga para las cuatro díadas estudiadas. A pesar de que la incorporación del cobre en las subunidades Cor se llevó a cabo con intención de estudiar un cambio en sus propiedades, se encontraron tiempos y mecanismos similares de separación de carga para las díadas **5**, **6** y **7**, obteniendo los mejores tiempos para la díada **4**, con valores máximos de 534 ps en tolueno. Adicionalmente, la díada **11** demostró ser capaz de canalizar toda la energía absorbida por la molécula hacia la subunidad SubPc, reforzando su papel como antena en sistemas de transferencia energética.

En la segunda sección, se llevó a cabo la síntesis de las díadas SubPc-Cor **14** y **15** unidas a través de la posición axial del Cor. Para ello, se empleó un Cor de fósforo sustituido en sus posiciones *meso*- por unidadesceptoras. Dado el escaso número de metodologías para la introducción de diferentes funcionalidades sobre la posición axial de los Cor de fósforo, nuestros estudios preliminares se centraron en la activación de dicha posición. Para ello, se siguió una estrategia empleando diferentes derivados de triflato, sin éxito. Finalmente, aprovechando la gran afinidad mostrada por el fósforo hacia las unidades hidroxí-, se lograron introducir dos unidades diferentes de SubPc a través de enlaces  $\mu$ -oxo. Los estudios de absorción y emisión revelaron para la díada **15** una posible transferencia de energía desde la SubPc hacia el Cor. Para la díada **14**, sin embargo, los resultados obtenidos llevaron a proponer la formación de un exciplex.

En el tercer apartado, se llevó a cabo la unión de unidades SubPc y Fc mediante un enlace etinilo. Durante este proceso, se logró optimizar la reacción de formación de la Cl-SubPcCl<sub>6</sub> **17**, incrementando su rendimiento de obtención al 67%. La síntesis de los nuevos derivados de SubPc se llevó a cabo mediante una estrategia de sustitución axial sobre la SubPc, que consiste en el uso de AlCl<sub>3</sub> y el etinil-TMS derivado en condiciones suaves. La unión entre las correspondientes SubPc-Etinilo y Fc se realizó mediante una

reacción Sonogashira de acoplamiento C-C catalizada por paladio, obteniendo las díadas **21** y **22**. Estudios preliminares fotofísicos mostraron una fuerte disminución de la intensidad de emisión de ambas díadas frente a sus correspondientes subunidades de referencia. Esto, junto con los antecedentes en la combinación de SubPcs y Fc mediante diferentes tipos de enlaces, nos llevó a sugerir la presencia de un estado de separación de carga en ambos sistemas.

En el cuarto y último apartado, se llevó a cabo la incorporación de una unidad tetraciano, con propiedades electrónicas fuertemente aceptoras, en el Cor dador **23**, a través de una de sus posiciones periféricas. Para ello, un fragmento de etinilanilina fue enlazado sobre la posición *meso*- del Cor **22** mediante una reacción de Sonogashira, permitiendo la posterior introducción de la unidad tetraciano sobre el Cor **23** mediante una reacción de cicloadición-retroelectrociclación, obteniendo el TCBD-Cor **24**. Con el fin de estudiar su comportamiento en función del pH del medio, se llevaron a cabo experimentos de absorción en diferentes fases de su equilibrio de protonación/desprotonación. Actualmente, se están llevando a cabo experimentos de emisión, espectroelectroquímica y espectrometría de absorción transitoria para determinar su uso potencial en sistemas biológicos, estudiando a fondo su comportamiento fotofísico en función del pH.

## **Capítulo 2. Subftalocianinas y naftalocianinas como materiales sensibles en sistemas de gravimetría de masas**

Gracias a sus particulares propiedades fotofísicas y electrónicas, la familia de los porfirinoides ha sido extensamente empleada como material sensible en dispositivos electrónicos. Además, la versitilidad sintética de estos macrociclos y la estrecha relación entre su estructura y sus propiedades hace que estas últimas puedan ser moduladas de manera precisa y efectiva.

En el presente capítulo, se llevaron a cabo estudios preliminares en la incorporación de SubPcs y naftalocianinas (NPCs) como materiales sensibles en dispositivos de detección de gases de amplia selectividad. El dispositivo empleado está basado en un conjunto de pequeños transductores de masa, en este caso microbalanzas de cuarzo (QMBs), cubiertos por una capa sensible que corresponde a cada uno de los compuestos empleados. La

interacción del analito con la capa sensible lleva a la modificación de una o varias de sus propiedades físicas. A su vez, el transductor se encarga de transformar dichas variaciones en señales eléctricas. Este dispositivo es comúnmente conocido como “nariz electrónica”, debido a su similitud con el sistema olfativo de los mamíferos, los cuales se basan en sistemas de detección no selectivos.

El sistema de detección de gases se compone de cuatro nuevas capas sensibles (SubPcs **s1**, **s2** y **s3**; Np **s5**) así como de una serie de Cors, Pcs y Pors ampliamente estudiados. De las nuevas capas introducidas, tres de ellas presentaron perfiles de sensibilidad distintivos que, en comparación con las capas sensibles ya conocidas, mostraron un conjunto diferente de afinidades frente a los compuestos volátiles orgánicos empleados. Se logró establecer una tendencia de distinción frente a la acidez del medio para las tres SubPcs empleadas, siguiendo un patrón de afinidad en función de sus propiedades electrónicas. Estos resultados convierten a las SubPcs en perfectos candidatos para su incorporación de manera general en dispositivos sensores de selectividad cruzada.